2011

# Pile Setup, Dynamic Construction Control, and Load and Resistance Factor Design of Vertically-Loaded Steel H-Piles

Kam Weng Ng
*Iowa State University*

**Pile setup, Dynamic construction control, and Load and Resistance Factor Design of vertically-loaded steel H-piles**

by

**Kam Weng Ng**

A dissertation submitted to the graduate faculty
in partial fulfillment of the requirements for the degree of
DOCTOR OF PHILOSOPHY

Major: Civil Engineering (Structural Engineering)

Program of Study Committee:
Sri Sritharan, Major Professor
Fouad Fanous
Jeramy Ashlock
Jennifer Shane
Igor Beresnev
Muhannad T. Suleiman

Iowa State University
Ames, Iowa
2011

## DEDICATION

I devote this dissertation to my family, Chooi Kim Lau and Sai Kit Ng, for their patience and support throughout these difficult years, which allow me to focus on my research, studies, and successfully achieve my lifelong goal. To my parents and brothers who always remind me the importance of higher education.

# TABLE OF CONTENTS

# LIST OF FIGURES

# LIST OF TABLES

# ABSTRACT

Because of the mandate imposed by the Federal Highway Administration (FHWA) on the implementation of Load Resistance Factor Design (LRFD) in all new bridge projects initiated after October 1, 2007, research on developing the LRFD recommendations for pile foundations that reflect local soil conditions and construction experiences for the State of Iowa becomes essential. This research focuses on the most commonly used steel H-pile foundation. The research scope is to (1) characterize soil-pile responses under pile driving impact loads, and (2) understand how the generated information could be used to improve design and construction control of piles subjected to vertical loads in accordance with LRFD.

It has been understood that efficiency of the pile foundation can be elevated, if the increase in pile resistance as a function of time (i.e., pile setup) can be quantified and incorporated into the LRFD. Because the current pile foundation practice involves different methods in designing and verifying pile performances, the resulting discrepancy of pile performances often causes an adjustment in pile specifications that incurs incremental construction costs, significant construction delays, and other associated scheduling issues. Although this research focuses on the most advanced dynamic analysis methods, such as Pile Driving Analyzer (PDA), Wave Equation Analysis Program (WEAP), and CAse Pile Wave Analysis Program (CAPWAP), the accuracy of these methods in estimating and verifying pile performances is highly dependent upon the input selection of dynamic soil parameters that have not been successfully quantified in terms of measured soil properties.

To overcome these problems and due to the limited data available from the Iowa historical database (PILOT), ten full-scaled field tests on the steel H-piles (HP 250 × 63) were conducted in Iowa. Detailed in-situ soil investigations using the Standard Penetration Test (SPT) and the Cone Penetration Test (CPT) were completed near test piles. Push-in pressure cells were installed to measure total lateral earth and pore water pressures during the life stages of the test piles. Soil characterization and consolidation tests were performed. Pile responses during driving, at the end of driving (EOD), and at restrikes were monitored

using PDA. PDA records were used in CAPWAP analysis to estimate the pile performances. In addition, hammer blow counts were recorded for WEAP analysis. After completing all restrikes, static load tests were performed to measure the pile resistance.

The information collected from the tests provided both qualitative and quantitative studies of pile setup. Unlike the empirical pile setup methods found in the literature, analytical semi-empirical equations are developed in terms of soil coefficient of consolidation, SPT N-value, and pile radius to systematically quantify the pile setup. These proposed equations do not require the performance of pile restrikes or load tests; both are time consuming and expensive. The successful validation of these proposed equations provides confidence and accuracy in estimating setup for steel H-piles embedded in cohesive soils. For the similar study on large displacement piles, the results indicate that the proposed methods provide a better pile setup prediction for smaller diameter piles.

Based on statistical evaluations performed on the available database, field tests, and sources found in the literature, it was determined that different uncertainties were associated with the estimations of the initial pile resistance at the EOD and pile setup resistance. To account for this difference, a procedure for incorporating the pile setup in LRFD was established by expanding the First Order Second Moment (FOSM) method, while maintaining the same target reliability level. The outcome of the research provides a methodology to determine resistance factors for both EOD and setup resistances based on any regional database. Therefore, the practical implementation of pile setup can now be included in a pile design, which has not been provided in the latest American Association of State Highway and Transportation Officials (AASHTO) Bridge Design Specifications.

Combining the PILOT database with the field test results, regionally calibrated resistance factors for bridge deep foundations embedded in clay, sand, and mixed soil profiles were established for the dynamic analysis methods. This regional calibration generated higher resistance factors and improved the efficiency of pile performances when compared with those recommended by the latest AASHTO Bridge Design Specifications.

Furthermore, using these calibrated results of the dynamic analysis methods that serve as the construction control methods, the resistance factors of the Iowa in-house method (Iowa Blue Book) that serves as the design method were enhanced through the development of a construction control procedure. Construction control consideration minimizes the discrepancy between design and field pile resistances, and integrates the construction control methods as part of the design process.

An improved CAPWAP signal matching procedure was developed to provide a better quantification of the dynamic soil damping factor and quake value with respect to different soil properties along the shaft and at the toe of a pile. Correlation studies resulted in the development of several empirical equations for quantifying the dynamic soil parameters using the measured SPT N-value. In addition, the results reveal the influences of pile setup and pile installation on the dynamic soil parameters. The application of these estimated dynamic soil parameters was validated through the improvement of a CAPWAP signal match quality.

# CHAPTER 1: INTRODUCTION

## 1.1. Background

Deep foundations are frequently selected by designers to support structures whenever the subsurface soils at structures are too soft or loose to support shallow foundations safely and economically. Deep foundations are referred to as pile foundations, which are classified into displacement and nondisplacement piles. Displacement piles, such as wood piles, steel H-piles, and precast concrete piles, are inserted into the ground by hammer driving with surrounding soil experiencing lateral displacements during pile installation. On the other hand, nondisplacement piles, such as drilled shafts, are cast in place at which concrete is placed into the void left after a volume of soil is excavated (Salgado, 2008).

The Iowa Department of Transportation (Iowa DOT) conducted a total of 264 static pile load tests between 1966 to 1989 to improve their pile foundation design practice. Of these tests, 164 (62 %) were performed on steel H-piles, 75 (28 %) were performed on wood piles, and the remaining 25 (10 %) were performed on other pile types such as pipe piles and drilled shafts. Recently, an electronic database known as PIle LOad Tests in Iowa (PILOT) was created by Roling et al. (2010) with all of the relevant test information stored electronically. PILOT provides significant amount of data needed for the proposed research. In addition, a recent survey completed by AbdelSalam et al. (2010) indicates that the steel H-pile foundation is the most common bridge foundation used in the United States, especially in the Midwest. Therefore, the proposed research focuses primarily on the steel H-pile foundations. This dissertation presents the experimental studies and response characterizations of axially-loaded steel H-piles using dynamic analysis methods while the investigation using static analysis methods and dynamic formulas have been performed in companion studies by AbdelSalam (2010) and Roling (2010).

Steel H-pile responses are related to soil-pile-water interaction. The surrounding soil is remolded during pile driving, and drainage of pore water in soil influences the effective

soil strength. The gain in effective soil strength increases the pile resistance, and the rate of effective strength increment dictates the gain in pile resistance over time. Specifically, a clay soil requires a longer time for pore water to drain out, has slower dissipation of any built-up pore pressure resulting from pile driving and has a smaller consolidation rate than a sand soil. Therefore, piles embedded in clay soil usually exhibit resistance increments due to consolidation, which are known as pile setup. In contrast, piles embedded in sand soil gain resistance immediately after the end of driving (EOD). Since clay soils are more common in the Midwest, the dissertation includes an extensive research and presents recommendations on pile setup for the Load and Resistance Factor Design (LRFD). Furthermore, the accuracy of pile resistance estimations using the dynamic analysis methods is largely dependent upon the selection of appropriate dynamic soil parameters (spring and damping characteristics of one-dimensional soil-pile model), and yet the quantification of these parameters possesses challenges.

### 1.1.1. Foundation design philosophy

Deep foundations are traditionally designed based on Allowable Stress Design (ASD) philosophy, which combines uncertainties of applied load (Q) and resistance (R) through a factor of safety (FS). The FS is highly dependent on an individual pile designer's experience and judgment, and the FS does not reflect the variation in pile types, soil conditions, and design methods. To overcome the limitations of the ASD, Load and Resistance Factor Design (LRFD) philosophy is being implemented for foundation designs throughout the United States. The basic principle of the LRFD uses probabilistic approaches and account for uncertainties individually for the resistance as well as for different design loads. The focus of LRFD is to achieve a consistent and reliable design by separating the variability of the load and resistance components. The load and resistance components are multiplied by load factor ($\gamma$) and resistance factor ($\varphi$), respectively. In foundation designs, the load factor takes the values used in the superstructure designs, and the resistance factor is calibrated using reliability analysis methods from available data.

### 1.1.2. Pile design and verification methods

The main challenge associated with the deep foundation design is the ability to accurately predict and verify pile resistance, which primarily stem from significant variations of soil properties. Furthermore, pile resistance can be estimated using static analysis methods, dynamic formulas, and dynamic analysis methods. Because of the empirical nature of some of the methods combined with the influence of variation in soil parameters, the resistance of a pile calculated based on different methods may differ significantly even if the different methods follow the same analysis concept (e.g., static analysis methods).

Driven pile foundations are normally designed using the static analysis methods. Static analysis methods approximately estimate the pile resistance based on soil properties obtained from both laboratory and in-situ soil tests. However, the static analysis methods cannot be used to verify the estimated pile resistance during pile driving. In recognizing this deficiency, the pile resistance is usually verified by an expensive and time consuming approach known as the static load test specified in the American Society for Testing and Materials (ASTM) as ASTM D 1143: Quick Load Test Method. In addition, pile driving formulas, which are formulated from the principle of conservation of work done, are conventionally used for verifying the pile resistance and introduce a means to limit the pile depth—this practice is often referred as construction control. Unfortunately, pile driving formulas produce unimpressive and conservative resistance (Coduto, 2001).

As a result, alternative methods, such as dynamic analysis methods, are desired to improve the pile design and verification. With the advent of digital computers, dynamic analysis methods have not only gained popularity and but also continue to be advanced. They are now used as routine methods for verifying pile performances and have been incorporated into a standard specification for testing deep pile foundations in the American Society for Testing and Materials (ASTM), ASTM D-4945. The advantages of using the dynamic analysis methods are as follows: (1) give accurate pile resistance estimation; (2) evaluate time dependent pile resistance; (3) provide pile driving control; (4) detect pile damage and

check pile integrity; (5) evaluate driving system performance; (6) assess soil resistance distribution; and (7) less expensive than static load test. For these reasons, dynamic analysis methods are used to evaluate pile performances and assess surrounding soil behaviors during and after pile driving in this research. The following methods were chosen: wave equation analysis using the Wave Equation Analysis Program (WEAP), pile driving analysis using the Pile Driving Analyzer (PDA) method, and pile resistance and dynamic soil properties estimations using the CAse Pile Wave Analysis Program (CAPWAP).

WEAP was developed based on Smith's (1962) numerical mathematical model that exploits the one-dimensional wave propagation concept to characterize the hammer-pile-soil system under a hammer impact. Subsequently, WEAP was further developed to incorporate all available hammers information by Goble, Rausche and Likins (GRL) into a commercial program, GRLWEAP. To accurately capture the hammer impact on a pile, Pile Dynamic Inc. (PDI) developed a data acquisition equipment known as PDA in the 1960s to measure strains and accelerations near the pile head during driving. PDA converts the measured strains and accelerations to forces and velocities respectively and uses them to estimate the pile resistance—this approach is known as Case method. Utilizing the PDA records, the Case method and the wave equation method, they developed an improved pile analysis method known as CAPWAP in the 1970s. CAPWAP uses the Smith's model and refines the Case method results by performing force and velocity signals matching process. Despite having numerous advantages over other methods, the aforementioned dynamic analysis methods have some challenges, such as finding suitable dynamic soil parameters, requiring understanding of wave mechanics and requiring operational as well as interpretational skills. The details of the dynamic analysis methods are described in Chapter 2 of the dissertation: Literature Review.

## 1.2. Current State of Knowledge

### 1.2.1. Soil properties

Standard Penetration Test (SPT) is the most commonly used in-situ soil tests in Iowa

and Cone Penetration Test (CPT) has becoming more popular in pile designs. Usually, both SPT and CPT are not concurrently available for pile designs. Therefore, correlations of soil properties are desired to estimate relevant soil properties in the absence of either method. Correlations between SPT and CPT soil properties have been investigated by many researchers, such as Kruizinga (1982) and Robertson et al. (1983). However, the correlations were not calibrated specifically to represent the local soil conditions in Iowa. Another in-situ soil test is the borehole shear test (BST), which was developed by an emeritus Professor Handy of Iowa State University, to directly and quickly measure the soil friction angle (φ) and cohesion (c). BST is commonly used in slope stability designs but not in pile designs. Currently, only the SPT soil properties can be directly applied in WEAP analysis.

### 1.2.2. Pile setup

Pile setup refers to the gain in pile resistance over time and it has been observed by many researchers. The setup phenomenon is mostly due to the dissipation of pore pressure and the healing of remolded soil near piles over time (Salgado 2008). Even though pile responses resulted from pile setup can be measured using dynamic analysis methods, the actual soil-pile interactive behavior that causes pile setup cannot be generally quantified. Furthermore, pile setup characterization using dynamic analysis methods requires the field data from re-striking of the pile at different times after the end of driving (EOD), which might not be practical and economical procedures for in routine construction practice. Nevertheless, many empirical relationships have been developed for quantifying pile setup, including the frequently used equation based on an empirical constant (A) and time ratio proposed by Skov and Denver (1988). The reliability of these empirical equations has yet to be proven especially in the context of LRFD. In addition, the available empirical equations have no relationship with commonly used soil properties, such as SPT N-value, CPT friction, or coefficient of consolidation ($C_v$). Komurka et al. (2003) had provided the discussion of several empirical relationships for estimating pile setup, and they concluded that the existing good pile testing data did not have promising subsurface information for pile setup correlation studies. Furthermore, Salgado (2008) highlighted that pile setup has not been

confidently accounted for in current pile designs because of insufficient data available for accurately estimating the pile setup evolution over a period of time.

### 1.2.3. Construction control

Construction control involves procedures and methods for nondestructive verification of designed pile resistance during construction. Iowa in-house method based on the Blue Book (originally written by Dirks and Patrick Kam, 1989) is currently used to design piles, and WEAP is generally used as the construction control method in current practices in Iowa. If the desired pile resistance is not attained, pile driving specifications will be adjusted accordingly, such as increasing pile length. The adjustment may result construction cost increment as well as significant delays and other associated scheduling issues. To improve the accuracy of pile resistance estimation during the design stage and the accuracy of cost estimation during the design and cost estimated stage, construction control using either WEAP or CAPWAP analysis is desired to be integrated as part of the design procedures. Although the procedure may not be the same, similar efforts are being examined by other states (e.g., Long et al. (2009) have examined a probability method to improve pile resistance estimation for the Illinois DOT).

### 1.2.4. LRFD resistance factors calibration

The latest American Association of State Highway and Transportation Officials (AASHTO) LRFD Bridge Design Specifications (2007) were published based on the studies of both Paikowsky et al. (2005) and Allen et al. (2006). The resistance factors for driven piles were developed based on the Davisson's criterion, the First Order Second Moment (FOSM) reliability method and AASHTO (2007) Strength I load combination. The recommended AASHTO (2007) resistance factors for dynamic analysis methods were calibrated for general driven pile and soil types. However, AASHTO allows every state to develop its regionally calibrated resistance factors that have better representation of the local soil conditions, local design and construction practices. A cost effective implementation of the regionally developed LRFD specifications can be achieved, and consistent and reliable

pile performances can be ensured. Currently, twenty-seven states have implemented the LRFD approach to foundation design while seventeen other states including Iowa are in transition from ASD to LRFD (AbdelSalam et al., 2008).

### 1.2.5. Dynamic soil parameters

The accuracy of dynamic analysis is dependent upon the proper input of suitable dynamic soil parameters: damping coefficient (c) and stiffness (k). The damping coefficient (c) was recommended by Smith (1962) as a product of ultimate static soil resistance ($R_u$) and Smith's damping factor (J). The spring stiffness (k) was assumed as the ratio of ultimate static soil resistance ($R_u$) and Smith's soil quake (q). Currently, the Smith's soil parameters are implemented in WEAP analysis. On the other, Goble et al. (1975) proposed the damping coefficient (c) as a product of Case damping factors ($J_c$) and pile impedance (Z) for use in PDA analysis. The Case damping factors were reported by Hannigan et al. (1998). Note that all the recommended dynamic soil parameters are only correlated with simple soil types and/or pile geometry, and no relationship has been developed to correlate them with measurable soil properties. Furthermore, Svinkin and Woods (1998) recognized that the present dynamic soil parameters cannot reflect the time dependent variation in the pile responses. They believed the use of variable dynamic soil parameters as a function of time will improve the pile resistance prediction.

## 1.3. Problem Statement

The Federal Highway Administration (FHWA) has mandated all new bridges initiated after October 1, 2007 should follow the LRFD design approach. Unfortunately, the current AASHTO LRFD Bridge Design Specifications (2010) have been developed for general soil conditions and pile types. Also, the current Iowa DOT pile design manual does not comply with the LRFD design philosophy. Even though AASHTO allows the use of regional calibrated resistance factors in LRFD pile designs, Iowa DOT has insufficient usable pile database, such as pile driving data with PDA records, for developing resistance factors for dynamic analysis methods. In recognizing the problems, the Iowa Highway Research

Board (IHRB) sponsored research project to develop LRFD bridge foundation design recommendations for the State of Iowa. One of the research objectives is to develop regionally calibrated LRFD resistance factors for dynamic analysis methods. The research focuses primarily on the most commonly used steel H-pile foundations in Iowa. In lieu with the problems encountered at the national and the state levels, technical problems listed below were examined in order to establish cost-efficient LRFD pile design guidelines at the state level.

1. Pile setup has not been successfully estimated and implemented in current pile designs;
2. Pile setup quantification methods have not been incorporated in current AASHTO (2007) LRFD Specifications;
3. Construction control has not been considered in pile designs prior to pile driving; and
4. Current recommended dynamic soil parameters are vague and have not been successfully correlated with any measurable soil properties.

### 1.4. Research Scope And Objectives

In light of the aforementioned challenges and opportunities, this research is on the characterization of soil-pile responses under pile driving impact loads and how this information could be used to improve design and construction control of piles subjected to vertical loads in accordance with LRFD. The scope of the proposed research was achieved through the following objectives:

1. Improve dynamic pile driving characterization of vertically loaded piles;
2. Investigate variation of pile resistance as a function of time and soil conditions;
3. Incorporate the advantages of pile setup into the LRFD;
4. Recommend regional LRFD design guidelines for dynamic analysis methods; and
5. Improve the estimation and verification of pile performances in terms of strength using dynamic analysis methods.

## 1.5. Research Tasks

The objectives noted above were accomplished by completing the following five tasks, which were described explicitly in this dissertation.

### 1.5.1. Task 1: Literature review

A literature review on dynamic analysis methods and the LRFD calibration procedure is an essential task for improving dynamic analysis methods and developing the regional LRFD recommendations. A literature review beginning with introduction of the history and theory of dynamic analysis methods (PDA, CAPWAP and WEAP) was performed. Past reliability studies of dynamic analysis methods published by other researchers were summarized. The LRFD philosophy and calibration procedures were described, and the latest LRFD resistance factor results reported by other researchers for driven piles were summarized. Next, a detailed literature review on pile setup was performed. Furthermore, brief literature reviews on construction control and dynamic soil parameters were also conducted in their respective chapters of the dissertation.

### 1.5.2. Task 2: Full-scale pile tests and soil characterizations

#### *1.5.2.1. Full-scale pile tests*

Full-scale pile tests were performed to increase the Iowa DOT insufficient usable pile database and to produce new data for pile setup investigation and LRFD resistance factor calibrations for dynamic analysis methods. Ten full-scale soil and pile tests were conducted on selected under construction bridge sites in Iowa with three different soil profiles (clay, sand, and mixed). Standard Penetration Test (SPT), Cone Penetration Test (CPT) with pore water dissipation tests and Borehole Shear Test (BST) were performed. At some of the test sites, push in pressure cells were installed adjacent to pile's flange to measure in-situ total lateral soil and pore water pressures during pile driving, restriking and load testing. Soil characterization tests (gradation, Atterberg limits and moisture content tests) were conducted using the collected disturbed soil samples, and one-dimensional consolidation tests using the

collected undisturbed soil samples were performed. HP 250 x 63 steel piles, the most common in Iowa, were instrumented with strain gauges mounted along the pile embedded lengths. PDA tests were performed during driving, at the end of driving (EOD) and at the beginning of restrikes (BORs) before axially and statically loading the test piles to failure. The restrikes were performed at several times after the EOD, and the pile resistance was eventually measured using static load tests.

#### *1.5.2.2. Soil profiles categorization*

To increase sample sizes for analyses and to improve accuracy of analyses with respect to different soil types, the PILOT database and the new field data have been categorized into sand, clay and mixed soil profiles. The significance of the soil profiles categorization approach has been evaluated using WEAP through the LRFD resistance factors comparison.

#### *1.5.2.3. Soil properties characterization*

As previously mentioned in the Section 1.2: Current State of Knowledge, pile setup is mainly influenced by the rate of soil consolidation, and pile setup predictions have not been quantified in terms of a coefficient of consolidation. Horizontal coefficients of consolidation ($C_h$) were estimated using the CPT test results based on strain path method reported by Houlsby and Teh (1988) and were compared with the in-situ soil properties, such as SPT N-value. Similarly, vertical coefficients of consolidation ($C_v$) measured from the one-dimensional soil consolidation tests were correlated with the SPT N-value. This correlation helps in estimating the $C_v$ or $C_h$ value from the SPT N-value for a practical pile setup quantification purpose.

### 1.5.3. Task 3: Pile setup investigation

#### *1.5.3.1. Dynamic analysis methods*

Pile responses as a function of time were monitored using PDA in the fields during pile driving, at EOD and at several restrikes. The amount of pile setup was evaluated using

both WEAP and CAPWAP. The contribution of pile setup to the increase in shaft and toe resistances of the surrounding soil was studied using CAPWAP. Qualitative correlation studies between pile setup distribution along embedded pile length and various soil properties, such as SPT N-value, coefficient of consolidation and plasticity index, were presented.

#### *1.5.3.2. Analytical setup quantification methods*

Instead of using the less reliable empirical equations proposed by other researchers in literature, the research focuses on developing better pile setup estimation methods in terms of measurable soil properties. The proposed analytical pile setup quantification methods incorporated measurable and commonly used soil properties, such as SPT N-values and horizontal coefficient of consolidation ($C_h$). The proposed methods do not require the performance of time consuming restrikes and use an initial pile resistance estimated at EOD using either WEAP or CAPWAP as a reference pile resistance. Validation of the proposed methods was conducted using both local PILOT database and data sources found in literature. Moreover, confident levels of the proposed methods were evaluated and suitably recommended. Although these proposed setup methods were originally developed from experimental studies on steel H-piles, their applications on other pile types were evaluated. These pile setup estimation methods were incorporated into the Iowa DOT design guidelines for practical applications.

### 1.5.4. Task 4: Construction control

To improve pile resistance estimations and to consider using dynamic analysis methods for verifying pile resistances in the design stage, estimated pile resistances using the Iowa DOT in-house method were compared with the predicted pile resistances using WEAP, and similar comparisons were performed for CAPWAP. Construction control correction factors for the Iowa in-house method with respect to different dynamic analysis methods at different soil profiles were determined based on a probability method. By applying the correction factors to estimated pile resistances using the Iowa in-house method, the

construction control was assimilated in pile designs with the intentions to improve the accuracy of pile resistance estimation using the Iowa DOT in-house method and to reduce the discrepency of pile resistances estimated during designs and measured during constructions.

### 1.5.5. Task 5: LRFD calibration

Regional LRFD resistance factor calibrations are allowed by FHWA to maintain consistent and reliable pile performances, to represent local soil condition and construction practices, and to design cost effective pile foundations. LRFD resistance factors for WEAP analysis were calibrated based on five different soil input procedures for sand, clay and mixed soil profiles, and the five procedures are DRIVEN, soil type based method (ST), SPT N-value based method (SA), Iowa in-house design chart, and current Iowa DOT approach. The soil profile input procedure that gives the highest efficiency coefficient ($\varphi/\lambda$), a ratio of the resistance factor and the corresponding resistance bias, at each soil profile was recommended. These comparisons provide a rational basis for pile designers to adopt varies soil input procedures for different soil profiles in WEAP. Besides, LRFD resistance factors were calibrated for CAPWAP. These newly and regionally calibrated LRFD resistance factors were compared with the latest AASHTO (2010) recommendations and with the resistance factors proposed by other researchers, such as Paikowsky et al. (2004) and Allen (2005).

Furthermore, a new procedure was developed to enabling incorporation of a resistance factor separately for pile setup such that the setup effect can be accounted in addition to the design resistance estimation for a pile at the End of Driving (EOD) for a chosen target reliability index. The procedure, which uses the First Order Second Moment (FOSM) method, not only allows incorporation of any form of setup estimate to the estimated pile resistance at EOD, but also facilitates inclusion of two resistances affected by each other to reach a target reliability level in accordance with the LRFD framework. The main benefit of this approach is that it eliminates the inappropriate means to use the same resistance factor for both setup and pile resistance estimation at EOD, which could result in an overestimated pile design.

### 1.5.6. Task 6: Dynamic soil parameters characterization

One of the challenges with dynamic analysis methods is to find suitable dynamic soil parameters for accurate pile resistance estimations and verifications. Dynamic soil parameters were estimated by matching the pile responses predicted using CAPWAP with the measured pile responses collected using PDA. Because of the current default CAPWAP matching procedure, constant dynamic soil parameters for an entire soil profile were estimated regardless of the different soil types and properties existed along a pile shaft. For this reason, correlation studies between these dynamic soil parameters and any measured soil properties become much more challenging. In lieu with this limitation with the current CAPWAP matching procedure, a new matching procedure based on variable dynamic soil parameters was proposed. The newly proposed matching procedure provided a good correlation between the estimated dynamic soil parameters and SPT N-value. The effects of pile installation and pile setup on the dynamic soil parameters were also investigated.

## 1.6. Thesis Outline

The dissertation was written in a journal paper format and consists eight chapters. Chapter 1 begins with an introduction, description of current state of knowledge pertinent to pile foundations, problem statement, research scope and objectives, and research tasks. Literatures on dynamic analysis methods, LRFD, and pile setup were reviewed in Chapter 2. Full scale pile tests and soil characterizations pertinent to pile setup were described in Chapter 3. Detailed pile setup analysis and verification were described in Chapter 4. The development of the proposed calibration procedure to incorporate pile setup in LRFD was illustrated in Chapter 5. The results of the LRFD resistance factors calibration, construction control consideration and recommendations were covered in Chapter 6. Quantification of dynamic soil parameters was included in Chapter 7. Summary, conclusions and suggested future researches were enumerated in Chapter 8. A brief description of each chapter is given as below.

- **Chapter 1 – *Introduction***: An overview of the current bridge pile foundations, the pile foundation design philosophies, and the driven pile foundation design and

verification methods. Current state of knowledge pertinent to pile foundations. Brief descriptions of problem statement, research scope and objectives, and research tasks.

- **Chapter 2 – *Literature Review***: Description of the history and theory of dynamic analysis methods. Summary of past reliability studies of dynamic analysis methods reported by other researchers. Detailed discussion of LRFD calibration methods and pile setup.
- **Chapter 3 – *Pile Setup in Cohesive Soil with Emphasis on LRFD-An Experimental Investigation***: Detailed description of the pile driving, restriking, dynamic testing, and static load testing procedures on test piles performed in Iowa. Full description of the in-situ and laboratory soil tests and results. Evidence of pile setup and its qualitative correlation with surrounding soil properties were presented.
- **Chapter 4 – *Pile Setup in Cohesive Soil with Emphasis on LRFD-Analytical Quantifications and Design Recommendations***: Pile setup investigation using dynamic analysis methods. Development, validation, and application of proposed pile setup prediction methods.
- **Chapter 5 – *A Procedure for Incorporating Pile Setup in Load and Resistance Factor Design of Steel H-Piles in Cohesive Soil***: Development of a new calibration procedure using First Order Second Moment (FOSM) reliability method to separately account for the uncertainties associated with initial pile resistance at EOD and pile setup resistance in accordance with LRFD framework.
- **Chapter 6 – *Integration of Construction Control and Pile Setup Into Design***: Development of regionally calibrated LRFD resistance factors for steel H-pile foundation for dynamic analysis methods with considering pile setup. Integration of construction control using dynamic analysis methods in pile designs based on a probability approach. Compared the newly and regionally calibrated resistance factors with the AASHTO (2010) recommendations as well as resistance factors determined by other researchers.
- **Chapter 7 – *An Improved CAPWAP Matching Procedure for the Quantification of Dynamic Soil Properties***: Development of an improved CAPWAP signal matching procedure. Correlation studies between dynamic soil parameters (damping and quake

values) and SPT and CPT measured soil properties for the enhancement of pile resistance estimations.

- **Chapter 8 – *Summary, Conclusions and Recommendations***: Summary of the research, conclusions, and recommendations for future research.

## 1.7. References

AASHTO. (1994). LRFD Bridge Design Specifications. First Edition, American Association of State Highway and Transportation Officials, Washington, D.C.

AASHTO. (2007). LRFD Bridge Design Specifications. Customary U.S. Units, Forth Edition, 2008 Interim, American Association of State Highway and Transportation Officials, Washington, D.C.

AASHTO. (2010). LRFD Bridge Design Specifications. Customary U. S. Units, Fifth Edition, 2010 Interim Revisions, American Association of State Highway and Transportation Officials, Washington, D.C.

AbdelSalam, S. S., Sritharan, S., and Suleiman, M. T. (2010). "Current Design and Construction Practices of Bridge Pile Foundations with Emphasis on Implementation of LRFD." Journal of Bridge Engineering, ASCE, 15(6), pp. 749-758.

Allen, T. M. (2005). Development of Geotechnical Resistance Factors and Downdrag Load Factors for LRFD Foundation Strength Limit State Design. FHWA-NHI-05-052, Federal Highway Administration, U.S. Department of Transportation, Washington, D.C.

American Society for Testing and Materials (ASTM). (2008). Standard Test Method for High-Strain Dynamic Testing of Piles. ASTM D 4945, 1916 Race Street, Philadelphia, PA 19103.

Coduto, D. P. (2001). Foundation Design: Principles and Practices. Second Edition, Prentice Hall, NJ.

Dirks, Kermit L., and Patrick Kam. (1989). Foundation Soils Information Chart Pile Foundation. Iowa DOT, Office of Road Design, Highway Division Soils Survey Section, January.

Goble, G. G., Likins, G. E., and Rausche, F. (1975). Bearing Capacity of Piles from Dynamic Measurements. Final Report, Department of Civil Engineering, Case Western Reserve University, Cleveland, OH.

Goble, G. G., Moses, F., and Snyder, R. (1980). "Pile Design and Installation Specification Based on Load Factor Concept." Transportation Research Record 749, Transportation Research Board, National Research Council, Washington, D.C., pp. 42-45.

Hannigan, P.J., Goble, G.G., Thendean, G., Likins, G.E. and Rausche, F. (1998). Design and Construction of Driven Pile Foundations – Volumn II, FHWA-HI-97-013. National Highway Institute, Federal Highway Administration, U.S. Department of Transportation, Washington, D.C.

Houlsby, G.T. and Teh, C.I. (1988). "Analysis of the Piezocone in Clay." Penetration Testing 1988, Vol. 2, Balkema, Rotterdam, The Netherlands, pp. 777-783.

Iowa DOT LRFD Design Manual (2010). Office Policies and Procedures, Office of Bridges and Structures. Iowa Department of Transportation Electronic Reference Library.

Komurka, Van E., Wagner, Alan B., and Edil, Tuncer. (2003). Estimating Soil/Pile Set-Up. WHRP Report No. 03-05, Wisconsin Highway Research Program #0092-00-14, September.

Long, James H., Hendrix, Joshua, and Baratta, Alma. (2009). Evaluation/Modification of IDOT Foundation Piling Design and Construction Policy. Research Report FHWA-ICT-09-037, Illinois Center for Transportation, University of Illinois at Urbana-Champaign, IL, March.

Paikowsky, S.G. with Contributions from Birgisson from Birgisson, B., McVay, M., Nguyen, T., Kuo, C., Baecher, G., Ayyab, B., Stenersen, K., O'Malley, K., Chernauskas, L., and O'Neill, M. (2004). Load and Resistance Factor Design (LRFD) for Deep Foundations, NCHRP Report, 507, Transportation Research Board, Washington, D.C.

Pile Dynamics, Inc. (2005). GRLWEAP Wave Equation Analysis of Pile Driving: Procedures and Models Version 2005, Cleveland, OH.

Roling, J. M. (2010). Establishment of a Suitable Dynamic Formula for the Construction Control of Driven Piles and its Calibration for Load and Resistance Factor Design.

MS. Thesis, Iowa State University, Ames, IA.

Roling, M., Sritharan, S., and Suleiman, M. T. (2010). Development of LRFD design procedures for bridge piles in Iowa – Electronic Database. Final Report Vol. I, Project No. TR-573, Institute of Transportation, Iowa State University, Ames, IA.

Salgado, Rodrigo. (2008). The Engineering of Foundations. McGraw-Hill, NY.

Skov, Rikard, and Denver, Hans. (1988). "Time Dependence of Bearing Capacity of Piles." Proceedings 3rd International Conference on Application of Stress-Waves Theory to Piles, Bitech Publisher, Ottawa, pp. 1-10.

Smith, E. A. L. (1962). "Pile-Driving Analysis by the Wave Equation." Journal of the Soil Mechanics and Foundations Division, ASCE, Paper No. 3306, Vol. 127, Part 1, pp.1145-1193.

Svinkin, M. R. and Woods, R. D. (1998). "Accuracy of Determining Pile Capacity by Dynamic Methods." Proceeding of the Seventh International Conference and Exhibition on Piling and Deep Foundations, Deep Foundation Institute, 15th to 17th June, Palais, Ferstel, Vienna, Austria, pp. 1.2.1-1.2.8.

# CHAPTER 2: LITERATURE REVIEW

This chapter provides a detailed review and background information on dynamic analysis methods, the Load and Resistance Factor Design (LRFD) in pile foundations, and pile setup. The dynamic analysis methods focused in this research project are Pile Driving Analyzer (PDA) method, Case Pile Wave Analysis Program (CAPWAP) method, and Wave Equation Analysis Program (WEAP). A historical summary, detailed literature reviews pertinent to these three methods and their reliability studies reported in literature are described in this chapter. Also, a detailed review on pile setup is also included in this chapter.

## 2.1. Introduction

Dynamic analysis methods have unique advantages over static analysis methods. One of the advantages is an application in estimating time dependent pile resistance (or capacity), which is increased by soil setup and decreased by soil relaxation. To measure the change in pile resistance, the pile is tested using dynamic analysis methods at the beginning of re-strike (BOR) over a specified duration after the end of driving (EOD). Besides, dynamic analysis methods are used to control pile driving, detect pile damage, evaluate driving system performance, assess soil resistance distribution, and determine dynamic soil parameters. Svinkin and Woods (1998) noted that dynamic analysis methods using the wave propagation theory were first proposed by St. Venant almost a century ago. In the United States, the dynamic analysis methods have been progressively developed over the past decades. They are now used as routine methods and thus are incorporated into a standard specification for deep foundations by the American Society for Testing and Materials (ASTM) D4945 (ASTM 2008). The historical summary of the dynamic analysis methods is described in Section 2.2. Literatures pertinent to PDA, CAPWAP and WEAP are reviewed in Sections 2.3, 2.4, and 2.5, respectively. Reliability studies on the dynamic methods are summarized in Section 2.6. Literatures that focus on evaluating the LRFD resistance factors for dynamic methods are reviewed in Section 2.7. Finally, pile setup was reviewed in

Section 2.8.

## 2.2. Historical Summary

Dynamic analysis methods were developed by applying the theory of wave propagation. Svinkin and Woods (1998) noted that the first solution to this dynamic analysis problem in the longitudinal direction of piles was suggested by St. Venant almost a century ago. In 1931, D. V. Isaacs was the first researcher to highlight the occurrence of wave action during pile driving, but it was E. N. Fox who published the first solution to this problem in 1938 (Smith 1962). Soon after the Second World War and with the advent of the digital computer, Smith (1962) developed a mathematical model of a hammer-pile-soil system to characterize the actual behavior of both the pile and surrounding soil under a hammer impact. Furthermore, Smith, who was one of the first to use a digital computer in solving pile problems, developed the first computer program for driving analysis of piles (Goble et al. 1980). Details of the Smith's model for pile dynamic analysis are discussed in Section 2.4.2. The Smith's model has been modified and improved by many researchers. One of these improved methods is known as the Case method that was developed by Professor G.G. Goble and his students in 1960s through funding from the Ohio Department of Transportation (ODOT) and Federal Highway Administration (FHWA) at Case Western Reserve University. Concurrently, a data acquisition system called the Pile Driving Analyzer (PDA) was developed using the Case method to measure strains and accelerations during pile driving.

In 1970, a rigorous numerical modeling technique called the Case Pile Wave Analysis Program (CAPWAP) was developed by Professor Goble and his students using the PDA data to evaluate the pile resistance (Hannigan et al. 1998). Both the PDA and CAPWAP software have been commercially available since 1972 (Coduto, 2001). After successfully developing the PDA and CAPWAP, the FHWA continuously supported Drs. Goble and Rausche for the development of a computer program known as WEAP using the Smith's concept. In 1976, the WEAP program was commercialized by GRL Engineers, Inc., and it has been continuously improved until the present time.

Today, the dynamic analysis methods have become a routine practice in the design and construction of pile foundations in the United States as well as in many other countries. The dynamic analysis methods have been incorporated into many design codes and specifications as highlighted by Likins et al. (2004) and described in details by Beim et al. (1998). For example, Australia Standard AS 2159, Brazil Standard NBR-13208, China Standard JGJ 106-97, and the United States Standard ASTM D 4945 and American Association of State Highway and Transportation Officials (AASHTO) T-298-33 are design standards that include PDA, CAPWAP and WEAP as the dynamic analysis methods for pile foundations.

## 2.3. Pile Driving Analyzer (PDA) Method

### 2.3.1. Introduction

Pile Driving Analyzer (PDA) is a data acquisition equipment that records strains and accelerations at locations typically near the pile top when a pile is driven or subjected to a re-strike with a pile driving hammer. For this purpose, two strain transducers and two accelerometers of PDA were installed at 750 mm (30-in) below the top of the pile. The strain transducers were bolted to both sides of the web along the centerline, and the accelerometers were attached to either sides of the web at a distance of 75 mm (3-in) left and right of the strain transducers to measure the strains and accelerations. The PDA converts the strain and acceleration signals to force and velocity records as a function of time using Eqs. (2.1) and (2.2), respectively (Hannigan et al. 1998).

$$F(t) = EA\varepsilon(t) \tag{2.1}$$

$$v(t) = \int_0^T a(t)dt \tag{2.2}$$

where,

F(t) = force at time t, kN or kip,

v(t) = velocity at time t, m/s or ft/s,

E = pile elastic modulus, kN/m$^2$ or ksi,

A = pile cross sectional area at gauge locations, m$^2$ or in$^2$,

ε(t) = strain at time t, mm/mm or in/in,

a(t) = acceleration at time t, $m^2$/s or $ft^2$/s, and

T = default maximum time limit which is 0.2048 second, s.

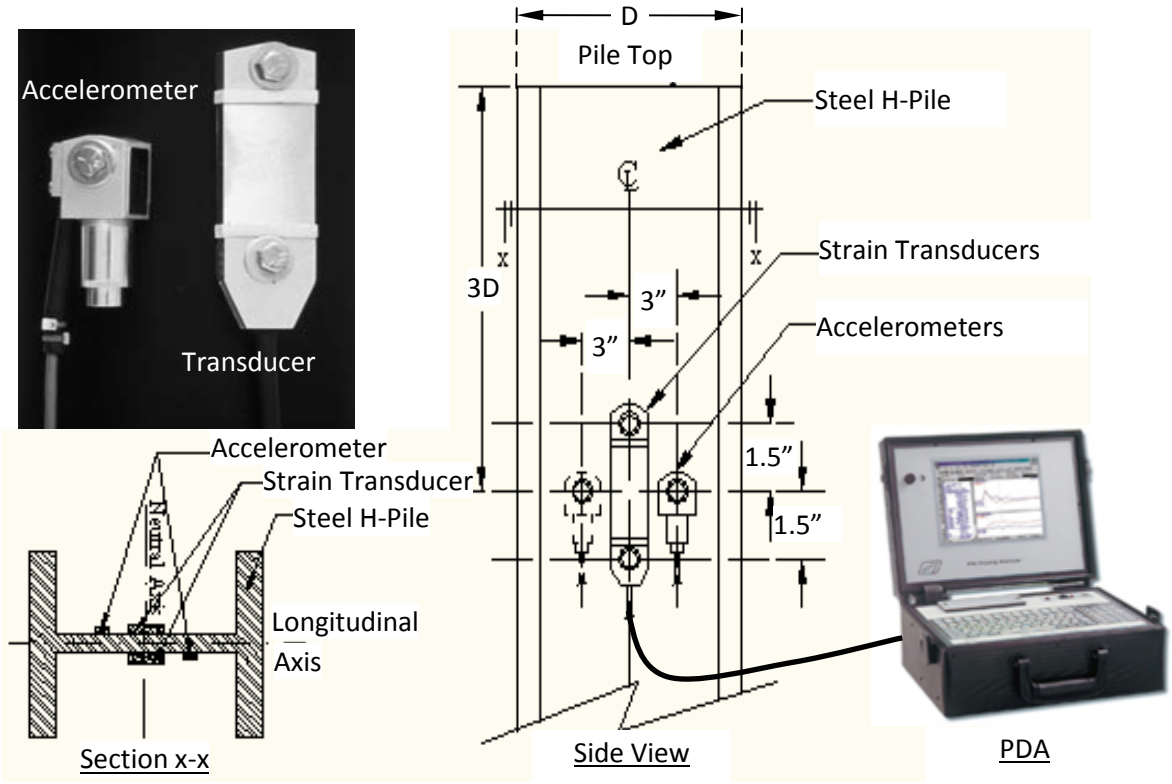


Figure 2.1: Typical locations of the PDA transducers and the accelerometers

The modern PDA equipment automatically computes the force and velocity and produce graphical and numerical summary of the pile responses as shown in Figure 2.2. The complete force and velocity records are digitally stored in PDA for the CAPWAP analysis to be performed after the pile driving is completed. With today's advancement in computational technology, a typical input preparation and running of the PDA program are straight forward. However, interpretation of PDA outputs requires skills for one to avoid misinterpretation of results. Thus, Goble G. and Likins G. (1996) recommended that the PDA data shall be analyzed by qualified engineers or specialists who have the knowledge of wave propagation and pile foundation. The PDA method has exhibited many advantages over the conventional static load test, and the most important benefit in pile testing is that it

can be performed quickly and economically (Fellenius and Altaee 2001). With more than twenty years of experience in using the PDA, Fellenius (1999) notes that he has numerous examples of good agreement between resistances determined from PDA and static load tests on various piles. A similar conclusion has been drawn by Wei et al. (1991) and Abe et al. (1990) through testing of steel H-piles. However, in some cases, the pile resistance prediction from the PDA method does not correlate well with that found from a static load test. The main reason for such discrepancy is attributed to time dependent issues such as the time between the compared tests, the changes in pile resistance with time, and the variation of soil properties with time are not considered in the comparison process (Svinkin & Woods 1998, and Long et al. 2002).

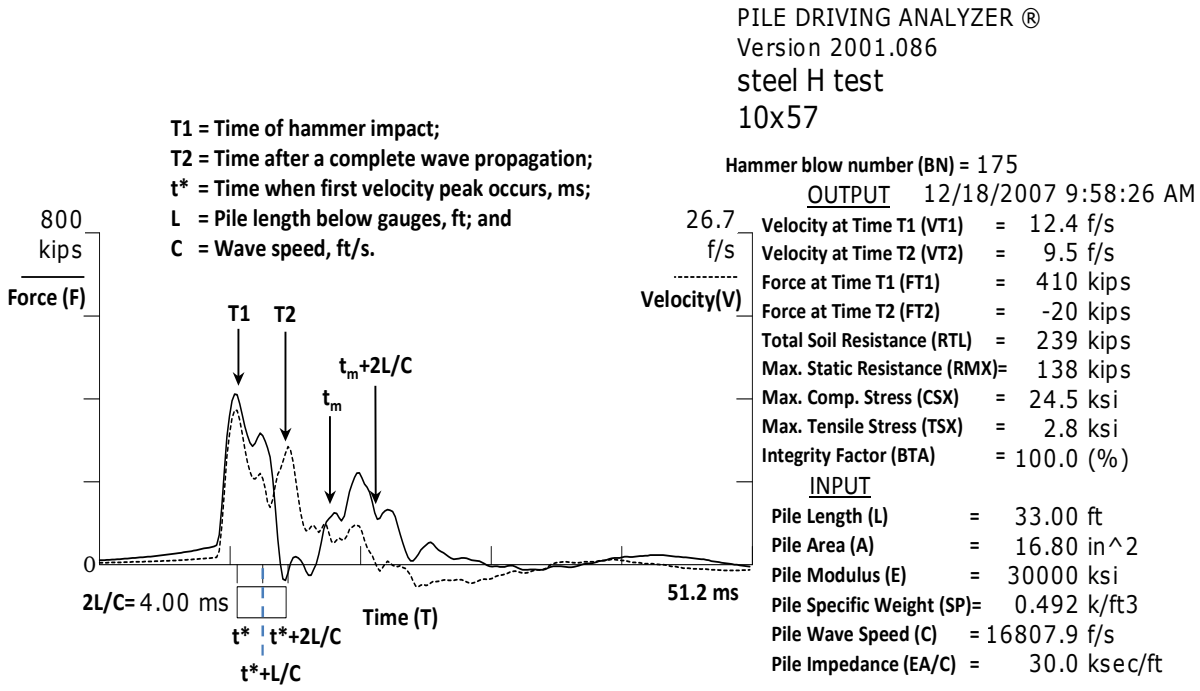


Figure 2.2: Typical PDA graphical and numeric summary outputs

### 2.3.2. Wave propagation concept

As described by Hannigan et al. (1998), when a pile is impacted by a hammer, it is only compressed at the ram pile interface and a compressive force pulse is generated. This compressive force pulse expands down toward the pile toe at a constant stress wave

propagation speed, C, as shown in Figure 2.3. The variable C depends on the density and elastic modulus of a pile material (see Eq. (2.4)). When the compressive force pulse travels along the embedded portion of the pile, its magnitude is decreased by the surrounding soil resistance. The incremental soil resistances along the pile shaft and at the pile toe generate a reflective force, which may be either a tensile or a compressive force pulse that travels back up the pile length. The compressive force pulse is typically considered as positive values and the tensile force pulse is treated as negative values. A permanent pile set (i.e., pile penetration into soil per hammer blow) is formed when the combined effects of the force pulses are large enough to overcome the effects of both the static and dynamic soil resistances. The total duration for the force pulse to travel near the pile head at the gauge location to the pile toe and returns is equal to 2L/C, where L is the vertical distance between the gauges and the pile toe. Because the time 2L/C is comparably shorter than the interval of hammer blows, Coduto D. P. (2001) noted that the effects of a single hammer blow can be characterized as shown in Figure 2.2.

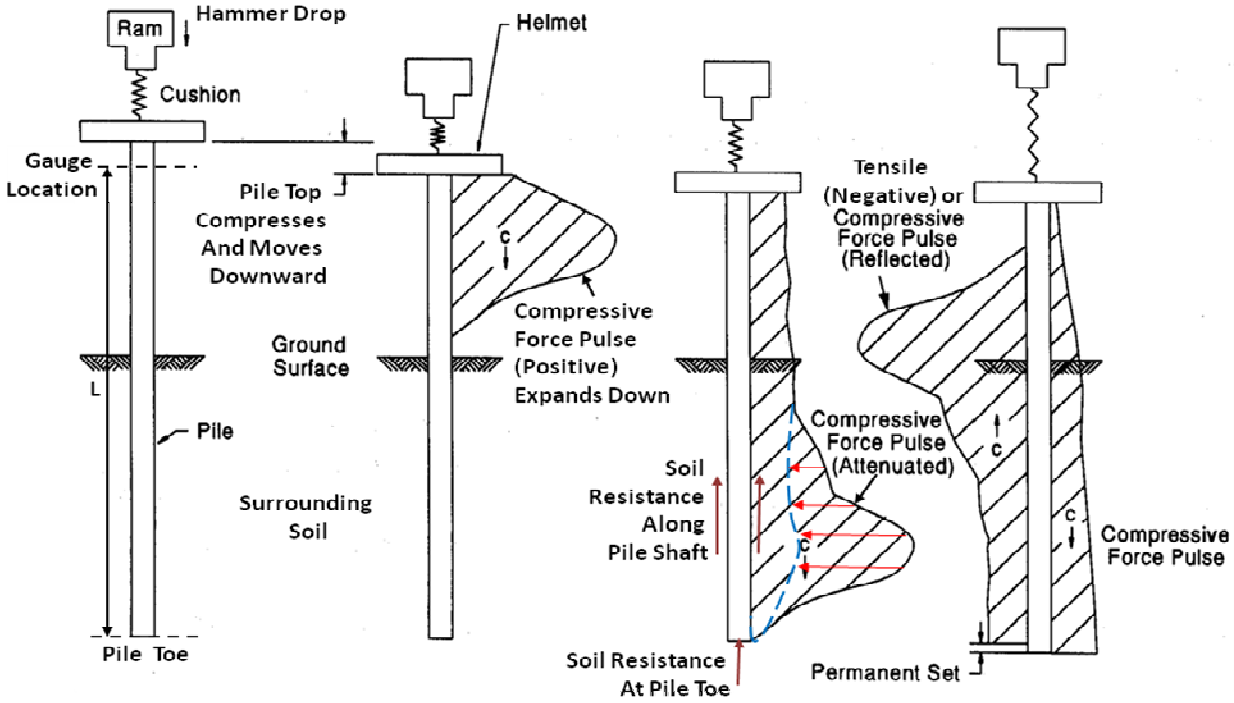


Figure 2.3: Wave propagation in a pile (adapted and modified from Cheney and Chassie, 1993)

### 2.3.3. Wave mechanics

The principle of wave mechanics is the basis for the Case method derivation that determines the static pile resistances. As described by Rausche et al. (1985), when a uniform elastic rod of cross sectional area (A), elastic modulus (E), and wave speed (C), is axially loaded by an impact force, the relationship between the force (F(t)) in the rod and the velocity of particle motion (v(t)) can be expressed using Eq. (2.3) as long as there are no resistance effects on the rod or no reflections arrive at the point under consideration. The term $\frac{EA}{C}$ is also known as rod impedance (Z).

$$F(t) = \left(\frac{EA}{C}\right) v(t) = Z\, v(t) \tag{2.3}$$

where,

F(t) = force in a uniform rod, kN or kip,

E = elastic modulus of a uniform rod, kN/mm$^2$ or ksi,

A = cross sectional area of a uniform rod, mm$^2$ or in$^2$,

v(t) = particle velocity in the a uniform rod, m/s or ft/s,

C = wave speed of a uniform rod, m/s or ft/s, and

Z = rod impedance, kN-s/m or kip-s/ft.

The wave speed can be expressed in terms of mass density (ρ) and elastic modulus (E) of a uniform rod material using Eq. (2.4). The detailed derivative of this equation is given by Timoshenko and Goodier (1951).

$$C = \sqrt{\frac{E}{\rho}} \tag{2.4}$$

where,

C = wave speed of a uniform rod, m/s or ft/s,

E = elastic modulus of a uniform rod, kN/m$^2$ or ksf, and

ρ = mass density of a uniform rod; kN-s$^2$/m$^4$ or kip-s$^2$/ft$^4$.

When a uniform free end rod is impacted by a mass, a compressive force pulse is created and travels down the rod at its material wave speed. Referred to Eq. (2.3), the particle velocity is directly proportional to the force and it moves in the same direction of the compressive force. At time L/C after the impact, the compressive force pulse arrives the free end of the rod. Since there are no resistance effects acting at the end of the rod, a same magnitude tensile stress wave occurs and reflects from the rod tip back toward the top. Thus, the compressive and tensile forces at the free end cancel each other and the net force becomes zero. However, the particle velocities from both the downward compressive force and the upward tensile force are moving in the same direction and thus, the particle velocity term doubles in magnitude.

On the other hand, for a uniform rod with a fixed end, the particle velocity at the fixed end is prevented from moving and becomes zero. However, the compressive force that travels down the rod at its wave speed reflects and superimposes at the fixed end. As a result, the net force doubles and the particle velocity becomes zero during reflection at the fixed end. By relating the above wave mechanics of a rod to a pile, the increase in soil resistance acting on a pile decreases the velocity record relatively more than the force record. This phenomenon can be seen from a typical force-velocity record collected from a PDA test as shown in Figure 2.2. The separation of the force and velocity records between the time of a hammer impact (T1) and the time for a complete wave propagation (T2) indicates the presence of soil resistance alongside of a pile. The extent of separation qualitatively describes the magnitude of the soil shaft resistance. For a primarily frictional pile with a relative small end bearing resistance as shown in Figure 2.2, the force approaches zero while the velocity increases immediately near time T2.

### 2.3.4. Case method

#### *2.3.4.1. Soil resistance*

Case method is a numerical technique used in the PDA to determine the static soil resistance (i.e., pile resistance), which is developed from the principles of wave mechanics. The Case method assumes a uniform cross section, linear, and elastic pile, which is subjected

to one-dimensional axial load and is embedded in a perfectly plastic soil. Under a hammer impulsive load, the total static and dynamic soil resistance (RTL) acting on a pile can be estimated using Eq. (2.5), for which the detailed derivation was reported in Rausche et al. (1985).

$$\mathrm{RTL} = \frac{1}{2}[\mathrm{FT1} + \mathrm{FT2}] + \frac{1}{2}[\mathrm{VT1} - \mathrm{VT2}]\frac{\mathrm{EA}}{\mathrm{C}} \tag{2.5}$$

where,

RTL = total static and dynamic soil resistance on a pile, kN or kip,

FT1 = measured force at time of initial impact, kN or kip,

FT2 = measured force at time of reflection of initial impact from pile toe (T1+2L/C), kN or kip,

VT1 = measured velocity at time of initial impact, m/s or ft/s,

VT2 = measured velocity at time of reflection of initial impact from pile toe (T1+2L/C), m/s or ft/s,

T1 = time of initial impact, s,

E = elastic modulus of a uniform pile, kN/mm$^2$ or ksi,

A = cross sectional area of a uniform pile, mm$^2$ or in$^2$, and

C = wave speed of a uniform pile, m/s or ft/s.

A correct static soil resistance is not represented by Eq. (2.5), because some dynamic soil resistances are included due to the rapid movement of piles. To avoid a serious error in the soil resistance computation, the total soil resistance is divided into both static and dynamic components. Assumptions made by Rausche et al. (1985) indicated that the dynamic resistance can be expressed as a linear function of the viscous damping coefficient and the pile toe velocity

$$\mathrm{R_d} = \mathrm{RTL} - \mathrm{R_s} = \mathrm{C_v v_b} \tag{2.6}$$

where,

$R_d$ = dynamic soil resistance, kN or kip,

RTL = total soil resistance, kN or kip,

$R_s$ = static soil resistance, kN or kip,

$C_v$ = linear viscous damping coefficient ≈ $J_c$ (EA/C), kN-s/m or kip-s/ft,

$J_c$ = Case damping factor, dimensionless, and

$v_b$ = velocity of pile toe at time T1+L/C, m/s or ft/s.

The pile toe velocity is expressed using Eq. (2.7), which is equal to the summation of the initial pile top velocity ($v_T$) and the net velocity, induced by the difference in pile force and soil resistance. Substituting Eq. (2.7) into Eq. (2.6) and replacing the $C_v$ with $J_c$ and EA/C, the static soil resistance can be rearranged as Eq. (2.8). Furthermore, the maximum static soil resistance can be determined by replacing the time t* with $t_m$, the time when maximum total resistance occurs, and by substituting RTL(t*) with Eq. (2.5). Hannigan et al. (1998) noted that Eq. (2.8) is best used for displacement piles and piles with large shaft resistance. Also, they noted that Eq. (2.9) is more appropriately used for piles with large toe resistances, piles with large toe quakes, and piles with delay in toe resistances.

$$v_b\left(t^* + \frac{L}{C}\right) = v_T(t^*) + \frac{C}{EA}[F_T(t^*) - RTL(t^*)] \tag{2.7}$$

$$R_s(t^*) = RTL(t^*) - J_c\left[\frac{EA}{C}v_T(t^*) + F_T(t^*) - RTL(t^*)\right] \tag{2.8}$$

$$\begin{aligned} R_s(t_m) = RMX \\ = \frac{1}{2}\Bigg\{(1 - J_c)\left[F(t_m) + \frac{EA}{C}v_T(t_m)\right] \\ + (1 + J_c)\left[F\left(t_m + \frac{2L}{C}\right) - \frac{EA}{C}v_T\left(t_m + \frac{2L}{C}\right)\right]\Bigg\} \end{aligned} \tag{2.9}$$

where,

RTL(t*)= total soil resistance at time t*, kN or kip,

$R_s$(t*) = static soil resistance at time t*, kN or kip,

$R_s(t_m)$ = maximum static soil resistance at time $t_m$, kN or kip,

$F_T$(t*) = measured force at pile top at time t*, kN or kip,

$v_T$(t*) = measured velocity at pile top at time t*, m/s or ft/s,

$t_m$ = time when maximum total resistance occurs, s,

t* = time corresponding to the maximum velocity, s,

$J_c$ = Case damping factor, dimensionless,

C = pile wave speed, m/s or ft/s,

E = modulus of elasticity of a pile material, kN/mm$^2$ or ksi,

A = cross sectional area of a pile, mm$^2$ or in$^2$, and

L = pile length below gauges, m or ft.

### *2.3.4.2. Case damping factor*

Referred to Eq. (2.9), all the variables on the right can be measured or determined except the Case damping factor $J_c$ which is a purely empirical value that describes the dynamic soil resistances. Rausche et al. (1985) pointed out that the $J_c$ can be calculated by substituting the maximum static soil resistance shown in Eq. (2.9) with the ultimate pile resistance determined from a static load test using the Davisson's criteria. The recommended $J_c$ values given by Hannigan et al. (1998) are shown in Table 2.1. The original $J_c$ values were determined by Goble et al. (1975) from 69 static load test data, and they were organized according to five soil types in the region of the pile toe. The data used in the original $J_c$ correlation were within 20% of the difference between Case method predicted results and the static load test results. In addition, a single best $J_c$ value was selected from the correlation study for each soil type and tabulated under the "Best Correlation Value" in Table 2.1. Subsequently, the $J_c$ values were updated by Pile Dynamic, Inc. (1996) with additional static load test data.

Table 2.1: Summary of Case damping factors (after Hannigan et al. 1998)

| Soil Type at Pile Toe | Original Case Damping Factors | Best Correlation Value | Updated Case Damping Factors |
|---|---|---|---|
| Clean Sand | 0.05 to 0.20 | 0.05 | 0.10 to 0.15 |
| Silty Sand, Sandy Silt | 0.15 to 0.30 | 0.15 | 0.15 to 0.25 |
| Silt | 0.20 to 0.45 | 0.3 | 0.25 to 0.40 |
| Silty Clay, Clayey Silt | 0.40 to 0.70 | 0.55 | 0.40 to 0.70 |
| Clay | 0.60 to 1.10 | 1.10 | 0.70 or higher |

For a pile with very hard driving, the pile toe velocity is very small and close to zero, and the total resistance is approximately equal to the static resistance. Thus, the pile resistance computation is insensitive to the selection of $J_c$. On the other hands, the pile toe velocity is higher in easy driving and the pile resistance computation is sensitive to $J_c$. Chiesura G. (1998) noted that a correct selection of $J_c$ is important in estimating a realistic static soil resistance. He suggested that both dynamic and static load tests should be carried out to obtain the right $J_c$ value. Furthermore, Hannigan et al. (1998) suggested that the $J_c$ should be at least 0.40 when the maximum static resistance Eq. (2.9) is used and it is usually on the order of 0.20 higher than the value used in the standard Case static resistance Eq. (2.8).

### 2.3.5. Pile driving stresses

Besides the pile resistance determination, PDA is used to calculate pile driving stresses. PDA calculates both compressive and tensile stresses at the gauge location and compares them with the maximum allowable stresses given in Table 2.2. In addition, the structural pile driving stress limits can be determined in accordance with AASHTO (2010) LRFD Bridge Design Specifications. The compressive stress is calculated using Eq. (2.10). Whereas, the tension stress is calculated based on the superposition of the upward and downward traveling stress waves, expressed in Eq. (2.11) given by Goble et al. (1980).

$$\sigma_c = \varepsilon E \tag{2.10}$$

$$\sigma_T = \frac{1}{2}\{(VT2)Z - FT2 - (VT3)Z - FT3\} \tag{2.11}$$

where,

$\sigma_c$ = compressive stress, kN/mm$^2$ or ksi,

$\varepsilon$ = measured strain at gauge location, mm/mm or in/in,

E = pile modulus of elasticity, kN/mm$^2$ or ksi,

$\sigma_T$ = tension stress, kN/mm$^2$ or ksi,

VT2 = measured velocity at time T2 = T1+2L/C, m/s or ft/s,

VT3 = measured velocity at time T3 = T1 + 2(L-x)/C, x is distance where tension

stress occurs measured below gauge location, m/s or ft/s,

FT2 = measured force at time T2, kN or kip,

FT3 = measured force at time T3, kN or kip,

Z = pile impedance = EA/C, kN-s/m or kip-s/ft,

L = pile length, m or ft,

E = pile modulus of elasticity, kN/mm$^2$ or ksi, and

C = pile wave speed, m/s or ft/s.

If the stress limits are exceeded, the PDA will give a warning by highlighting the maximum compression stress (CSX) or the maximum tensile stress (TSX). Thus, the warning allows the construction personnel in the field to check the driving process and to employ the required steps to prevent any damage caused by overstressing during driving.

Table 2.2: Recommended Driving Stress Limits (after Pile Dynamic, Inc. 2001)

| Stress Type | Stress Limits in SI Unit | Remarks |
|---|---|---|
| Steel Compression | 0.90 $F_y$ | $F_y$ = Steel yield strength |
| Steel Tension | 0.90 $F_y$ | |
| Prestressed Concrete Compression | 0.85 $f'_c - f_{pe}$ | $f'_c$ = Concrete 28 day strength |
| Prestressed Concrete Tension | $f_{pe} + 0.25 (f'_c)^{0.5}$ | $f_{pe}$ = Effective prestress (MPa) |
| Regular Reinforced Concrete Compression | 0.85 $f'_c$ | |
| Regular Reinforced Concrete Tension | 0.70 $F_y$ ($A_s/A_c$) | $A_s$ = Steel reinforcement area<br>$A_c$ = Concrete area |
| Timber | 3 MPa* | *- Allowable static stress |

### 2.3.6. Structural integrity

PDA can be used to check integrity of piles below ground surface. Hannigan et al. (1998) noted that the convergence between the force and velocity records occurred before 2L/C indicates a reduction in the pile impedance (Z). For a uniform cross section pile, a sharp reduction in pile impedance means a possible pile damage. Rausche and Goble (1979) derived the integrity factor (BTA) given by Eq. (2.12) to describe the degree of convergence as illustrated in Figure 2.4.

$$\text{BTA} = \frac{1-\alpha}{1+\alpha}\ ;\ \alpha = \frac{\Delta u}{2(\text{FT1} - \Delta R)} \tag{2.12}$$

where,

BTA = integrity factor used in PDA, %;

α = a defining term, dimensionless;

Δu = the change between force and the apparent velocity at the location where change in pile impedance occurs, kN or kip;

FT1 = the force at pile top at the time of impact, kN or kip; and

ΔR = the soil resistance at the time before the sudden increase in the velocity becomes noticeable, kN or kip.

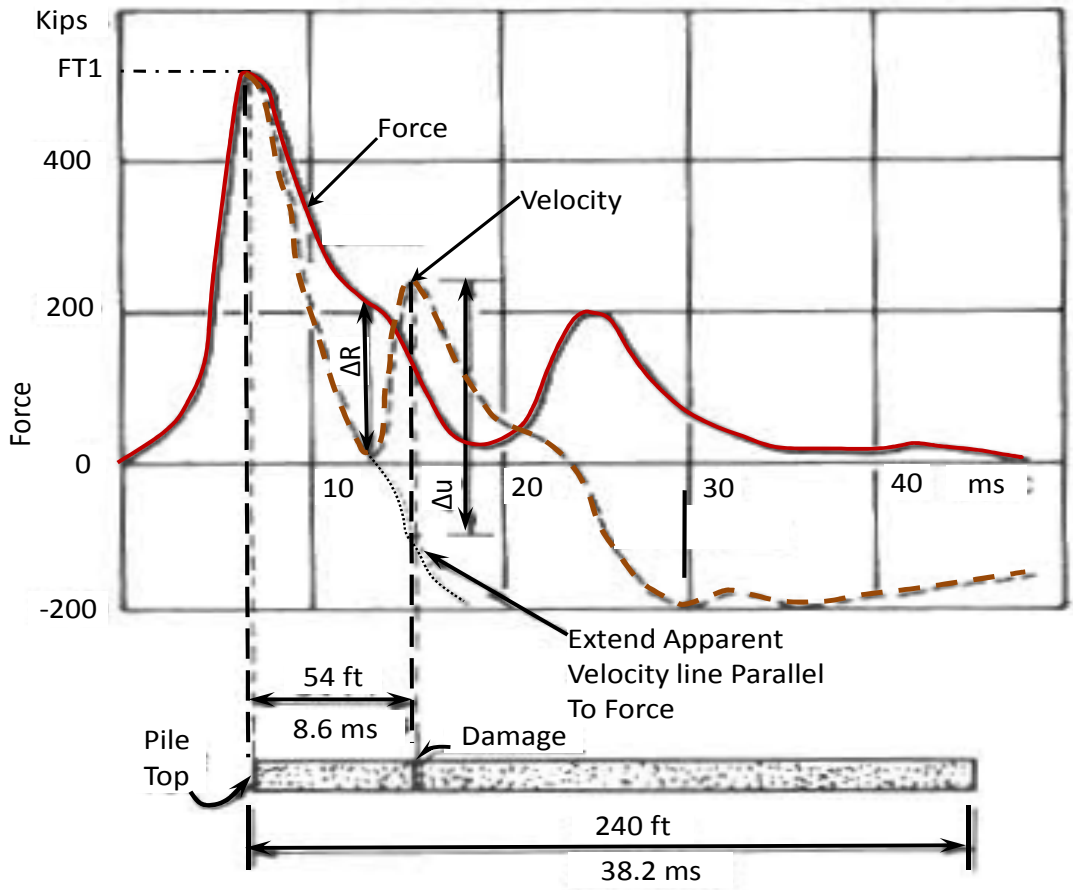


Figure 2.4: A typical pile damage force and velocity record (after Rausche and Goble, 1979)

Rausche and Goble (1979) classified the damage as given in Table 2.3 under the presumption that BTA indicates how much the pile cross section is remained. Webster and Teferra (1996) noted that most of the pile damages were caused by pile overstressing, either in compression or tension, during driving. However, piles may also be damaged due to bending. They suggested that the difference between maximum compressive stress at the gauge location (CSX) and the individual compressive stress measured from a single gauge (CSI) should be kept minimal to avoid any excessive bending.

Table 2.3: Pile damage classification (Rausche and Goble 1979)

| BTA (Percentage) | Severity of Damage |
|---|---|
| 1.0 (100%) | Undamaged |
| 0.8 – 1.0 (80% - 100%) | Slight damage |
| 0.6 – 0.8 (60% - 80%) | Damage |
| Below 0.6 (below 60%) | Broken |

### 2.3.7. Hammer/driving system

PDA monitors the hammer energy transferred to a pile to reduce the probability of pile damage and to ensure an efficient hammer performance. Hussein et al. (2002) noted that the hammer driving energy is dependent on hammer ram weight, stroke, mechanical efficiency, hammer and cushion characteristics, pile dimension, pile properties, and soil resistance effects. Hannigan et al. (1998) expressed the transferred energy using

$$E_p(t) = \int_0^T F(t)\, v(t) dt \tag{2.13}$$

where,

$E_p(t)$ = transferred energy at gauge location as a function of time t, kN-m or kip-ft,

F(t) = measured force, calculated using Eq. (2.1) as a function of time t, kN or kip,

v(t) = the measured velocity calculated using Eq. (2.2) as a function of time t, m/s or ft/s, and

T = default maximum time limit, which is 0.2048 second, s.

Hammer efficiency defines the performance of a hammer and driving system, and it can be expressed in percentage using Eq. (2.14). Wei et al. (1991) noted that the average efficiencies of 58 kN (6.5 ton), 62 kN (7 ton), and 71 kN (8 ton) hydraulic hammers are about 56%, 68% and 57%, respectively. In addition, the average efficiency of a 22 kN (2.5 ton) diesel hammer is about 37 %.

$$\text{Efficiency} = \frac{\text{Transferred Energy to Pile Head Using Eq. (2.13)}}{\text{Manufacturer Rated Hammer Energy}} \tag{2.14}$$

Hussein and Goble (1987) revealed that the separation between the force and velocity records before impact (between time zero and T1 of Figure 2.2) is caused by the precompression in the hammer combustion chamber. The separation increases and the immediate peak (at time T1) reduces if the gases are ignited before any impact. In addition, they pointed out that a cushion has a large influence on a successful pile driving installation. Used cushion will induce a higher peak force and a shorter rise time. Webster and Teferra (1996) emphasized the importance of proper selection of pile driving equipment and adequate cushioning used, so pile overstressing or damage can be prevented.

Hussein et al. (1996) suggested several general guidelines for selecting a hammer used in the PDA testing on drilled shafts. They recommended that the hammer weight should be at least 1.5% of the anticipated static test load. The hammer stroke should be approximately 8.5% of the pile length or a minimum of 2 m (6.6 ft). The cushion thickness of $t_c = L^2/2D$, where L = pile length and D = pile diameter, is suggested with a minimum value of 100 mm (4-in), and an additional of 150 mm (6-in) should be added when the pile length exceeds 30.5 m (100 ft). Likins et al. (2004) related the hammer stroke of an open-end diesel hammer to an equivalent blow rate using

$$\text{H} = \left[4.02\left(\frac{60}{\text{BPM}}\right)^2 - 0.3\right] \tag{2.15}$$

where,

H = hammer stroke, ft, and

BPM = equivalent blow rate, blows per minute.

### 2.3.8. Interpretation and calculation of PDA results

Goble and Likins (1996) suggested that final PDA results interpretation should be performed by qualified engineers who understand wave propagation concept, Case method, pile design, and pile driving. Soil resistance effects on pile can be evaluated qualitatively from the force and velocity records. Noted that the velocity record has been multiplied by the pile impedance Z, and it is plotted together with the force record. Figure 2.5 illustrates the pile responses induced by various soil resistance conditions. The pile loading section happens between the time of impact when the first peak of both force and velocity records occur and the time at 2L/C. The unloading section occurs after the time 2L/C. The separation between the force and velocity records between the time of impact and the time 2L/C represents the shaft resistance, and the toe resistance is identified at the time 2L/C.

Figure 2.5(a) shows a minimal separation between force and velocity within the loading section. The velocity peaks and the force decreases to negative at the time 2L/C. These typical responses indicate that only small shaft and toe resistances acting on the pile which is similar to a free end rod as described in Section 2.3.3. Within the unloading section, the force increase from negative to positive value and rises above the velocity record that decreases from positive to negative value. Similar to the loading section, the small separation between the force and velocity records show a small shaft resistance on the pile. Figure 2.5(b) shows a similar response as observed in Figure 2.5(a) at the loading section. However, the force increases and velocity decreases significantly at time 2L/C, indicating a small shaft resistance and a large toe resistance on the pile. At the unloading section, because of high toe resistance, the force continues above the velocity before a dissipation of the force. In contrast, Figure 2.5(c) shows a large separation between the force and velocity records during the loading section. These typical responses show that the pile has a large shaft resistance, and a similar observation is noticed in the unloading section. Detailed interpretation of the PDA results can be referred to Hannigan et al. (1998) and Hussein and Goble (1987).

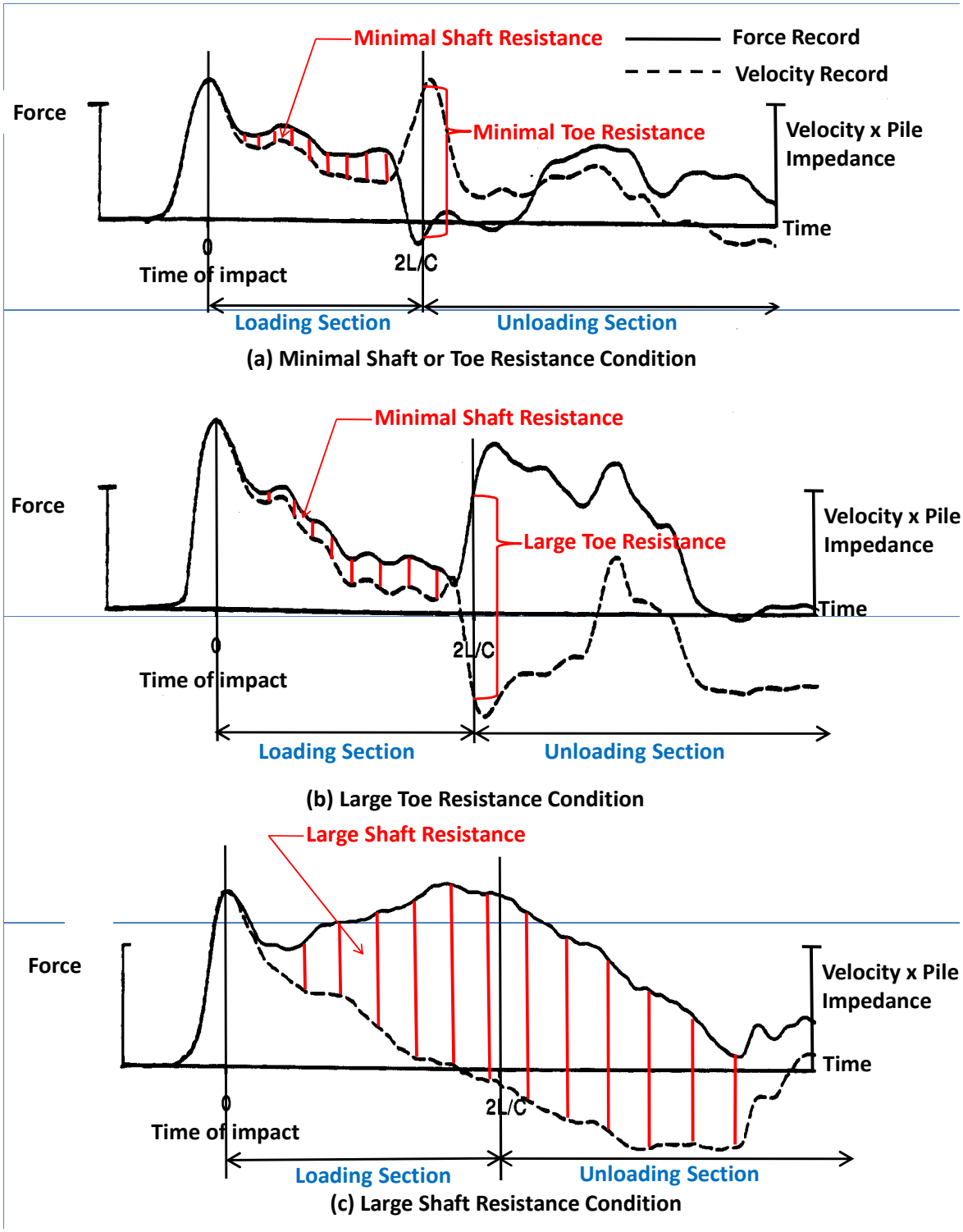


Figure 2.5: Typical force and velocity records for various soil resistance conditions (after Hannigan et al. 1998)

### 2.3.9. Example calculation

Referred to the PDA record shown in Figure 2.2, the measured forces and velocities at time of initial impact (T1) and at time of reflection of initial impact from pile toe (T2) after a duration of 2L/C as well as the steel H-pile properties are listed as below:

1. FT1 = 410 kips;
2. FT2 = -20 kips;
3. VT1 = 12.4 ft/s;
4. VT2 = 9.5 ft/s;
5. E = 30,000 ksi;
6. A = 16.8 $in^2$; and
7. C = 16,807.9 ft/s.

Using these numerical values, the total static and dynamic soil resistance on the pile (RTL) was calculated using Eq. (2.5) as follows

$$\mathrm{RTL} = \frac{1}{2}[\mathrm{FT1} + \mathrm{FT2}] + \frac{1}{2}[\mathrm{VT1} - \mathrm{VT2}]\frac{\mathrm{EA}}{\mathrm{C}}$$

$$\mathrm{RTL} = \frac{1}{2}[410 - 20] + \frac{1}{2}[12.4 - 9.5]\frac{30{,}000 \times 16.8}{16{,}807.9} = 239 \text{ kips}$$

The maximum static resistance (RMX) was found to occur at a time of 7.4 ms after the time of initial impact (T1). Thus, referred to the PDA record shown in Figure 2.2, the force and velocity at the time when RMX occurred ($t_m$) were 115 kips and 2.5 ft/s, respectively. The force and velocity after the time ($t_m$) for a duration of 2L/C were 107.9 kips and -0.7 ft/s, respectively. Using Eq. (2.9) and assuming a case damping factor ($J_c$) of 0.7 for a typical cohesive soil in Iowa, the calculation of the RMX was shown as below. In addition, the percent shaft resistance and end bearing are estimated using the PDA, and the procedure was illustrated in Ng et al. (2011).

$$R_s(t_m) = \frac{1}{2}\left\{(1 - J_c)\left[F(t_m) + \frac{EA}{C}v_T(t_m)\right] + (1 + J_c)\left[F\left(t_m + \frac{2L}{C}\right) - \frac{EA}{C}v_T\left(t_m + \frac{2L}{C}\right)\right]\right\}$$

$$\mathrm{RMX} = \frac{1}{2}\{(1 - 0.7)[115 + 30 \times 2.5] + (1 + 0.7)[107.9 - 30 \times -0.7]\} = 138 \text{ kips}$$

## 2.4. Case Pile Wave Analysis Program (CAPWAP)

### 2.4.1. Introduction

Case Pile Wave Analysis Program (CAPWAP) method was developed by Professor Goble and his students in the 1970s. It is a computer program for a more accurate numerical estimation of the soil resistance distribution, and dynamic soil parameters. The CAPWAP pile model adapted the Smith's model that was introduced in the 1960s. The Smith's model is described in Section 2.4.2 and the CAPWAP model is described in Section 2.4.3. CAPWAP uses the PDA records, the force-time and velocity-time information, as an input data and improves the pile resistance estimation by performing signals matching process. The analysis produces several important information, such as the ultimate pile resistance, soil distribution along a pile, soil Smith and Case damping factors, and soil quakes. Coduto (2001) noted that CAPWAP results could be further used to provide more accurate input parameters for the wave equation analysis discussed in Section 2.5, provide a specific Case damping factor for PDA analysis, measure soil setup or relaxation by analyzing data collected at EOD and BOR, and produce predicted static load test results.

### 2.4.2. Smith's models

In the late 1950s, Smith developed a mathematical model using the one-dimensional wave equation for the hammer-soil-pile system and used the digital computer in his pile driving analysis. Svinkin and Woods (1998) acknowledged that Smith was one of the pioneers in using a mathematical model to analyze pile driving. Today, his mathematical model is called the Smith's model that idealized the soil deformation and actual driven piles behaviors by taking into account of the accumulated experience on pile driving. Smith (1962) illustrated that his model divided the pile, hammer, and driving accessories into a series of short distinct sectional weight (W) and springs (K) as shown in Figure 2.6. The interface between the side of a pile and its surrounding soil is modeled with a series of instantaneous shaft damping resistances ($R_3$ to $R_{11}$). Similarly, a toe damping resistance ($R_{12}$) is placed at the bottom of a pile. During any pile driving, the time is divided into small time intervals, such as 1/4000 second, for an accurate numerical analysis. The mathematical

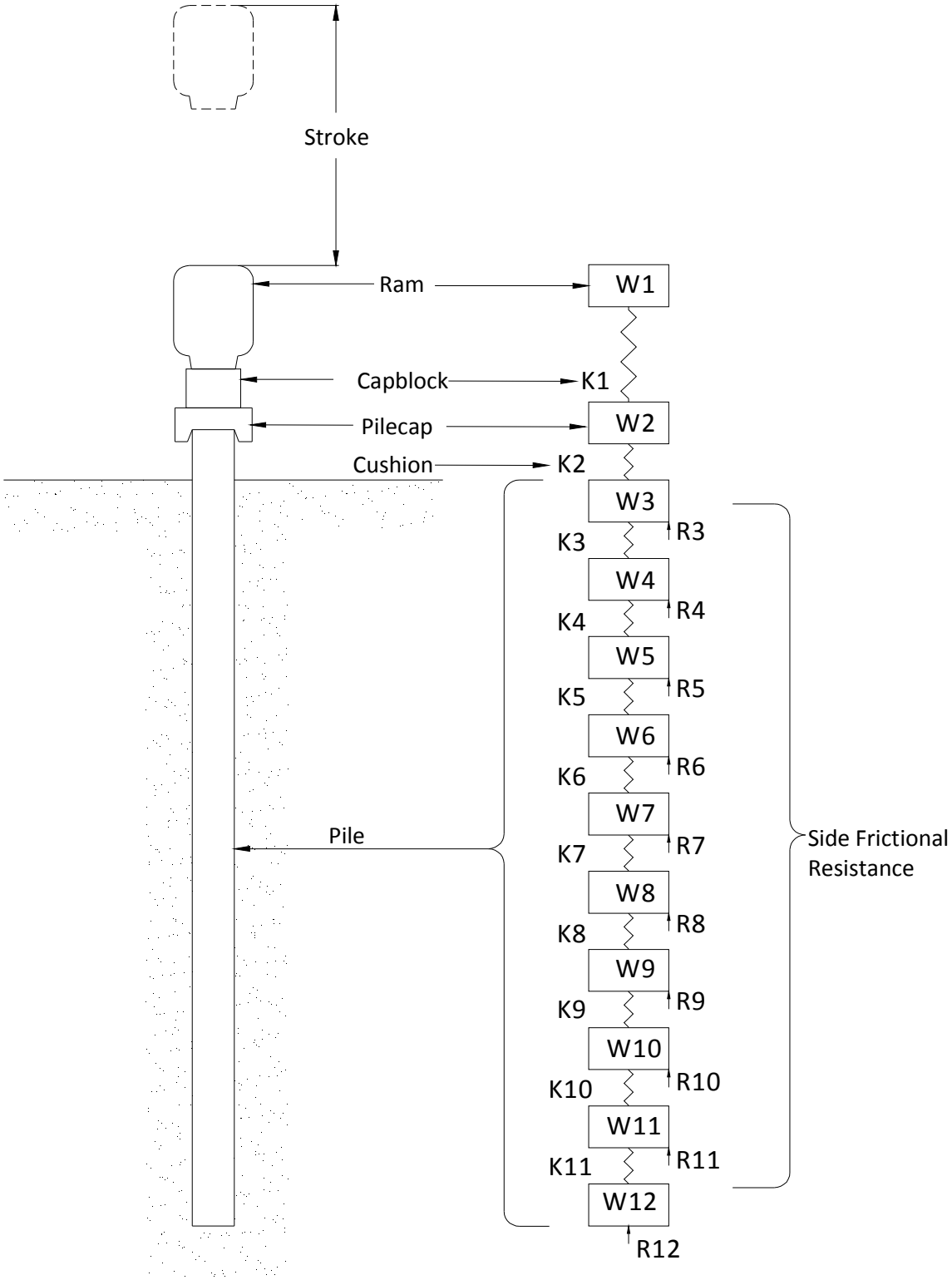


Figure 2.6: Smith's Model (after Smith 1962)

computation is stable only when the time increment is shorter than the critical wave travel time of any pile segment (Pile Dynamic Inc. 2005). Because a fairly long wave is usually induced during pile driving, a division of pile lengths from 1.5 m (5 ft) to 3m (10 ft) will usually produce a stable computation with an acceptable accuracy. The hammer ram as shown in Figure 2.6, is represented by a rigid, heavy and short single weight W1 without any elasticity. The cap block is represented by a spring K1 that can only transmit compression but not tension. The pile cap likes the ram is represented by a single weight W2 without any elasticity. The cushion is used under the pile cap to protect the piles from damaging and it is represented by a non-tensional spring K2. The pile is divided in ten sectional weights from W3 to W12 and they are connected with springs from K3 to K11.

Smith adapted Chellis's concept of soil mechanics, which soil compresses elastically to a displacement called quake (q) and fails plastically with a constant ultimate static soil resistance ($R_u$) as illustrated with a black solid line OABC shown in Figure 2.7. Smith developed a mathematical equation which accounts for both static and dynamic soil behaviors as illustrated with a dash line OA′BC shown in Figure 2.7. The total soil resistance at any point x′ with x deformation on the line OA′BC is given by

$$R = R_s + R_d = Kx + J_s R_s v_p = R_s\left(1 + J_s v_p\right) \tag{2.16}$$

where,

R = total soil resistance, kN or kip,

$R_s$ = static soil resistance, kN or kip,

$R_d$ = dynamic soil resistance, kN or kip,

$J_s$ = Smith damping constant, s/m or s/ft,

$v_p$ = instantaneous velocity of a pile segment, m/s or ft/s,

K = spring constant for soil model, kN/m or kip/ft, and

x = soil deformation, m or ft.

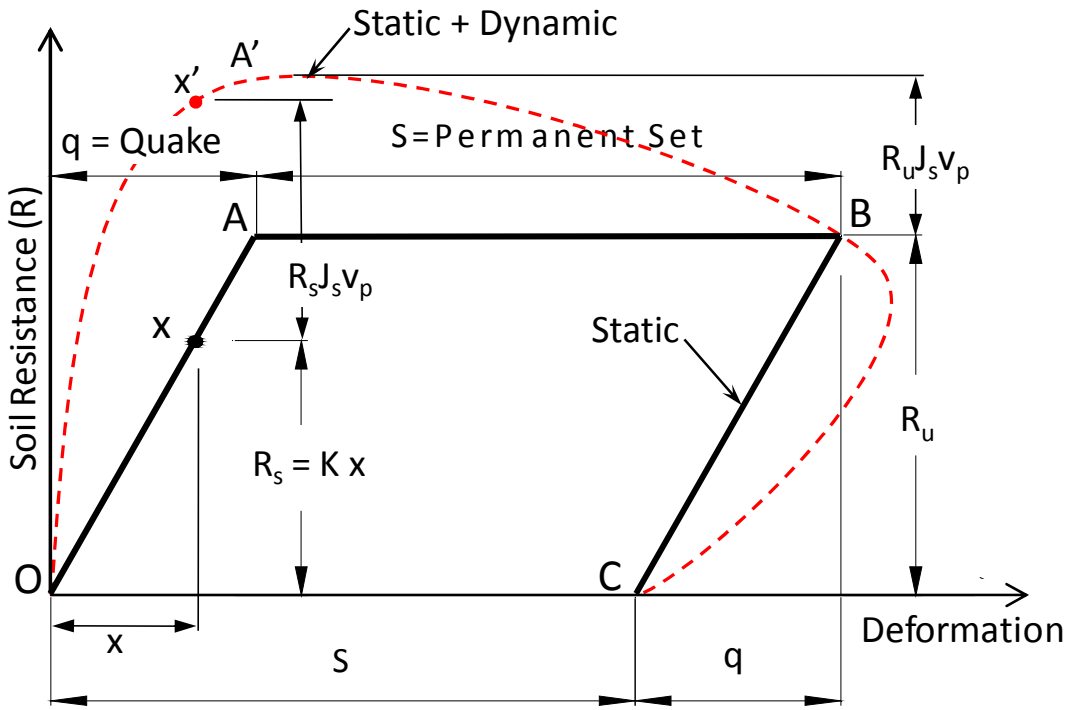


Figure 2.7: Stress strain diagram of the soil resistance at a pile point (after Coyle and Gibson, 1970 and Smith, 1962).

Smith (1962) described that the velocity of any particular pile segment at any particular time interval produces a displacement, which serves as a boundary condition for the next time interval. Then, the displacements of two adjacent pile segments produce a compression in the spring between them and create a spring force. The spring force and the resistance acting on the particular segment produce a net force. This net force accelerates or decelerates the segment and produces a new velocity which in turn produces a new displacement in the next succeeding time interval. This process is repeated for each segment and each spring at each time interval until all downward velocities are dissipated. The displacement of a pile given by Smith can be expressed by Eq. (2.17). The shaft resistance alongside of a pile can be expressed by Eq. (2.18), and the toe resistance can be expressed by Eq. (2.19). The difference between the pile displacement and the corresponding ground displacement (D – D′) is represented by a soil quake (q). Soil quake along shaft ($q_s$) and soil quake at toe ($q_T$) are denoted to describe the difference in deformation alongside of a pile ($D_m - D'_m$) and at the pile toe ($D_p - D'_p$), respectively.

$$D_m = 2d_m - d_m^* + \frac{g\Delta t^2}{W_m}[(d_{m-1} - d_m)K_{m-1} - (d_m - d_{m+1})K_m - R_m] \quad (2.17)$$

$$R_m = (D_m - D'_m)K'_m(1 + J'v_m) = q_s K'_m(1 + J'v_m) \quad (2.18)$$

$$R_p = (D_p - D'_p)K'_p(1 + Jv_p) = q_T K'_p(1 + Jv_p) \quad (2.19)$$

where,

$D_m$ = displacement along pile segment m at time interval n, m or ft,

$d_m$ = displacement along pile segment m at time interval n-1, m or ft,

$d^*_m$ = displacement along pile segment m at time interval n-2, m or ft,

$g$ = acceleration due to gravity, $m/s^2$ or $ft/s^2$,

$\Delta t$ = time interval used in calculation, sec,

$W_m$ = pile weight, kN or kip,

$R_m$ = shaft resistance along pile segment m at time interval n, kN or kip,

$K_m$ = pile spring constant, kN/m or kip/ft,

$D'_m$ = ground plastic side displacement at time interval n, m or ft,

$K'_m$ = ground spring constant along pile segment m, kN/m or kip/ft,

$J'$ = damping constant applicable to resistance along a pile, s/m or s/ft,

$v_m$ = instantaneous velocity along pile segment m at time interval n-1, m/s or ft/s,

$R_p$ = toe resistance at the pile point, kN or kip,

$D_p$ = pile toe displacement at time interval n, m or ft,

$D'_p$ = ground displacement at pile toe at time interval n, m or ft,

$K'_p$ = ground spring constant at pile toe, kN/ft or kip/ft,

$J$ = damping constant applicable to pile toe, s/m or s/ft,

$v_p$ = instantaneous velocity at pile toe in time interval n-1, m/s or ft/s,

$q_s$ = soil quake along a pile shaft, m or ft,

$q_T$ = soil quake at a pile toe, m or ft,

$n$ = time interval for which calculations are being made, and

$m$ = subscript denoting the general pile segment m.

Smith established four routines that act as the bases for his pile driving computer program. The condition in the routine No. 1, which is applied only to friction alongside the pile, is the ground displacement $D'_m$ will remain unchanged unless either $D'_m$ is less than $D_m$– q or $D'_m$ is greater than $D_m$+q. Routine No. 2, which is applied only to the pile toe, sets the condition that the ground displacement $D'_p$ will remain unchanged unless $D'_p$ is less than $D_p$– q. Routine No. 3 takes into account the inelasticity of spring K1 for capblock and delivers the ability to use Eq. (2.20) for compression and Eq. (2.21) for restitution alternatively. Similar to the routine No. 3, routine No. 4 is applied to spring K2 for cushion. Eqs. (2.20) and (2.21) are similarly applied to spring K2 by changing the subscript 1 to 2. The only exception is the force $F_2$ in routine No. 4 has an alternative of being zero, negative, or positive value.

$$F_1 = C_1 K_1 \tag{2.20}$$

$$F_1 = \left[\frac{K_1}{(e_1)^2}\right] C_1 - \left[\frac{1}{(e_1)^2} - 1\right] K_1 C_{1\,max} \tag{2.21}$$

where,

$F_1$ = force exerted by spring 1 at time interval n, kN or kip,

$C_1$ = spring 1 compression at time interval n, m or ft,

$C_{1max}$ = maximum value of C1, m or ft,

$K_1$ = spring 1 constant, kN/m or kip/ft, and

$e_1$ = coefficient of restitution for spring K1.

Svinkin and Woods (1998) highlighted that one of the limitations of Smith soil model is the difficulty with determining the soil parameters, soil quakes (q) and damping factors (J), from any standard geotechnical tests. Robert Liang and Sheng (1993) realized that the accuracy of dynamic analysis using the Smith's model depends upon the proper input of representative Smith's soil parameters. Robert Liang and Zhou (1997) used a probability method to determine a better representative of the Smith soil parameters and to establish an alternative approach to estimate pile resistance. Although experimental investigations have

been carried by many researchers for the estimation of these dynamic soil parameters, the accuracy and reliability of the pile resistance prediction are yet to be achieved. Table 2.4 and Table 2.5 summarize the suggested values of soil quakes and Smith damping factors from ten references. Additional references on recommended Smith's soil parameters can be referred to Soares et al. (1984) for all soil types and Swann & Abbs (1984) for calcareous soils. Robert Liang and Sheng (1993) concluded that the size of the penetrating shaft exerts significant influence on the soil quake and Smith damping factor, and they gave the relationship between the penetrating velocity ($v_p$) and acceleration ($\dot{v}_p$) and the Smith damping factor. It can be concluded from Table 2.4 and Table 2.5 that the soil quakes and damping factors are not only dependent on soil types, but the quakes also depend on pile dimension while the damping factors also depend on both pile dimension and pile penetration rate.

### 2.4.3. CAPWAP model

Similar to Smith's model, CAPWAP model is divided into pile and soil models. CAPWAP uses the PDA data to quantify the two of the three unknowns, which are the pile force and velocity. The remaining unknown is the pile boundary conditions, which are defined by the soil resistance distribution, soil quake and soil damping factors of the soil model (Hannigan et al. 1998). By adjusting the boundary conditions, CAPWAP calculates an equilibrium pile head force, which is comparable to the PDA measured force. Several iteration adjustments are made to the soil model until the best matching signal between the calculated and measured force is obtained. The schematic of a CAPWAP model is shown in Figure 2.8. Goble and Rausche (1980) described that the pile is modeled with a series of masses and springs, and the soil resistances are modeled alongside and at toe of the pile with elasto-plastic springs and linear dashpots. CAPWAP model is similar to Smith's except CAPWAP model does not include the driving systems and the pile section above the PDA gauges.

Table 2.4: Summary 1 of dynamic soil parameters for Smith's soil model

| Description | Hill (1950) | Smith (1962) | Timoshenko and Goodier (1970) | Coyle and Gibson (1970) | Coyle et al. (1973) | Randolph and Wroth (1978) | Swann and Abbs (1984) |
|---|---|---|---|---|---|---|---|
| Quake Shaft ($q_S$) | N/A | 2.5 mm | N/A | N/A | 2.5 mm | $\frac{f_s r_o}{G}\ln\left(\frac{r_m}{r_o}\right)$ | N/A |
| Quake Toe ($q_T$) | $\frac{1+\nu}{2E}P_y\left(\frac{D}{2}\right)$ | 2.5 mm | $\frac{q_b D(1-\nu^2)}{E}I_b$ | N/A | 2.5 mm | N/A | N/A |
| Smith Shaft Damping Factor ($J_S$) | N/A | 0.16s/m | N/A | N/A | 0.66 s/m (clay), 0.16 s/m (sand), 0.33 s/m (silt) | N/A | 0.16 s/m (gravel & sand), 0.33s/m to 0.49 s/m (silt), 0.66 s/m (clay) |
| Smith Toe Damping Factor ($J_T$) | N/A | 0.49s/m | N/A | $\frac{1}{v^N}\left(\frac{P_d}{P_s}-1\right)$ | 0.03 s/m (clay), 0.49 s/m(sand & silt) | N/A | 0.16 s/m to 0.33 s/m (gravel); 0.33 s/m to 0.66 s/m (sand); 0.33 s/m to 1.64 s/m (silt); 0.03 s/m to 3.28 s/m (clay) |

where,

$\nu$ = soil poisson's ratio
E = soil Young's modulus
$P_y$ = yielding stress on cavity
D = pile diameter

$q_b$ = stress intensity at pile toe
$I_b$ = influence coefficient, 0.78 to 0.5
D = pile diameter
E = soil Young's modulus.

$P_d$ = peak dynamic load
$P_s$ = peak static load
v = velocity of soil deformation
N = exponential power modification, 0.2 (sand) and 0.18 (clay)

$f_s$ = unit shaft resistance
$r_o$ = radius of pile,
$r_m$ = radius of the influence zone
G = average shear modulus in the influence zone

Table 2.5: Summary 2 of dynamic soil parameters for Smith's soil model

| Dynamic soil properties | Robert Liang and Sheng (1992) | Robert Liang and Abdullah I. Husein (1993) | Hannigan et al. (1998) | Coduto (2001) |
|---|---|---|---|---|
| Quake Shaft ($q_S$) | N/A | N/A | 2.5 mm | 2.5 mm per 300 mm of pile diameter |
| Quake Toe ($q_T$) | N/A | N/A | D/120 for very dense and hard soil; D/60 for soft materials; D in inches | 2.5 mm per 300 mm of pile diameter |
| Smith Shaft Damping Factor ($J_S$) | N/A | $\frac{0.1}{V_{pd}}\log\left(\frac{V_{pd}}{V_{ps}}\right)$ | 0.66 s/m for cohesive soil, 0.16 s/m for non-cohesive soil | N/A |
| Smith Toe Damping Factor ($J_T$) | $\frac{\rho}{3f_T}\left(2r_o\frac{\dot{v}_p}{v_o}+3v_p\right)$ | N/A | 0.49 s/m for all soils | N/A |

where,
$\rho$ = soil density,
$f_T$ = unit toe resistance,
$\dot{v}_p$= pile penetration acceleration,
$v_p$ = pile penetration velocity,
$V_{pd}$ = pile penetration rate under dynamic condition, and
$V_{ps}$ = pile penetration rate under quasistatic condition.

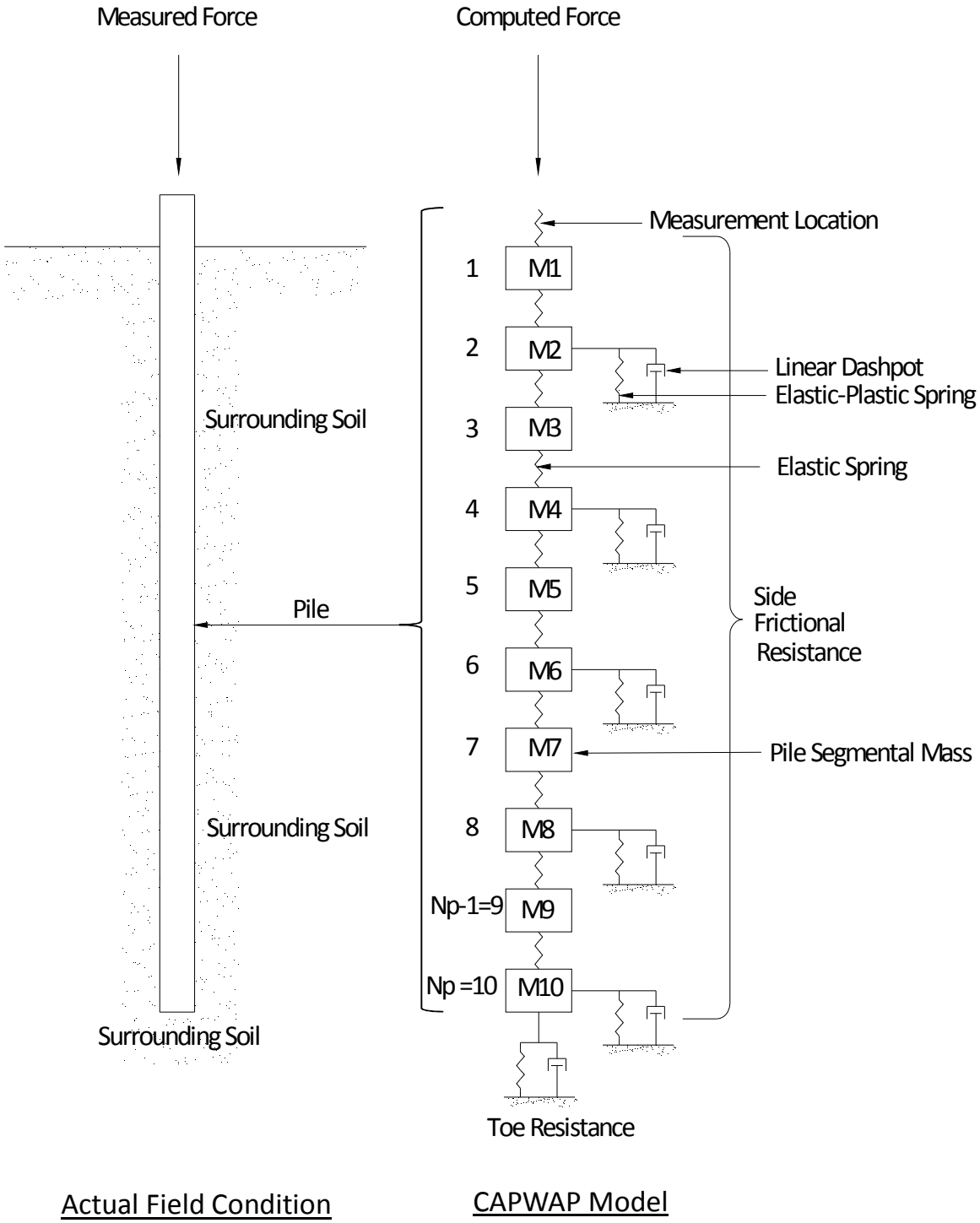


Figure 2.8: CAPWAP model (after Goble & Rausche, 1980 and Hannigan et al., 1998)

#### *2.4.3.1. Pile model*

Pile Dynamics, Inc. (2000) described that a typical uniform cross section pile in CAPWAP is divided into $N_p$ segments of pile masses (M) with each has approximate 1 m (3.3 ft) equal length ($\Delta L$) and each pile mass is connected with a series of elasto-plastic springs. The sum of all $\Delta L$ equals to the total pile length (L) and the sum of all wave travel time $\Delta t$ equals the total wave travel time L/C. A pile can be divided into different lengths as according to their material properties. For piles with variable cross section, force reflection happens between segments with different geometries. Thus, based on the wave propagation concept, reflected waves traveling upward will superimpose with the downward waves. CAPWAP assumes that all pile segments are unstressed before driving; however, in reality, residual forces could develop in pile segments during driving when unbalanced pile forces occur before coming to rest. Hannigan and Webster (1987) stated that the summation of pile forces must be in equilibrium at which pile segments with residual compressive forces are balanced by segments with residual tension forces.

#### *2.4.3.2. Soil model*

The CAPWAP soil model at each pile mass is represented by an elasto-plastic spring and a linear dashpot as shown in Figure 2.9. Generally, the soil model can be described by three parameters: soil resistance (R), quake (q), and viscous damping coefficient ($C_v$) at a soil segment k and pile segment i with a relationship given by Eq. (2.22), which is equal to the summation of soil static and dynamic resistances. The static soil resistance ($R_{sk}$) represented by a spring is equal to the product of the spring constant or soil stiffness (k) and the pile displacement (u). Whereas, the dynamic soil resistance ($R_{dk}$) represented by a linear dashpot is presented by a product of the viscous damping coefficient ($C_v$) and the instantaneous velocity ($\dot{u}$).

$$R_k = R_{sk} + R_{dk} = k_{sk} u_i + C_{v_k} \dot{u}_i \tag{2.22}$$

where,

$R_k$ = total soil resistance force at soil segment k, kN or kip,

$R_{sk}$ = static soil resistance force at soil segment k, kN or kip,

$R_{dk}$ = dynamic soil resistance at soil segment k, kN or kip,

$k_{sk}$ = soil stiffness of the k-th segment resistance, kN/m or kip/ft,

$u_i$ = pile displacement at segment i, m or ft,

$C_{v_k}$ = viscous damping coefficient at soil segment k, kN-s/m or kip-s/ft, and

$\dot{u}_i$ = instantaneous pile velocity at segment i, m/s or ft/s.

The CAPWAP soil model introduces a linear viscous damping coefficient ($C_v$) to replace the Smith damping coefficient ($J_sR_s$) used in Eq. (2.16). This linear damping coefficient can be approximately related to the Smith damping factor ($J_s$) and the Case damping factor ($J_c$) using the Eqs (2.23) and (2.24), respectively (Rausche et al. 1992). However, any change in ultimate static resistance ($R_u$) will change the $J_s$ value but not the $J_c$ value.

$$J_s \approx \frac{C_v}{R_u} \tag{2.23}$$

$$J_c \cong \frac{\sum C_v}{Z} \tag{2.24}$$

where,

$J_s$ = Smith damping factor, s/m or s/ft,

$J_c$ = Case damping factor, dimensionless,

$C_v$ = linear viscous damping coefficient, kN-s/m or kip-s/ft,

$R_u$ = ultimate static resistance, kN or kip, and

$Z$ = pile impedance, kN-s/m or kip-s/ft.

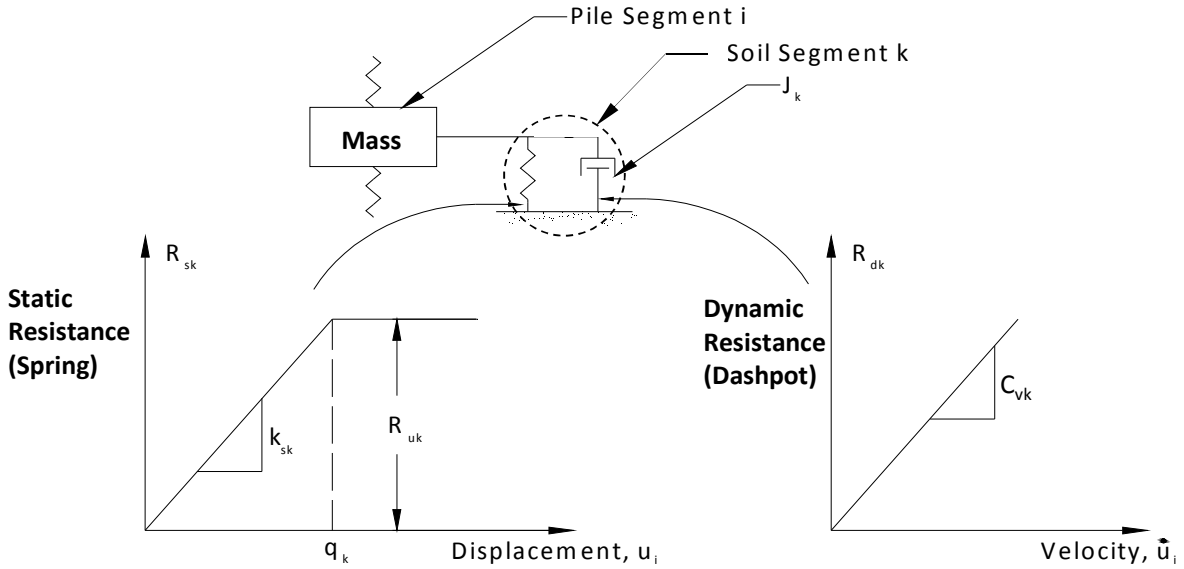


Figure 2.9: CAPWAP soil model (after Pile Dynamic, Inc. 2000)

An extended CAPWAP soil model shown in Figure 2.10 includes a radiation damping model that simulates the surrounding soil motion. It provides an improved model for a better correlation with static load tests by limiting the maximum Smith's shaft damping factor to 1.3 s/m (0.4 s/ft) (Likins et al. 1992). For the shaft radiation damping model, a soil mass ($M_s$) and a dashpot with damping coefficient ($C_{sk}$) are used to replace the rigid soil support of the traditional Smith model. Similarly, the toe radiation model uses a soil mass ($M_t$) and a dashpot with a damping coefficient ($C_{BT}$). The model allows the energy dissipation in the soil-pile interface and prevents interface failures. Likins et al. (1992) suggested that the radiation damping model is used only when the Smith damping factors exceed 0.79 s/m (0.24 s/ft). Furthermore, a toe gap is included in the extended CAPWAP model. A gap (g) between the pile toe and the soil happens when the pile is driven on a very hard soil layer. The static toe resistance is developed when the toe displacement exceeds the gap. For a full activation of soil toe resistance, the sum of the toe gap and the quake must be less than the maximum pile toe displacement, and the static soil resistance can be revised as

$$R_{sk} = k_{sk}(u_i - g_i) \tag{2.25}$$

where,

$R_{sk}$ = static soil resistance force at soil segment k = $N_s$+1, kN or kip,

$k_{sk}$ = soil stiffness of the k-th segment resistance, kN or kip,

$u_i$ = pile displacement at segment i = $N_p$, m or ft, and

$g_i$ = pile gap beneath pile toe, m or ft.

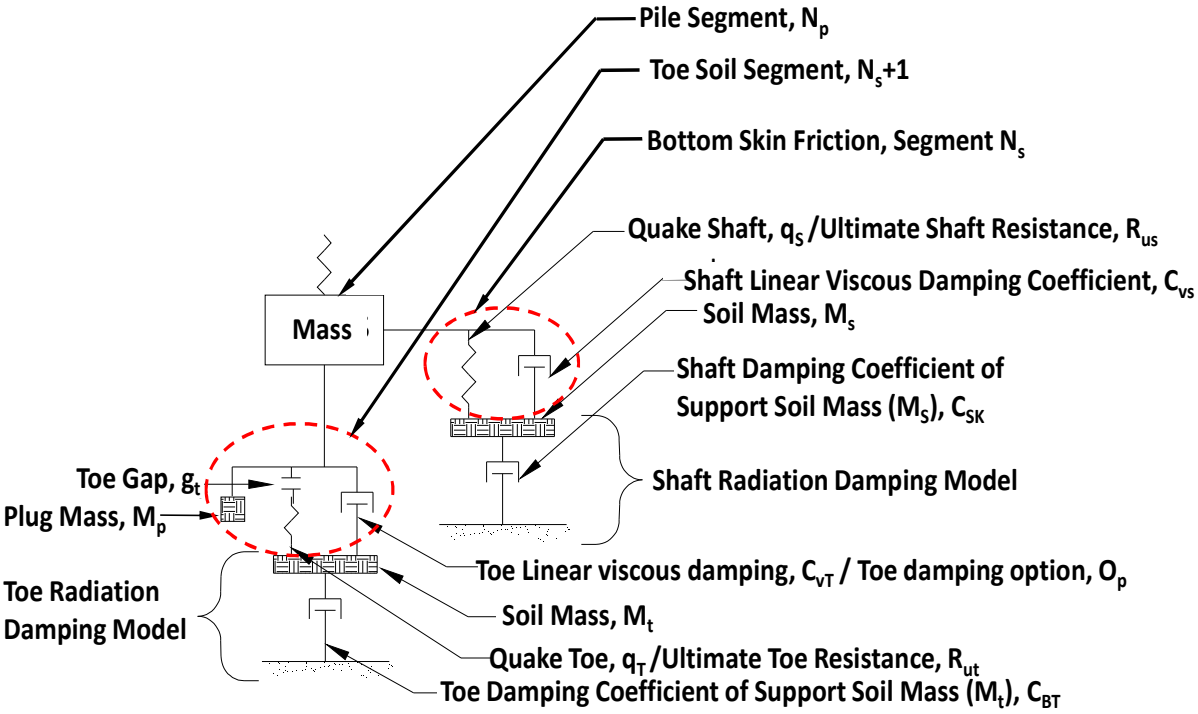


Figure 2.10: The extended CAPWAP soil resistance model includes toe gap, plug mass, and radiation damping (after Pile Dynamic, Inc. 2000)

Another consideration is the pile plug which is modeled with a soil mass ($M_p$) as shown in Figure 2.10. The soil mass exerts an external resistance force ($R_M$) on pile toe at time j. The additional external resistance due to pile plug force can be expressed as

$$R_{Mj} = \frac{M_p\left(\dot{u}_{b_j} - \dot{u}_{b_{j-1}}\right)}{\Delta t} \tag{2.26}$$

where,

$R_{Mj}$ = external resistance force due to pile plug at time j, kN or kip,

$M_p$ = soil mass in pile plug, kN-s$^2$/m or kip-s$^2$/ft,

$\dot{u}_{b_j}$ = pile bottom velocity at time j, m/s or ft/s,

$\dot{u}_{b_{j-1}}$ = pile bottom velocity at previous time j-1, m/s or ft/s, and

$\Delta t$ = computational time increment, s.

With this new radiation damping model shown in Figure 2.10, the relative displacement and velocity between pile and the support soil mass at any pile segment can be computed using the Eqs. (2.27) and (2.28)**,** respectively. These two equations are written for all shaft segments; however, the $M_s$ and $C_{sk}$ can be replaced with $M_t$ and $C_{BT}$ for the toe calculation. The pile segment i and soil segment k at time counter j are selected for a generalization.

$$u_{ri} = u_i - \left[u_{ssi,j-1} + \left(\dot{u}_{ssi,j-1}\right)\Delta t\right] \tag{2.27}$$

$$\dot{u}_{ri} = \dot{u}_i - \dot{u}_{ssi,j-1} - \frac{\left(R_k + C_{vk}\dot{u}_i - C_{sk}\dot{u}_{ssi,j-1}\right)}{\left(C_{sk} + \frac{M_s}{\Delta t}\right)} \tag{2.28}$$

where,

$u_{ri}$ = relative displacement between pile segment i and its soil mass, m or ft,

$u_i$ = pile displacement at segment i, m or ft,

$u_{ss,i,j-1}$ = soil mass displacement at time j-1 and pile segment i, m or ft,

$\dot{u}_{ssi,j-1}$ = soil mass velocity at time j-1 and pile segment i, m/s or ft/s,

$\Delta t$ = computational time increment, s,

$\dot{u}_{ri}$ = relative velocity between pile and support soil mass, m/s or ft/s,

$\dot{u}_i$ = pile velocity at segment i, m/s or ft/s,

$R_k$ = total soil resistance force at soil segment k, kN or kip,

$C_{vk}$ = linear viscous damping coefficient at soil segment k, kN-s/m or kip-s/ft,

$C_{sk}$ = radiation damping coefficient at soil segment k, kN-s/m or kip-s/ft, and

$M_s$ = support soil mass at soil shaft segment k, kN-$s^2$/m or kip-$s^2$/ft.

### 2.4.4. CAPWAP signal matching

The main objective of CAPWAP analysis is to achieve the best signal matching between the computed and measured signals through the simultaneous adjustments of pile model and soil model. In CAPWAP, the quality of the signal matching is measured in terms of a match quality (MQ). The match quality is calculated by summing the absolute values of

the relative differences between measured ($F_m$) and computed ($F_c$) signals at individual points in time divided by the maximum pile top signal ($F_x$) given by Eq. (2.29). Also, due to the difference between measured and computed hammer blow counts, the match quality is penalized by a blow count penalty (BCP). The signal matching is improved as the MQ value reduces closer to zero.

$$MQ = \sum_{Period} \sum_{Time} \left| \frac{F_m - F_c}{F_x} \right| + BCP \tag{2.29}$$

where,

BCP = blow count penalty (BCP = 0 if $\Delta_{set} < 1$ mm, or BCP = $\Delta_{set}$ □ 1 if $\Delta_{set} \geq 1$ mm), and

$\Delta_{set}$ = absolute difference between measured and computed pile sets.

In order to reduce the analytical time required to achieve a reasonably good signal matching, default and automated CAPWAP (AC) matching procedure is normally used during practices. Referred to Figure 2.11, the AC procedure simultaneously adjusts the resistance at each pile segment shown in Window 2 and dynamic soil parameters listed in Window 3 until the best MQ value shown in Window 1 is achieved. The summation of the resistances for all pile segments yields the total shaft resistance ($R_s$) as indicated in Window 2. The total end bearing is equal to the summation of all resistances at the Toe, Toe2, and Toe3. Toe2 and Toe3 refer to as second and third toe cross sections of a composite pile. The addition of the total shaft resistance and end bearing gives the ultimate pile resistance ($R_{ult}$), which is considered as the total pile resistance estimated using CAPWAP. The limitations with AC procedure are described below:

1. Unrealistic high resistance near pile top may be generated,
2. Unrealistic low resistance near pile bottom may be generated,
3. The estimated soil resistance distribution may not represent the actual soil profile and properties,
4. Constant dynamic soil parameters, such as shaft damping factor ($J_S$ or SS in CAPWAP) and shaft quake ($q_S$ or QS in CAPWAP) as shown in Window 3, are

assigned for the entire embedded pile length regardless of different soil layers, and

5. Non-unique solution is generated from matching the same measured PDA signal due to the indeterminate nature of the AC procedure.

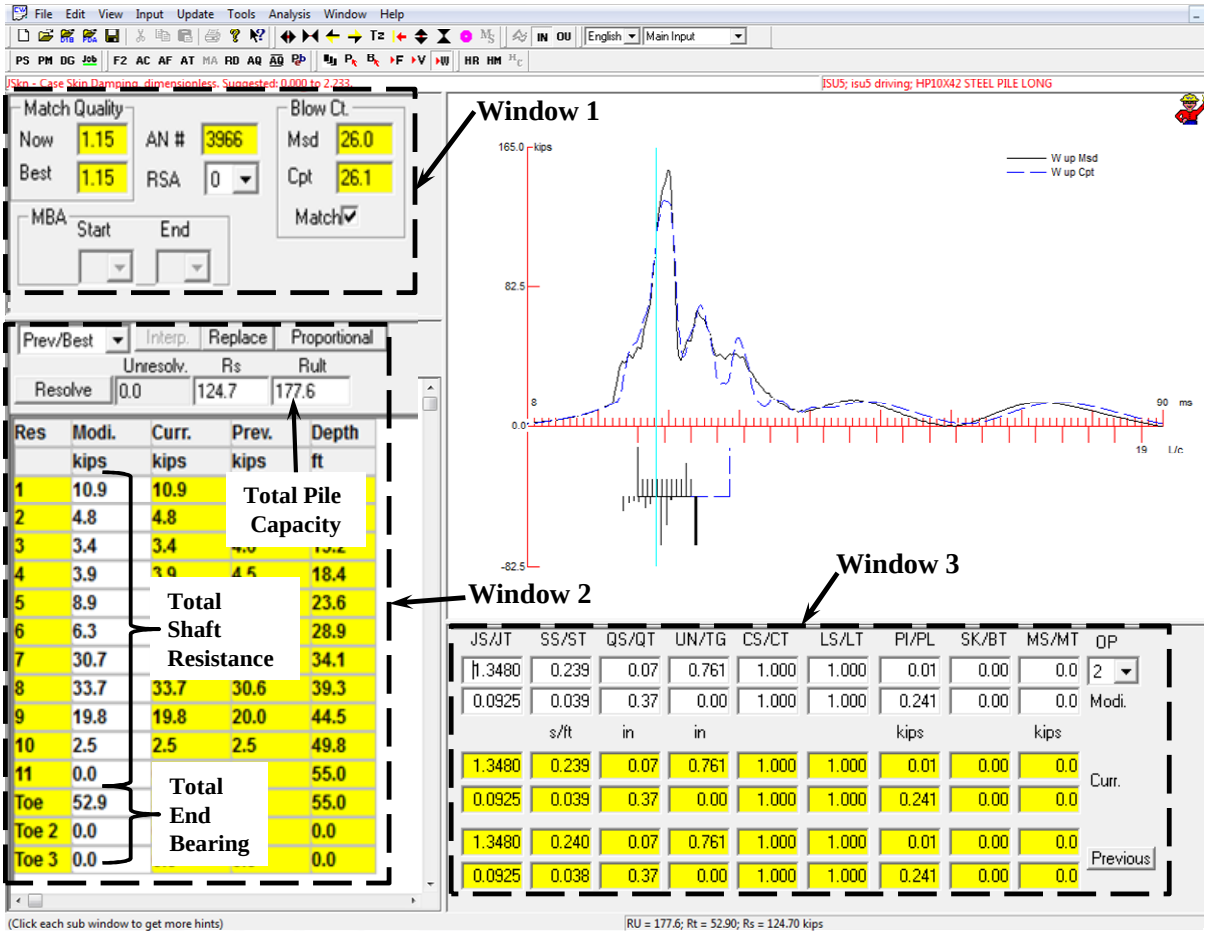


Figure 2.11: Windows of CAPWAP analysis

## 2.5. Wave Equation Analysis Program

### 2.5.1. Introduction

Wave equation analysis method was first introduced by Smith in the early 1950's and was applied to the Wave Equation Analysis Program (WEAP) by Goble and Rausche (1976). The WEAP was developed extensively, upgraded to the latest Window version, and commercialized by Pile Dynamic, Inc. WEAP simulates the motion and force on a pile when driven by an impact or vibratory hammer. Long et al. (2002) highlighted that wave equation analysis can be used to assess the behavior of a pile with different hammers used before the pile is actually driven. He concluded that the wave equation method provides a more accurate and reliable result than dynamic formulae. In fact, Coduto (2001) urged the replacement of dynamic formulae with wave equation method. Based on a statistical comparison of 99 static pile load tests, Rausche et al. (2004) concluded that the wave equation method generally under predicted the pile resistance by 18% and gave a high coefficient of variation (COV) of 0.44 when the end of driving (EOD) blow counts were used. In addition, because of the uncertainty in recording the exact blow count and the hammer performance, he found that the wave equation method over predicted the pile resistance by approximately 22 % and gave a relatively lower COV of 0.35 when the beginning of re-strike (BOR) blow counts were used. Furthermore, Paikowsky (2004) stated that the evaluation for pile resistance predictions using WEAP is difficult due to a large range of input parameters that are greatly affected by the actual field conditions.

WEAP requires the modeling of hammer, driving system, pile, splice, and soil as the inputs for wave equation analysis. Similar to the Smith's model, WEAP models the hammer, the pile, and the soil resistance in a series of masses, springs, and viscous dashpots as shown in Figure 2.12. This program computes the blow count, the axial driven stress on a pile, the hammer performance, and the pile resistance. Each model is briefly discussed in the following sections.

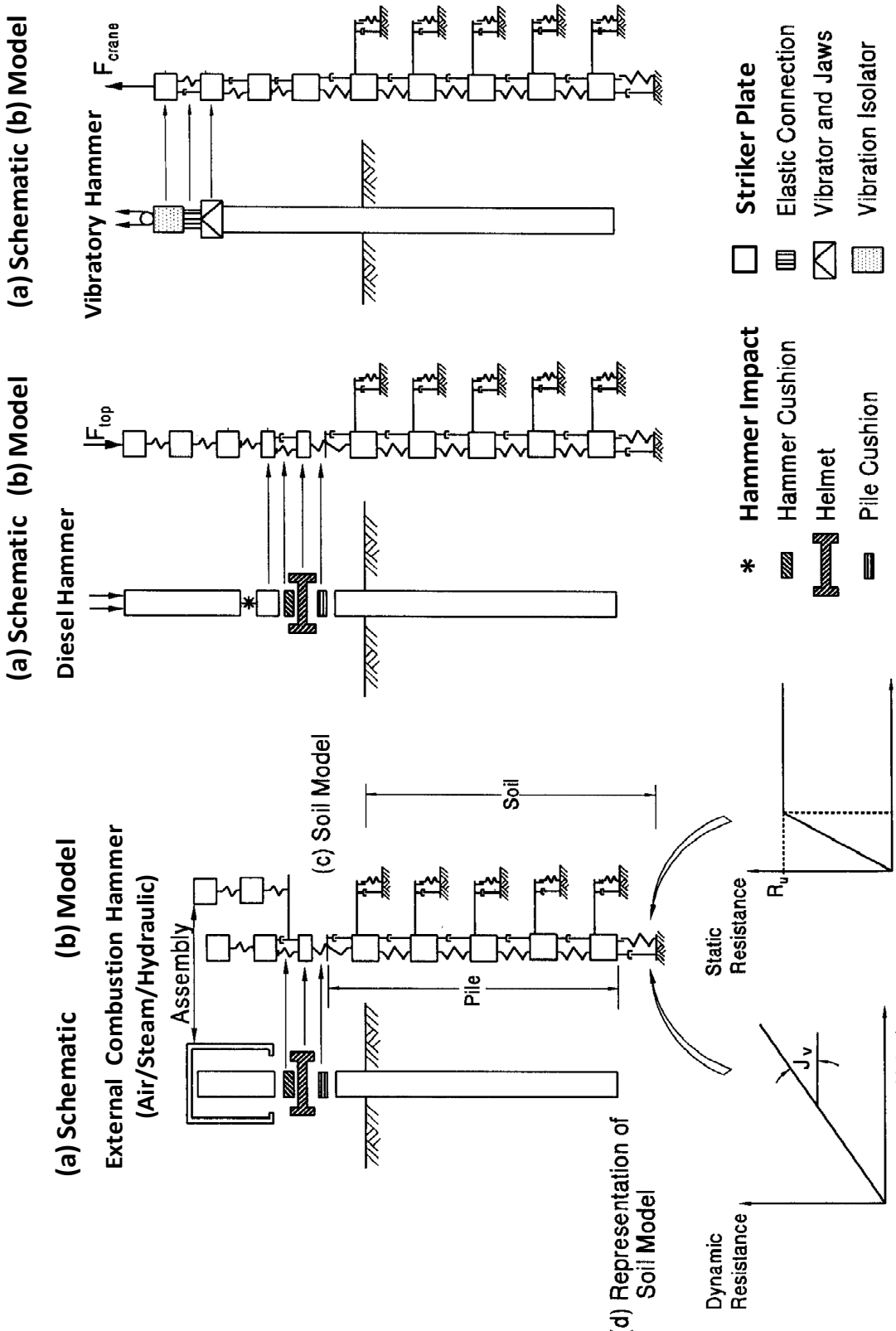


Figure 2.12: Wave equation models for different hammers (adapted from Hannigan et al. 1998)

### 2.5.2. Hammer model

Hammers can be divided into either internal or external combustion hammers. All diesel and vibratory hammers are internal combustion hammers, and the hydraulic and drop hammers are external combustion hammers. Diesel hammers can be classified as liquid injection, atomized injection, open end, and closed end. Hydraulic hammers can be categorized into single acting, double acting, drop, and power assisted, and their energy can be transferred by steam, compressed air, pressurized hydraulic fluid, or simply a hoist and a rope.

In WEAP hammer modeling, a ram segment is usually about 900 mm (3 ft) long and a slender ram is connected with a series of ram springs. Different hammer types are modeled with different combination of masses, springs, and/or dashpots, and the hammer assembly for the external combustion hammer is shown in Figure 2.12. The WEAP 2005 version has a database of various hammer types, and modifications of hammer efficiency, pressure, and stroke values that represent the actual hammer used are allowed.

### 2.5.3. Driving system model

The WEAP driving system model consists of a striker plate, hammer cushion, helmet, and a pile cushion which are represented by masses and springs. The weight of each piece should be included in the mass. The driving system model also has a dashpot that is placed parallel with the hammer cushion spring as illustrated in Figure 2.12, and its damping constant can be computed using

$$C_{dh} = \frac{1}{50} C_{dhi} \sqrt{k_r m_a} \tag{2.30}$$

where,

$C_{dh}$ = damping constant for hammer cushion, kN-s/m or kip-s/ft,

$C_{dhi}$ = non-dimensionalized input value, default value of 1.0, dimensionless,

$k_r$ = hammer cushion stiffness, kN/m or kip/ft, and

$m_a$ = either the impact block mass density for diesel hammer or helmet mass density for external combustion hammer, kN-s$^2$/m or kip-s$^2$/ft.

### 2.5.4. Pile model

Pile model is divided into pile segmental masses with each has approximate 900 mm (3 ft) long. The masses are connected together with a series of springs and dashpots. The mass, the spring stiffness, and the dashpot damping constant at each pile segment i can be computed using Eqs. (2.31), (2.32), and (2.33), respectively. The pile input data also consists of pile material yield strength, perimeter, toe area, and pile size and type.

$$m_{pi} = A(\Delta L)\rho \tag{2.31}$$

$$k_{pi} = \frac{EA}{\Delta L} \tag{2.32}$$

$$C_{dp} = \frac{1}{50} C_{dpi} \frac{EA}{C} \tag{2.33}$$

where,

$m_{pi}$ = pile mass at segment i, g or lb,
A = pile cross sectional area, $m^2$ or $ft^2$,
$\Delta L$ = pile length at segment i, m or ft,
$\rho$ = pile material density, $g/m^3$ or $lb/ft^3$,
$k_{pi}$ = pile spring stiffnes, kN/m or kip/ft,
E = pile material modulus of elasticity, $kN/m^2$ or $kip/ft^2$,
$C_{dp}$ = pile damping constant at pile segment i, kN-s/m or kip-s/ft,
$C_{dpi}$ = non-dimensionalized input value for pile, and
C = pile wave speed, m/s or ft/s.

### 2.5.5. Splice model

Splice model is included in WEAP for modeling cushion, helmet, and pile top. The splice model is represented by a slack ($d_{sl}$), a coefficient of restitution ($c_a$), and a round out deformation ($d_{sc}$). Referring to Figure 2.13, when the spring model is compressed, the force increases nonlinearly to $F_{lim}$ at a round out deformation and later increases linearly with a slope given by a nominal spring stiffness, k. When the model expanses during unloading, the force decreases linearly with a slope $k/c_a^2$. On the other hand, during the spring extension,

the spring stiffness develops only when it has extended beyond the slack distance ($d_{sl}$), and the spring force is always zero within the slack distance. Normally, a splice model is required when some forceless deformation is desired such as the mechanical splices of concrete piles.

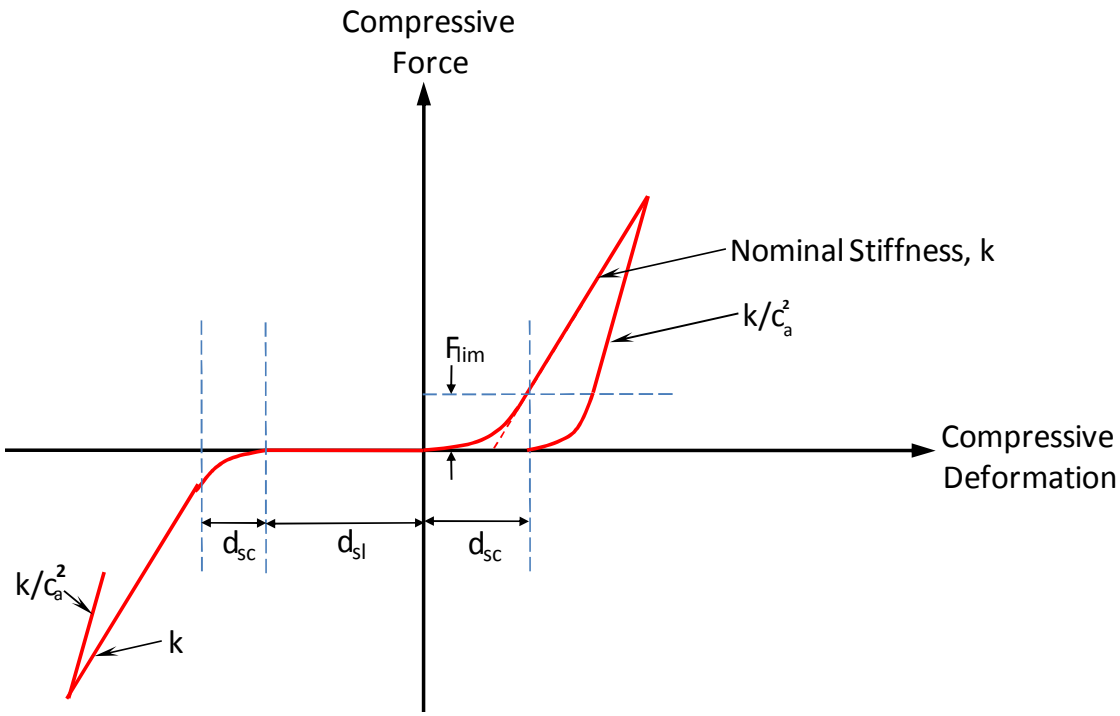


Figure 2.13: Force deformation curve for slack model (after Pile Dynamic Inc., 2005)

### 2.5.6. Soil model

WEAP used the Smith's approach to model the surrounding soil with springs and dashpots as shown in Figure 2.12. Quake and the damping factor are the two soil parameters that describe the soil model, and their estimates have been recommended by Hannigan et al. (1998) as listed in Table 2.5 for WEAP analysis.

Five soil damping models are available in WEAP. The standard Smith and Smith viscous damping models are the most common in practices. The remaining models are the Case non-dimensionalized viscous damping, Coyle and Gibson damping, and Rausche damping, and they are mainly used for research applications. The standard Smith damping

model calculates the dynamic soil resistance using Eq. (2.16), whereas the Smith viscous soil model replaces the static soil resistance ($R_s$) used in Eq. (2.16) with ultimate soil resistance ($R_u$) for dynamic soil resistance computation. The Smith viscous model is recommended for residual stress analysis because it produces damped pile motions after pile rebounds, especially when the static resistances are small (Pile Dynamic Inc. 2005). Also, this model is preferable for vibratory hammer because of the relative small velocities of vibratory driven piles. The Case non-dimensionalized viscous damping model computes the dynamic soil resistance at pile segment i using Eq. (2.34). The Coyle and Gibson approach uses Eq. (2.35) to compute the dynamic soil resistance. Because of numerical problems with Coyle and Gibson approach, Rausche et al. (1994) proposed Eq. (2.36) for dynamic soil resistance computation. The accuracies of these three methods are yet to be proven for different pile types, soil conditions and driving conditions.

$$R_{di} = J_{ci} v_i \sqrt{k_{pi} m_{pi}} \tag{2.34}$$

$$R_{di} = R_{si} J_{gi} v_i^N \tag{2.35}$$

$$R_{di} = R_{ai} J_{Ri} v_i^N \left(\frac{v_i}{v_{xi}}\right) \tag{2.36}$$

where,

$R_{di}$ = dynamic soil resistance, kN or kip,

$J_{ci}$ = Case damping factor, dimensionless,

$v_i$ = pile segment velocity, m/s or ft/s,

$k_{pi}$ = pile segment stiffness = $\frac{EA}{L}$, kN/m or kip/ft,

$m_{pi}$ = pile mass density, kN-s$^2$/m or kip-s$^2$/ft,

$R_{si}$ = static soil resistance, kN or kip,

$J_{gi}$ = Gibson damping factor with units of time over length to the 1/N power (refer to Table 2-14 in Coyle and Gibson (1970)), (s/ft)$^{1/N}$,

N = exponential power typically 0.2 for sand and 0.18 for clay, dimensionless

$R_{ai}$ = maximum activated static resistance, kN or kip,

$J_{Ri}$ = Rausche damping factor; converted from standard Smith damping factor

using Figure 5 in Rausche (1994), $(s/ft)^{1/N}$, and

$v_{xi}$ = maximum pile velocity, m/s or ft/s.

### 2.5.7. WEAP computation and analysis

As described in Section 2.4.2, the time increment adapted in WEAP is chosen as the smallest of the wave travel time increment through any hammer and pile segments. To ensure stability in WEAP computation, the minimum time is divided by a factor ϕ given by

$$\Delta t = \frac{\min\left(\frac{L_i}{C_i} \text{ or } \sqrt{\frac{m_i}{k_i}}\right)}{\phi} \tag{2.37}$$

where,

$\Delta t$ = time increment, s,

$L_i$ = pile length at segment i, mor ft,

$C_i$ = wave speed at pile segment i, m/s or ft/s,

$m_i$ = a lump segment mass, kN-$s^2$/m or kip-$s^2$/ft,

$k_i$ = hammer or driving system stiffness, kN/m or kip/ft, and

ϕ = a reduction factor greater than 1, WEAP default value is 1.6.

WEAP performs a pre-integration for velocity from acceleration and for displacement from velocity. The initial acceleration is taken as the gravitational acceleration of the hammer. WEAP computed the spring force by multiplying spring stiffness to relative displacements of the neighboring pile segments. Also, the dashpot force is calculated by multiplying pile damping factor to relative velocities of neighboring pile segments. Using Newton's Second law, the acceleration of a pile segment i at time step j is revised using the external resistance forces given by Eq. (2.38). Thereafter, the velocity and displacement are refined and all forces are recalculated. The computation will repeat until either the required iteration steps have exceeded or the convergence of top and bottom velocities are achieved.

$$a_{ij} = g_p + \frac{\left(F^t_{sij} + F^t_{dij} - F^b_{sij} - F^b_{dij} - R_{sij} - R_{sij}\right)}{m_i} \tag{2.38}$$

where,

$a_{ij}$ = acceleration at a pile segment i, m/s or ft/s,

$g_p$ = gravitational acceleration of the pile, m/s$^2$ or ft/s$^2$,

$F^t_{sij}$ = force at top spring on pile segment i, kN or kip,

$F^t_{dij}$ = force at top dashpot on pile segment i, kN or kip,

$F^b_{sij}$ = force at bottom spring on pile segment i, kN or kip,

$F^b_{dij}$ = force at bottom dashpot on pile segment i, kN or kip,

$R_{sij}$ = external resistance spring force at the end of previous time step, kN or kip,

$R_{dij}$ = External resistance dashpot force at the end of previous time step, kN or kip,

$m_i$ = pile segment mass density, kN-s$^2$/m or kip-s$^2$/ft.

WEAP computes the permanent set from the difference between maximum toe displacement and average toe quake, and the blow count is the inverse of permanent set given by Eq. (2.39) for the non-residual force analysis.

$$s = u_{mt} - q_{ave} = u_{mt} - \frac{\sum[R_{ui} q_i]}{R_{ut}} = \frac{1}{B_{ct}} \tag{2.39}$$

where,

$s$ = permanent set, m/blow or ft/blow,

$u_{mt}$ = maximum toe displacement, m or ft,

$q_{ave}$ = average quake, m or ft,

$q_i$ = individual quake, m or ft,

$R_{ui}$ = individual ultimate resistance, kN or kip,

$R_{ut}$ = total ultimate resistance, kN or kip, and

$B_{ct}$ = blow count, blow/m or blow/ft.

WEAP performs residual stress analyses (RSA) and allows the input of the number of trial iterations. Residual stress happens when the surrounding soil exhibits skin friction forces on a pile. Residual stress usually occurs on long and flexible piles with large toe quakes. However, little studies have been done on using RSA and it has been proven only

for monotube piles. Furthermore, RSA cannot be performed together with two-pile analysis, two pile toe analysis, vibratory analysis, and on piles involving slacks. Likins et al. (1996) suggested that RSA is useful for piles with high blow count and not recommended for piles with easy driving situations. Nevertheless, RSA provides better approximations than the traditional Smith's method on piles with residual forces.

### 2.5.8. Soil profile input procedures

Soil type based method (ST) and SPT N-value based method (SA) are the two soil profile input procedures customized in WEAP, which yield a rough estimate of static soil resistance. In addition, three other procedures: (1) Driven program developed by the Federal Highway Administration (FHWA) FHWA; (2) Iowa Blue Book (Iowa DOT steel pile Design Chart); and (3) the Iowa DOT current procedure are enumerated here. Table 2.6 summarizes the five soil profile input procedures with respect to different soil types.

The soil type based method (ST) simplifies the soil resistance calculation and aids in the input process for both bearing graph and driveability analyses in WEAP. The soil parameters used in the analysis are based on the Bowles (1996) and Fellenius (1991) recommendations as shown in Table 2.7 and Table 2.8 for non-cohesive soils and cohesive soils, respectively. This method uses the β-method, an effective stress method, to estimate the unit shaft and toe resistances for non-cohesive soils. However, a modified α-method, a total stress method, is used to predict the unit shaft and toe resistances for cohesive soils.

The SPT N-value based method (SA) is based on soil types, soil unit weights, and SPT uncorrected N-values, which are limited to 60. The correlation between all these input soil parameters can be referred to Bowles (1988) as shown in Table 2.9 and Table 2.10 for granular soils and cohesive soils respectively. Table 2.6 shows that the unit shaft resistance for sands, gravels and clays can be calculated based on the basic theory of soil mechanics given by Eq. (2.40). The toe unit resistances for sands, gravels and clays are calculated based on SPT uncorrected N-value. In addition, Bjerrum-Borland β-method is used to calculate

Table 2.6: Summary of static analysis methods using five soil input procedures

| Options | Soil Types | | | | | | | |
|---|---|---|---|---|---|---|---|---|
| | Sand (Non-cohesive, drained) | | Silt (Non-cohesive, drained) | | Silt (Cohesive, drained) | | Clay (Cohesive, undrained) | |
| | Unit Shaft | Unit Toe | Unit Shaft | Unit Toe | Unit Shaft | Unit Toe | Unit Shaft | Unit Toe |
| ST (Soil Type Based Method) | β-method (Esrig and Kirby 1979) | | β-method (Esrig and Kirby 1979) | | Modified α-method based on unconfined compressive strength | | Modified α-method based on unconfined compressive strength | |
| SA (SPT N-Value Based Method) | $k_o \tan(\delta)\ \sigma'_v \leq 250$ kPa | 200 N ≤ 12000 kPa | Bjerrum-Borland β-method (Based on Fellenius 1996 linear interpolation of β) | $N_t\ \sigma'_v \leq$ 6000 kPa ($N_t$ from Fellenius 1996) | Bjerrum-Borland β-method (Based on Fellenius 1996 linear interpolation of β) | $N_t\ \sigma'_v \leq$ 6000 kPa ($N_t$ from Fellenius 1996) | $k_o \tan(\delta)\ \sigma'_v \leq 75$ kPa | 54 N ≤ 3240 kPa |
| DRIVEN (FHWA, Mathias and Cribbs, 1998) | Nordlund (1963,1979) Thurman (1964) | Nordlund/ Thurman limited by Meyerhof (1976) | Nordlund (1963,1979) Thurman (1964) | Nordlund/ Thurman limited by Meyerhof (1976) | α-method (Tomlinson 1971) | $9S_u$ (Tomlinson 1971) | α-method (Tomlinson 1971) | $9S_u$ (Tomlinson 1971) |
| Blue Book (Iowa DOT Design Chart ) | Meyerhoff's semi-empirical method | Wave Equation Concept Using SPT N-values | Meyerhoff's semi-empirical method | Wave Equation Concept Using SPT N-values | α-method (Tomlinson 1971) | Wave Equation Concept Using SPT N-values | α-method (Tomlinson 1971) | Wave Equation Concept Using SPT N-values |
| Iowa DOT current practice | Used SPT N-values and variable pile profile option in the WEAP | | | | | | | |

shaft unit resistances, and Fellenius (1996) method is used to calculate the toe unit resistances for silts.

$$q_s = k_o \tan(\delta)\sigma'_v \tag{2.40}$$

where,

$q_s$ = unit shaft resistance, kN/m$^2$ or kip/ft$^2$,

$k_o$ = earth pressure coefficient at rest, dimensionless,

$\delta$ = pile-soil effective friction angle ($\phi'$) degree, and

$\sigma'_v$ = effective vertical static geotechnical stress, kN/m$^2$ or kip/ft$^2$.

Table 2.7: Soil Parameters for non-cohesive soils

| Soil Type | SPT N-value | Friction Angle (Degree) | Unit Weight (kN/m³) | Beta coefficient, β | Toe bearing coefficient, $N_t$ | Limit Unit Shaft Resistance, $q_s$ (kPa) | Limit Unit Toe Resistance, $q_t$ (kPa) |
|---|---|---|---|---|---|---|---|
| Very Loose | 2 | 25 - 30 | 13.5 | 0.203 | 12.1 | 24 | 2400 |
| Loose | 7 | 27 – 32 | 16.0 | 0.242 | 18.1 | 48 | 4800 |
| Medium | 20 | 30 - 35 | 18.5 | 0.313 | 33.2 | 72 | 7200 |
| Dense | 40 | 35 - 40 | 19.5 | 0.483 | 86.0 | 96 | 9600 |
| Very Dense | 50+ | 38 - 43 | 22.0 | 0.627 | 147.0 | 192 | 19000 |

Table 2.8: Soil Parameters for cohesive soils

| Soil Type | SPT N-value | Unconfined compressive strength, $q_u$ (kPa) | Unit Weight (kN/m³) | Limit Unit Shaft Resistance, $q_s$ (kPa) | Limit Unit Toe Resistance, $q_t$ (kPa) |
|---|---|---|---|---|---|
| Very Soft | 1 | 12 | 17.5 | 3.5 | 54 |
| Soft | 3 | 36 | 17.5 | 10.5 | 162 |
| Medium | 6 | 72 | 18.5 | 19 | 324 |
| Stiff | 12 | 144 | 20.5 | 38.5 | 648 |
| Very Stiff | 24 | 288 | 20.5 | 63.5 | 1296 |
| Hard | 32+ | 384+ | 19 – 22 | 77 | 1728 |

Table 2.9: Empirical values for □, $D_r$, and γ of granular soils based on corrected N-value

| Description | Very Loose | Loose | Medium | Dense | Very Dense |
|---|---|---|---|---|---|
| Relative Density, $D_r$ | 0 - 0.15 | 0.15 - 0.35 | 0.35 - 0.65 | 0.65 - 0.85 | 0.85 - 1.00 |
| Corrected N-values | 0 - 4 | 4 - 10 | 10 - 30 | 30 - 50 | 50+ |
| Approximate frictional angle, ϕ | 25 - 30˚ | 27 - 32˚ | 30 - 35˚ | 35 - 40˚ | 38 - 43˚ |
| Approximate moist unit weight, γ (kN/m³) | 11 – 15.7 | 14 – 18 | 17.3 – 20.4 | 17.3 – 22 | 20.4 – 23.6 |

Table 2.10: Empirical values for $q_u$ and γ of cohesive soils based on uncorrected N-value

| Description | Very Soft | Soft | Medium | Stiff | Very Stiff | Hard |
|---|---|---|---|---|---|---|
| Unconfined compressive strength, $q_u$ (kPa) | 0 – 24 | 24 – 48 | 48 – 96 | 96 – 192 | 192 – 384 | 384+ |
| Uncorrected N-values | 0 - 2 | 2 - 4 | 4 - 8 | 8 - 16 | 16 - 32 | 32+ |
| Saturated unit weight, γ (kN/m³) | 15.8 – 18.8 | 15.8 – 18.8 | 17.3 – 20.4 | 18.8 – 22 | 18.8 – 22 | 18.8 – 22 |

DRIVEN program generates the entire soil profile of a full pile depth and creates an input file for WEAP analysis. It requires the soil unit weight for all soil types, which are obtained either from laboratory soil tests or from Table 2.9 and Table 2.10 for granular soils and cohesive soils, respectively. Furthermore, SPT N-value and undrained shear strength ($S_u$) are required for defining the granular soil strength and cohesive soil strength respectively. The undrained shear strength ($S_u$) is estimated either from Cone Penetration Test (CPT) or by taking half of the unconfined compressive strength ($q_u$) given in Table 2.8. General pile adhesion for cohesive soils after Tomlinson (1980) is selected. Next, the unit shaft and toe resistances are calculated based on the static analysis methods as listed in Table 2.6. The detailed descriptions of the DRIVEN program can be referred to the FHWA DRIVEN User's Manual written by Mathias and Cribbs (1998).

WEAP analysis based on the Iowa Blue Book method uses the Iowa DOT pile design charts found in the Iowa DOT LRFD Design Manual Section 6 under the website (URL://www.iowadot.gov/bridge/manuallrfd.htm) for determining the unit shaft ($q_s$) and unit toe ($q_t$) resistances. The Iowa Blue Book method initially applied the wave equation concepts to develop the end bearing chart and applied the Meyerhoff's semi empirical method and Tomlinson method to develop the shaft resistance chart. The charts obtained from the combination of these methods were adjusted to correlate with the static load test results performed during the past 30 years in Iowa. The unit shaft resistance is determined by dividing the friction value in kips per foot chosen from the design chart with corresponding to the width of the steel H-pile, the soil description and the SPT N-value with the perimeter of the boxed section of a steel H-pile. However, a coating perimeter for H section was assumed for calculating the unit shaft for sand or cohesionless soil. The total toe resistance in kips is determined by multiplying the unit end bearing value in ksi with the cross sectional area of the H-pile for any soil conditions, assuming soil plug does not occur in cohesive or clay soil.

Iowa DOT method uses the SPT N-values as the only soil parameter which is input into the WEAP's variable resistance distribution table with respect to the depth where the SPT N-values are taken. Static geotechnical analysis and driveability analysis cannot be performed because the SPT N-values are only served to define the relative and approximate stiffness of the soil profile. Nevertheless, the bearing graph analysis can be performed to estimate pile resistance.

### 2.5.9. Output options

The three WEAP analysis output options are (1) bearing graph calculation; (2) driveability analysis; and (3) Inspector's Chart. The first option is the most commonly used WEAP analysis. In the bearing graph calculation, ultimate pile resistance, hammer stroke, pile stresses are plotted as a function of hammer blow count. Figure 2.14 shows the sample output of the bearing graph analysis, which also lists the hammer type, dynamic soil parameters, pile information, and the soil skin friction distribution. Since the hammer blow

count is typically recorded during pile drivings, the pile responses can be estimated using this bearing graph. For instance, if 197 blows/m (60 blows/ft) of pile penetration is recorded, the ultimate pile resistance is estimated to be 1068 kN (240 kips), which is considered as the pile resistance estimated using WEAP for the Load Resistance Factor Design (LRFD) resistance factors calibration discussed in Section 2.7. In addition, the hammer stroke is expected to reach at least 2.9 m (9.6 ft) to achieve the 60 blow counts. The pile compressive and tensile stresses are expected to be 290 MPa (42 ksi) and 15 MPa (2.2 ksi), respectively, which provide the necessary information for comparison with the allowable driving stress limits listed in Table 2.2.

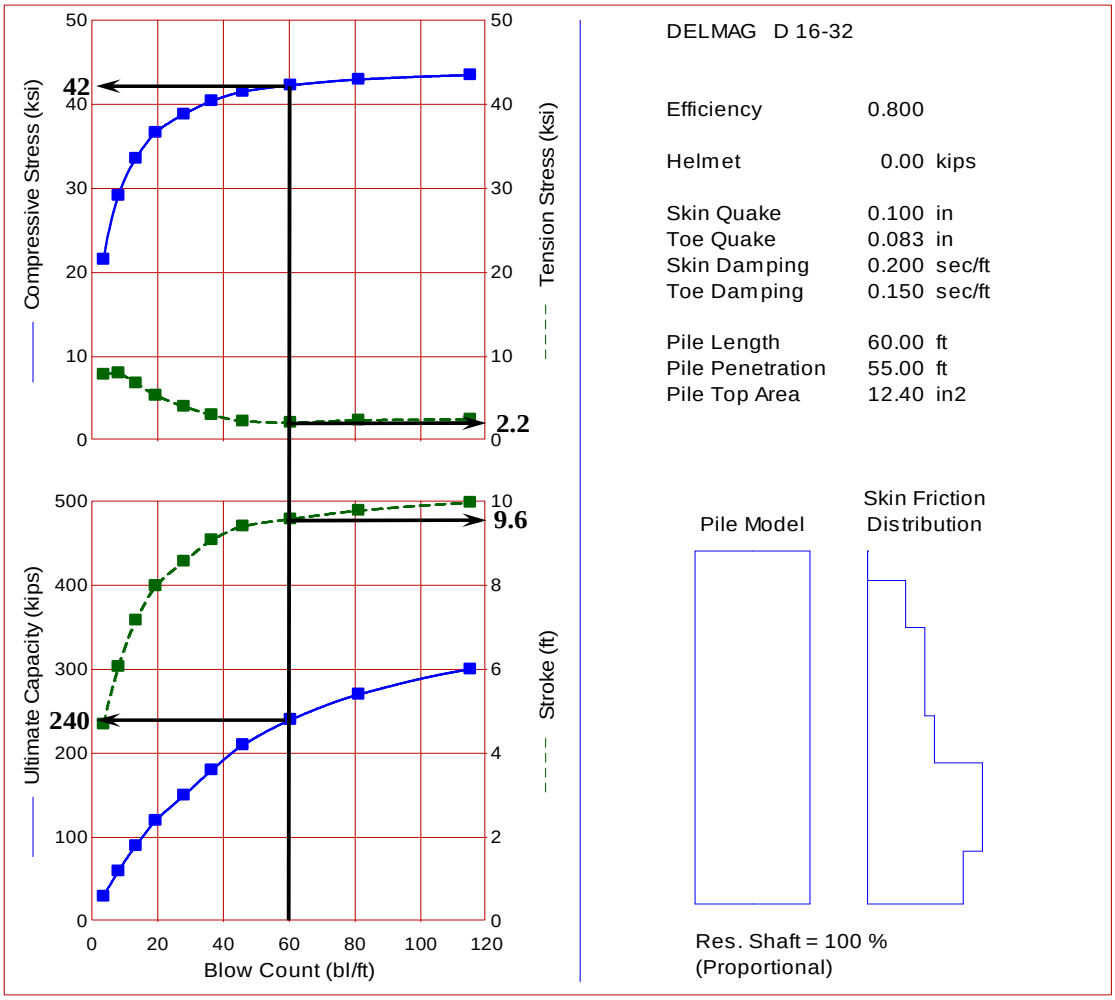


Figure 2.14: Sample output of WEAP bearing graph analysis

The second output option is the driveability analysis. This analysis calculates the static soil resistance, pile stresses, blow count, hammer performance, and soil distribution as a function of a pile penetration depth. The third output option is the Inspector's Chart, which calculates and plots the hammer strokes as a function of hammer blow counts at a desired pile resistance. It provides a flexible driving criterion to the field inspector to adjust the hammer stroke in order to satisfy the field requirements.

## 2.6. Reliability of Dynamic Analysis Methods

The reliability of dynamic analysis methods have been studied by many researchers, especially Pile Dynamic Inc., in the past 30 years. The dynamic analysis methods described here are PDA, CAPWAP and WEAP. All the reliability studies were correlated with static load test results based the Davisson's criterion. Paikowsky (2004) concluded that Davisson's criterion was the best failure resistance interpretation method for driven piles with diameters of 610 mm (2 ft) or less. The following simple guidelines described by Likins & Rausche (2004) and Hannigan & Webster (1987) are required to obtain reliable correlations between the dynamic and the static load test results.

1. A sufficient time is allowed before performing re-strike tests after EOD, so that the changes in soil resistance are stabilized.
2. Ideally, dynamic tests and static load tests should be carried out in a closer time period after EOD. Hannigan and Webster (1987) suggested that the best correlation between static load test and CAPWAP results can be achieved by limiting the time of dynamic re-strike testing to 24 to 48 hours prior to the static load test.
3. The test piles must experience sufficient displacement during dynamic testing in order to mobilize the full dynamic resistance. In fact, Pile Driving Contractors Association (PDCA) specification 102-07 (2007) suggested that the hammer used for re-striking shall be warmed up in order to achieve the required energy to mobilize the test piles. The maximum penetration required during re-strike shall be 75 mm (3-in) or the maximum total number of hammer blows required shall be 20, whichever occurs first. Hannigan and Webster (1987) believed that an order of 36 blows/m (11

blows/ft) or less is required to fully mobilize the soil resistance. Also, re-strike testing is recommended with a few hammer blows to minimize the loss of the effect of soil setup or soil relaxation.

4. A driving hammer shall have the sufficient impact force to mobilize the pile during the re-strike tests. Hannigan and Webster (1987) suggested the following guidelines for dynamic testing.

$$\text{Minimum impact force for steel piles} = \frac{\text{Ultimate Pile Resistance}}{0.8}$$

$$\text{Minimum impact force for concrete piles} = \frac{\text{Ultimate Pile Resistance}}{0.4}$$

$$1 < \frac{\text{Hammer Ram Weight}}{\text{Pile Weight}} < 3$$

In order to improve the reliability of dynamic analysis methods, Svinkins and Woods (1998) suggested the implementation of time dependent soil properties in estimating the pile resistance. They concluded that the time between static and dynamic tests has to be within a short duration at which the time difference should not exceed 1 to 2 days. They used the ratio of pile resistances obtained from dynamic and static tests as the main criterion for comparison and correlation studies. Lo et al. (2008) stated that the advantages of using the ratio are to avoid the total uncertainty in innate variability, effects of pile installation on soil properties, prediction model, and input parameters for resistance calculation using dynamic measurements. This ratio is treated as a random variable, and it is characterized by the mean and the coefficient of variation (COV). The COV is calculated by dividing standard of deviation by the mean. Lo et al. (2008) implied that dynamic analysis methods will tend to give a conservative pile resistance in a pile design and a conservative method is not necessary a better method from a probabilistic point of view. In addition, the degree of conservatism of a method and its related variability should be considered when establishing statistical resistance factors for limit state design of pile foundations.

Past correlation studies of the dynamic and static tests have been performed extensively starting from 1980's and the results are chronologically arranged and

summarized in Table 2.11, Table 2.12, and Table 2.13 for PDA, CAPWAP, and WEAP respectively. The piles tested included timber piles, screwed piles, steel H-piles, closed and open ended steel pipe piles, precast concrete square piles, drilled shafts, prestressed concrete cylinder spun piles, monotube piles, and composite steel, and concrete piles. The number of test database (N) used in the analyses varied from one (1) to as large as two hundred and six (206). The average mean ratio values of PDA, CAPWAP, and the WEAP are 1.118, 0.979, and 1.008 respectively. The results depict that dynamic analysis methods using PDA and WEAP tend to over-predict the pile resistance and CAPWAP tends to give conservative results. By comparing the mean values, WEAP provides the best dynamic method in estimating pile resistance with the closest mean ratio to one; PDA gives the relative less accurate results, and CAPWAP in between. In fact, many of the WEAP analyses were refined using CAPWAP soil parameters determined at BOR, and this could be the reason for generating good estimations from WEAP. Among the three methods, CAPWAP is the most popular dynamic analysis method in estimating the pile resistance and many studies were published to compare CAPWAP results with static load tests. Table 2.11 shows that the ratios for PDA method vary from 0.734 to 2.132. In addition, the ratios for CAPWAP as shown in Table 2.12 vary from 0.725 to 1.457. As for WEAP shown in Table 2.13, the ratios vary from 0.873 to 1.295. This study illustrates that PDA has a larger scatter prediction than CAPWAP and WEAP.

The average COV of all cases used in the PDA, CAPWAP, and the WEAP analyses are 0.200, 0.166, and 0.166 respectively. Generally, the average pile resistance estimation within each case is relatively more scatter for PDA than CAPWAP and WEAP. The range of COV for CAPWAP and WEAP are between 0.014 to 0.411 and 0.065 to 0.350, respectively, whereas the range for PDA is from 0.059 to 0.329. Furthermore, the COV for the PDA method increases from cases with single material piles such steel or concrete piles to composite piles as noticed by comparing Cases 4 and 11 with Cases 6 and 9. Similar observations are noticed in the CAPWAP and WEAP.

The relationship between soil profile and the mean ratios of the dynamic analysis

methods is obscure and it cannot be easily developed. The relationship is rather complicated because other factors such as pile types, time of static load tests, soil variability, and number of database used have some influences on the analyses.

Instead, the relationship between the time of static load tests performed and the mean ratio for CAPWAP is studied and the results are plotted in Figure 2.15. Unfortunately, similar analysis cannot be performed for PDA and WEAP which have insufficient database. As shown in Figure 2.15, the mean ratio of pile resistances predicted from the CAPWAP and the static load tests is drawn against the time difference between the static load test and the dynamic test. The lower and upper ranges of each case drawn together with the average day represented by solid square markers are best fitted with a dash polynomial line. Generally, the dash line is above zero, which indicates that all the dynamic tests using CAPWAP were performed before the corresponding static load tests were carried out. The profile of the dash polynomial line shows that the mean ratio shifts away from unity when the day delay increases. The result is consistent with the recommendation made by Svinkins and Woods (1998) to conducting the static load and dynamic tests within a close period of time, 1 to 2 days, in order to obtain a good correlation study.

In summary, based on these literature studies, dynamic analysis methods are concluded as reliable methods for pile resistance prediction and site verification purposes. Therefore, these methods are included in the latest AASHTO (2010) LRFD Bridge Design Specifications shown in Table 2.16.

Table 2.11: Correlation studies between PDA and static load tests

| Case | Reference | Pile type | Number of test database (N) | Soil profile | Days delay (ahead) of SLT after PDA | Ave. ratio of PDA and SLT | COV | Remarks |
|---|---|---|---|---|---|---|---|---|
| 1 | Holm et al. (1984) | 10.6 × 10.6 in precast concrete piles | 5 | Loose silty sand and sand | 21 to 28 | 1.283 | 0.24 | Used $J_c$ = 0.2; Settlement limit method was used as SLT failure criteria |
| 2 | Seitz J. M. (1984) | 2.3 ft, 4 ft, and 5 ft concrete bored piles | 3 | Medium dense sand above gravel | Some months | 2.132 | 0.194 | PDA performed some months after SLT; Use $J_c$ = 0.1 |
| 3 | Abe et al. (1990) | HP12 × 53 steel pile | 1 | Silt | N/A | 0.986 | N/A | Hammer ICE 640 was used for re-strike at one day after EOD |
| 4 | Wei at al. (1991) | Varies steel H-piles | 35 | Varies soil types (sandy silt, clayey silt or marine clay) | 4 to 33 | 0.876 | 0.09 | Sites in Singapore; The static load test is based on the elastic-plastic soil model that is similar to dynamic formula energy concept |
| 5 | York et al. (1994) | 14 in monotube piles | 5 | Glacial sand with fine gravel | Close | 0.734 | 0.123 | JFK airport project at New York; Ground water from 4 to 8 ft |
| 6 | Lee et al. (1996) | 14 to 19.7 in outside diameter soil-cement injected prestressed concrete spun cylinder piles | 10 | Water borne sand with gravel deposit | (20) to (2) =5 piles, 1 to 27 =5 piles | 1.435 | 0.319 | The cement filled was not considered in the CAPWAP analysis; Korea |

Table 2.11: (continue)

| Case | Reference | Pile type | Number of test database (N) | Soil profile | Days delay (ahead) of SLT after PDA | Ave. ratio of PDA and SLT | COV | Remarks |
|---|---|---|---|---|---|---|---|---|
| 7 | Lee et al. (1996) | 14 to 17.7 in prestressed concrete spun cylinder piles | 9 | Water borne sand with gravel deposit | (6) to (1) = 3 piles, 1 to 15 =6 piles | 1.304 | 0.150 | |
| 8 | Lee et al. (1996) | Three 20 in and one 24 in diameter Steel cylinder piles | 4 | Water borne sand with gravel deposit | 4 to 11 | 1.310 | 0.171 | |
| 9 | McVay et al. (2000) | Mixture of concrete and steel piles | 48 (EOD) 42 (BOR) | Varies soil types | N/A | 0.744 (EOD) 0.965 (BOR) | 0.329 (EOD) 0.322 (BOR) | Florida perspective |
| 10 | Long et al. (2002) | HP12 × 53 steel pile | 1 | Six soil layers from 23 ft silty clay to 20 ft sandy till with till below | 0<br>(15) | 1.077<br>0.815 | N/A<br>N/A | SLT 22 days after EOD |
| 11 | Sellountou and Roberts (2007) | 14 in square precast prestressed concrete piles | 3 | 13 ft sandy clay on 10 ft silty sand and 75 ft stiff clay/sandy clay | (180) | 0.870 | 0.059 | Piles were driven into mainly clay and sandy clay at Louisiana; BOR performed 6 months after SLT |
| | | | | | Average | 1.118 | 0.200 | |

Table 2.12: Correlation studies between CAPWAP and static load tests

| Case | Reference | Pile type | Number of test database (N) | Soil profile | Days delay (ahead) of SLT after CAPWAP | Ave. ratio of CAP-WAP and SLT | COV | Remarks |
|---|---|---|---|---|---|---|---|---|
| 1 | Goble et al. (1980) | Mostly closed end steel pipe piles | 77 | All soil types | N/A | 1.010 | 0.168 | Test Piles pre-dominantly in Ohio |
| 2 | Holm et al. (1984) | 10.6 × 10.6 in precast concrete piles | 5 | Loose silty sand and sand | 7 | 0.996 | 0.128 | Driven into loose sand; Settlement limit method used as SLT failure criteria |
| 3 | Hannigan and Webster (1987) | 17.7 in square prestressed concrete piles | 2 | Carbonate Sand | Immediate ly after SLT | 1.001 | 0.057 | |
| 4 | Hannigan and Webster (1987) | 17.7 in square prestressed concrete piles | 1 | Sandy silt | 8 | 0.728 | N/A | |
| 5 | Hannigan and Webster (1987) | 10 in, 14 in, and 54 in steel pipe piles | 3 | Silty clay with fine sand | Close | 0.88 | 0.077 | |
| 6 | Hannigan and Webster (1987) | HP 10×42 steel pile | 1 | Silty clay | Close | 0.992 | N/A | |
| 7 | Denver and Skov (1988) | 10 x 10 in square concrete piles | 14 | Layers of sand and clay | Interpolat-ed to SLT time | Close to 1.0 | Close to 0.13 | The standard of deviation is 0.13 |
| 8 | Hunt and Baker (1988) | 14 in steel pipe pile | 2 | 7 ft sand fill, 33 ft silt/clay fill, 7 ft dense sand or gravel, 20 ft lacustrine, and 7 ft basal sand | N/A | 0.966 | 0.014 | Hammer efficiency and blow by PDA used in BOR analysis; Water level 6.5 to 10 in below |

Table 2.12: (continue)

| Case | Reference | Pile type | Number of test database (N) | Soil profile | Days delay (ahead) of SLT after CAP-WAP | Ave. ratio of CAP-WAP and SLT | COV | Remarks |
|---|---|---|---|---|---|---|---|---|
| 9 | Fellenius et al. (1989) | HP 12 × 63 steel pile | 2 | 20 ft earth fill, 66 ft silty clay, and 89 ft glacial deposit | (1) and (3) | 1.118 | 0.089 | |
| 10 | Abe et al. (1990) | 12 in diameter prestressed pile | 1 | Sandy and clayey silt | 0 | 1.024 | N/A | North Carolina. Conmaco 65E5 hammer |
| 11 | Ho and Weber (1991) | High strength steel H-pile (HP 14 × 14.5) | 1 | 16 ft Loose sandy clay to 33 ft medium dense silty sand to completely decomposed granite | 30 | 0.725 | N/A | |
| 12 | Likins et al. (1992) | 17.7 in solid prestressed concrete pile | 2 | 36 ft silty sand, 13 ft clay, and 36 ft silty clayey sand | 10 | 1.036 | 0.014 | Water table at 2 ft |
| 13 | Likins et al. (1992) | 24 in square prestressed concrete pile with 10.2 in diameter void | 2 | 36 ft silty sand, 13 ft clay, and 36 ft silty clayey sand | 13 | 0.941 | 0.032 | Water table at 2 ft |
| 14 | Likins et al. (1992) | 35 in square prestressed concrete pile with 22 in diameter void | 2 | 36 ft silty sand, 13 ft clay, and 36 ft silty clayey sand | 14 | 0.791 | 0.086 | Water table at 2 ft |

Table 2.12: (continue)

| Case | Reference | Pile type | Number of test database (N) | Soil profile | Days delay (ahead) of SLT after CAP-WAP | Ave. ratio of CAP-WAP and SLT | COV | Remarks |
|---|---|---|---|---|---|---|---|---|
| 15 | Paikowsky et al. (1994) | All pile types | 206 | All soil types | Any time | 0.732 | 0.390 | Based on all soil types and on any testing time of SLT and CAPWAP |
| | | All pile types | 109 | All soil types | BOR | 0.789 | 0.336 | Based on all soil types and CAPWAP BOR results |
| | | All pile types | 83 | Sand | BOR | 0.780 | 0.316 | Based on sand regions and CAPWAP BOR results |
| | | All pile types | 23 | Clay | BOR | 0.797 | 0.411 | Based on clay regions and CAPWAP BOR results |
| 16 | York et al (1994) | 14 in monotube piles | 5 | Glacial sand with fine gravel | Close | 0.888 | 0.077 | Using radiation damping model |
| 17 | Thendean et al. (1996) | Combination of steel and concrete piles from GRL database | 99 | Various soil types | ≤ 3 (59 piles) > 3 (40 piles) | 0.920 | 0.22 | Based on measured PDA BOR data |
| 18 | Likins et al. (1996) | Mixture of concrete piles, steel piles, a timber pile, and a monotube pile | 41 | Various soil types | (3) to 3 | 0.950 | 0.15 | Based on best match analysis and time ratio between 0.33 to 1.25 |

Table 2.12: (continue)

| Case | Reference | Pile type | Number of test database (N) | Soil profile | Days delay (ahead) of SLT after CAP-WAP | Ave. ratio of CAP-WAP and SLT | COV | Remarks |
|---|---|---|---|---|---|---|---|---|
| 19 | Lee et al. (1996) | 14 in to 20 in outside diameter soil-cement injected prestressed concrete spun cylinder piles | 10 | Water borne sand with gravel deposit | (20) to (2) = 5 piles, 1 to 27 =5 piles | 1.381 | 0.219 | The cement filled was not considered in the CAPWAP analysis; Korea |
| 20 | Lee et al. (1996) | 14 in to 18 in prestressed concrete spun cylinder piles | 9 | Water borne sand with gravel deposit | (6) to (1) = 3 piles, 1 to 15 = 6 piles | 1.309 | 0.199 | |
| 21 | Lee et al. (1996) | Three 20 in and one 24 in diameter Steel cylinder piles | 4 | Water borne sand with gravel deposit | 4 to 11 | 1.220 | 0.197 | |
| 22 | Liang and Zhou (1997) | HP10x42 and HP14x89 steel piles | 2 | Silty clay over till (HP10), Clayey sand over sand (HP14) | BOR | 1.111 | 0.293 | |
| 23 | Liang and Zhou (1997) | 12.6 in closed end pipe piles | 1 | Silty clay over till | BOR | 1.029 | | |
| 24 | Liang and Zhou (1997) | 12 in & 14 in prestressed concrete piles | 2 | Silty clay over till | BOR | 0.828 | 0.041 | |
| 25 | Cannon (2000) | 6.6 in tube with 27.6 in screw pile | 1 | Dense to medium sand | N/A | 0.964 | N/A | Sydney Int. Airport. |
| | | 8.6 in tube with 33.5 in screw pile | 1 | Weathered sandstone | Some months | 1.206 | N/A | Redcliff Hospital at Brisbane |

Table 2.12: (continue)

| Case | Reference | Pile type | Number of test database (N) | Soil Profile | Days delay (ahead) of SLT after CAP-WAP | Ave. Ratio of CAP-WAP and SLT | COV | Remarks |
|---|---|---|---|---|---|---|---|---|
| 26 | McVay et al. (2000) | Mixture of concrete and steel piles | 44 (EOD) 79 (BOR) | Varies soil types | N/A | 0.626 (EOD) 0.794 (BOR) | 0.350 (EOD) 0.347 (BOR) | |
| 27 | Fellenius and Altaee (2001) | Monotube piles | 1 | Fine to course, medium dense to dense glacial sand | 2 | 0.965 | N/A | New York |
| | | Steel taper tube piles | 1 | | 2 | 0.990 | N/A | |
| 28 | Long et al. (2002) | HP12 x 53 steel pile | 1 | Six soil layers from 7m silty clay to 6m sandy till with till below | 0 | 1.051 | N/A | |
| | | | | | (15) | 0.903 | N/A | SLT 22 days after EOD |
| 29 | Hussein et al. (2002) | 30 in square prestressed concrete pile with 18 in circular void | 1 | 8 ft fat clay, 48 ft coarse sand and hard mixture of clay, sand, shell and gravel. | 41 = EOD and (2) = BOR | 0.991 | N/A | Use super-position of CAPWAP end bearing from EOD and shaft resistance from BOR. Water table 7.6 ft |
| 30 | Likins and Rausche (2004) | 70 driven concrete piles, 46 driven steel piles, 23 drill shafts and flight augercast, and 4 others | 143 | All soil types | Vary | 0.993 | 0.165 | Combined database from all six Stresswave Conferences from 1980 to 2000 |
| 31 | Rausche et al. (2004) | 24 in steel pipe pile | 1 | Sandy clay over silty sand | Close | 1.457 | N/A | At Louisiana |
| 32 | Rausche et al. (2004) | 24 in prestressed concrete piles | 1 | Sandy silty clay over sandy clay | Close | 1.264 | N/A | At Louisiana |

Table 2.12: (continue)

| Case | Reference | Pile type | Number of test database (N) | Soil Profile | Days delay (ahead) of SLT after CAP-WAP | Ave. ratio of CAP-WAP and SLT | COV | Remarks |
|---|---|---|---|---|---|---|---|---|
| 33 | Rausche et al. (2004) | 16 in prestressed concrete piles | 3 | Clay over clayey sand | Close | 0.865 | 0.048 | At Louisiana |
| 34 | Rausche et al. (2004) | 14 in prestressed concrete piles | 1 | Silty clayey sand over silty clay | Close | 1.223 | N/A | At Louisiana |
| 35 | Fung et al. (2005) | Nine 12 in x 12 in x 10 lb/in and four 12 in x 12 in x 8.3 lb/in H-piles | 13 | Granite saprolites | N/A | 0.944 | 0.119 | Test locations in Hong Kong. |
| 36 | Alvarez et al. (2006) | 16 in auger pressure grouted displacement pile | 1 | N/A | N/A | 1.041 | N/A | Based on maximum measured resistance using embedded dynamic sensors modules |
| 37 | Sellountou and Roberts (2007) | 14 in square precast prestressed concrete piles | 3 | Mainly clay and sandy clay | (160) | 1.060 | 0.033 | At Louisiana |
| 38 | Lo et al. (2008) | Mostly 12 in x 12 in x 12.4 lb/in H-piles | 15 | Granite saprolites | N/A | 0.766 | 0.119 | Test locations in Hong Kong |
| | | | | | Average | 0.979 | 0.166 | |

Table 2.13: Correlation studies between WEAP and static load tests

| Case | Reference | Pile type | Number of test database (N) | Soil Profile | Days delay (ahead) of SLT after WEAP | Ave. Ratio of WEAP and SLT | COV | Remarks |
|---|---|---|---|---|---|---|---|---|
| 1 | Hunt and Baker (1988) | 14 in steel pipe pile | 11 | 2m sand fill, 10m silt/clay fill, 2m dense sand/gravel, 6m lacustrine, and 2m basal sand. | N/A | 0.995 | 0.082 | Hammer efficiency and blow by PDA used in BOR analysis. Water level 2 to 3m below. |
| 2 | Abe et al. (1990) | 12 in diameter prestressed pile | 1 | Sandy and clayey silt | 0 | 0.951 | N/A | North Carolina. Conmaco 65E5 hammer. |
| 3 | York et al (1994) | 14 in monotube piles | 5 | Glacial sand with fine gravel | Close | 0.982 | 0.065 | Based on adjusted input hammer efficiency from PDA. |
| 4 | Thendean et al. (1996) | Combination of steel and concrete piles from GRL database | 99 | Various soil types | ≤ 3 (59 piles)<br>> 3 (40 piles) | 1.16 | 0.35 | Based on adjusted WEAP analysis using measured PDA BOR data. |
| 5 | Svinkin (1997) | 24 in square prestressed concrete pile with 12 in diameter hollow center | 1 | Gray clay | 13 | 0.908 | N/A | |
| 6 | Long et al. (2002) | HP12 x 53 steel pile | 1 | Six soil layers from 7m silty clay to 6m sandy till with till below | 0<br>(15) | 1.295<br>0.901 | N/A<br>N/A | (22 days after EOD) |
| 7 | Widjaja (2006) | 19.7 in concrete spun pile | 1 | Clay and silt | Close | 0.873 | N/A | Water table 26.3 to 28 ft. Jakarta, Indonesia |
| | | | | | Average | 1.008 | 0.166 | |

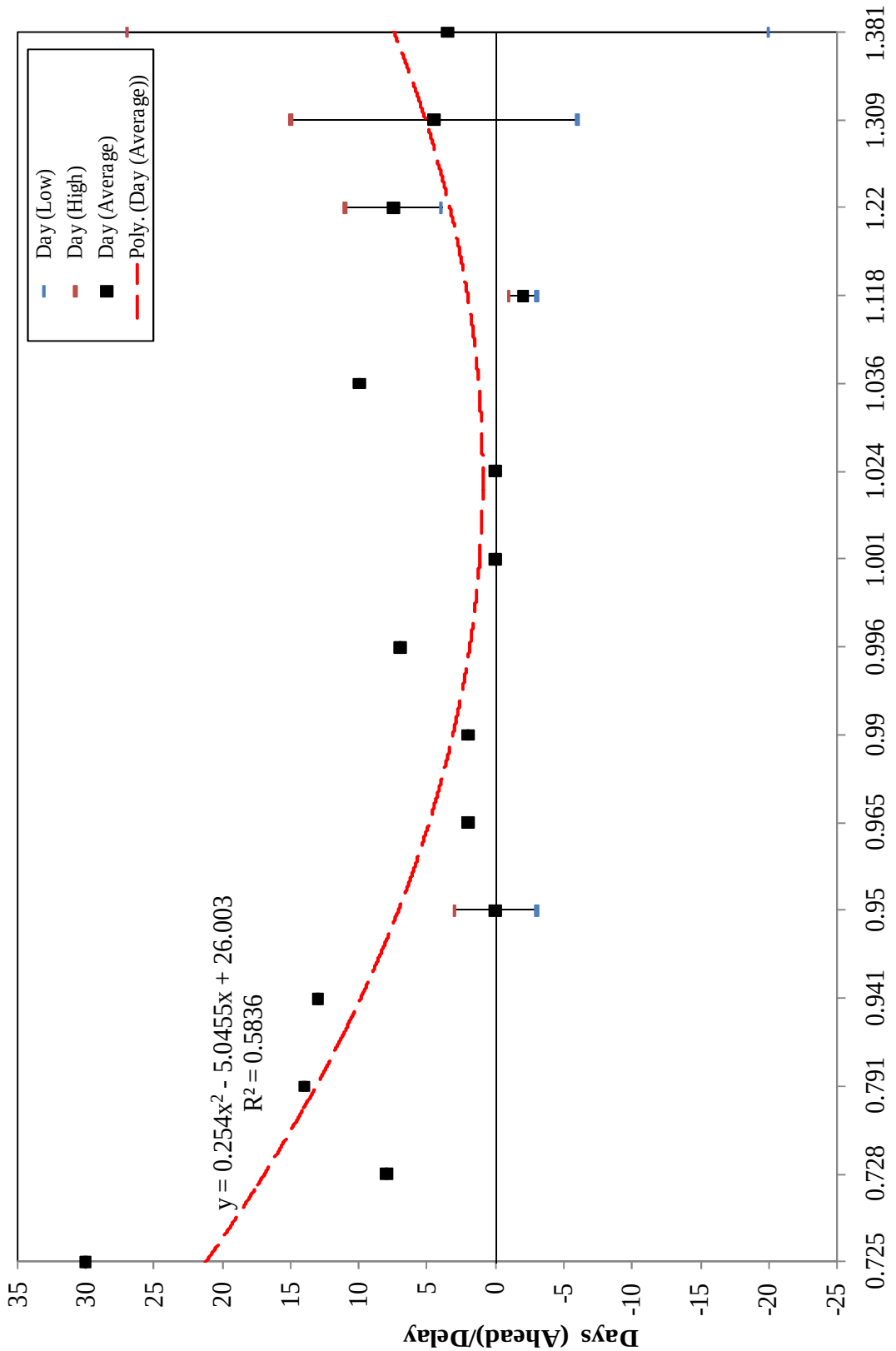


Figure 2.15: A graph illustrates the effect of mean ratios of CAPWAP and static load tests with the day delay or ahead

## 2.7. LRFD Resistance Factors for Dynamic Analysis Methods

### 2.7.1 Introduction

A study by Transportation Research Board (TRB) in 1987 concluded that the American Association of State Highway and Transportation Officials (AASHTO) standard specifications for highway bridges contain gaps and inconsistencies and did not use the latest design philosophy and knowledge, the limit state design or also known as Load and Resistance Factor Design (LRFD). The relative slow LRFD development in deep foundation is associated with the challenges of high variability in soil properties and the ability in predicting realistic pile resistance. The initial LRFD resistance factors calibration was carried out by Barker et al. (1991). A review of worldwide LRFD codes for deep foundations was performed by Goble (1999), and the short summary of each code was described by Paikowsky et al. (2004). LRFD gains acceptance over the conventional allowable stress design (ASD) in the recent several decades, because LRFD provides uniform level of safety and reliability by calibrating the resistance and load factors from actual bridge databases. In addition, a more uniform level of safety that should ensure superior bridge serviceability and long term maintainability. Most importantly, LRFD is believed as a more cost effective and efficient design method. Because of the LRFD's impact on the safety, reliability, and serviceability of National Bridge Inventory (NBI) which contains more than 590,000 bridges in the United States, the AASHTO in concurrence with the Federal Highway Administration (FHWA) has mandated that all bridges initiated after October 1, 2007, must be designed in according to the LRFD specification. According to the AASHTO Oversight Committee (OC) 2005 survey, sixteen (16) States have fully implemented LRFD, and the remaining States are in the transition of full implementation. In 2007, the AASHTO Oversight Committee (OC) updated that forty-four (44) of fifty (50) states will fully implement LRFD for all new bridges by October 1, 2007. In response to the recommendation by FHWA to improve the AASHTO LRFD specifications that have a better represent of local soil and local experience, the Iowa Department of Transportation (Iowa DOT) in cooperation with Iowa State University (ISU) began the LRFD foundation research project TR-573 in July 2007. The main objective of this research project is to examine current pile design and

construction procedures used by the Iowa DOT, and recommend changes and improvements to the current AASHTO LRFD bridge design specification. In addition to TR-573, dynamic analysis methods using PDA, CAPWAP, and WEAP for pile design and construction control were added in the research project TR-583 that allows the development and/or improvement of LRFD foundation design for dynamic analysis methods. The fundamental difficulties of developing LRFD resistance factors for dynamic analysis methods are correct identification of pile penetration, static resistance calculation, and time dependent pile resistance (Paikowsky et al., 2004). Many studies have been made on developing LRFD for deep foundations in the recent years, especially by Paikowsky et al. (2004) and Allen (2005), which were adopted in the recent AASHTO (2010) Bridge Design Specifications.

### 2.7.2 Reliability theory approaches

The principle of LRFD is to incorporate the margin of safety through the combination of load and resistance factors. The uncertainties involve in the load and resistance are quantified using statistical based methods to achieve a consistent level of reliability. Uncertainties in loads are small compared with soil resistances. This fundamental relationship can be given by Eq. (2.41). As noticed from this equation, partial safety factors are applied separately to the load (Q) and resistance (R).

$$\sum \eta_i \gamma_i Q_i \leq \varphi R \tag{2.41}$$

where,

$\eta_i$ = a modifier factor to account for effects of ductility, redundancy and operational importance,

$\gamma_i$ = load factor,

$Q_i$ = load, kN or kip,

$\varphi$ = resistance factor, and

R = ultimate resistance, kN or kip.

Figure 2.16 shows probability density functions (PDFs) for load (Q) and resistance (R). In principle, failure happens when the load exceeds the resistance, and the probability of failure ($p_f$) is related to the extent to which the two probability density functions overlap. By combining both the probability density functions, the margin of safety or the reliability index (β) can be expressed as shown in Figure 2.17. The reliability index (β) is defined as the number of standard deviations of the derived PDFs separating the mean safety margin and the nominal failure value of zero (Paikowsky et al., 2004), or simply the distance measured in standard deviations between the mean safety margin and the failure limit (Allen, 2005).

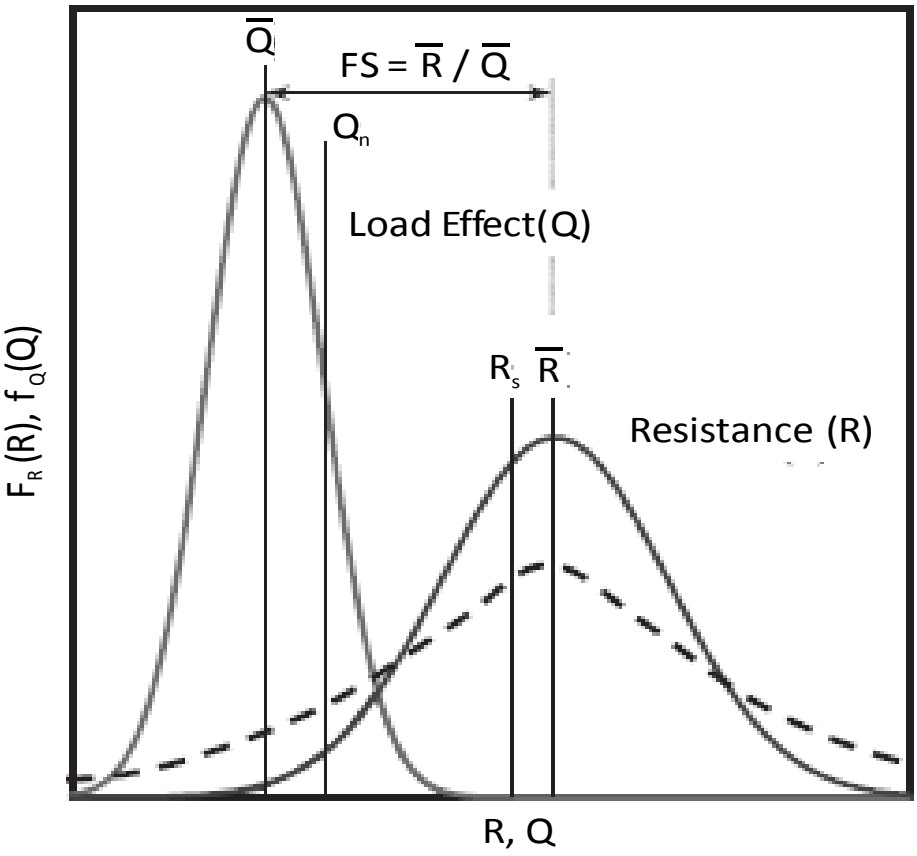


Figure 2.16: Probability density functions for load and resistance (Adapted after Paikowsky et al. 2004)

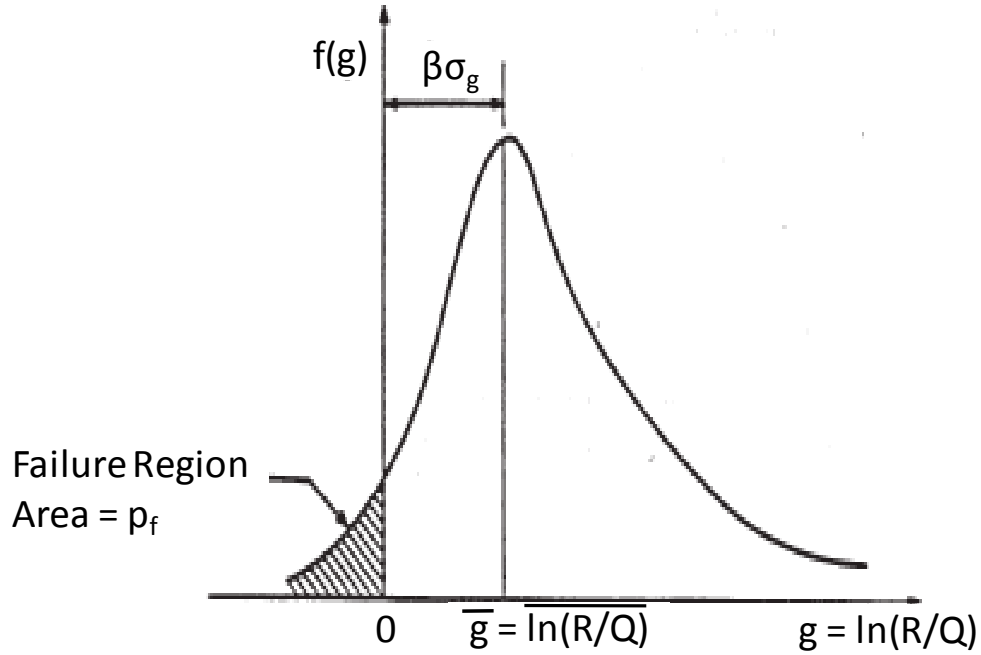


Figure 2.17: Combined PDFs that represents the safety margin and reliability index (Adapted after Paikowsky et al. 2004)

Two statistical methods are commonly used in the resistance and load factors calibration, and they are First-Order Second-Moment (FOSM) and First-Order Reliability Method (FORM). Existing AASHTO specifications are based on the FOSM analysis. A comparison in calculating resistance factors using both methods has been studied by Paikowsky et al. (2004). They concluded that FORM provides higher resistance factors than the FOSM by approximate 10%. Kim (2002) described that the load (Q) and resistance (R) are lognormally distributed, mutually independent, and ln(Q) and ln(R) are normally distributed. Thus, the mean value of limit state function g(Q,R) can be expressed by Eq. (2.42) and its standard of deviation ($\sigma_g$) can be expressed by Eq. (2.43). By definition, the reliability index ($\beta$) is the ratio of $\bar{g}$ over $\sigma_g$ given by Eq. (2.44). Replacing R with Eq. (2.41) and rearranging Eq. (2.44), the resistance factor ($\varphi$) is given by Eq. (2.45). Paikowsky et al. (2004) described that the probabilistic characteristics of the random variables for dead load ($Q_D$) and live load ($Q_L$) are based on the assumption used by current AASHTO and load combination for strength I as listed in Table 2.14**,** which are different from the initial factors proposed by Barker et al. (1991).

$$\bar{g} = \overline{\ln(R)} - \overline{\ln(Q)} = \ln\frac{\bar{R}}{\sqrt{1+COV_R^2}} - \ln\frac{\bar{Q}}{\sqrt{1+COV_Q^2}} = \ln\left[\frac{\bar{R}}{\bar{Q}}\sqrt{\frac{1+COV_Q^2}{1+COV_R^2}}\right] \quad (2.42)$$

$$\sigma_g = \sqrt{\sigma_{\ln(R)}^2 + \sigma_{\ln(Q)}^2} = \sqrt{\ln\left[(1+COV_R^2)(1+COV_Q^2)\right]} \quad (2.43)$$

$$\beta = \frac{\bar{g}}{\sigma_g} = \frac{\ln\left[\frac{\lambda_R R}{\lambda_D Q_D + \lambda_L Q_L}\sqrt{\frac{\left(1+COV_{Q_D}^2+COV_{Q_L}^2\right)}{\left(1+COV_R^2\right)}}\right]}{\sqrt{\ln\left[(1+COV_R^2)(1+COV_{Q_D}^2+COV_{Q_L}^2)\right]}} \quad (2.44)$$

$$\varphi = \frac{\lambda_R\left(\frac{\gamma_D Q_D}{Q_L}+\gamma_L\right)\sqrt{\left[\frac{\left(1+COV_{Q_D}^2+COV_{Q_L}^2\right)}{\left(1+COV_R^2\right)}\right]}}{\left(\frac{\lambda_D Q_D}{Q_L}+\lambda_L\right)e^{\left\{\beta_T\sqrt{\ln\left[(1+COV_R^2)\left(1+COV_{Q_D}^2+COV_{Q_L}^2\right)\right]}\right\}}} \quad (2.45)$$

where,

$\bar{R}$ = mean value of the resistance = $\lambda_R R$, kN or kip,

$\bar{Q}$ = mean value of the load = $\lambda_D Q_D + \lambda_L Q_L$, kN or kip,

$COV_R$ = coefficient of variation of resistance,

$COV_Q$ = coefficient of variation of load,

$\sigma_g$ = standard of deviation of function g,

$\beta$ = reliability index,

$\beta_T$ = target or desired reliability index,

$\lambda_R$ = resistance bias factor = Ratio of measured to predicted value for resistance,

$\lambda_D$ = dead load bias factor = Ratio of measured to predicted value for dead load,

$\lambda_L$ = live load bias factor = Ratio of measured to predicted value for live load,

$\gamma_D$ = dead load factor,

$\gamma_L$ = live load factor,

$Q_D$ = dead load, kN or kip, and

$Q_L$ = live load, kN or kip.

Table 2.14: AASHTO assumed random variables for dead load and live load

| Load (Q) | Load Factor ($\gamma$) | Load Bias ($\lambda$) | Coefficient of Variation ($COV_Q$) |
|---|---|---|---|
| Dead (D) | 1.25 | 1.05 | 0.1 |
| Live (L) | 1.75 | 1.15 | 0.2 |

The calibration of LRFD factors requires a proper selection of a set of target reliability levels that are represented by target reliability index and determine the probability of failure. An approximate relationship between the probability of failure and the target reliability index for lognormal distribution can be given by Eq. (2.46). However, this approximation is not accurate for $\beta$ below 2.5, which is at the mid zone of interested $\beta$ (from 2 to 3) for foundation design (Baecher, 2001). According to Barker et al. (1991), the target reliability index for driven piles can be reduced to a value between 2.0 and 2.5 especially for a group system effect. The initial target reliability index used by Paikowsky et al. (2004) is between 2 to 2.5 for pile groups and as high as 3.0 for single piles. After following the reviews, Paikowsky et al. (2004) developed their recommendations for the target reliability index as listed in Table 2.15.

$$p_f = 460e^{-4.3\beta_T} \tag{2.46}$$

where,

$p_f$ = probability of failure, and
$\beta_T$ = target reliability index.

Table 2.15: Recommended probability of failure and target reliability index

| Pile Support Type | No. of piles per cap | Probability of Failure, $p_f$ | Target Reliability Index, $\beta_T$ |
|---|---|---|---|
| Non-Redundant | Less than or equal 4 | 0.1 % | 3.00 |
| Redundant | 5 or more | 1.0 % | 2.33 |

Another parameter used in the Eq. (2.45) is the ratio of dead load to live load ($Q_D/Q_L$). The ratio shows little sensitivity to the resistance factor calculations, and a typical value of 2.0 is reasonably chosen by Paikowsky et al. (2004) and a value of 3.0 is chosen by Allen (2005). Despite the proper selection of the parameters, the efficiencies of the design methods are not reflected from the resistance factors. McVay et al. (2000) proposed an efficiency factor, which is defined by the ratio of the resistance factor to the bias factor ($\varphi/\lambda$), to better present the economic value of the design methods and to avoid the misconception

between the economy of the design methods and their high resistance factors.

The FORM approach, another statistical method, has been used in the LRFD calibration for structural design. To maintain a consistency in bridge design, FORM approach is urged by Nowak (1999) to be used in the LRFD resistance factors calibration for deep foundation. The failure events in deep foundation design can be associated with ultimate resistance and serviceability, and they are described by a limit state function $g(X_i)$, where the vector $X_i$ is defined as basic random variables representing resistances and loads. The following steps to determinate the reliability index ($\beta$) using this FORM method have been described by Assakkaf and Ayyub (1995) and Faber (2001).

1. The basic random variables are transformed into standardized normally distributed random variables using Eq. (2.47).
2. However, for non-normal distributed random variables, they are approximated by both original probability distribution functions as represented by Eq. (2.48) and original probability density functions as represented by Eq. (2.49). Combining Eqs. (2.48) and (2.49), the equivalent mean and standard deviation of the approximating normal distribution can be obtained using Eqs. (2.50) and (2.51), respectively.
3. Let the standardized normally distributed random variables ($X_i'^*$) in a function of reliability index ($\beta$) and a directional cosine ($\alpha_i^*$). The directional cosine ($\alpha_i^*$) is calculated using Eq. (2.52).
4. With $\alpha_i^*$, $\mu'_{X_i}$, and $\sigma'_{X_i}$ are now known, the Eq. (2.53) can be solved for the root reliability index ($\beta$).
5. Using the $\beta$ obtained from step 4, a new design point can be obtained from Eq. (2.54).
6. Repeat steps 1 to 5 until a convergence of $\beta$ is achieved.
7. Following the above procedures and for the given values of $\beta$, probability distributions and moments of the load variables (means and standard deviations), and the coefficient of variation for resistance, the resistance factor can be computed using Eq. (2.55).

$$X_i'^{*} = \frac{X_i^{*} - \mu_{X_i}}{\sigma_{X_i}} \tag{2.47}$$

$$F_{X_{ii}}(X_i^{*}) = \Phi\left(\frac{X_i^{*} - \mu'_{X_i}}{\sigma'_{X_i}}\right) \tag{2.48}$$

$$f_{X_{ii}}(X_i^{*}) = \frac{1}{\sigma_{X_i}}\varphi\left(\frac{X_i^{*} - \mu'_{X_i}}{\sigma'_{X_i}}\right) \tag{2.49}$$

$$\mu'_{X_i} = X_i^{*} - \Phi^{-1}\left[F_{X_i}(X_i^{*})\right]\sigma'_{X_i} \tag{2.50}$$

$$\sigma'_{X_i} = \frac{\varphi\left(\Phi^{-1}\left[F_{X_i}(X_i^{*})\right]\right)}{f_{X_i}(X_i^{*})} \tag{2.51}$$

$$\alpha_i^{*} = \frac{\left(\frac{\partial g}{\partial X_i}\right)_{*}\sigma'_{X_i}}{\sqrt{\sum_{i=1}^{n}\left[\left(\frac{\partial g}{\partial X_i}\right)_{*}\sigma'_{X_i}\right]^2}} \text{ for } i = 1,2,\ldots\ldots,n \tag{2.52}$$

$$g\left[\left(\mu'_{X_i} - \alpha^{*}_{X_i}\sigma'_{X_i}\beta\right),\ldots,\left(\mu'_{X_n} - \alpha^{*}_{X_n}\sigma'_{X_n}\beta\right)\right] = 0 \tag{2.53}$$

$$X_i^{*} = \mu'_{X_i} - \alpha^{*}_{X_i}\sigma'_{X_i}\beta \tag{2.54}$$

$$\varphi = \frac{\sum_{i=1}^{n}\gamma_i\mu_{Qi}}{\mu_R} \tag{2.55}$$

where,

$X_i'^{*}$ = a design point in reduced coordinate system,

$X_i^{*}$ = a design point in regular coordinate system,

$\mu_{X_i}$ = mean value of the basic random variables,

$\mu'_{X_i}$ = equivalent mean of the approximating normal distribution,

$\mu_{Qi}$ = mean value of the load variable,

$\mu_R$ = mean value of the resistance variable,

$\sigma_{X_i}$ = standard deviation of the basic random variables,

$\sigma'_{X_i}$ = equivalent standard deviation of the approximating normal distribution,

$F_{X_{ii}}(X_i^{*})$ = original probability distribution function of basic random variables in design coordinates,

$f_{X_{ii}}(X_i^{*})$ = original probability density function of basic random variables in

design coordinates,

$\Phi(\ )$ = cumulative distribution function of the standard normal distribution,

$\varphi(\ )$ = probability density function of the standard normal distribution,

$\beta$ = reliability index,

$\alpha_i^*$ = directional cosines for i = 1, 2,….., n, and

$\gamma_i$ = given set of load factor refer to Table 2.15.

### 2.7.3 Fitting to ASD approach

The fitting to allowable stress design (ASD) approach is always used as a reference whenever there is a fundamental change in either design philosophy or design specification format (Allen, 2005). Barker et al. (1991) developed resistance factors using the statistical data and calibration by fitting to ASD approach based on Strength I which focuses only on dead load ($Q_D$) and live load ($Q_L$). The general formula used to calculate a resistance factor by fitting to ASD is given by Eq. (2.56). Based on the current AASHTO recommended load factors as listed in Table 2.14 and a dead load to live load ratio of 3.0 chosen by Allen (2005), Eq. (2.56) can be simplified to Eq. (2.57)**.**

$$\varphi = \frac{\gamma_D \left(\frac{Q_D}{Q_L}\right) + \gamma_L}{\left(\frac{Q_D}{Q_L} + 1\right) FS} \tag{2.56}$$

$$\varphi = \frac{1.375}{FS} \tag{2.57}$$

where,

$\gamma_D$ = dead load factor,

$\gamma_L$ = live load factor,

$Q_D$ = dead load, kN or kip,

$Q_L$ = live load, kN or kip, and

FS = allowable stress design factor of safety.

### 2.7.4 Recommended LRFD resistance factors

According to Allen (2005), the initial source of the resistance factors in the AASHTO LRFD Design Specifications (AASHTO 2004), Section 10, was based on the recommendation reported by Barker et al. (1991). However, the latest AASHTO (2010) Interim Revisions presented the resistance factors for driven piles are based on the studies by Paikowsky et al. (2004) and Allen (2005). Table 2.16 was adapted from the revised AASHTO (2010) LRFD Bridge Design Specifications for dynamic analysis methods.

Table 2.16: LRFD resistance factors for driven piles (AASHTO, 2010)

| Condition/Resistance Determination Method | | Resistance Factor |
|---|---|---|
| Nominal Bearing Resistance of Single Pile – Dynamic Analysis and Static Load Test Methods, $\varphi_{dyn}$ | Driving criteria established by successful static load test of at least one pile per site condition and dynamic testing[(a)] of at least two piles per site condition, but no less than 2% of the production piles | 0.80 |
| | Driving criteria established by successful static load test of at least one pile per site condition without dynamic testing | 0.75 |
| | Driving criteria established by dynamic testing[(a)] conducted on 100% of production piles | 0.75 |
| | Driving criteria established by dynamic test[(a)], quality control by dynamic testing[(a)] of at least two piles per site condition, but no less than 2% of the production piles | 0.65 |
| | Wave equation analysis, without pile dynamic measurements or load test but with field confirmation of hammer performance | 0.50 |

(a)  Dynamic testing requires signal matching, and best estimates of nominal resistance are made from a restrike. Dynamic tests are calibrated to the static load test, when available.

As described in the AASHTO (2010) Section 10.5.5.2.3 for driven piles, if the resistance factors shown in Table 2.16 are to be applied to non-redundant pile groups as described in Table 2.15, the factors should be reduced by 20 % to reflect a higher target reliability index ($\beta_T$) of 3.0 or more. Furthermore, the resistance factors were determined mainly from load test results obtained on piles with diameters of 610 mm (2 ft) or less. A static or dynamic load test should be considered if piles larger than 610 mm (2 ft) diameter are used during design using static analysis methods. The combination of static and/or dynamic tests should be established based on the degree of site variability, which is characterized using field and laboratory exploration and test program. Noted that the

resistance factors (0.65 and 0.75) listed in Table 2.16 for dynamic testing without static load testing were developed for the beginning of restrike (BOR) conditions, and their applications for the end of driving (EOD) conditions may yield conservative results because of soil setup up. The 0.50 resistance factor for wave equation analysis is established based on calibration by fitting to past allowable stress design practice. Local experience or test results should be used in wave equation analysis to enhance the confidence of pile resistance estimation, and field verification of the hammer performance should be conducted.

### 2.7.5 Other LRFD resistance factors

Based on the calibration procedures described in Section 2.7.2, resistance factors for driven piles were calculated by other researchers based on upon their available regional database. Table 2.17 summarizes the resistance factors and the corresponding efficiency factors for the dynamic testing with signal matching procedure (CAPWAP) and the wave equation analysis.

Table 2.17: Other LRFD resistance factors for driven piles

| Dynamic Analysis Method | Reference | Source of Database | EOD or BOR | Resistance Factor, φ ($\beta_T$ = 2.33) | Efficiency Factor, φ/λ |
|---|---|---|---|---|---|
| Dynamic testing requires signal matching | Perez (1998) | Florida DOT | EOD<br>BOR | 0.73[(c)]<br>0.58[(c)] | 0.46<br>0.46 |
| | Paikowsky et al. (2004) | National | EOD<br>BOR | 0.64<br>0.65 | 0.40<br>0.56 |
| | Allen (2005) | Paikowsky et al. (2004) | BOR | 0.71[(a)] | n/a |
| | Abu-Farsakh et al. (2009) | Louisiana DOT | EOD<br>BOR (14 days) | 1.31[(b)]<br>0.55 | 0.36<br>0.44 |
| Wave equation analysis | Paikowsky et al. (2004) | National | EOD | 0.39 | 0.24 |
| | Transportation Research Board (2009) | Florida DOT | EOD | 0.35[(c)] | n/a |
| | Allen (2005) | Paikowsky et al. (2004) | EOD | 0.40 | n/a |

(a) □ Based on Monte-Carlo simulation method; (b) □ For Lousiana soft soil; (c) □ Based on $\beta_T$ = 2.50.

## 2.8. Pile Setup

### 2.8.1 Introduction

Pile setup refers to the increase in resistance of driven piles over time, especially piles embedded in cohesive soils. When a pile is driven, the surrounding soil is displaced primarily radially along the pile shaft and moves downward and radially below pile toe. As a result of this pile installation process, the surrounding soil is remolded and excess pore water pressure is generated. Randolph et al. (1979) stated that pile driving disturbs soil stress up to a distance about 20 pile radii, and the amount of excess pore water pressure can exceed the existing overburden geostatic stress at a region within one pile diameter. A research on closed-ended pipe piles performed by Pestana et al. (2002) revealed that the magnitude of excess pore water pressure decreases at an inverse relationship with the square of the distance from the pile. When healing of remolded soils and/or dissipation of the excess of pore water pressure occur, effective stress of the surrounding soil increases, which increases the shear strength and bearing resistance of the pile. Because of these mechanisms happen over a period of time depending on the rate of soil recovery and consolidation, the pile resistance increases as a function of time. Soderberg (1961) reported that the time of excess pore water dissipation is directly proportional to the square of the pile width and inversely proportional to the surrounding soil's horizontal coefficient of consolidation ($C_h$). Because soil disturbance and excess pore water pressure generation and dissipation occur primarily along the shaft, it is suggested that pile setup is primarily attributed to the increase in shaft resistance (Axelsson, 2002; Bullock, 1999; and Chow et al., 1998). However, experiment results relate pile setup to soil disturbance and pore water dissipation rarely exist.

Pile setup has become an important research topic, because the successful incorporation of setup in pile foundation designs contributes economic advantages to our civil infrastructure systems. A literature review on the effect of pile and soil on pile setup is summarized in the following sections. Furthermore, current methods available in literature to measure and estimate pile setup are described.

### 2.8.2 Effect of pile

It was reported by Camp and Parmar (1999) with focus on a stiff, overconsolidated cohesive calcareous soil that a displacement pile (such as a closed-ended pipe pile), which exerts greater disturbance to the surrounding soil than a low displacement pile (such as a steel H-pile), takes a longer time to fully gain its resistance (i.e., a slower setup rate). However, based on a database of pile static load and dynamic tests collected from literature, Long et al. (1999) found no clear evidence of difference in setup time between large displacement and low displacement piles driven into mixed and clay soil profiles. A report by Finno (1989) indicated that a closed-ended pipe pile generated higher excess pore water pressure than steel H-pile; however, the unit shaft resistances for both pile types matched after 43 weeks. It is anticipated that pre-stressed concrete piles exhibit larger setup than steel H-pile, which is due to a higher coefficient of friction along the soil-concrete pile interface as reasoned by Priem et al. (1989). Furthermore, more permeable wooden piles, which absorb water and allow faster dissipation of pore water pressure, have higher setup rate than other less permeable piles (Bjerrum et al., 1958 and Yang, 1956).

### 2.8.3 Effect of soil

Many research outcomes have confirmed the effect of different soil types on pile setup. Occurrence of pile setup has been recognized in both cohesive and cohesionless soils. In cohesive soils, Komurka et al. (2003) qualitatively explained that excess pore water pressure dissipates slowly and dictates the pile setup rate, which moderately relates to logarithmic nonlinear relationship (Zone 1), mainly relates to logarithmic linear relationship (Zone 2), and slightly involves aging mechanism (Zone 3) shown in Figure 2.18. Randolph et al. (1979) stated that the variation in soil stress around a pile after installation is independent of the soil's overconsolidation ratio (OCR). However, Whittle and Sutabutr (1999) indicated that reliable pile setup estimations for large diameter open-ended pipe piles depend on accurate measurement of OCR value and hydraulic conductivity. Compiling pile load test information published in literature, Long et al. (1999) found that piles embedded in soft clays experience more setup than in stiff clays. They noticed piles embedded in clay soil

experiencing setup by a factor of 1 to more than 6 of its initial resistance estimated immediately after installation, while piles in a mixed profile exhibited over a range between those for sand and those for clay. Although effect of soil on pile setup is apparent, necessary data to quantitatively estimate pile setup in terms of soil properties is rarely available.

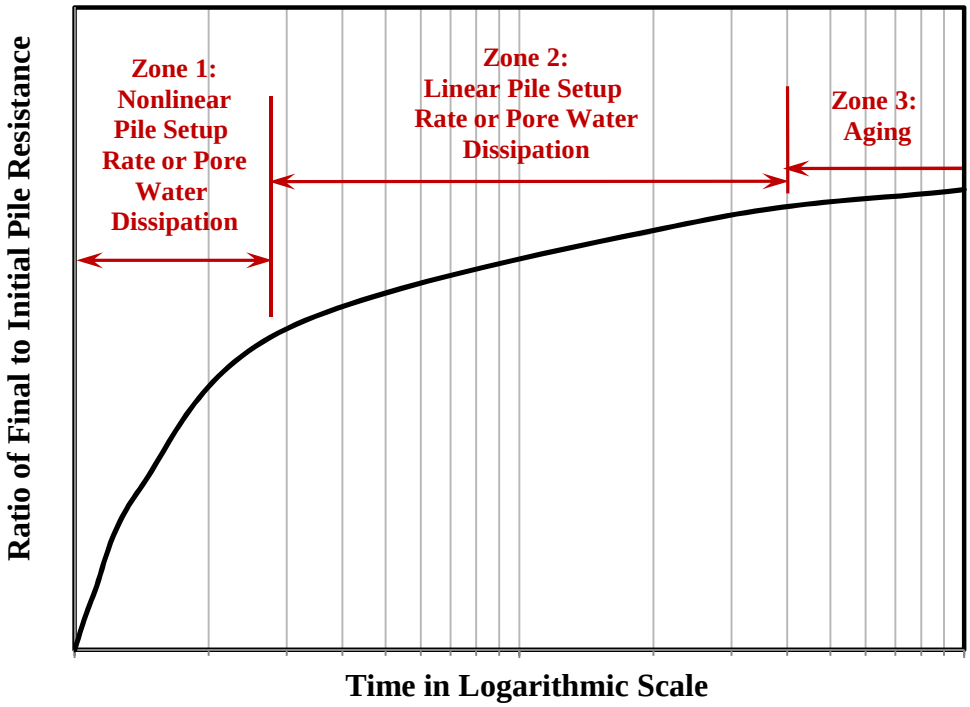


Figure 2.18: Idealized schematic of pile setup zones (after Komurka et al. 2003)

For the case of piles embedded in cohesionless soils, Komurka et al. (2003) stated that excess pore water pressure dissipates rapidly. As a result, pile setup occurs with a logarithmic linear relationship (Zone 2 in Figure 2.18) and mostly associates with aging in the soil (Zone 3 in Figure 2.18) (Axelsson, 2002). Aging refers to a time-dependent change in soil properties at a constant effective stress. The effect of aging increases soil shear modulus, stiffness, and dilatancy, and reduce soil compressibility (Axelsson, 1998; and Schmertmann, 1991). Research performed by Chow et al. (1998) on open-ended pipe piles driven into dense marine sand showed an 85% increase in shaft resistance during the interval between 6 months and 5 years after installation. They concluded pile setup was caused by the changes in the stress regimes created during pile installation and the creeping effect leading to the breakdown of arching around the pile shaft that allows radial stress to increase

close to the pile. Axelsson (2002) showed an average pile resistance increase of 40% per log cycle of time, while Koutsoftas (2002) reported a pile resistance increase of 25% to 50% in cohesionless soils. Based on an extensive research performed on 457 mm (18 in) square prestressed concrete piles, Bullock et al. (2005a) concluded that all pile segments embedded in different soil layers exhibited side shear setup with similar magnitude in both cohesive and cohesionless soils.

### 2.8.4 Measuring pile setup

At least two field determinations of pile resistance with one taken at the end of driving (EOD) and the other at a delayed time are required to measure pile setup. Static load tests and dynamic analysis methods can be used to measure pile setup. Because of the construction sequence in setting up a reaction system, a top-loaded static load test usually requires several days after pile installation before testing can be performed. Hence, this method is considered impractical to determine the initial resistance at EOD (Komurka et al., 2003). On the other hand, a static load can be applied at a pile toe using an Osterberg's cell. This method determines either the maximum end bearing or the maximum shaft resistance since both resistances are used as reactions to test each other. Since pile setup is mainly attributed to the increase in shaft resistance, it will be suitable to evaluate pile setup from bottom-loaded static load tests that fail in shaft resistance, if the pile is internally instrumented with strain gauges or tell-tales. However, this bottom-loaded static load test is not suitable for driven pile. Due to a time required for setting up the testing equipment and a high cost of performing this test, it is practically infeasible to measure pile setup.

On the other hands, dynamic analysis methods, such as PDA with CAPWAP as described in previous sections, are typically used to measure pile setup. PDA allows measurement of pile responses during driving, which is appropriate for determining the initial pile resistance at EOD. The gain in resistances is measured by performing multiple pile restrikes at various times after EOD, and the distribution of pile setup along the pile can be determined. The challenges with using dynamic analysis methods are (1) the ability of a driving hammer to fully mobilize the pile resistance (i.e., causing pile displacement to

mobilize the resistance along the pile-soil interface) for an accurate measurement of pile responses; (2) the use of representative dynamic soil parameters that greatly influence the pile setup quantifications; and (3) the performance of time consuming and inconvenient pile restrikes. In fact, AASHTO (2010) acknowledges that it is not feasible in practices to perform static load or dynamic restrike tests over a long period of time to quantify the pile setup.

### 2.8.5 Estimating pile setup

Pile setup can be estimated using empirical, analytical, or numerical methods. Eleven methods and their limitations are chronologically summarized in Table 2.18 and are explicitly depicted in the following paragraphs. Based on a large number of load test data on concrete piles driven into Shanghai clay soils, Pei and Wang (1986) observed a considerable pile setup and proposed Eq. (2.58) to estimate the pile resistance at any time (t) after EOD. This setup equation is purely empirical and does not incorporate any soil and pile properties. Furthermore, this method requires the determination of a maximum pile resistance ($R_{max}$) defined at 100% consolidation of the surrounding soil (i.e., complete dissipation of excess pore water pressure), which is usually difficult to estimate in practices.

$$\frac{R_t}{R_{EOD}} = 0.236[\log(t) + 1]\left(\frac{R_{max}}{R_{EOD}} - 1\right) + 1 \tag{2.58}$$

where,

$R_t$ = pile resistance at any time (t) after EOD, kN or kip,

$R_{EOD}$ = initial pile resistance estimated at EOD, kN or kip, and

$R_{max}$ = maximum pile resistance after completing soil consolidation, kN or kip.

Table 2.18: Summary of available methods for pile setup estimations

| Reference | Setup Equation or Method | Soil Type | Limitations |
|---|---|---|---|
| Pei and Wang (1986) | $\frac{R_t}{R_{EOD}} = 0.236[\log(t)+1]\left(\frac{R_{max}}{R_{EOD}}-1\right)+1$ | Shanghai clay | – Purely empirical<br>– Site specific<br>– No soil and pile properties<br>– Difficult to determine $R_{max}$ |
| Zhu (1988) | $\frac{R_{14}}{R_{EOD}} = 0.375S_t + 1$ | Shanghai clay | – Only predict pile resistance at 14$^{th}$ day<br>– No consolidation effect is considered |
| Skov and Denver (1988) | $\frac{R_t}{R_o} = A\log\left(\frac{t}{t_o}\right)+1$ | Clay, chalk, or sand | – Require restrikes<br>– Wide range and non-uniqueness of A parameter |
| Lukas and Bushell (1989) | $\Delta R = \sum_{i=1}^{n}\left[S_{a_i}(\text{long}) - S_{a_i}(\text{short})\right]\times A_s$ | Silty clay | – Challenge with determining correct adhesion factor (AF) unless load tests are performed over time |
| Svinkin (1996) | $R_t = 1.4\,R_{EOD}t^{0.1}$ (upper bound)<br>$R_t = 1.025\,R_{EOD}t^{0.1}$ (lower bound) | Glacial sandy soil | – Purely empirical<br>– No soil and pile properties |
| Titi and Wathugala (1999) | A general numerical procedure using (HiSS)-$\delta^*_{2i}$ soil model, strain path method and finite element nonlinear analysis. | Sabine clay | – Highly technical and complex for general applications by pile designers |
| Whittle and Sutabutr (1999) | A general numerical procedure using strain path model, MIT-E3 soil model, and finite element nonlinear analysis | Marine clay | – Highly technical and complex for general applications by pile designers<br>– Require detailed soil tests |
| Svinkin and Skov (2000) | $\frac{R_t}{R_{EOD}} = B[\log(t)+1]+1$ | General cohesive soil | – Require restrikes<br>– B parameter has not been extensively quantified<br>– No clear relationship between B and soil or pile properties. |
| Paikowsky et al. (2004) | Determine a suitable time for a pile restrike at when the pile achieves 75% of its maximum resistance | Clay and granular soil | – Does not estimate pile setup but suggests time of pile testing |
| Karlsrud et al. (2005) | $\frac{R_t}{R_{100}} = A\log\left(\frac{t}{t_{100}}\right)+1$ ;<br>$A = 0.1+0.4\left(1-\frac{PI}{50}\right)OCR^{-0.8}$ | Clay | – Assumed complete dissipation after 100 days is not true<br>– Not practical to use $R_{100}$ |
| Jeon and Rahman (2007) | A backpropagation neural network (BPNN) | All soils | – Dependent on quality of database<br>– Insufficient data |

Based on about 70 test piles at more than 20 sites in the coastal areas of East China, Zhu (1988) proposed a pile setup Eq. (2.59) in terms of cohesive soil sensitivity ($S_t$). This equation was developed to specifically estimate a pile resistance at 14$^{th}$ day ($R_{14}$), which is not always practical due to the inflexibility of the method to predict a pile resistance at any desirable time.

$$\frac{R_{14}}{R_{EOD}} = 0.375S_t + 1 \tag{2.59}$$

Based on data collected in Demark and Germany summarized in Table 2.19, Skov and Denver (1988) developed a pile setup Eq. (2.60) for three soil types: clay, chalk and sand based on case history Nos. 1, 3 and 4, respectively. Due to the limited pile test data, case history No. 2 was not selected. Using the pile resistances measured from static load tests and pile restrikes using CAPWAP, logarithmic lines were best fitted through the data points with the appropriate assumption of the initial reference times ($t_o$) of 1 day, 5 days, and 0.5 day for clay, chalk, and sand, respectively. Figure 2.19 shows that different soil conditions resulted in the pile setup relationship with different slopes represented by the pile setup parameter (A). It was found that piles embedded in chalk generated the highest A value of 5.0 while piles in clay and sand had A values of 0.6 and 0.2, respectively. Skov and Denver (1988) noted that the suggested values of $t_o$ and A were valid for these case histories, but they may be used in other cases with caution.

$$\frac{R_t}{R_o} = A\ \log_{10}\left(\frac{t}{t_o}\right) + 1 \tag{2.60}$$

where,

R = pile resistance at any time (t) after installation kN or kip,

$R_o$ = initial pile resistance estimated at time $t_o$, kN or kip,

A = pile setup parameter, and

$t_o$ = initial reference time.

Table 2.19: Summary of piling projects implemented by Skov and Denver (1988)

| Case | Location | Pile Type | Pile Length (m) | Soil Type | Hammer | No. of Restrikes | Delay of SLT (day) |
|---|---|---|---|---|---|---|---|
| 1 | Albory, Germay | 250×250 mm concrete piles | 19[(a)] and 21[(b)] | Clay | UDCOMB H5H | 3 | 29 |
| 2 | Hamburg, Germany | 762 mm ϕ steel pipe pile | 33.7 | Sand | MRB600[(c)] and Delmag D46-02[(d)] | 1 | 7 |
| 3 | Nykobing F, Denmark | 300×300 mm concrete piles | 11 | Chalk | BANUT | 6 | 14 |
| 4 | Hamburg, Germany | 350×350 mm concrete piles | 21 | Sand | UDCOMB H5H | 4 | 19 |

(a) – Piles selected for restrikes; (b) – Pile selected for a static load test; (c) – Hammer used during driving; and (d) – Hammer used during the restrike.

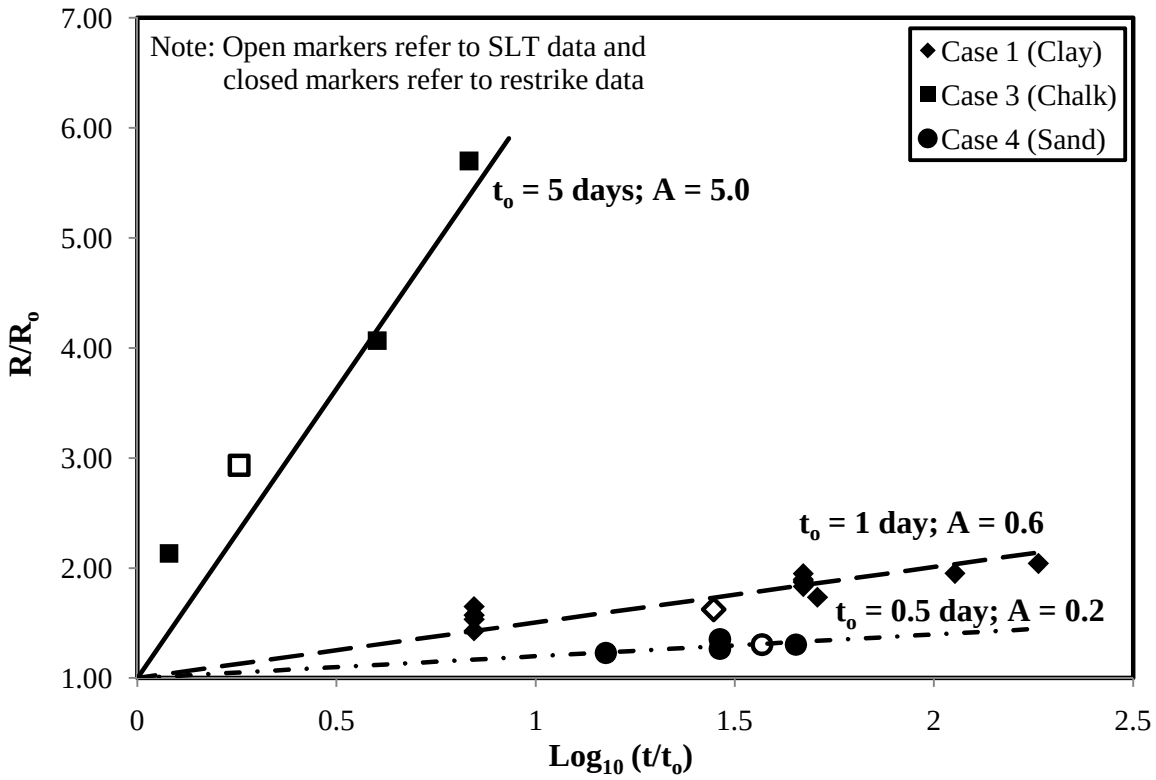


Figure 2.19: The development of Skov and Denver (1988) pile setup relationship

The determination of $t_o$ and A values is challenging, and they are usually assumed from literature, or back-calculated from experimental results (Komurka et al. 2003). Bullock (1999) noted that the setup parameter (A) is a function of the $t_o$ value, or vice-versa.

Komurka et al. (2003) noted that the $t_o$ value is a function of soil type and pile size. For instance, Camp and Parmer (1999) concluded that piles with larger diameter have larger $t_o$ values. Due to the variability of soil and pile types, Svinkin et al. (1994), Bullock et al. (2005a), and Yang & Liang (2006) reported A values ranging from 0.1 to 1.0. For practical application, Bullock et al. (2005b) recommended using a conservative and default value of A=0.1 for piles embedded in mixed soil profiles without performing restrikes. The non-uniqueness of the A value, which is usually determined from restrikes, has not been successfully correlated with soil properties, which limits the general application of this equation. In order to improve the estimation of setup using the estimated pile resistance at EOD, Long et al. (1999) and Svinkin and Skov (2000) respectively proposed the use of 0.01 day and 0.1 day for $t_o$.

Using pile load tests conducted at five separate sites in the Chicagoland area with four compression tests and one tension test, Lukas and Bushell (1989) estimated pile setup in clayey soils by first determining average undrained shear strength ($S_u$) along the pile. Next, they found that the soil-pile adhesion ($S_a$) at short period of time after driving can be approximated by the remolded shear strength ($S_r$), which is the ratio of $S_u$ and soil sensitivity ($S_t$). Based on the field test results, the long term $S_a$ values corresponding to the time between 30 and 80 days did not reach the measured $S_u$ value. For this reason, the long term $S_a$ value was suggested as the product of $S_u$ and an adhesion factor (AF). The increase in pile resistance ($\Delta R$) was estimated by summing the product of the gain in adhesion (difference between long-term and short-term $S_a$ values) and the corresponding segmental pile shaft surface area given by Eq. (2.61). They suggested the adhesion factors of 0.83 and 0.64 for stiff clay and soft to medium clay soils, respectively. The challenge with this approach is the determination of a suitable adhesion factor at a time of consideration unless field pile load tests are performed over a period of time.

$$\Delta R = \sum_{i=1}^{n} \left[ S_{a_i}(\text{long term}) - S_{a_i}(\text{short term}) \right] \times A_s \qquad (2.61)$$

where,

$\Delta R$ = increase in pile resistance, kN or kip,

i = pile segment i,

n = total n number of pile segments,

$S_{a_i}(\text{long term})$ = long term soil-pile adhesion = $S_u \times AF$, kN/m$^2$ or ksi,

AF = adhesion factor (0.83 for stiff clay and 0.64 for soft to medium clay),

$S_{a_i}(\text{short term})$ = short term soil-pile adhesion $\approx S_r$, kN/m$^2$ or ksi,

$S_r$ = remolded shear strength = $S_u/S_t$; kN/m$^2$ or ksi,

$S_t$ = soil sensitivity, and

$A_s$ = segmental pile shaft surface area, m$^2$ or in$^2$.

Using pile load test data in mostly glacial sandy soil, Svinkin (1996) presented the upper and lower boundaries to estimate the pile setup of driven piles in sandy soil given by Eq. (2.62). He found that the rate of pile setup with respect to the time (t) from the pile test data was generally the same (i.e., time t has the same power 0.1), but the setup coefficient ranged between 1.025 and 1.4. He also concluded that the pile setup in sandy soils was influenced by the level of ground water table. Similarly, this equation is purely empirical and no soil or pile properties were incorporated for general applications.

$$R_t = 1.4\, R_{EOD} t^{0.1} \text{ (upper bound)}$$
$$R_t = 1.025\, R_{EOD} t^{0.1} \text{ (lower bound)} \quad (2.62)$$

Titi and Wathugala (1999) presented a general numerical method for estimating the variation of pile resistance with time for driven friction piles embedded in saturated clay. The numerical analysis formulated the completed life stages of the pile, starting from pile installation, subsequent consolidation of surrounding soil to loading. This analysis was performed using Hierarchical Single Surface (HiSS)-$\delta^*_{2i}$ model, strain path method, and nonlinear analysis of porous media through a commercial finite element program ABAQUS. The (HiSS)-$\delta^*_{2i}$ model was adapted, based on the nonassociative anisotropic (HiSS)-$\delta^*_2$ model

developed by Wathugala and Desai (1991), to characterize soil behavior at the pile-soil interface and at the far-field. This model is capable of predicting very low effective stresses at the interface during and immediately after pile installation. The numerical simulation procedure is summarized in the following steps.

1. Estimate the strain fields induced in the soil around the pile due to pile installation using the principles of the strain path method presented by Baligh (1985).
2. Determine the effective stress paths for the soil particles around the pile during pile installation by integrating the constitutive equations of the (HiSS)-$\delta_{2i}^{*}$ model along the strain paths estimated in step 1.
3. Determine the equilibrated effective stresses and pore water pressures at the end of pile installation using the coupled theory of nonlinear porous media.
4. Simulate the subsequent soil consolidation around the pile using the finite element program ABAQUS.
5. Simulate the pile load tests at different times during soil consolidation around the pile using ABAQUS.

This numerical procedure was successfully verified based on field experiments conducted on 43.7 mm (1.7-in) and 76.2 mm (3-in) diameter instrumented pile segment models installed at Sabine Pass, Texas. Using the Sabine clay soil condition, Titi and Wathugala (1999) simulated the complete process of two full-stage 10 m (32.8 ft) long piles with diameters of 300 mm (11.8-in) and 500 mm (19.7-in), starting from pile installation, subsequent soil consolidation, and static load test. Although the proposed numerical procedure can be used for full-scale piles, no full-scale field pile load tests were available to validate the simulated responses. It is a highly technical and complex procedure that requires in depth understanding of soil mechanics and involves simulation using finite element methods. For this reason, it is practically infeasible for pile designers to estimate pile setup using this procedure.

Similar to the numerical procedure proposed by Titi and Wathugala (1999), Whittle

and Sutabutr (1999) proposed a numerical procedure to predict pile setup specifically for large diameter, open-ended steel piles used to anchor offshore platform. They used the strain path model presented by Baligh (1985) to characterize pile installation disturbance for a given pile geometry. MIT-E3 soil model formulated by Whittle and Kavvadas (1994) was used to predict effective stress-strain strength properties throughout pile installation and setup based on specified initial stress state, stress history, and material input parameters determined from one-dimensional consolidation tests and undrained triaxial shear tests. Subsequently, one-dimensional finite element model was used to simulate nonlinear coupled consolidation that occurs radially around the pile shaft. The proposed procedure for pile setup estimation was validated using (1) Piezo lateral stress (PLS) cell data on a closed-ended model pile in a clay deposit performed at the Saugus site reported by Azzouz and Morrison (1988); and (2) an instrumented model pile with 104 mm outside diameter and 6 m long embedded in a soft marine clay at Bothkennar site developed at Imperial College, London, by Lehane and Jardine (1994). Again, the numerical procedure is highly technical and complex which may not conveniently implemented by pile designers for practical pile setup estimations.

Maintaining the opportunity of using the logarithmic time scale by setting the reference time ($t_o$) given in Eq. (2.60) to 0.1 day, Svinkin and Skov (2000) presented an alternative setup Eq. (2.63) that accounts for the actual time elapses immediately after EOD and independent of $t_o$. Although this method has taken into an account the actual time after EOD ($t_{EOD}$) by allowing the reference pile resistance to be estimated at the EOD condition, the alternative soil dependent setup factor (B) value was not quantified in terms of any soil properties and relied on pile restrikes for pile setup estimation.

$$\frac{R_t}{R_{EOD}} = B\,[\log_{10}(t) + 1] + 1 \tag{2.63}$$

Using an extensive database of pile load tests and restrikes with CAPWAP analysis on closed-ended piles, Paikowsky et al. (2004) concluded that the actual increase in pile resistances measured using static load tests was much slower than that exhibited by the

dynamic analysis methods. They suggested that scheduling of construction or pile testing for setup measurement should consider the following recommended times in hours elapsed after the pile installation to reach 75% of the maximum resistance ($t_{75\%}$) in terms of a pile radius (r). For open-ended pipe piles, the pile radius (r) can be taken as one-half of the outside diameter. For a square shape pile, the radius (r) can be assumed as half of its side dimension. The depth from the outer edge of one flange to the outer edge of the other flange can considered the equivalent radius (r) for steel H-piles. This approach does not estimate pile setup, but it suggests when pile static or dynamic tests are performed to measure the increase in pile resistance at 75% of the maximum value.

1. <u>For piles embedded completely in clay:</u>
   For static testing purpose: $t_{75\%} = 1540r^2$
   For dynamic testing purpose: $t_{75\%} = 85r^2$

2. <u>For piles embedded in alternating soil conditions (granular and cohesive):</u>
   For dynamic testing purpose: $t_{75\%} = 39r^2$

Karlsrud et al. (2005) tried to relate soil properties to pile setup by incorporating the plasticity index (PI) and overconsolidation ratio (OCR) in Eq. (2.64), based on a Norwegian Geotechnical Institute (NGI) database that consisted of 36 well documented pile tests on steel pipe piles with outer diameters greater than 200 mm and supplemented results given in Flaate (1968). Referred to Eq. (2.64), the term $\left[0.1 + 0.4\left(1 - \frac{PI}{50}\right)OCR^{-0.8}\right]$ is a dimensionless resistance increase for a ten-fold time increase, and it is limited to a range between 0.1 and 0.5. Fellenius (2008) concluded that the reference resistance at 100 days ($R_{100}$) by assuming complete pore water dissipation at this time was not true and not feasibly determined in practices.

$$\frac{R_t}{R_{100}} = \left[0.1 + 0.4\left(1 - \frac{PI}{50}\right)OCR^{-0.8}\right]\log\left(\frac{t}{t_{100}}\right) + 1 \qquad (2.64)$$

Jeon and Rahman (2007) developed a backpropagation neural network (BPNN) to estimate the increase of ultimate pile resistance based on a database from a variety of case

studies available in literature. The database was established from a total of 96 field dynamic tests using PDA and CAPWAP. These 96 data points were randomly split into two groups. The first group of 73 points was used for training the neural network model, while the remaining 23 points were used for testing the model. Six input parameters, soil type, pile type, pile diameter, pile length, time after pile installation, and effective stress at pile tip, were selected in the development of the model. To demonstrate the accuracy of this method, pile resistances estimated by the neural network model were compared with those from four empirical relationships: Skov and Denver (1988), Svinkin (1996), Skov and Denver (1998) with Long et al. (1999) suggestion, and Svinkin and Skov (2000). The results of the comparison indicated that the neural network model provided a better prediction, verified based on a higher coefficient of determination ($R^2$) and a smaller root-mean squared error (RMSE). Jeon and Rahman (2007) acknowledged that additional data are needed in future for further training of the model to improve the quality of the pile setup estimation.

## 2.9. References

AASHTO. (2004). Interim Guidelines on Foundations, AASHTO LRFD Bridge Design SpecificationsAmerican Association of State Highway and Transportation Officials, Washington, D.C.

AASHTO. (2010). Interim Revisions, AASHTO LRFD Bridge Design Specifications. Customary U.S. Units, 5th Edition 2010, American Association of State Highway and Transportation Officials, Washington, D.C.

Abe, S., Likins, G. E. and Morgano, C. M. (1990). "Three Case Studies on Static and Dynamic Testing of Piles." Geotechnical News Magazine, Vol. 8, No. 4: Richmond, B. C., Canada, December, pp. 26-28.

Abu-Farsakh, M. Y., Yoon, S. M., and Tsai, C. (2009). Calibration of Resistance Factors Needed in the LRFD Design of Driven Piles. Louisiana Transportation Research Center, FHWA/LA.09/449, Federal Highway Administration, U.S. Department of Transportation, Washington, D.C.

Allen, T. M. (2005). Development of Geotechnical Resistance Factors and Downdrag Load

Factors for LRFD Foundation Strength Limit State Design, FHWA-NHI-05-052, Federal Highway Administration, U.S. Department of Transportation, Washington, D.C.

Alvarez, C., Zuckerman, B., Lemke, J., (2006). "Dynamic Pile Analysis Using CAPWAP and Multiple Sensors." ASCE GEO Congress: Atlanta, Georgia, February. (CD-ROM).

Assakkaf, I. A. and Ayyub, B. M. (1995). "Reliability-based Design of Unstiffened Panels for Ship Structures." Proceedings of the Joint ISUMA-NAFIPS'95, edited by Ayyub, IEEE-CS, April, College Park, MD, pp. 692-697.

Axelsson, G. (1998). "Long Term Setup of Driven Piles in Non-Cohesive Soils Evaluated from Dynamic Tests on Penetration Rods." Proceedings of the 1st International Conference on Site Characterization, Vol. 2, pp. 895-900.

Axelsson, G. (2002). "A Conceptual Model of Pile Setup for Driven Piles in Non-Cohesive Soil." Deep Foundations Congress, Geotechnical Special Publication, No. 116, Vol. 1, ASCE, Reston, Va., pp. 64-79.

ASTM D4945 (2008). Standard Test Method for High-Strain Dynamic Testing of Piles. American Society for Testing and Materials, 1916 Race St., Philadelphia, PA 19103.

Baecher, G. (2001). LRFD Deep Foundations Design. Contribution to a progress research report as part of Project NCHRP 24-17, (unpublished document).

Baligh, M. M. (1985). "Strain Path Method." Journal of Geotechnical Engineering, ASCE, Vol. 111, No. GT7, pp. 1108-1196.

Barker, R., Duncan, J., Rojiani, K., Ooi, P., Tan, C., and Kim, S. (1991). NCHRP Report 343: Manuals for the Design of Bridge Foundations. Transportation Research Board, National Research Council, Washington, D.C.

Beim, J., Grävare, C. J., Klingmüller, O., and Qing, L. D. (1998). "Standardization and Codification of Dynamic Pile Testing." Proceeding of the 7th International Conference and Exhibition on Piling and Deep Foundations, Deep Foundation Institute, 15th to 17th June, Palais, Ferstel, Vienna, Austria, pp. 2.2.1-2.2.8.

Bjerrum, L, Hansen, and Sevaldson. (1958). "Geotechnical Investigations for a Quay Structure in IIorton." Norwegian Geotechnical Publication, No. 28, Oslo.

Bowles, J. E. (1996). Foundation Analysis and Design. 5th Edition, McGraw-Hill Book Company, 1004.

Bullock, P. J. (1999). Pile Friction Freeze: A Field and Laboratory Study, Vol. 1. Ph.D. Dissertation, University of Florida, FL.

Bullock, P. J., Schmertmann, J. H., McVay, M. C., and Townsend, F. C. (2005a). "Side Shear Setup I: Test Piles Driven in Florida." Journal of Geotechnical and Geoenvironmental Engineering, 131(3), ASCE, pp. 292-300.

Bullock, P. J., Schmertmann, J. H., McVay, M. C., and Townsend, F. C. (2005b). "Side Shear Setup II: Results From Florida Test Piles." Journal of Geotechnical and Geoenvironmental Engineering, 131(3), ASCE, pp. 301-310.

Camp, W. M., and Parmar, H. S. (1999). "Characterization of Pile Capacity with Time in the Cooper Marl: A Study of the Applicability of a Past Approach to Predict Long-Term Pile Capacity." Transportation Research Record 1663, Paper No. 99-1381, Transportation Research Board, Washington, D.C., pp. 1-19.

Cannon J. G. (2000) "The Application of High Strain Dynamic Pile Testing to Screwed Steel Piles." In J. Beim & S. Niyama (Eds), Application of Stress-Wave Theory to Piles: Quality Assurance on Land and Offshore Piling: At Taylor & Francis, Balkema Rotterdam, September, pp. 393-398.

Cheney, R. S. and Chassie, R. G. (1993). Soils and Foundations Workshop Manual. 2nd Edition, Report No. HI-88-009, U. S. Department of Transportation, Federal Highway Administration, Office of Engineering, Washington, D.C., pp. 353-362.

Chiesura, Guido (1998). "Some Dynamic Parameters of Drilled Piles under Low-and High-Energy Tests. Correlation with the Static Pattern." Proceeding of the 7th International Conference and Exhibition on Piling and Deep Foundations, Deep Foundation Institute, 15th to 17th June, Palais, Ferstel, Vienna, Austria, pp. 1.5.1-1.5.11.

Chow, F. C., Jardine, R. J., Brucy, F., and Nauroy, J. F. (1998). "Effect of Time on Capacity of Pipe Piles in Dense Marine Sand." Journal of Geotechnical and Geoenvironmental Engineering, 124(3), ASCE, pp. 254-264.

Coduto, D. P. (2001). Foundation Design: Principles and Practices. 2nd Edition, Prentice Hall,

New Jersey.

Coyle, H. M, Bartoskewitz, R. E., and Berger, W. J. (1973). Bearing Capacity by Wave Equation Analysis – State of Art. Texas Transportation institute, Texas A & M University, TX, August.

Coyle, H. M. and Gibson, G. C. (1970). "Empirical Damping Constants for Sands and Clays." Journal of Soil Mechanics and Foundation Division, ASCE, Vol. 96, No. SM3, May, pp. 949-965.

Denver, H. and Skov, R. (1988). "Investigation of the Stress-Wave Method by Instrumented Piles." Proceedings of the 3rd International Conference on the Application of Stress-Wave Theory to Piles, BiTech Publisher, Ottawa, Canada, pp. 613-625.

Esrig, M. E. and Kirby, R. C. (1979). "Advances in General Effective Stress Method for the Prediction of Axial Capacity for Driven Piles in Clay." Proceedings, 11th Annual Offshores Technology Conference, pp. 437-449.

Faber, M. H. (2001). "Methods of Structural Reliability Theory – An Introduction." Swiss Federal Institute of Technology, Lectures Notes on Risk and Reliability in Civil Engineering, pp. 1-11.

Fellenius, B. H. (1991). Foundation Engineering Handbook. 2nd Edition. H.S. Fang, Editor, Van Nostrand Reinhold Publisher, NY.

Fellenius, B. H. (1996). Basics of Foundation Design. BiTech Publishers, Richmond, British Columbia, 134 p.

Fellenius, B. H. (1999). Using the Pile Driving Analyzer. Pile Driving Contractors Association, PDCA, Annual Meeting, San Diego, February 19-20, pp. 1-4.

Fellenius, B. H. (2008). "Effective Stress Analysis and Set-up for Shaft Capacity of Piles in Clay." From Research To Practice In Geotechnical Engineering, GSP No. 180, ASCE, pp. 384-406.

Fellenius, B. H. and Altaee, A. (2001). "Pile Dynamics in Geotechnical Practice – Six Case Histories." ASCE, International Deep Foundation Congress, An International Perspective on Theory, Design, Construction, and Performance, Geotechnical Special Publication GSP No. 116, Edited by M.W. O'Neill, and F.C. Townsend, Orlando, Florida, February 14-16, 2002, Vol. 2, pp. 619-631.

Fellenius, B. H., Riker, R. E., Brien, A. O., and Tracy G. R. (1989). "Dynamic and Static Testing in Soil Exhibiting Set-Up." The Journal of Geotechnical Engineering, Vol. 115, No. 7, July, Reston, VA, pp.984-1001.

Finno, R. J., Cosmao, T., and Gitskin, B. (1989). "Results of Foundation Engineering Congress Pile Load Tests." Predicted and Observed Axial Behavior of Piles. Geotechnical special Publication No. 23, ASCE, pp. 338-355.

Flaate, K. (1968). "Bearing Capacity of Friction Piles in Clay." NGF Stipend 1967-1968, Veglaboratoriet, Oslo.

Fung, W. K., Kwong, M. K., and Wing, C. T. (2005). "Observations of using the Energy Obtained from Stress Qwave Measurements in the Hiley Formula." Transactions, Hong Kong Institution of Engineers, 12, pp. 19-21.

Goble, G. G. and Likins, G. (1996). "On the Application of PDA Dynamic Pile Testing." Fifth International Conference on the Application of Stress-Wave Theory to Piles (STRESSWAVE 96): Orlando, FL, September, pp. 263-273.

Goble, G. G., Likins, G. E., and Rausche, F. (1975). Bearing Capacity of Piles from Dynamic Measurements. Final Report, Department of Civil Engineering, Case Western Reserve University, Cleveland, OH.

Goble, G. G. and Rausche, F. (1976). Wave Equation Analysis of Pile Driving – WEAP Program, U.S. Department of Transportation, Federal Highway Administration, Offices of Research and Development, Washington, D.C., Vols. I-IV.

Goble, G. G. and Rausche, F. (1980). "Pile Drivability Predictions by CAPWAP." Institution of Civil Engineers. Numerical methods in offshore piling. ICE, London, pp. 29-36.

Goble, G. G., Rausche, F., and Likins, G. E. (1980). "The Analysis of Pile Driving – A State of the Art." Presented at the First Seminar on the Application of Stress-Wave Theory on Piles, 4-5$^{th}$ June, Stockholm, Sweden, pp.131-161.

Hannigan, P.J., Goble, G.G., Thendean, G., Likins, G.E. and Rausche, F. (1998). Design and Construction of Driven Pile Foundations – Volumn II, FHWA-HI-97-013. National Highway Institute, Federal Highway Administration, U.S. Department of Transportation, Washington, D.C.

Hannigan, P. J. and Webster, S. D. (1987). "Comparison of Static Load Test and Dynamic Pile Testing Results." Proceedings of the 2nd International Symposium, DFI, Luxembourg, May.

Hill, R. (1950). The Mathematical Theory of Plasticity. Oxford University Press, New York, N.Y.

Hirsch, T. J., Carr, L. and Lowery, L. L. (1976). Pile Driving Analysis, TTI Program, U.S. Department of Transportation, Federal Highway Administration, Offices of Research and Development, IP-76-13, Washington, D.C., Vols. I-IV.

Ho, J. and Weber, L. (1991). "The Use of High Strength H Bearing Piles In Hong Kong." Proceedings of the 4th International conference on Piling and Deep Foundations, Stresa, Italy, 7-12th April, Vol. 1, pp. 249-254.

Hou ShiTao, Gou Dian Quan G. et al. (1991). "Effect Analysis on Static and Dynamic Tests of Pile Foundations." Theory and Practice of Piling and Deep Foundations in China. Proceedings of the 4th International Conference on Piling and Deep Foundartions, Stresa, Italy, April, pp. 161-170.

Hunt, S. W. and Baker, C. N. (1988). "Use of Stress-wave Measurements to Evaluate Piles in High Set-up Conditions." Fellenius B. (ed.), Proceedings of the 3rd International Conference on the Application of Stress-Wave Theory to Piles, Bitech Publisher, Ottawa, pp. 689-705.

Hussein, M. and Goble, G. G. (1987). "Qualitative Evaluation of Force and Velocity Measurements during Pile Driving." Dynamic Response of Pile Foundations:Reston, VA, April, pp. 166-183.

Hussein, M., Likins, G., and Rausche, F. (1996). "Selection of a Hammer for High-Strain Dynamic Testing of Cast-In-Place Shafts." Fifth International Conference on the Application of Stress-wave Theory to Piles (STRESSWAVE '96): Orlando, FL, pp. 759-772.

Hussein, M., Sharp, M. R., and Knight, W. F. (2002). "The Use of Superposition for Evaluating Pile Capacity." Proceedings of the Conference American Society of Civil Engineers, February 14-16th, Orlando, FL, pp. 6-21.

Jeon, J. J., and Rahman, M. S. (2007). "A Neural Network Model for Prediction of Pile

Setup." Journal of the Transportation Research Board, No. 2004, Transportation Research Board, Washington, D.C., pp. 12-19.

Karlsrud, K., Clausen, C. J. F., and Aas, P. M. (2005). "Bearing Capacity of Driven Piles in Clay, the NGI Approach." Proceedings of 1st International Symposium on Frontiers in Offshore Geotechnics, Balkema, Perth, Australia, pp.775-782.

Kim, Kyung Jun. (2002). Development of Resistance Factors for Axial Capacity of Driven Piles in North Carolina. PhD Dissertation submitted to the Graduate Faculty of North Carolina State University. 272 pp.

Komurka, V. E., Wagner, A. B., and Edil, T. B. (2003). Estimating Soil/Pile Set-Up. Final Report Submitted to the Wisconsin Department of Transportation, September, Wisconsin Highway Research Program #0092-00-14, 55 pp.

Koutsoftas, D. C. (2002). "High Capacity Piles in Very Dense Sands." Deep Foundation Congress, Geotechnical Special Publication, No. 116, Vol. 1, ASCE, Reston, VA, pp. 632-646.

Lee, W., Lee, I. M., Yoon, S. J., and Choi, Y. J. (1996). "Bearing Capacity Evaluation of the soil-Cement Injected Pile Using CAPWAP." Proceedings of the 5th International Conference on the Application of Stress-Wave Theory to Piles, Orlando, University of Florida, pp.409-419.

Lehane, B. M., and Jardine, R. J. (1994). "Displacement-Pile Behavior in a Soft Marine Clay." Canadian Geotechnical Journal, Vol. 31, pp. 181-191.

Likins, G., DiMaggio, J., Rausche, F., and Teferra, W. (1992). "A Solution for High Damping Constants in Sands." Proceedings of the 4th International Conference on the Application of Stress-Wave Theory to Piles: The Netherlands, September, pp. 117-120.

Likins, G., Piscsalko, G., Rausche, F., and Hussein, M. (2004). "Real-Time Monitoring Solutions for Deep Foundation Testing." Compendium of Papers CD-ROM, 83rd Annual Transportation Research Board Meeting: Washington, D.C., January, pp. 1-18.

Likins, G. and Rausche, F. (2004). "Correlation of CAPWAP with Static Load Tests." Proceedings of the 7th International Conference on the Application of Stress-Wave

Theory to Piles, Petaling Jaya, Selangor, Malaysia, August, pp. 153 – 165.

Likins, G., Rausche, F., Thendean, G., and Svinkin, M. (1996). "CAPWAP Correlation Studies." Proceedings of the 5th International Conference on the Application of Stresswave Theory to Piles. University of Florida, Orlando, FL.

Liu, C., Lin, Q., and Shi, F. (1996). "Determining the Bearing Capacity of Large-Diameter Bored Cast-In-Situ Piles by High Strain Dynamic Pile Testing." Proceedings of the 5th International Conference on the Application of Stress-Wave Theory to Piles, Orlando, University of Florida, pp.409-419.

Lo, S. R., Li, K. S., and Lam J. (2008). "Driven High Capacity H-Piles in Hong Kong Saprolites: A Reliability Evaluation of Two Methods." Canada Geotechnical Journal, Vol. 45, pp. 124-130.

Long, J. H., Kerrigan, J. A., and Wysockey, M. H. (1999). "Measured Time Effects forAxial Capacity of Driving Piling." Transportation Research Record 1663, Paper No.99-1183, Transportation Research Board, Washington, D.C., pp. 8-15.

Long, J. H., Maniaci, M. and Samara, E. A. (2002). "Measured and Predicted Capacity of H-Piles." Geotechnical Special Publication No.116, Deep Foundations, An International Perspective on Theory, Design, Construction, and Performance, Vol. 1, Proceedings of the International Deep Foundations, Congress 2002, 14-16th February, Orlando, FL, ASCE, pp. 542-558.

Mathias, Dean and Cribbs, Michelle (1998). Driven 1.0: A Microsoft Windows ™ Based Program for Determining Ultimate Vertical Static Pile Capacity. Publication No. FHWA-SA-98-074, National Highway Institute, Federal Highway Administration, U.S. Department of Transportation, Washington, D.C.

McVay, M., Birgisson, B., Zhang, L., Perez., A, and Putcha, S. (2000). "Load and Resistance Factor Design (LRFD) for Driven Piles Using Dynamic Methods – A Florida Perspective." Geotechnical Testing Journal, Vol. 23, No.1, pp. 55-66.

Meyerhof, G. G. (1976). "Bearing Capacity and Settlement of Pile Foundations." Journal of Geotechnical Engineering Division, ASCE, Vol. 102, No. GT3, Proc. Paper 11962, pp. 195-228.

Morgano, C. M., and White, B. A. (2004). "Identifying Soil Relaxation from Dynamic

Testing." Proceeding of the 7th International Conference on the Application of Stress Wave Theory to Piles, Petaling Jaya, Selangor, Malaysia, August, pp.415-421.

Ng, K. W., Suleiman, M. T., Sritharan, S., Roling, M., and AbdelSalam, S. S. (2011). Development of LRFD Design Procedures for Bridge Piles in Iowa – Soil Investigation and Full-Scaled Pile Tests. Final Report Vol. II. IHRB Project No.TR-573. Institute of Transportation, Iowa State Univeristy, Ames, Iowa.

Nordlund, R. L. (1963). "Bearing Capacity of Piles in Cohesionless Soils." ASCE, SM&F Journal SM-3.

Nordlund, R. L. (1979). "Point Bearing and Shaft Friction of Piles in Sand." 5th Annual Fundamentals of Deep Foundation Design, University of Missouri-Rolla.

Nowak, A. (1999). NCHRP Report 368: Calibration of LRFD Bridge Design Code. Transportation Research Board, Washington, D.C.

Paikowsky, S.G. with Contributions from Birgisson from Birgisson, B., McVay, M., Nguyen, T., Kuo, C., Baecher, G., Ayyab, B., Stenersen, K., O'Malley, K., Chernauskas, L., and O'Neill, M. (2004). Load and Resistance Factor Design (LRFD) for Deep Foundations, NCHRP Report 507, Transportation Research Board, Washington, D.C.

Paikowsky, S. G., Regan, J. E., and McDonnell, J. J. (1994). A Simplified Field Method for Capacity Evaluation of Driven Piles. Publication No. FHWA-RD-94-042. National Highway Institute, Federal Highway Administration, U.S. Department of Transportation, Washington, D.C.

Pei, J., and Wang, Y. (1986). "Practical Experiences on Pile Dynamic Measurement in Shanghai." Proceedings of International Conference on Deep Foundations, Beijing, China, pp. 2.36-2.41.

Perez, A.P. (1998). Load Resistance Factor Design (LRFD) for Driven Piles Based on Dynamic Methods with Assessment of Skin and Tip Resistance from PDA Signals. MS. Thesis, University of Florida, FL.

Pestana J. M., Hunt, C. E., and Bray, J. D. (2002). "Soil Deformation and Excess Pore Pressure Field Around A Closed-Ended Pile." Journal of Geotechnical and Geoenvironmental Engineering, ASCE, Vol. 128, No. 1, January 1, pp.1-12.

Pile Driving Contractors Association (2007). Installation Specification for Driven Piles

PDCA Specification 102-07, PDCA Technical Committee, January.

Pile Dynamic, Inc. (1996). Pile Driving Analyzer Manual; Model PAK, Cleveland, OH.

Pile Dynamics, Inc. (2000). CAPWAP for Windows Manual 2000, Cleveland, OH.

Pile Dynamics, Inc. (2001). Pile Driving Analyzer-W Help: For use with PDA Models PAK and PAL, Version: July, Cleveland, OH.

Pile Dynamics, Inc. (2005). GRLWEAP Wave Equation Analysis of Pile Driving: Procedures and Models Version 2005, Cleveland, OH.

Priem, M. J., March, R., and Hussein, M. (1989). "Bearing Capacity of Piles in Soils with Time Dependent Characteristics." Piling and Deep Foundations, Vol. 1, pp. 363-370.

Poulos, H. G. and Davis, E. H. (1980). Pile Foundation Analysis and Design. John Wiley and Sons, NY. .

Randolph, M. F. and Wroth, C. P. (1978). "Analysis of Deformation of Vertically Loaded Piles." Journal of Geotechnical Engineering Division, ASCE, 104(12), pp. 1465-1488.

Rausche, F., and Goble, G. G. (1979). "Determination of Pile Damage by Top Measurements." American Society for Testing and Materials, Philadelphia, PA, pp. 500-506.

Rausche, F., Goble, G. G. and Likins, G. E. (1985). "Dynamic Determination of Pile Capacity." Journal of Geotechnical Engineering, ASCE, Vol. III, No.3, Reston, VA, January, pp. 367-383.

Rausche, F., Goble, G. G. and Likins, G. E. (1992). "Investigation of Dynamic Soil Resistance on Piles using GRLWEAP." Proceeding of the 4th International Conference on Application of Stress-Wave Theory to Piles, Frans B. J. Barends, ed., A. A. Balkema, The Hague, The Netherlands, pp. 137-142.

Rausche, F., Likins, G. E., and Goble, G. G. (1994). "A Rational and Usable Wave Equation Soil Model Based on Field Test Correlation." Proceedings Design and Construction of Deep Foundations, Federal Highway Administration, Washinton, D. C.

Rausche, F., Robinson, B., and Likins, G. E. (2004). "On The Prediction of Long Term Pile Capacity from End of Driving Information." Current Practices and Future Trends in Deep Foundations, Geotechnical Special Publication No. 125, Di Maggio, J.A. and

Hussein, M.H., Eds, ASCE, Reston, VA, August, pp. 77-95.

Randolph, M. F., Carter, J. P., and Wroth, C. P. (1979). "Driven Piles in Clay – the Effects of Installation and Subsequent Consolidation." Geotechnique 29, No.4, pp.361-393.

Robert Y. Liang and Abdullah I. Husein. (1993). "Simplified Dynamic Method for Pile-Driving Control." Journal of Geotechnical Engineering, ASCE, Vol.119, No.4, April, pp. 694-713.

Robert Y. Liang and Sheng, Y. (1992). "Interpretation of Smith Model Parameters Based on Cavity Expansion Theory." Proceeding of the 4th International Conference on Application of Stress-Wave Theory to Piles, Frans B. J. Barends, ed., A. A. Balkema, The Hague, The Netherlands, pp. 111-116.

Robert Y. Liang and Sheng Y. (1993). "Wave Equation Parameters from Driven-Rod Test." Journal of Geotechnical Engineering, ASCE, Vol.119, No.6, June, pp. 1037-1057.

Robert Y. Liang and Zhou, Jian. (1997). "Probability Method Applied to Dynamic Pile-Driving Control." Journal of Geotechnical and Geoenvironmental Engineering, Vol. 123, No. 2, February, pp. 137-144.

Schmertmann, J. H. (1991). "The Mechanical Aging of Soils." Journal of Geotechnical Engineering, Vol. 117, No. 9, September, ASCE, pp. 1288-1330.

Sellountou, E. A. and Robert, T. L. (2007). "The Cost Effectiveness of Dynamic Pile Installation Monitoring: A Case Study." Proceedings of the 7th International Symposium on Field Measurements in Geomechanics, ASCE, September 24-27, Boston, MA. 12 pp.

Skov, R., and Denver, H. (1988). "Time-Dependence of Bearing Capacity of Piles." Proceedings of 3rd International Conference on the Application of Stress-Wave Theory to Piles, B. H. Fellenius, ed., Ottawa, Ontario, Canada, pp.879-888.

Smith, E. A. L. (1962). "Pile-Driving Analysis by the Wave Equation." Journal of the Soil Mechanics and Foundations Division, ASCE, Paper No. 3306, Vol. 127, Part 1, pp.1145-1193.

Soares, M. M., Matos, S. F. D., and de Mello, J. R. C. (1984). "Pile Driveability Studies, Pile Driving Measurements." Proceedings of the 2nd International Conference on the Application of Stress-Wave Theory on Piles, Stockholm, May 27-30, pp.64-71.

Soderberg, L. O. (1962). "Consolidation Theory Applied to Foundation Pile Time Effects." Geotechnique, 12(3), pp.217-225.

Svinkin, M. R. (1996). "Setup and Relaxation in Glacial Sand – Discussion." Journal of Geotechnical Engineering, ASCE, 122(4), pp. 319-321.

Svinkin, M. R. (1997). "Time Dependent Capacity of Piles in Clayey Soils by Dynamic Methods." Proceedings of the 14th International Conference on Soil Mechanics and Foundation Engineering, Hamburg, Germany, September, Vol.2, pp. 1045-1048.

Svinkin, M. R., Morgano, C. M., and Morvant, M. (1994). "Pile Capacity as a Function of Time in Clayey and Sandy Soils." Deep Foundation Institute, 5th International Conference and Exhibition on Piling and Deep Foundations, pp. 1.11.1-1.11.8.

Svinkin, M. R., and Skov, R. (2000). "Set-Up Effect of Cohesive Soils in Pile Capacity." Proceedings of 6th International Conference on Application of Stress-Waves Theory to Piles, Niyama, S., and Beim, J., ed., Balkema, A. A., Sao Paulo, Brazil, pp.107-111.

Svinkin, M. R. and Woods, R. D. (1998). "Accuracy of Determining Pile Capacity by Dynamic Methods." Proceeding of the 7th International Conference and Exhibition on Piling and Deep Foundations, Deep Foundation Institute, 15th to 17th June, Palais, Ferstel, Vienna, Austria, pp. 1.2.1 – 1.2.8.

Swann, L. H. and Abbs, A. F. (1984). "The Use of Wave Equation in Calcareous Soils and Rocks." Proceedings of the 2nd International Conference on the Application of Stress-Wave Theory on Piles, Stockholm, May 27-30, pp. 421-434.

Thendean, G., Rausche, F., Svinkin, M. and Likins, G. (1996). "Wave Equation Correlation Studies." Proceedings of the 5th International Conference on the Application of Stress-Wave Theory to Piles, 1996, Orlando, University of Florida, pp. 144-162.

Timoshenko, S. and Goodier, J. N. (1951). Theory of Elasticity, 2nd Edition, McGraw-Hill Book Corporation, NY.

Titi, H. H., and Wathugala, G. W. (1999). "Numerical Procedure for Predicting Pile Capacity - Setup/Freeze." Transportation Research Record 1663, Paper No. 99-0942, Transportation Research Board, Washington, D.C., pp. 25-32.

Thurman, A. G. (1964). Computed Load Capacity and Movement of Friction and End

Bearing Piles Embedded in Uniform and Stratified Soil. Ph.D. Thesis, Carnegie Institute of Technology.

Tomlinson, M. J. (1980). Foundation Design and Construction. 4th Edition, Pitman Advanced Publishing, Boston, MA.

Transportation Research Board. (2009). Implementation Status of Geotechnical Load and Resistance Factor Design in State Departments of Transportation. Transportation Research Circular Number E-C136, June, Washington, D.C.

Wathugala, G. W., and C. S. Desai. (1991). "Hierarchical Single-Surface Model for Anisotropic Hardening Cohesive Soils." Proceedings of 7th International Conference of the International Association for Computer Methods and Advances in Geomechanics (J. Beer, J. R. Booker, and J. P. Carter, eds.), Cairns, Australia, pp. 1249-1254.

Webster, S. D. and Teferra, W. (1996). "Pile Damage Assessments Using the Pile Driving Analyzer." Fifth International Conference on the Application of Stress-Wave Theory to Piles (STRESSWAVE 96): Orlando, FL, September, pp. 980-990.

Wei, J., Heng, Y. S., Lok, C. S. and Chong, M. K. (1991). "Dynamic Testing of H-Piles and HDB Sites." Proceedings of the 4th International Conference on Piling and Deep Foundations, Stresa, Italy, 7-12th April, Vol. 1, pp. 665-671.

Whittle, A. J., and Kavvadas, M. J. (1994). "Formulation of MIT-E3 Constitutive Model for Overconsolidated Clays." Journal of Geotechnical Engineering, ASCE, 120(1), pp. 173-199.

Whittle, A. J., and Sutabutr, T. (1999). "Prediction of Pile Setup in Clay." Transportation Research Record 1663, Transportation Research Board, Washington, D.C., pp. 33-40.

Widjaja, Budijanto. (2006). "Wave Equation Analysis and Pile Driving Analyzer for Driven Piles: 18th Floor Office Building Jakarta Case." International Civil Engineering Conference: Towards Sustainable Civil Engineering Practice, Surabaya, Indonesia, August 25-26, pp. 201-208.

Yang, N. C. (1956). "Redriving Characteristics of Piles." Journal of the Soil Mechanics and Foundations Division, ASCE, Vol. 82, Paper 1026, SM3, July.

Yang, L., and Liang, R. (2006). "Incorporating Setup into Reliability-Based Design of

Driven Piles in Clay." Canadian Geotechnical Journal, Vol. 43, pp. 946-955.

York , D. L., Brusey, W. G., Clemente, F. M. and Law, S. K. (1994). "Setup and Relaxation in Glacial Sand." Journal of Geotechnical Engineering, ASCE, 120(9), pp. 1498-1513.

Zhu, G. Y. (1988). "Wave Equation Applications for Piles in Soft Ground." Proceedings of 3rd International Conference on the Application of Stress-Wave Theory to Piles, B. H. Fellenius, ed., Ottawa, Ontario, Canada, pp. 831-836.

# CHAPTER 3: PILE SETUP IN COHESIVE SOIL WITH EMPHASIS ON LRFD: AN EXPERIMENTAL INVESTIGATION

Ng, K. W.[1]; Roling, M.[1]; AbdelSalam, S. S.[1]; Suleiman, M. T.[2]; and Sritharan, S.[3]

A paper to be submitted to the Journal of Geotechnical and Geoenvironmental Eng., ASCE

## 3.1. Abstract

Setup of piles driven in cohesive soils has been a known phenomenon for several decades. However, a systematic field investigation providing the needed data to develop analytical approaches for integrating pile setup into the design method rarely exists. This paper summarizes recently completed field investigation on five fully instrumented steel H-piles embedded in cohesive soils, while a companion paper discusses the development of the pile setup method and its incorporation into the Load and Resistance Factor Design (LRFD) approach. During the field investigation, detailed soil characterization, monitoring of soil total lateral stress and pore water pressure using push-in pressure cells, collection of pile dynamic restrike data as a function of time, and vertical static load tests were completed. Restrike measurements confirm that pile setup occurs with a logarithmic increase following the end of driving and its development correlates well with the rate of dissipation of the measured pore water pressure. The field data further concluded that only the skin friction component, not the end bearing, is largely contributes to the setup, which can be accurately estimated for practical purposes using soil properties, such as SPT *N*-value and coefficient of consolidation.

**CE Database Keywords:** Pile Setup; Load tests; Cohesive soil; WEAP; CAPWAP; Coefficient of consolidation; SPT *N*-value; *PI*; Damping factor; Quake; LRFD.

---

[1]Research Assistants, Dept. of Civil, Construction and Environmental Engineering, Iowa State Univ., Ames, IA 50011. E-mail: kwng@iastate.edu, roling@iastate.edu, and ssabdel@iastate.edu

[2]Assistant Professor, Dept. of Civil and Environmental Engineering, Lehigh University, Bethlehem, PA, 18015. E-mail: mts210@lehigh.edu

[3]Wilson Engineering Professor and Associate Chair, Dept. of Civil, Construction and Environmental Engineering, Iowa State Univ., Ames, IA 50011. E-mail: sri@iastate.edu

## 3.2. Introduction

Many researchers and practitioners have recognized the increase in resistance (or capacity) of driven piles embedded in cohesive soils over time, and this phenomenon is referred to as pile setup. The mechanisms of pile setup are related to the healing of remolded cohesive soils, the increase in lateral stresses, and the dissipation of pore water pressure (Soderberg 1962 and Randolph et al. 1979). When accounted for accurately during design, the integration of pile setup can lead to more cost-effective design as it will reduce the number of piles and/or pile lengths. Unfortunately, experimental data required for detailed pile setup studies rarely exists.

Static or dynamic tests can be performed to evaluate pile setup; however, it is not feasible in practice to perform these tests over a period of time as acknowledged in the interim report by the American Association of State Highway and Transportation Officials (AASHTO) (2008). Empirical methods to estimate pile setup have been proposed by several researchers, such as Pei and Wang (1986), Skov and Denver (1988) and Svinkin and Skov (2000). However, these methods have several shortcomings. For instance, Pei and Wang (1986)'s method was purely empirical, specifically developed for Shanghai soil, and lack of generalization in terms of soil properties. Skov and Denver (1988)'s and Svinkin and Skov (2000)'s methods require inconvenient and costly restrikes for the estimation of pile setup factors, and lack of generalization in terms of soil properties. Due to insufficient experimental data, these methods have not been substantially validated for accurate practical applications. For these reasons, empirical methods have not been included as part of the AASHTO (2008) LRFD Specifications to account for pile setup.

To account for pile setup in the LRFD approach, the followings are needed for commonly used foundation types: a) sufficient and detailed dynamic and static field test data as a function of time for accurate pile setup evaluation; b) detailed subsurface investigations and monitoring of soil stresses to quantify pile setup (Komurka et al. 2003); and c) a systematic reliability-based method to account for pile setup in the LRFD approach.

A literature review by the writers concluded that published information on pile setup lacks detailed dynamic and static field test data as a function of time for both small-displacement piles (i.e., H-piles and open-ended pipe piles) and large-displacement piles (closed-end pipe piles and precast concrete piles). In addition, quality setup data on small-displacement piles is relatively scarce according to the published data of pile setup reported by Long et al. (1999), Titi and Wathugala (1999), and Komurka et al. (2003). Furthermore, despite the fact that pile setup is influenced by properties of soil surrounding the pile and pore water pressure, the necessary data to quantitatively describe the relationship between pile setup and surrounding soil properties and dissipation of pore water pressure is not available. This raises a question if the pile setup of small-displacement driven piles is significant. If this is significant, then its dependency on surrounding soil properties and pore water pressure and its incorporation into the LRFD approach need to be studied. Given that a recent survey of more than 30 State Departments of Transportation (DOTs) conducted by AbdelSalam et al. (2010) revealed that steel H-pile is the most common foundation type used for bridges in the United States, the setup investigation reported herein focuses on steel H-pile.

## 3.3. Background

One of the first observations of setup for steel H-piles was reported by Yang (1956) on 58 m long HP 360 × 174 piles embedded in silty clay layers at the Tappen Zee Bridge site in New York. In this case, the pile resistance based on hammer driving resistance measurements increased from 1 blow/0.3m to 8 blows/0.3m after 2 days from the EOD. Similar soil setup observations for various steel H-piles embedded in cohesive soils (see Figure 3.1) have been reported by Huang (1988) and Lukas & Bushell (1989), and more recently by Long et al. (2002) and Fellenius (2002). Figure 3.1 summarize the setup found in the literature for steel H-piles in terms of a resistance ratio defined as the total pile resistance at any time after the EOD ($R_t$) divided by the reference total pile resistance at the EOD ($R_{EOD}$). The total pile resistances ($R_t$) were determined either using the measured response from a static load test or based on Pile Driving Analyzer (PDA) measurements in conjunction

with CAPWAP analysis at different times of restrike. The reference pile resistances at the EOD ($R_{EOD}$) were based on CAPWAP analysis of PDA data. For comparison purposes, a predominant soil type along the pile shaft and a weighted average SPT *N*-value ($N_a$) were determined for each data source. Figure 3.1 shows that pile resistances typically increase immediately after the EOD and the rate of increase decreases with time. The extent of setup, however, varies between sites. It can be observed in general that piles embedded in a soil profile with a relatively smaller $N_a$ value (i.e., weighted average SPT *N*-value) exhibited a higher resistance ratio ($R_t/R_{EOD}$), indicating a higher pile setup. However, the test pile reported by Lukas & Bushell (1989) exhibited a higher resistance ratio than that of Fellenius (2002) despite similar $N_a$ values for both sites, confirming that setup is influenced by other soil parameters. Although the mechanisms of pile setup are related to the increase in lateral stresses and the dissipation of pore water pressure, consolidation test results, in-situ lateral stresses, and pore water pressure measurements were not reported by the authors. Recognizing the difficulty in understanding the pile setup based solely on the data available in the literature, the current study focused on collecting sufficient and good-quality soil data for performing accurate pile setup evaluations, including SPT *N*-values, vertical coefficient of consolidation ($C_v$), horizontal coefficient of consolidation ($C_h$) using Piezocone Penetration Test (CPTu), over consolidation ratio (*OCR*), and Atterberg limits.

Besides the aforementioned pile setup reported by other researchers, pile setup was also realized using the PIle LOad Test (PILOT) database that currently reports quality assured historical pile load test data available in Iowa (Rolling et al. 2010). Using eight sets of data, Ng et al. (2010) reported an average of 39% increase in vertical load resistance of steel H-piles after five days of the EOD when comparing the measured pile resistance from static load tests with the initial pile resistance at the EOD estimated using WEAP. This finding confirmed the occurrence of pile setup in cohesive soils at a regional setting, where four different geological formations (i.e., loess, loess on top of glacial, Wisconsin glacial and loamy glacial) exist as shown in Figure 3.2.

## 3.4. Field Investigation

### 3.4.1. Test locations

As part of an effort to establish LRFD guidelines in Iowa, ten steel H- piles were driven and load tested in the field in different Iowa counties representing five geological regions (Vol. II by Ng et al. (2011a)). Five of these piles were driven into cohesive soils to investigate the effects of setup, whereas three were tested in mixed soils and the other two in sand profiles. The test piles embedded in cohesive soil profiles were referred to as ISU2, ISU3, ISU4, ISU5, and ISU6 (see Figure 3.2). ISU2 at Mills County, ISU3 at Polk County, and ISU6 at Buchanan County were located in loess, Wisconsin glacial, and loamy glacial geological formations, respectively. Both ISU4 at Jasper county and ISU5 at Clarke County were in the geological formation of loess soil deposits on top of glacial clay. Following a detailed presentation of results for ISU5 and ISU6, data from all five tests is used to develop a rational approach for quantifying pile setup. More detailed information gathered for all test piles can be found in Ng et al. (2011a).

### 3.4.2. Soil characterizations

Each test site was characterized using in-situ subsurface investigations, which consisted of Standard Penetration Tests (SPTs) and Piezocone Penetration Tests with pore water pressure dissipation measurements (CPTu), and laboratory soil classification and one-dimensional consolidation tests. SPTs and CPTs were performed within a distance of 3.7 m from test piles ISU2, ISU3 and ISU6 and 15 m from test piles ISU4 and ISU5. For piles ISU5 and ISU6, Figure 3.3 presents the measured SPT *N*-values (adjacent to the solid boxes) along the pile length and summarizes the measured CPT tip resistance ($q_c$) and skin friction ($f_s$). During the CPTs, pore water pressure dissipation tests were conducted at all sites. Based on these CPTs that achieved 50% pore water pressure dissipation, the values of horizontal coefficient of consolidation ($C_h$) were estimated (see Table 3.1) using the strain path method as described in Houlsby and Teh (1988).

Disturbed soil samples were collected for laboratory soil classification in accordance with the Unified Soil Classification System (USCS). Table 3.1 includes the USCS for all soil layers, soil unit weight ($\gamma$), liquid limit (*LL*), and plasticity index (*PI*). Table 3.1 shows that almost all soil layers were classified as low plasticity clay (CL). Based on the sensitivity analysis conducted by Ng et al. (2010) on using various soil profile input procedures in WEAP for pile resistance estimations, a pile with at least 70% of its cumulative length embedded in cohesive soil layers (clay or silt with *PI* of at least 4) was considered to be embedded in a cohesive soil profile. The average total unit weight was 20.7 kN/m$^3$ (132 pcf), and the liquid limit and the plasticity index ranged from 18.2% to 47.5% and from 4% to 28.4%, respectively.

Undisturbed soil samples collected using 75 mm (3-in) Shelby tubes were tested using one-dimensional consolidation tests in accordance with American Standard Testing Method (ASTM) Standard D2435 (ASTM 2004). The over consolidation ratio (*OCR*) was estimated using a graphical procedure proposed by Casagrande (1936) and the vertical coefficient of consolidation ($C_v$) was estimated using a square root of time method. Table 3.1 shows that almost all soil layers were normally consolidated to slightly overconsolidated. The high over-consolidation ratio (*OCR*) values above 4.0 obtained near the ground surface of ISU3 and ISU5 were suspected to be due to mechanical compaction of the top soil layers during past road construction; ISU3 was situated within an interchange, whereas ISU5 was located at an old road median. The $C_v$ values were estimated between 0.033 and 0.152 cm$^2$/min (0.005 and 0.023 in$^2$/min).

For ISU5, the 7.6 m (25 ft) thick top soil layer with loess origin was classified as low plasticity clay (CL), and the glacial till underlined layer classified as low plasticity clay with sand (CL). The ground water table (GWT) was located approximately 11 m (36 ft) below the ground surface. The SPT *N*-values ranged from 3 to 23, indicating a soft to stiff soil. The 7.6 m (25 ft) thick top low plasticity clay layer has an average SPT *N*-value of 8 overlaying sandy low plasticity clay with an average SPT *N*-value of 16. The CPT results show that the $q_c$ and $f_s$ values ranged from 527 kPa (76 psi) to 6,569 kPa (953 psi) and from 19 kPa (3 psi)

to 201 kPa (29 psi), respectively. The average $S_u$ value of the top low plasticity clay layer was 92 kPa (13 psi) underlain by sandy low plasticity clay having an average $S_u$ of 142 kPa (21 psi). The *OCR* values ranged from 1.3 to 4.5, and the $C_v$ values ranged from 0.051 to 0.107 $cm^2$/min (0.008 to 0.017 $in^2$/min).

For ISU6, which was situated in the loamy glacial region subjecting to a historical outwash, the soil profile was divided into four layers consisting of 4 m (13 ft) of a mixed fill of clayey sand and low plasticity clay (SC and CL) overlaying a 2.1 m (7 ft) of silty sand (SM), 9.05 m (30 ft) of sandy low plasticity clay (CL) with 0.35 m (1 ft) of silty sand (SM) and approximately 3.55 m (11.6 ft) of low plasticity silt (ML). The ground water table (GWT) was located approximately 4.6 m (15 ft) below the ground surface. The SPT *N*-values ranged from 8 to 23 with a softest layer of sandy low plasticity clay at the depth between 6.1 and 8.95 m (20 and 29 ft). The $q_c$ and $f_s$ values ranged from 488 kPa (71 psi) to 12,353 kPa (1,792 psi) and from 10 kPa (1.5 psi) to 645 kPa (93.5 psi), respectively. The average $S_u$ values ranged from 71 kPa (10.3 psi) for the sandy low plasticity clay layer between 6.1 to 9.0 m (20 to 30 ft) underlain by sandy low plasticity clay having an average $S_u$ of 348 kPa (50.5 psi). The horizontal coefficient of consolidation at the depth of 15.2 m (50 ft) was 0.008 $cm^2$/min (0.0013 $in^2$/min). The *OCR* values ranged from 1.1 to 1.2, and the $C_v$ values ranged from 0.033 to 0.057 $cm^2$/min (0.005 to 0.009 $in^2$/min).

Since the CPT dissipation test was not conducted for all soil layers at each site and it requires excessively long time to achieve 50% pore water pressure dissipation during a CPT for a $C_h$ estimation, a relationship between $C_h$ and SPT *N*-values was established as shown in Figure 3.4. Using this relationship, the $C_h$ values were estimated for cohesive layers where the dissipation test was not performed. Table 3.2 lists the weighted average SPT *N*, $C_h$, and $C_{v,}$ values along each pile shaft. The weighted average *N*-value was calculated by weighting the measured soil property for the cohesive soil layer by its thickness divided by the total length for all cohesive layers located along the embedded pile length.

### 3.4.3. Instrumentation

All test piles were instrumented with strain gauges in pairs on either side of the web along the centerline of the embedded pile length as shown in Figure 3.3 and Figure 3.5. All strain gauges were covered with a black flexible rubbery membrane and aluminum tape for protection against welding sparks, heat and water. The strain gauge cables were also wrapped with aluminum foil. As seen in Figure 3.5, the gauges and the cables were covered with 50 mm × 50 mm × 5 mm steel angles welded to the webs of the pile to prevent damages caused by direct soil contact during pile installation. Despite the addition of the two steel angles, the shaft surface area in contact with the soil increases only by 4%. The steel angles were chamfered at the pile toe to form a pointed end to minimize any increase in the toe cross-sectional area.

Prior to the pile installation, two strain transducers and two accelerometers of PDA were installed at 750 mm (30-in) below the top of the pile. The strain transducers were bolted to both sides of the web along the centerline, and the accelerometers were attached to either sides of the web at a distance of 75 mm (3-in) left and right of the strain transducers. The PDA recorded the strains and accelerations during pile driving and restrikes, which were later converted to force and velocity records.

### 3.4.4. Push-In pressure cells

To measure the total lateral earth pressure and pore water pressure during pile driving, restrikes and static load tests (SLTs), Geokon Model 4830 push-in pressure cells (PCs) were inserted into the soil at a horizontal distance ranging from 200 mm (0.65 ft) to 610 mm (2 ft) from test piles ISU5 and ISU6; PCs were not installed near ISU2, ISU3 and ISU4. The PCs were installed one to two days before pile driving to ensure stabilization of lateral stress and pore water pressure readings as recommended by Suleiman et al. (2010). To install each PC, a 100-mm (4-in) diameter borehole was drilled to a specified depth below the ground surface using a hollow-stemmed auger. The PC was then lowered through the hollow-stemmed auger and pushed approximately 350 mm (1.15 ft) below the bottom of the

borehole such that the piezometer and the flat pressure surface faced the flange of the test pile. Measurements were taken every 4 seconds during pile driving, restrikes and SLT, while readings were taken at 30-minute intervals between restrikes as well as between the last restrike and SLT. The push-in pressure cell denoted as PC1 in Figure 3.3 (a) was installed approximately 7 m (23 ft) below the ground surface and 200 mm (0.65 ft) away from the flange of ISU5. Given the deep water table (11 m or 36 ft)) encountered at ISU5's site, PC1 was installed above the water table (i.e., at 7 m or 23 ft) to avoid damage to the connection between the top of the pressure cell and the drilling rod during installation and retrieval as witnessed previously. For ISU6 shown in Figure 3.3 (b), two push-in pressure cells (PC3 and PC4) were installed below the GWT at approximately 10 m (33 ft) below the ground surface and 230 mm (0.75 ft) and 610 mm (2 ft) away from the flange, respectively. Given that ISU6 was the last test pile driven in a cohesive soil profile, a higher risk was taken to measure the dissipation of pore water pressure at a deeper location. Due to the space limitation, only the pore water pressure measurements are included in this paper and completed measurements are reported in Ng et al. (2011a).

### 3.4.5. Pile driving and restrikes

Single-acting, open-ended diesel hammers were used to drive and restrike all test piles as summarized in Table 3.3 and to install all reaction piles. Before driving each test pile, two 18.3 m (60 ft) long HP 250×63 (HP 10×42) reaction piles were driven by aligning their webs as shown in Figure 3.6. To avoid the effect of reaction pile installations on soil properties initially measured at the test pile location, the reaction piles were installed at an equal distance of 2.44 m (8 ft) on both sides of the test pile (see Figure 3.6 (a)) except for ISU6 (see Figure 3.6 (b)), in which case reaction piles were installed at distances of 1.73 m (5.7 ft) and 3.12 m (10 ft) on either side of the test pile as another test pile (ISU7) was included with a shallower embedded length of only 5.8 m (20 ft). In all cases, the reaction piles were installed with an exposed length of 1.8 m (6 ft) to connect them with a horizontal reaction beam. The test pile was then driven and the PDA data were recorded during both pile driving and restrikes. To help with pile setup evaluations, the time and the pile

embedded length before and after each restrike were precisely recorded for each test pile (see Table 3.3). Furthermore, pile driving resistance in terms of the total number of hammer blows per 300 mm (1 ft) of pile penetration (i.e., hammer blow count) was accurately obtained using videos recorded during pile installation restrikes. Figure 3.7 depicts the gathered data for ISU5 as a function of hammer blow count for the pile to penetrate 300 mm depth, which increased from 30 at the EOD to 72 at the beginning of restrike No. 6 (i.e., BOR6) over a period of 7.92 days. This substantial rise in hammer blow count without significantly increasing the pile embedded length is mainly caused by pile setup, ultimately increasing the pile resistance.

### 3.4.6. Dynamic analysis methods

With the available pile, soil, and hammer information and the recorded hammer blow count, the total pile resistance of each restrike was estimated using the WEAP SPT *N*-value based method (i.e., SA method specified by Pile Dynamic, Inc. 2005). Two assumptions were made to complete the WEAP analyses: (1) since the bearing graph (pile resistance versus hammer blow rate) generated from WEAP is independent of the water table and all restrikes were conducted within 10 days at most (see Table 3.3), water table at each test site remained constant at the EOD and at every BOR; and (2) the percentage of shaft resistance estimated from a driveability analysis was reasonably used for a bearing graph analysis, because our sensitivity studies revealed that the increase in percent shaft resistance from 50% to 99% does not vary the estimated pile resistances by more than 10%.

Furthermore, the measured force and velocity records near the pile head from PDA were used in CAPWAP analysis to calculate the total pile resistance at each event as summarized in Table 3.3. Unlike WEAP where a total shaft resistance is estimated from the driveability analysis, CAPWAP estimates the resistance distribution along the pile length. In both methods, the end bearing components are also estimated. Figure 3.8 presents the CAPWAP estimated pile shaft resistance distributions for ISU5 from EOD to the $6^{th}$ restrike (BOR6).

### 3.4.7. Static load tests

Following completion of all restrikes, vertical SLTs were performed on test piles following the "Quick Test" procedure of ASTM D 1143 according to the schedule indicated in Table 3.3. In addition to recording the strain data along the pile shaft, four 250 mm (0.8 ft)-stroke displacement transducers installed at the four extreme edges of the test pile flanges recorded the pile vertical movement during each loading and unloading step. For each pile, the pile resistance (or the total nominal resistance) was calculated using the measured load-displacement curve and the Davisson's criterion (Davisson, 1972), whereas the variation in pile force along the depth was estimated using the measured strain data at every load step as shown in Figure 3.9. By extending the slope of the pile force resistance along the pile length over the bottom two pairs of strain data, the end bearing contribution was also estimated at the toe of each pile. The nominal pile resistance of ISU 5 was found to be 1081 kN (243 kip), and its distribution along the pile length is shown in Figure 3.9 (by the solid line without markers) as established from interpolation of the force distribution curves corresponding to 1051 kN (236 kip) and 1114 kN (250 kip). In this case, the end bearing component was 247 kN (56 kip) or 23% of the total pile resistance of 1081 kN.

Subtracting the end bearing resistance from the total nominal pile resistance, the shaft resistance for ISU5 was determined to be 834 kN (188 kip). Table 3.3 lists the shaft resistance and end bearing for all test piles except ISU4 and ISU6, for which large number of strain gauges failed during the test and thus this information could not be extracted with sufficient accuracy.

## 3.5. Results

### 3.5.1. Observed pile setup

In addition to the increase in hammer blow counts observed Figure 3.7 between the EOD condition and BOR6 for ISU5, Table 3.4 summarizes the percent of pile resistance increase at different times ($\Delta R_t$) with reference to the calculated pile resistance at EOD

($R_{EOD}$) from CAPWAP analyses. The increases in total pile resistance, shaft resistance and end bearing resistance are listed separately to illustrate the different effects on setup. Both shaft resistance and end bearing increased with time after EOD. Referring to the last restrikes of all test piles, the increase in CAPWAP calculated shaft resistance ranged from 51% to 71% while the end bearing resistance increased by 8% to 21%. Since the end bearing component on average was about 16% of the total resistance, the impact of setup estimated for this component is not significant. Furthermore, the CAPWAP pile setup estimate on shaft resistance correlated well with the corresponding SLT measurements in Table 3.4 that indicates 52% to 66% increase in shaft resistance due to setup. This observation concludes that the setup largely affects the shaft resistance of steel H-piles.

### 3.5.2. Assessment of pile setup trend

Using the restrike and static load test results of ISU6, the percent increase in pile resistances normalized with its initial pile resistance estimated at EOD ($\Delta R_t/R_{EOD}$) were plotted as a function of time ($t$) after EOD in Figure 3.10. Four mathematical best-fit trends as summarized in Table 3.5 were selected to describe the relationship between the increase in pile resistance and the time given in Figure 3.10. Compared among the four trends in terms of the calculated coefficient of determination ($R^2$), the exponential equation gives the least confidence while the rational equation gives the best confidence in predicting the resistance gain. For long-term pile setup estimation, the constant estimation using the exponential equation does not agree with the continuous increase in pile resistance as observed from the field test results. Both rational and square root equations estimate relative higher increase in pile resistance than the logarithmic equation. Nevertheless, long-term restrike and load test data are not available to evaluate them. Since restrikes and load test are normally performed within 14 days after EOD, the estimation of short-term pile setup is adequate for practical applications. Although the rational equation, which has four empirical constants, gives the best correlation, the simpler logarithmic equation, which involves with only two empirical constants, provides a comparable confidence in the short-term pile setup prediction.

### 3.5.3. Logarithmic trend

When plotted as a function of time (t), the percent increase in total resistance, shaft resistance, and end bearing with respect to the corresponding resistance at EOD ($\Delta R_t/R_{EOD}$ in Table 3.4) obtained using CAPWAP generally followed a logarithmic trend for ISU5 as shown in Figure 3.11 (a) & (b). Figure 3.11 (a) depicts the logarithmic trend over a short duration immediately after EOD, and Figure 3.11 (b) confirms the same trend over a period of 9 days. As shown in this figure, total, shaft and end bearing resistances increased immediately after EOD with rapid gains within the first day, followed by increase at a slower rate after the second day. The same observation holds for the calculated total resistance from WEAP. Furthermore, the extrapolated WEAP and CAPWAP logarithmic trends provide good estimates of the measured pile resistance from SLT. Figure 3.12 shows a similar observation for all test piles, in which the percent increase in total resistance with respect to the corresponding resistance at EOD from CAPWAP followed the logarithmic trend.

### 3.5.4. Pore water pressure

Pore water pressures recorded using PC3 and PC4 at 10 m (33 ft) below ground surface with the groundwater table at 4.6 m (15 ft) at ISU6 are plotted in Figure 3.13 as function of time. Figure 3.13 (a) shows the recorded data for the first 20 minutes period. Accordingly, pore water pressure recorded using PC3 experienced some drop in readings before the pile toe reached the depth of the device. Significant change was recorded as the pile passed through the gauge location during driving. The recorded pore pressure progressively increased from 84 kPa (12 psi) to 101 kPa (14.6 psi) at PC3 and from 55 kPa (8 psi) to 64 kPa (9.3 psi) at PC4 between the time when the pile passed through the devices and BOR3. This observation is attributed to the compression of the normally consolidated (*OCR* = 1.1 between 9.3 m (30.5 ft) and 15.5 m (51 ft)) and sandy low plasticity clay soil during pile installation, resulting in the subsequent increase in the pore water pressure. In addition, the sandy low plasticity clay layer in which the PCs were installed has a small measured horizontal coefficient of consolidation ($C_h$) of 0.008 $cm^2$/min (0.0013 $in^2$/min) (see Table 3.1), which delayed the dissipation of pore water pressure. After BOR3, fluctuations in data

due to restrike and SLT as well as graduate dissipation of pressure with time were generally seen (Figure 3.13 (b).

For PC3 that was closer to the pile, the pore water pressure dissipation generally followed a logarithmic trend and reached a value of about 68 kPa (10 psi) within a day (i.e., around BOR5) and almost its hydrostatic state, which indicates complete dissipation in about seven days (i.e., around BOR7). Re-plotting the dissipated PC3 pore water pressure in percentage of the pressure measured at EOD (93 kPa) as function of time (t), Figure 3.14 confirms the logarithmic trend with a relative high coefficient of determination ($R^2$) of 0.79. The minimal difference in the gradients of the logarithmic best fits (i.e., 0.55 for resistance and 0.50 for pore water pressure dissipation in equations included in Figure 3.14) suggests that the logarithmic increase in total pile resistance followed the rate of the pore water pressure dissipation. The difference between the increase of pile resistance curves and the percent of pore water pressure dissipation curve, which is mainly due to the difference in the intercept values of 0.33 for resistance and 0.25 for pore water pressure as shown by equations presented in Figure 3.14, is believed due to remolding and healing process occurring in the soil disturbed by pile driving. With a lesser influence from pile installation, the PC4 pore water pressure reduced to the hydrostatic pressure within a day.

### 3.5.5. Influence of soil properties

Since the pile setup largely increases the shaft resistance, a detailed correlation study between soil properties and percent increase in shaft resistance ($\Delta R/R_{EOD}$) was performed. The percent increase in shaft resistance calculated for ISU5 using CAPWAP between EOD and the last restrike is plotted along the embedded pile length in Figure 3.15 together with the measured vertical coefficient of consolidation ($C_v$) and SPT $N$-value. A similar distribution of $\Delta R/R_{EOD}$ for the SLT, the percent difference between the measured shaft resistance from SLT at 9 days after EOD, and the CAPWAP calculated shaft resistance at EOD are also included in Figure 3.15 for comparative purposes. It is interesting to note that the distributions of the percent increase in shaft resistance ($\Delta R/R_{EOD}$) for both CAPWAP and

SLT have a similar trend. The magnitudes are sometimes significantly different which is attributed to the current CAPWAP signal matching procedure of using constant damping and quake values to achieve a best match.

Referring to the $\Delta R/R_{EOD}$ distribution based on SLT (the dashed line), Figure 3.15 shows that the $\Delta R/R_{EOD}$ increased by about 5% in the top 5 m (16.4 ft) thick soil layer, which was characterized with relative large $C_v$ values ranging between 0.107 cm$^2$/min (0.017 in$^2$/min) and 0.089 cm$^2$/min (0.0142 in$^2$/min) and small SPT *N*-values ranging between 6 and 9. The $\Delta R/R_{EOD}$ continued to reduce to a depth of about 11 m from the ground surface, where the surrounding cohesive soil layer has the smallest $C_v$ of 0.051 cm$^2$/min (0.008 in$^2$/min) and the highest SPT *N*-value of 22. With the combined effects of the overburden pressure and the reduction in SPT *N*-value from 22 to 13 below the 11 m (36 ft) depth, the $\Delta R/R_{EOD}$ indicated a peak increase of about 25%. This observation suggests a direct relationship between pile setup along the shaft and the coefficient of consolidation, and an inverse relationship between pile setup and the SPT *N*-value (or a direct relationship with the horizontal coefficient of consolidation as indicated by Figure 3.4).

Besides comparing with SPT *N*-value and coefficient of consolidation, pile setup was compared with other soil properties (overconsolidation ratio (*OCR*), compressibility index ($C_c$) and plastic index (*PI*)). Figure 3.15 reveals an inverse relationship between the measured *PI* and the $\Delta R/R_{EOD}$. For instance, within the cohesive soil layers with low *PI* values of 5.6% and 8.6% at 3 m (10 ft) and 14 m (13 ft), respectively, the shaft resistances increased. In other words, a pile embedded in a cohesive soil with low *PI* will experience a large $\Delta R/R_{EOD}$ at a given time. Furthermore, Zheng et al. (2010) concluded that a low compressive cohesive soil with a small $C_c$ value dissipated the excess pore water pressure faster. Relating this conclusion to pile setup, the $C_c$ value will have an inverse relationship with $\Delta R/R_{EOD}$. However, Figure 3.15 reveals no such inverse relationship, especially at the 11 m (36 ft) depth where $\Delta R/R_{EOD}$ reduced with the lowest $C_c$ of 0.124. Furthermore, a relationship between pile setup and *OCR* could not be established in Figure 3.15.

### 3.5.6. Quantitative studies between pile setup and soil properties

To further expand upon the observations presented above using data from ISU5, the percent increase in total pile resistance, shaft resistance, and end bearing estimated for all five test piles using CAPWAP were compared with weighted average SPT $N$, $C_h$, $C_v$, and $PI$ values, allowing variation of soil thicknesses along the embedded pile length to be included. For soil layers where the CPT dissipation test was not conducted or the 50% consolidation was not achieved, the horizontal coefficient of consolidation ($C_h$) was estimated using the SPT $N$-value based on the correlation developed from field test results presented in Figure 3.4. Table 3.2 summarizes the findings together with the weighted average soil properties along the pile shaft and near the pile toe for each test site, whereas Figure 3.16 presents graphical representations of the same data for each of the soil variable affecting pile setup at a common time of approximately 1 day after EOD.

At 1 day after EOD, Figure 3.16 (a) shows that the increase in total pile resistance and shaft resistance is inversely proportional to SPT N-value for all five piles. Similarly, Figure 3.16 (b) and (c) show that the total pile resistance and shaft resistance of a pile increase linearly with the $C_h$ and $C_v$ values, respectively. However, Figure 3.16 (d) shows that the total pile resistance and shaft resistance increase with $PI$ between 8% and 12%, which mainly represent the sandy low plasticity clay soils surrounding test piles ISU3 and ISU6 (see Table 3.1). However, the continuous increase in $PI$ above 12%, which represents the mostly low plasticity clay soils with higher affinity for water at the test sites of ISU2, ISU4 and ISU5, reduces both the total pile resistance and shaft resistance. Although the end bearing components were included in these figures, as expected, no clear correlations between the soil properties and the end bearing component are seen. This is largely due to relative large scatter in the data resulting from a) smaller contributions of the end bearing to the total pile resistance, and b) small errors in the estimation of shaft resistance causing larger error to the end bearing components. The insignificant impact of the end bearing is also been confirmed by the comparable trends observed for both the shaft resistance and total pile resistance.

Most importantly, Figure 3.16 strongly supports the possibility of using routine in-

situ (i.e., SPTs, and/or CPTs with pore pressure dissipation tests) and/or laboratory soil tests (i.e., one-dimensional consolidation tests) to quantitatively estimate pile setup and use in LRFD approach, which is investigated in the companion paper (Ng et al. 2011b or Chapter 4).

## 3.6. Conclusions

Motivated by insufficient information on pile setup of small-displacement piles in the literature, a detailed experimental investigation was conducted to quantify the pile setup for widely used steel H-piles. Five full-scale dynamic and static load tests were conducted on HP 250×63 steel piles embedded in cohesive soils. Gain in pile resistances and changes in soil responses were monitored from the time of driving until the piles were tested to failure under vertical static loads. In addition, the surrounding cohesive soil properties were characterized using both in-situ and laboratory tests. From the analyses of the pile and soil test data, the following conclusions were drawn:

1. Tested steel H-piles experienced the effects of setup along the pile shaft and at the pile toe in cohesive soils, with the larger setup effect occurring to the shaft resistance in the range between 51% and 71% of the CAPWAP estimated pile resistance at EOD. Despite an average contribution of about 16% towards the total resistance, the end bearing component only increased 8% to 21% by setup. The influence of pile setup was also evident by the significant increase in pile driving resistance in terms of hammer blow counts recorded between EOD and BORs. All of these observations were confirmed by the static load test measurements.
2. Steel H-piles exhibited a logarithmic trend for the gain in total pile resistance with time. The same trend was also true for the shaft resistance and the end bearing components. All pile resistances increased immediately and rapidly within a day after EOD and continuously increased at a slower rate after the second day. A comparison of the gradients of the best fits obtained for various data revealed that the logarithmic increase in total pile resistance generally followed the rate of the pore water pressure dissipation.

3. The experimental investigation confirmed that the amount of setup at a given time depends on soil properties including the coefficient of consolidation, the SPT *N*-value as well as the thicknesses of the cohesive soil layers along the embedded pile length. Piles embedded in a cohesive soil with a larger coefficient of consolidation exhibited higher percent increase in total pile resistances. However, piles embedded in a softer soil characterized by a smaller SPT *N*-value led higher percent increase in setup. The collected experimental data showed sufficient information for quantifying the pile setup using properties of surrounding soil, which is rarely available in the published literature.
4. The successful correlation between pile setup and the relevant soil properties indicates a cost-effective means to estimate the pile setup using SPTs, CPTs with pore pressure dissipation tests, and/or one-dimensional consolidation tests. In addition, detailed laboratory soil classifications and soil layers identification are also required. However, this approach is far more easily adoptable than those requiring pile restrikes or lacking generalization in terms of soil properties.

A systematic investigation on the quantification of pile setup in terms of the surrounding soil properties is presented in the companion paper (Chapter 4).

## 3.7. Acknowledgments

The writers would like to thank the Iowa Highway Research Board for sponsoring the research presented in this paper. The writers also express their gratitude to the following members of the project Technical Advisory Committee for their guidance and advice: Ahmad Abu-Hawash, Dean Bierwagen, Lyle Brehm, Ken Dunker, Kyle Frame, Steve Megivern, Curtis Monk, Michael Nop, Gary Novey, John Rasmussen and Bob Stanley. The members of this committee represent Office of Bridges and Structures, Soils, Design Section, and Office of Construction of the Iowa DOT, FHWA Iowa Division, and Iowa County Engineers. The writers would also like to thank the various bridge and soil contractors for their contributions to the field tests. Special thanks are due to Douglas Wood, Donald Davidson and Erica Velasco for their assistances with the field and laboratory tests.

## 3.8. Notation

The following symbols are used in this paper:

$C_c$ = Compressibility index

$C_v$, $C_{vh}$ = vertical or horizontal coefficient of consolidation

$LL$, $PI$ = Liquid limit or plastic index

$OCR$ = Overconsolidation ratio

$q_c$, $f_s$ = CPT measured tip resistance or skin friction

$R$, $R_{EOD}$ = Total pile resistance at any time $t$ or the reference pile resistance at the EOD

$\Delta R$ = Gain in pile resistance with respect to resistance estimated at EOD

$q_u$, $S_u$ = Unconfined compressive strength or undrained shear strength

$t$ = Time after end of driving

$\sigma_h$, $\mu$ = Lateral earth pressure or hydrostatic pressure

## 3.9. References

AbdelSalam, S. S., Sritharan, S., and Suleiman, M. T. (2010). "Current Design and Construction Practices of Bridge Pile Foundations with Emphasis on Implementation of LRFD." Journal of Bridge Engineering, ASCE, 15(6), pp. 749-758.

American Association of State Highway and Transportation Officials (AASHTO). (2008). LRFD Bridge Design Specifications Customary U.S. Units 4th Edition. Interim, Washington, D.C.

American Standard Test Method (ASTM) Standard D2435. (2004). Standard Test methods for One-Dimensional Consolidation Properties of Soils Using Incremental Loading, ASTM International, West Conshohocken, PA.

Casagrande, A. (1936). "Determination of the Preconsolidation Load and Its Practical Significance." Proceedings of 1st International Conference on Soil Mechanics and Foundation Engineering, Cambridge, Massachusetts, Vol. 3, pp. 60-64.

Davisson, M. (1972). "High Capacity Piles". Proceedings, Soil Mechanics Lecture Series on Innovations in Foundation Construction, ASCE, IL Section, Chicago, IL, pp. 81–112.

Fellenius, B. H. (2002). "Pile Dynamics in Geotechnical Practice-Six Case Histories."

Geotechnical Special Publication No. 116, ASCE, Proceedings of International Deep Foundations Congress 2002, Feb 14-16, M. W. O'Neill and F. C. Townsend, ed., Orlando, Florida, pp. 619-631.

Houlsby, G., & Teh, C. (1988). "Analysis of the Peizocone in Clay." Penetration Testing 1988, 2, pp. 777-783.

Huang, S. (1988). "Application of Dynamic Measurement on Long H-Pile Driven into Soft Ground in Shanghai." Proceedings of 3rd International Conference on the Application of Stress-Wave Theory to Piles, B. H. Fellenius, ed., Ontario, Canada, pp. 635-643.

Komurka, V. E., Wagner, A. B., and Edil, T. B. (2003). Estimating Soil/Pile Set-Up. Final Report. Wagner Komurka Geotechnical Group, Inc. and University ofWisconsin-Madison, Wisconsin.

Long, J. H., Kerrigan, J. A., and Wysockey, M. H. (1999). "Measured Time Effects forAxial Capacity of Driving Piling." Transportation Research Record 1663, Paper No.99-1183, Transportation Research Board, Washington, D. C., pp. 8-15.

Long, J. H., Maniaci, M., and Samara, E. A. (2002). "Measured and Predicted Capacity ofH-Piles." Geotechnical Special Publication No.116, Advances in Analysis, Modeling& Design, Proc. Of Int. Deep Foundations Congress 2002, ASCE, Feb 14-16, M. W. O'Neill and F. C. Townsend, ed., Orlando, Florida, pp. 542-558.

Lukas, R. G., and Bushell, T. D. (1989). "Contribution of Soil Freeze to Pile Capacity." Foundation Engineering: Current Principles and Practices, Vol. 2. Fred H. Kulhawy, ed., ASCE, pp. 991-1001.

Ng, K.W., Suleiman, M.T., and Sritharan, S. (2010). "LRFD Resistance Factors Including the Influence of Pile Setup for Design of Steel H-Pile Using WEAP." Geotechincal Special Publication No. 199, Advances in Analysis, Modeling & Design, Proc. of the Annual Geo-Congress of the Geo-Institute, ASCE, Feb 20-24, Fratta, D., Puppala, A. J., and Muhunthan, B., ed., West Palm Beach, Florida, pp. 2153-2161.

Ng, K. W., Suleiman, M. T., Sritharan, S., Roling, M., and AbdelSalam, S. S. (2011a). Development of LRFD Design Procedures for Bridge Piles in Iowa – Soil Investigation and Full-Scaled Pile Tests. Final Report Vol. II. IHRB Project No.TR-573. Institute of Transportation, Iowa State Univeristy, Ames, Iowa.

Ng, K.W., Suleiman, M.T., and Sritharan, S. (2011b). "Pile Setup in Cohesive Soil with Emphasis on LRFD: Analytical Quantifications and Design Recommendations." Journal of Geotechnical and Geoenvironmental Engineering, ASCE (Under Review).

Pei, J., and Wang, Y. (1986). "Practical Experiences on Pile Dynamic Measurement in Shanghai." Proceedings of International Conference on Deep Foundations, Beijing, China, pp. 2.36-2.41.

Pile Dynamic, Inc. (2005). GRLWEAP Wave Equation Analysis of Pile Driving: Procedures and Model Version 2005. Cleveland, Ohio.

Randolph, M. F., Carter, J. P., and Wroth, C. P. (1979). "Driven Piles in Clay-The Effects of Installation and Subsequent Consolidation." Geotechnique, 29(4), pp. 361-393.

Skov, R., and Denver, H. (1988). "Time-Dependence of Bearing Capacity of Piles." Proceedings of 3rd International Conference on the Application of Stress-Wave Theory to Piles, B. H. Fellenius, ed., Ottawa, Ontario, Canada, pp. 879–888.

Soderberg, L. O. (1962). "Consolidation Theory Applied to Foundation Pile Time Effects." Geotechnique, 12(3), pp. 217-225.

Suleiman, M. T., Stevens, L. Jahren, C. T., Ceylan, H., and Conway, W. M. (2010). Identification of Practices, Design, Construction, and Repair Using Trenchless Technology. Institute of Transportation, Final Research Report. Iowa Department of Transportation Project Number IHRB-06-09.

Svinkin, M. R., and Skov, R. (2000). "Set-Up Effect of Cohesive Soils in Pile Capacity." Proceedings of 6th International Conference on the Application of Stress-Wave Theory to Piles, Edited by Niyama, S., and Beim, J., Sao Paulo, Brazil, pp. 107–111.

Titi, H. H., and Wathugala, G. W. (1999). "Numerical Procedure for Predicting Pile Capacity-Setup/Freeze." Transportation Research Record 1663, Paper No. 99-0942, Transportation Research Board, Washington, D. C., pp. 25-32.

Yang, N. C. (1956). "Redriving Characteristics of Piles." Journal of Soil Mechanics Division, 82, SM3, ASCE, 17 pp.

Zheng, J. J., Lu, Y. E., Yin, J. H., and Guo, J. (2010). "Radial Consolidation with Variable Compressibility and Permeability Following Pile Installation." Computers and Geotechnics. 37(3), Elsevier Ltd., pp. 408-412.

Table 3.1: Summary of soil profiles and results of soil tests for all test sites

| Test pile | Soil depth (m) | USCS soil classification | Ave. SPT *N*-value at each layer | Unit weight (kN/m$^3$) | *LL* (%) | *PI* (%) | *OCR*[a] (sample depth in m) | $C_v$[b] (cm$^2$/min) | $C_h$[c] (cm$^2$/min); Depth in m |
|---|---|---|---|---|---|---|---|---|---|
| ISU2 | 0 to 4.88 | Clayey sand (SC) | 3 | - | 28.7 | 13.4 | 1.0 (2.7) | 0.152 | - |
| | 4.88 to 6.1 | Low plasticity clay (CL) | 14 | 19.1 | 43.7 | 25.0 | 1.1 (6.1) | 0.052 | - |
| | 6.1 to 10.98 | Low plasticity clay (CL) | 3 | 22.3 | 43.2 | 19.2 | 1.1 (9.1) | 0.126 | 0.892; 10.8 |
| | 10.98 to 13.42 | Clay | 4 | - | - | - | - | - | - |
| | 13.42 to 17.03 | Low plasticity clay (CL) | 4 | 23.0 | 47.5 | 28.4 | 1.0 (16.8) | 0.113 | - |
| ISU3 | 0 to 2.35 | Sandy low plasticity clay (CL) | - | - | 36.5 | 18.7 | 4.7[d] (0.9) | 0.072 | - |
| | 2.35 to 10.37 | Sandy low plasticity clay (CL) | 8 | 19.1 | 21.4 | 4.5 | 1.5 (8.2) | 0.077 | 0.192; 6.8 |
| | 10.37 to 15.55 | Low plasticity clay w/ sand (CL) | 10 | 19.0 | 30.6 | 10.8 | 1.3 (15.2) | 0.041 | - |
| ISU4 | 0 to 2.35 | Sandy low plasticity clay (CL) | 3 | 19.7 | 29.3 | 11.4 | - | - | - |
| | 2.35to 2.7 | Well graded sandy w/ clay (SW-SC) | - | 21.2 | - | - | - | - | - |
| | 2.7 to 6.05 | Silty sand (SM) | 5 | 20.2 | - | - | - | - | - |
| | 6.05 to 6.45 | Well graded sand (SW) | - | 21.6 | - | - | - | - | - |
| | 6.45 to 12.55 | Low plasticity clay w/ sand (CL) | 12 | 22.2 | 27.5 | 13.5 | 1.6 (8.2) | 0.077 | 0.036; 6.4<br>0.019; 6.5 |
| | 12.55 to 17.31 | Sandy low plasticity clay (CL) | 13 | 21.6 | 26.0 | 13.2 | 1.0 (13.7) | 0.076 | 0.009; 12.5<br>0.025; 15.4 |
| ISU5 | 0 to 7.7 | Low plasticity clay (CL) | 8 | 20.5 | 38.4 | 20.8 | 4.5[d] (2.4)<br>1.3 (7.6) | 0.107<br>0.089 | - |
| | 7.7 to 17.5 | Low plasticity clay w/ sand (CL) | 16 | 20.3 | 38.6 | 22.2 | n/a[e] (10.7) | 0.051 | - |
| ISU6 | 0 to 4.0 | Mixed fill (SC/CL) | 12 | - | 24.8 | 17.2 | 1.2 (3.7) | 0.033 | - |
| | 4.0 to 6.1 | Silty sand (SM) | 23 | 19.7 | 18.2 | 4.0 | - | - | - |
| | 6.1 to 9.0 | Sandy low plasticity clay (CL) | 8 | 19.2 | 24.8 | 10.9 | - | - | - |
| | 9.0 to 9.3 | Sandy to silty sand | 10 | - | - | - | - | - | - |
| | 9.3 to 15.5 | Sandy low plasticity clay (CL) | 21 | 23.5 | 26.7 | 13.1 | 1.1 (14.9) | 0.039 | 0.008; 15.2 |
| | 15.5 to 19.05 | Silt (ML) | 22 | 20.6 | 31.0 | 23.6 | n/a[e] (18) | 0.057 | |

[a] Estimated using Casagrande (1936) graphical procedure from one-dimensional consolidation test.
[b] Estimated using square root of time method from one-dimensional consolidation test.
[c] Estimated from CPT with pore pressure dissipation test using strain path method.
[d] Unusual high OCR due to mechanical compaction during road construction.
[e] The lack of concave or "break" in the e-log(σ) curve made the determination of the preconsolidation stress difficult.

Table 3.2: Weighted average soil properties along pile shaft and near pile toe

| Test pile | SPT *N*-value | | $C_h$ (cm$^2$/min) | | $C_v$ (cm$^2$/min) | | *PI* (%) | |
|---|---|---|---|---|---|---|---|---|
| | Shaft | Toe | Shaft | Toe | Shaft | Toe | Shaft | Toe |
| ISU2 | 5 | 4 | 0.208 | 0.178 | 0.126 | 0.113 | 14.86 | 28.40 |
| ISU3 | 8 | 10 | 0.045 | 0.026 | 0.102 | 0.097 | 9.95 | 8.15 |
| ISU4 | 10 | 13 | 0.056 | 0.015 | 0.094 | 0.100 | 15.44 | 13.06 |
| ISU5 | 12 | 13 | 0.028 | 0.015 | 0.090 | 0.085 | 18.17 | 22.33 |
| ISU6 | 14 | 22 | 0.022 | 0.005 | 0.085 | 0.092 | 9.22 | 7.43 |

Table 3.3: Summary of the five test piles and their results

| Test pile | Hammer | Type of event | Time after EOD, *t* (day) | Emb. pile length (m) | Blow per 300 mm | WEAP total resistance (kN) | CAPWAP pile resistance (kN) | | | SLT pile resistance (kN) | | |
|---|---|---|---|---|---|---|---|---|---|---|---|---|
| | | | | | | | Total | Shaft | End Bearing | Total | Shaft | End Bearing |
| ISU2 | Delmag D19-42 | EOD | 0 | 16.46 | 10 | 343 | 359 | 297 | 63 | 556 (9 days after EOD) | 492 | 64 |
| | | BOR1 | 0.17 | 16.77 | 14 | 448 | 517 | 451 | 66 | | | |
| | | BOR2 | 0.92 | 16.87 | 18 | 547 | 578 | 508 | 70 | | | |
| | | BOR3 | 2.97 | 17.02 | 22 | 617 | 578 | 507 | 71 | | | |
| ISU3 | Delmag D19-32 | EOD | 0 | 14.63 | 10 | 363 | 439 | 379 | 60 | 667 (36 days after EOD) | 605 | 62 |
| | | BOR1 | 2.85E-03 | 14.79 | 16 | 493 | 459 | 393 | 66 | | | |
| | | BOR2 | 7.30E-03 | 14.94 | 16 | 493 | 467 | 398 | 69 | | | |
| | | BOR3 | 1.66E-02 | 15.09 | 16 | 493 | 577 | 504 | 73 | | | |
| | | BOR4 | 1.11 | 15.3 | 18 | 539 | 637 | 564 | 73 | | | |
| | | BOR5 | 1.96 | 15.55 | 20 | 586 | 657 | 584 | 73 | | | |
| ISU4 | Delmag D19-42 | EOD | 0 | 16.77 | 13 | 422 | 453 | 392 | 60 | 685 (16 days after EOD) | Incomplete Readings | |
| | | BOR1 | 4.05E-03 | 16.87 | 15 | 472 | 469 | 398 | 71 | | | |
| | | BOR2 | 1.58E-02 | 16.97 | 18 | 543 | 484 | 414 | 71 | | | |
| | | BOR3 | 0.04 | 17.09 | 16 | 497 | 538 | 476 | 62 | | | |
| | | BOR4 | 0.74 | 17.18 | 21 | 592 | 601 | 532 | 69 | | | |
| | | BOR5 | 1.74 | 17.25 | 24 | 653 | 642 | 573 | 69 | | | |
| | | BOR6 | 4.75 | 17.31 | 26 | 687 | 685 | 616 | 69 | | | |
| ISU5 | Delmag D16-32 | EOD | 0 | 16.77 | 30 | 636 | 790 | 550 | 240 | 1081 (9 days after EOD) | 834 | 247 |
| | | BOR1 | 5.38E-03 | 16.87 | 36 | 791 | 842 | 600 | 243 | | | |
| | | BOR2 | 1.26E-02 | 16.97 | 37 | 809 | 957 | 713 | 244 | | | |
| | | BOR3 | 4.78E-02 | 17.07 | 38 | 823 | 979 | 732 | 246 | | | |
| | | BOR4 | 0.92 | 17.15 | 44 | 902 | 1035 | 778 | 257 | | | |
| | | BOR5 | 2.9 | 17.22 | 54 | 1013 | 1044 | 787 | 258 | | | |
| | | BOR6 | 7.92 | 17.28 | 72 | 1140 | 1088 | 829 | 259 | | | |
| ISU6 | Delmag D19-42 | EOD | 0 | 16.87 | 21 | 615 | 644 | 546 | 98 | 946 (14 days after EOD) | Incomplete Readings | |
| | | BOR1 | 1.60E-03 | 16.96 | 20 | 590 | 644 | 547 | 97 | | | |
| | | BOR2 | 4.36E-03 | 17.04 | 22 | 632 | 662 | 558 | 104 | | | |
| | | BOR3 | 1.17E-02 | 17.12 | 25 | 679 | 658 | 553 | 105 | | | |
| | | BOR4 | 6.71E-02 | 17.18 | 29 | 739 | 786 | 678 | 109 | | | |
| | | BOR5 | 0.83 | 17.27 | 38 | 879 | 831 | 721 | 110 | | | |
| | | BOR6 | 2.82 | 17.35 | 44 | 965 | 875 | 762 | 113 | | | |
| | | BOR7 | 6.79 | 17.41 | 53 | 1065 | 938 | 823 | 115 | | | |
| | | BOR8 | 9.81 | 17.44 | 60 | 1121 | 937 | 823 | 114 | | | |

Table 3.4: Percent increase in pile resistance based on WEAP, CAPWAP and SLT

| Test pile | Type of event | Time after EOD, $t$ (day) | WEAP, $\Delta R_t/R_{EOD}$ (%) | CAPWAP, $\Delta R_t/R_{EOD}$ (%) | | | SLT | | | |
|---|---|---|---|---|---|---|---|---|---|---|
| | | | | | | | $\Delta R_t/R_{EOD\text{-}WEAP}$ (%) | $\Delta R_t/R_{EOD\text{-}CAPWAP}$ (%) | | |
| | | | | Total | Shaft | End Bearing | Total | Total | Shaft | End Bearing |
| ISU2 | BOR1 | 0.17 | 31 % | 44 % | 52 % | 6 % | 62 % | 55 % | 66 % | 3 % |
| | BOR2 | 0.92 | 59 % | 61 % | 71 % | 12 % | | | | |
| | BOR3 | 2.97 | 80 % | 61 % | 71 % | 13 % | | (9 days after EOD) | | |
| ISU3 | BOR1 | 2.85E-3 | 36 % | 4 % | 4 % | 10 % | 84 % | 52 % | 60 % | 3 % |
| | BOR2 | 7.30E-3 | 36 % | 6 % | 5 % | 16 % | | | | |
| | BOR3 | 1.66E-2 | 36 % | 31 % | 33 % | 22 % | | | | |
| | BOR4 | 1.11 | 49 % | 45 % | 49 % | 21 % | | (36 days after EOD) | | |
| | BOR5 | 1.96 | 61 % | 49 % | 54 % | 21 % | | | | |
| ISU4 | BOR1 | 4.05E-3 | 12 % | 4 % | 1 % | 17 % | 62 % | 51 % | Incomplete Readings | |
| | BOR2 | 1.58E-2 | 29 % | 7 % | 5 % | 17 % | | | | |
| | BOR3 | 0.04 | 18 % | 19 % | 19 % | 15 % | | | | |
| | BOR4 | 0.74 | 40 % | 33 % | 36 % | 14 % | | | | |
| | BOR5 | 1.74 | 55 % | 42 % | 46 % | 13 % | | (16 days after EOD) | | |
| | BOR6 | 4.75 | 63 % | 51 % | 57 % | 14 % | | | | |
| ISU5 | BOR1 | 5.38E-3 | 24 % | 7 % | 9 % | 1 % | 70 % | 37 % | 52 % | 3 % |
| | BOR2 | 1.26E-2 | 27 % | 21 % | 30 % | 2 % | | | | |
| | BOR3 | 4.78E-2 | 30 % | 24 % | 33 % | 3 % | | | | |
| | BOR4 | 0.92 | 42 % | 31 % | 41 % | 7 % | | | | |
| | BOR5 | 2.90 | 59 % | 32 % | 43 % | 7 % | | (9 days after EOD) | | |
| | BOR6 | 7.92 | 79 % | 38 % | 51 % | 8 % | | | | |
| ISU6 | BOR1 | 1.60E-3 | -4 % | 0 % | 0 % | 0 % | 54 % | 47 % | Incomplete Readings | |
| | BOR2 | 4.36E-3 | 3 % | 3 % | 2 % | 6 % | | | | |
| | BOR3 | 1.17E-2 | 10 % | 2 % | 1 % | 7 % | | | | |
| | BOR4 | 6.71E-2 | 20 % | 22 % | 24 % | 11 % | | | | |
| | BOR5 | 0.83 | 43 % | 29 % | 32 % | 12 % | | | | |
| | BOR6 | 2.82 | 57 % | 36 % | 40 % | 15 % | | (14 days after EOD) | | |
| | BOR7 | 6.79 | 73 % | 46 % | 51 % | 17 % | | | | |
| | BOR8 | 9.81 | 82 % | 46 % | 51 % | 16 % | | | | |

Table 3.5: Summary of four best-fit trends and their coefficient of determinations for ISU6

| Type of Trend | Best-Fit Equation | Number of Empirical Constant | Coefficient of Determination, $R^2$ |
|---|---|---|---|
| Exponential | $\frac{\Delta R_t}{R_{EOD}} = 0.4394 - 0.2207e^{(-1.251\,t+0.5862)}$ | 4 | 0.9124 |
| Square Root | $\frac{\Delta R_t}{R_{EOD}} = 0.7952\sqrt{t^{0.1503}} - 0.4873$ | 3 | 0.9753 |
| Logarithmic | $\frac{\Delta R_t}{R_{EOD}} = 0.1192\log_{10}(t) + 0.3263$ | 2 | 0.9680 |
| Rational | $\frac{\Delta R_t}{R_{EOD}} = \frac{-3.065\,t}{-0.3558 - 9.054\,t^{0.8714}}$ | 4 | 0.9818 |

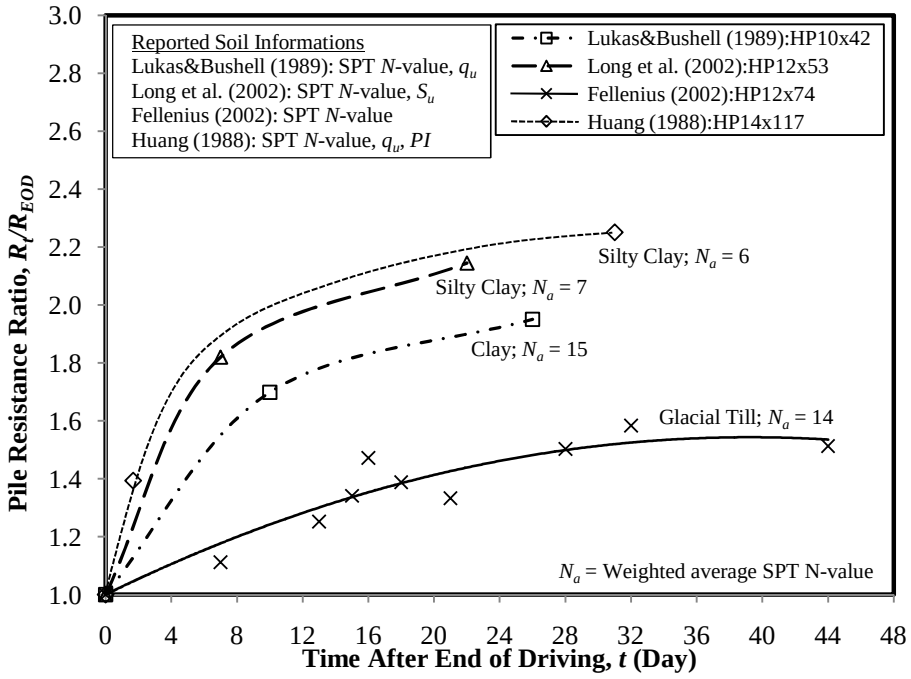


Figure 3.1: Summary of steel H-pile resistance ratio from literatures

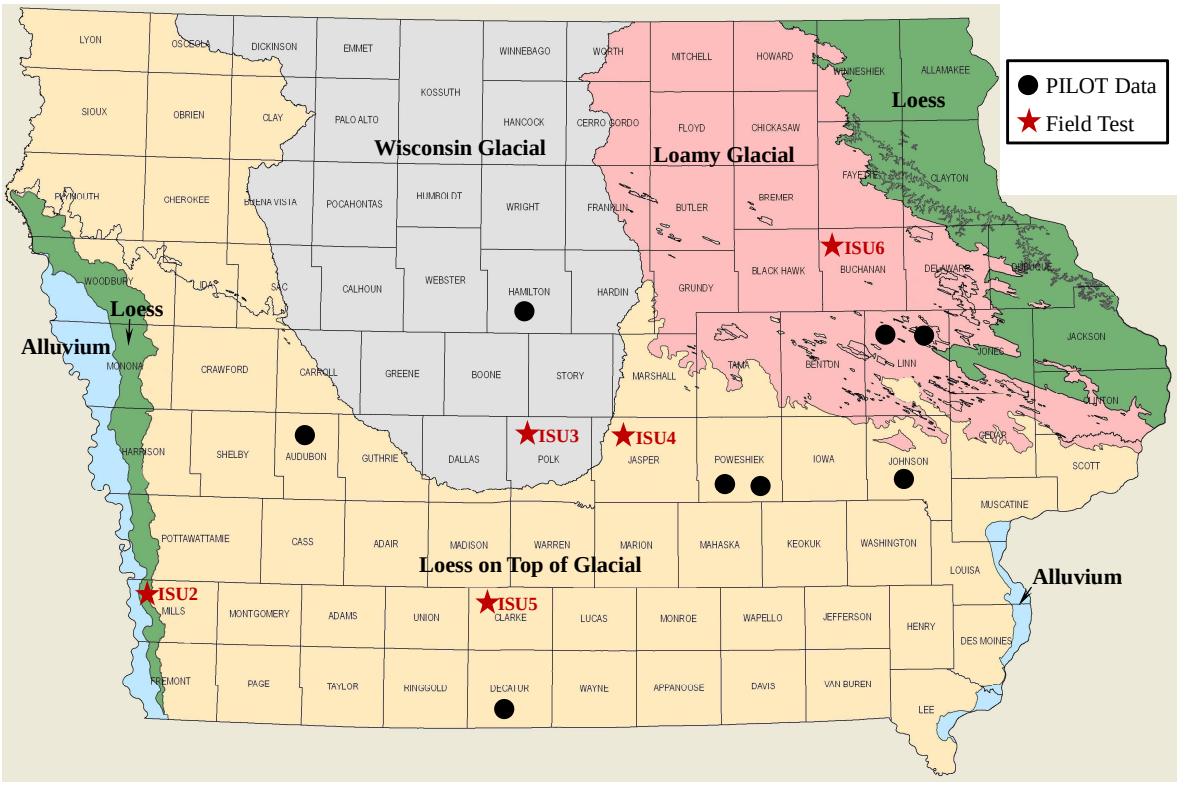


Figure 3.2: Locations of steel H-piles tested in the state of Iowa

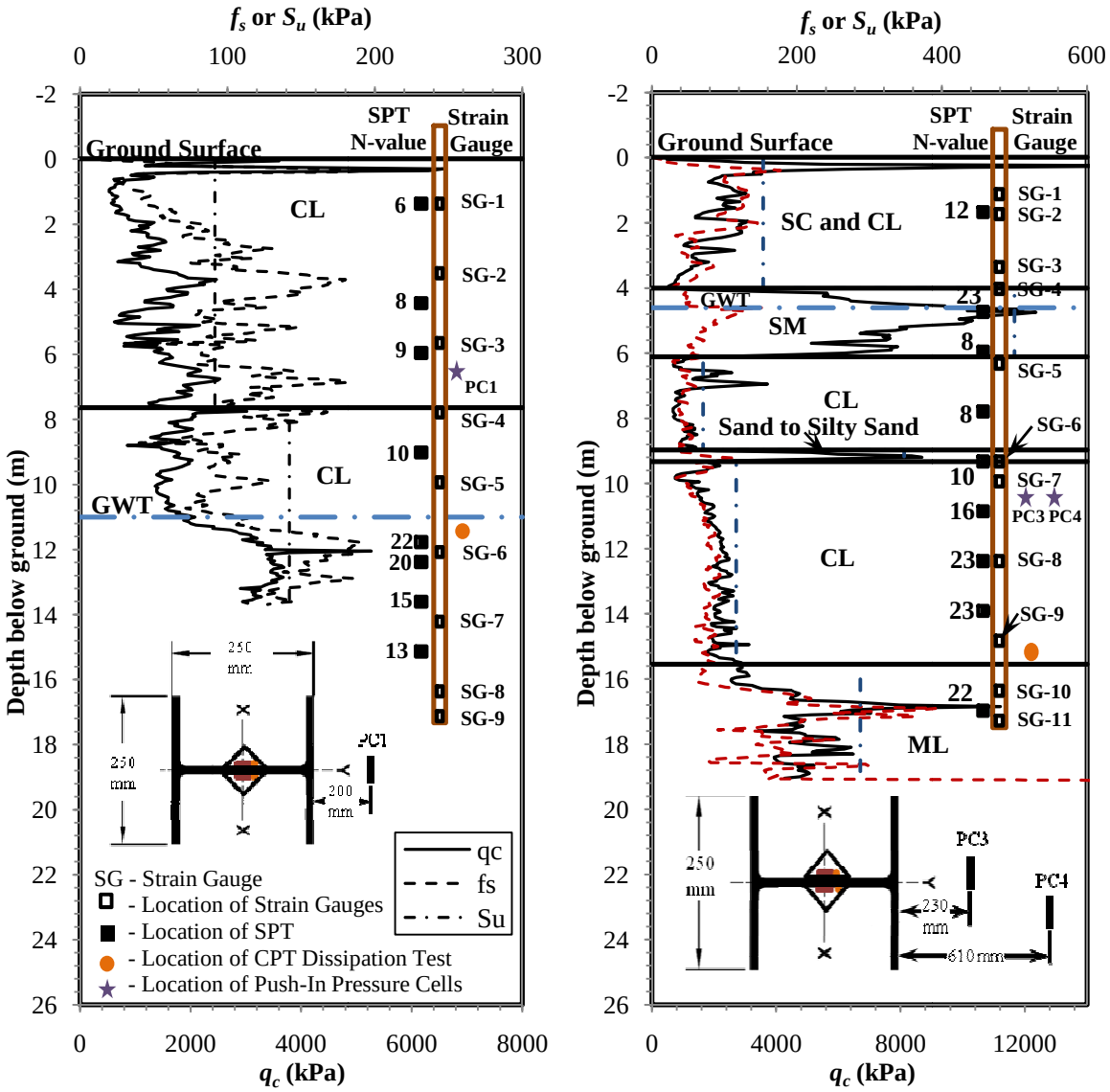


(a) For ISU5 (b) For ISU6

Figure 3.3: Soil profiles, soil test results, and test pile instrumentation schematics

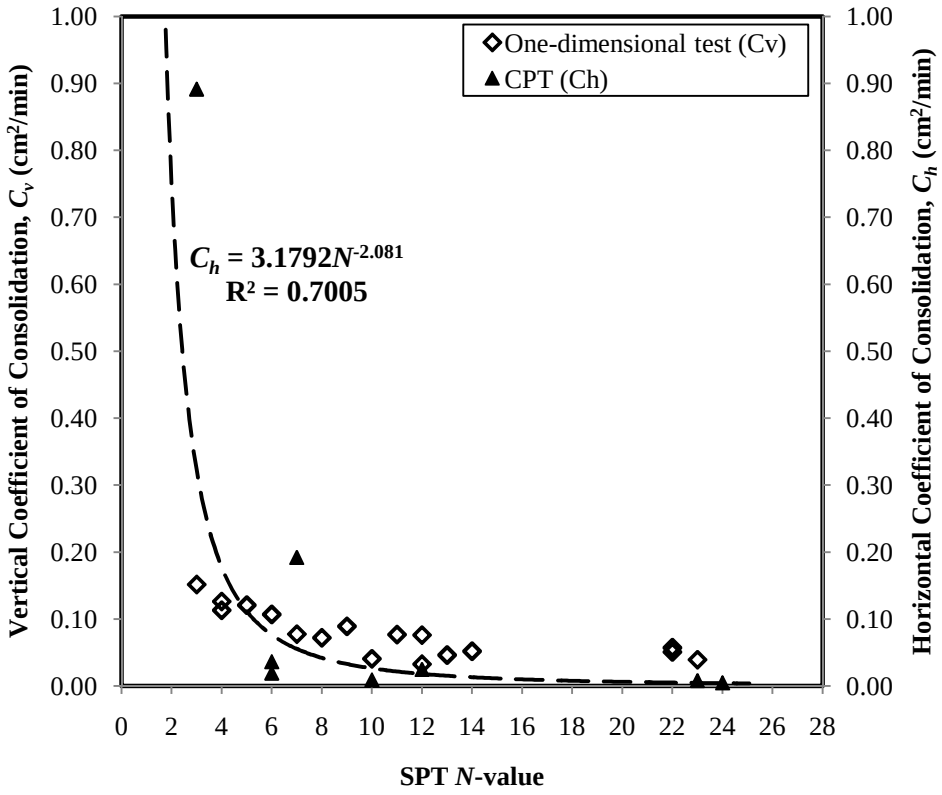


Figure 3.4: Proposed relationships between horizontal and vertical coefficients of consolidation and SPT N-value

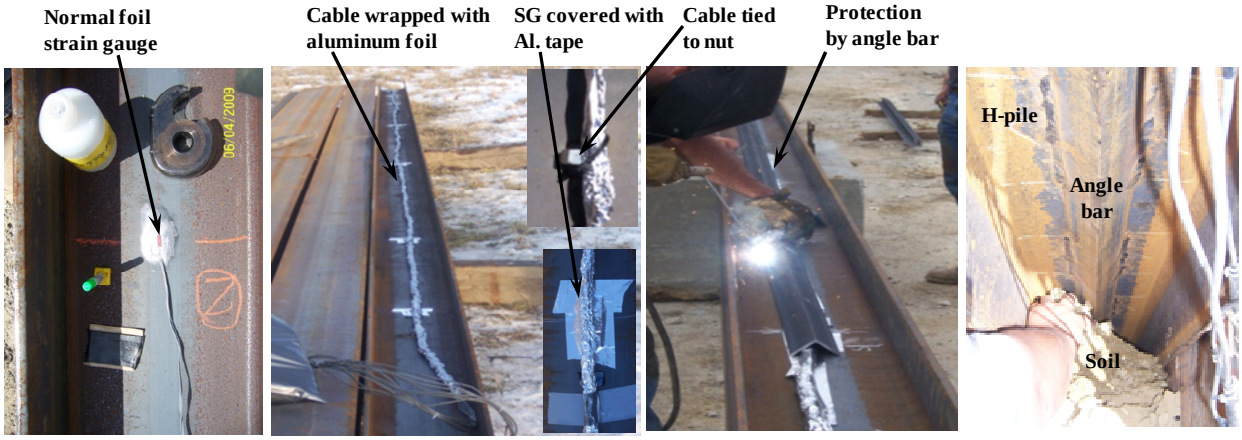


(a) strain gauges installation (b) cable protection (c) angle bar welded on the web (d) protected gauge region

Figure 3.5: Pile instrumentation with strain gauges

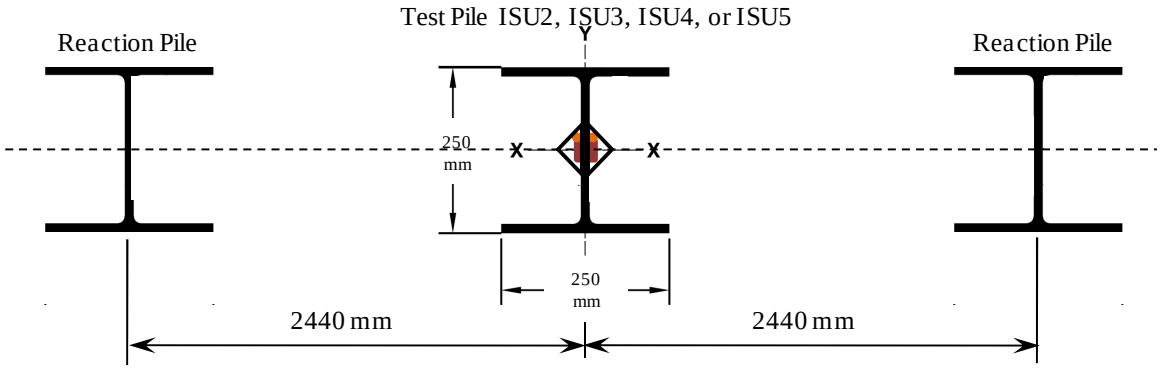


(a) For ISU2, ISU3, ISU4 and ISU5

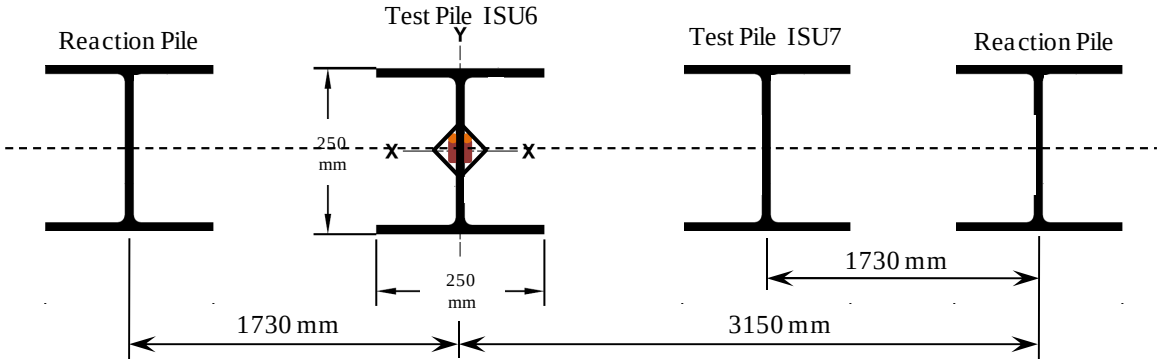


(b) For ISU6 and ISU7

Figure 3.6: Plan view of test configuration for reaction piles and test pile (a) for ISU2, ISU3, ISU4, and ISU5; and (b) for ISU6 and ISU7

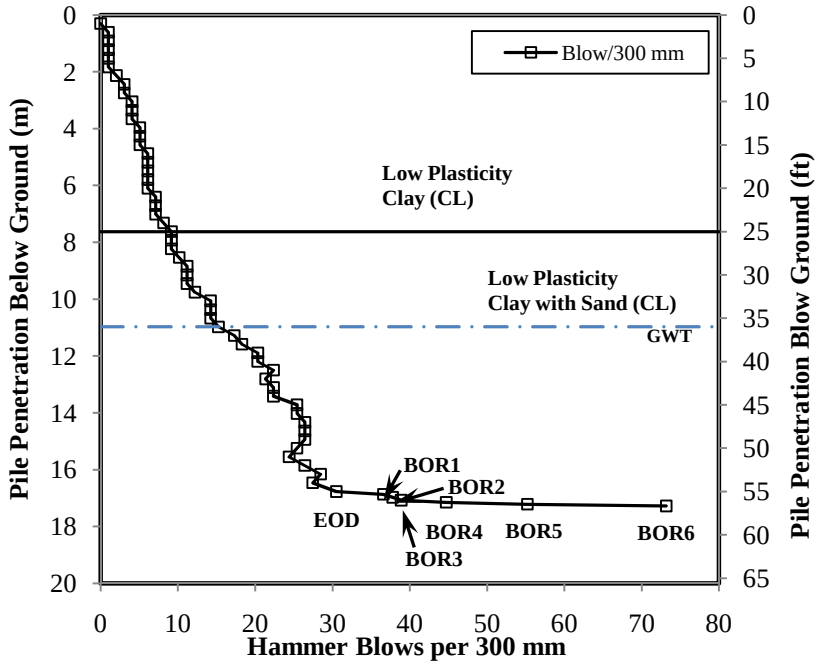


Figure 3.7: Pile driving resistance observed for ISU5

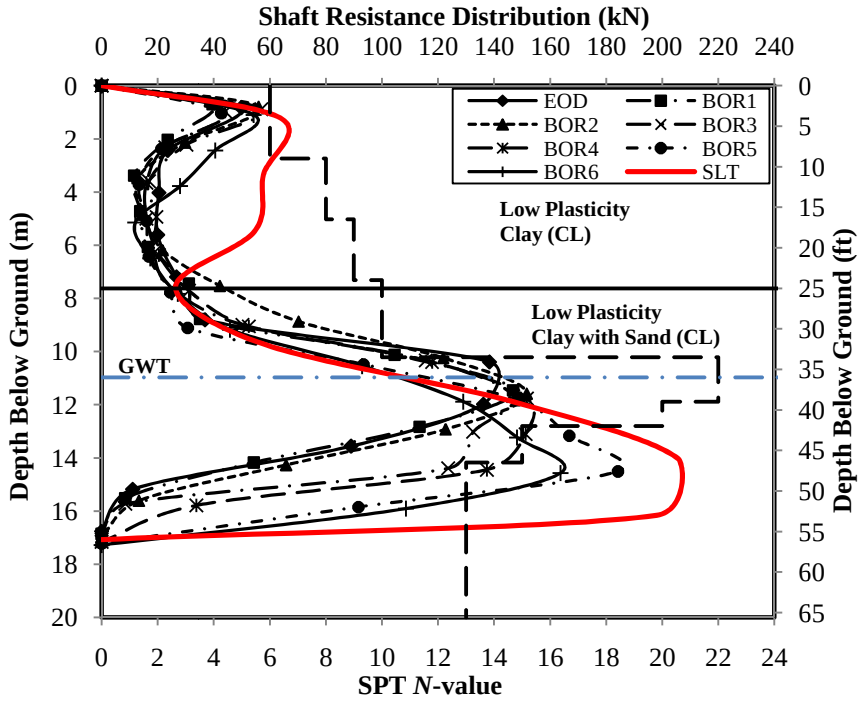


Figure 3.8: CAPWAP estimated and SLT measured pile shaft resistance distributions for ISU5

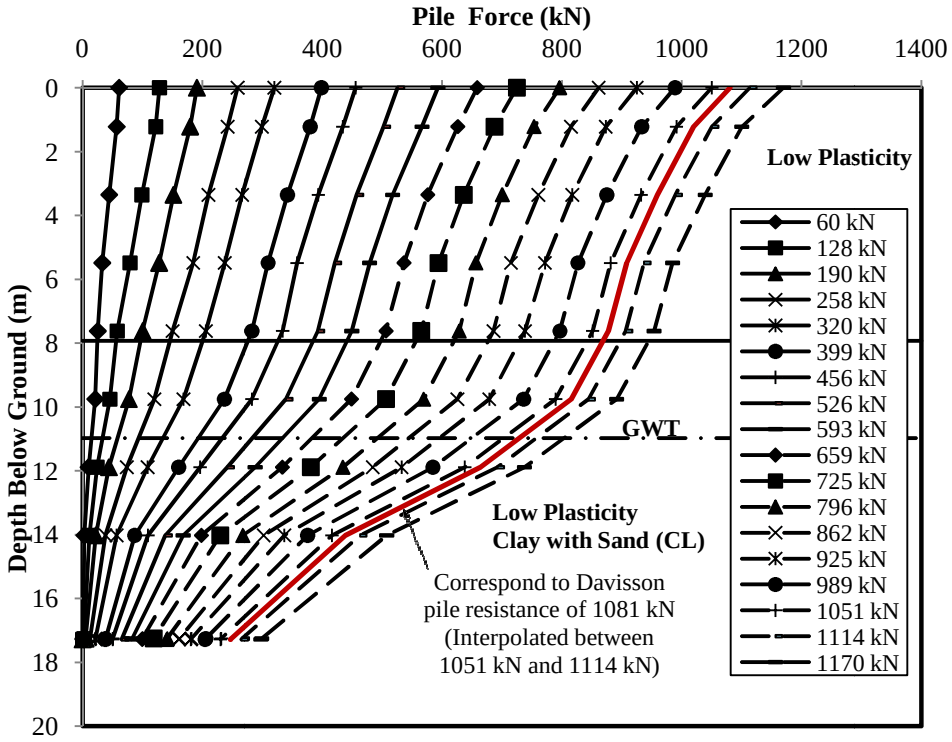


Figure 3.9: Measured force distribution along the pile length during SLT at each load increment for ISU5

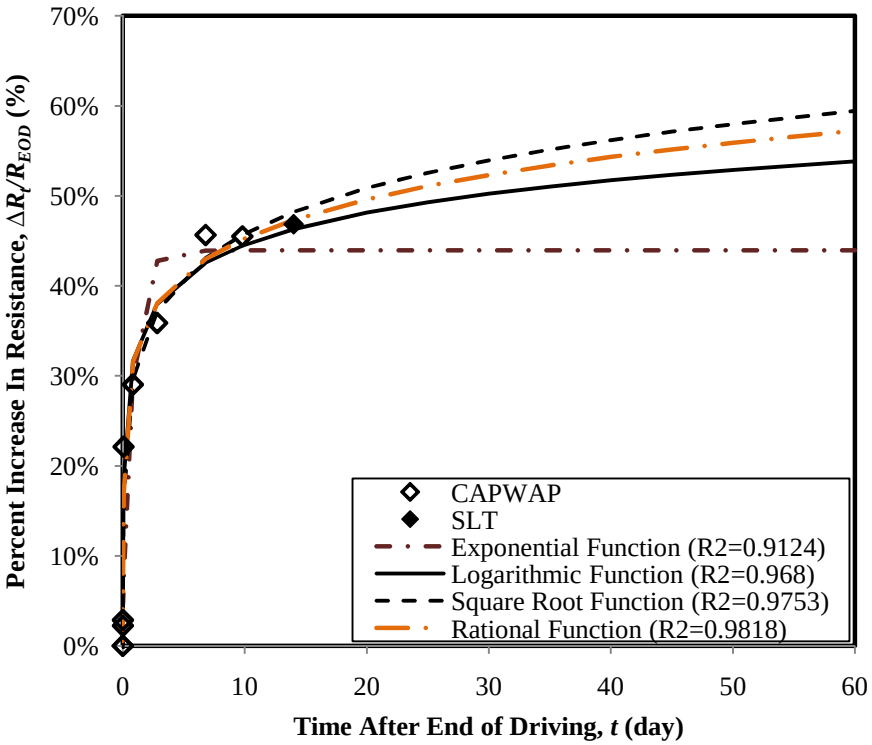


Figure 3.10: Four trends of percent increase in pile resistance to time based on restrike and static load test results of ISU6

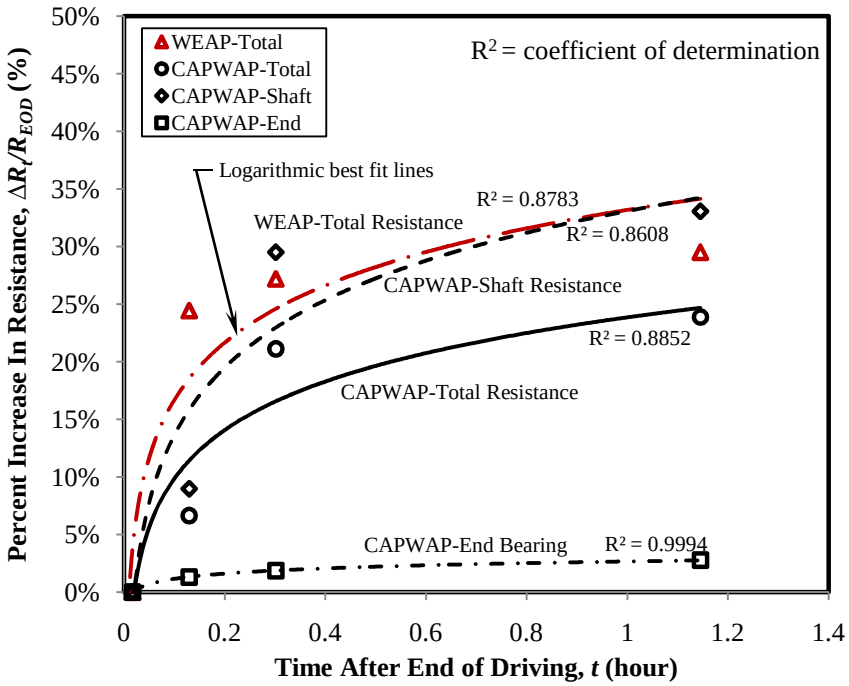


(a) For time in hour

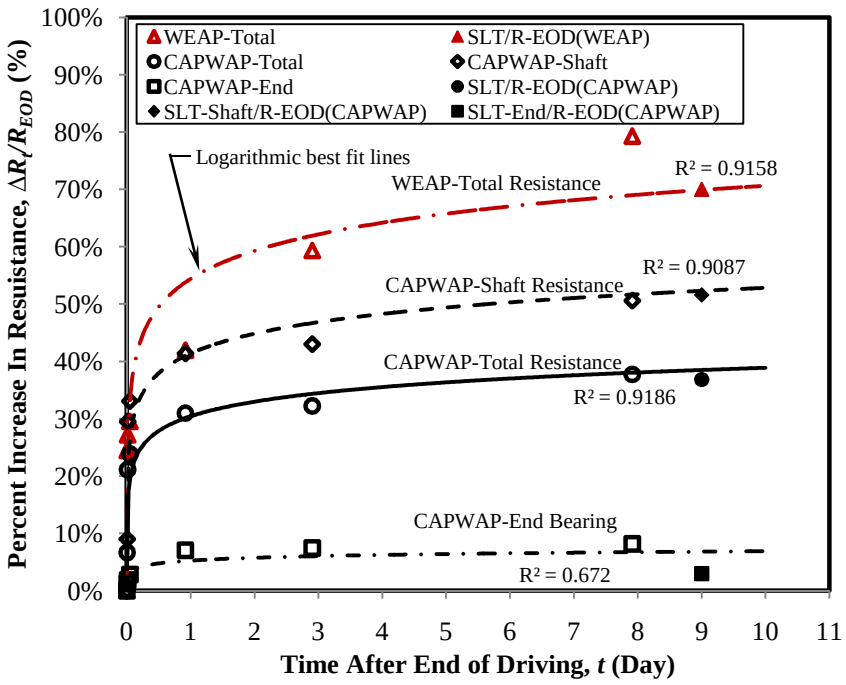


(b) For time in day

Figure 3.11: Estimated and measured percent increase in pile resistance for ISU5 with time after EOD in (a) hours; and (b) days

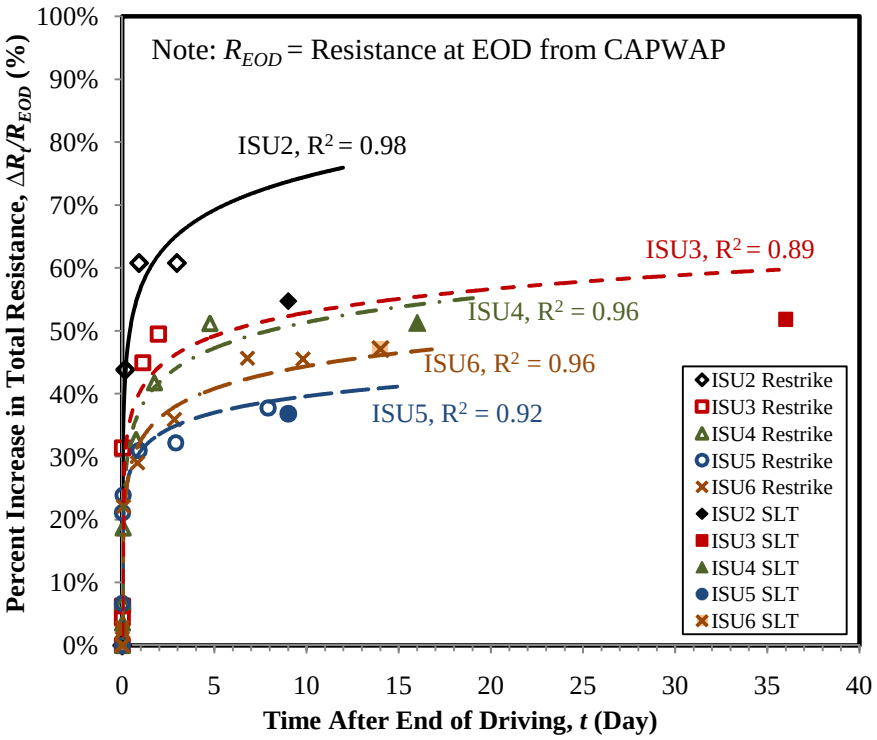


Figure 3.12: Percent increase in total resistance for all five test piles

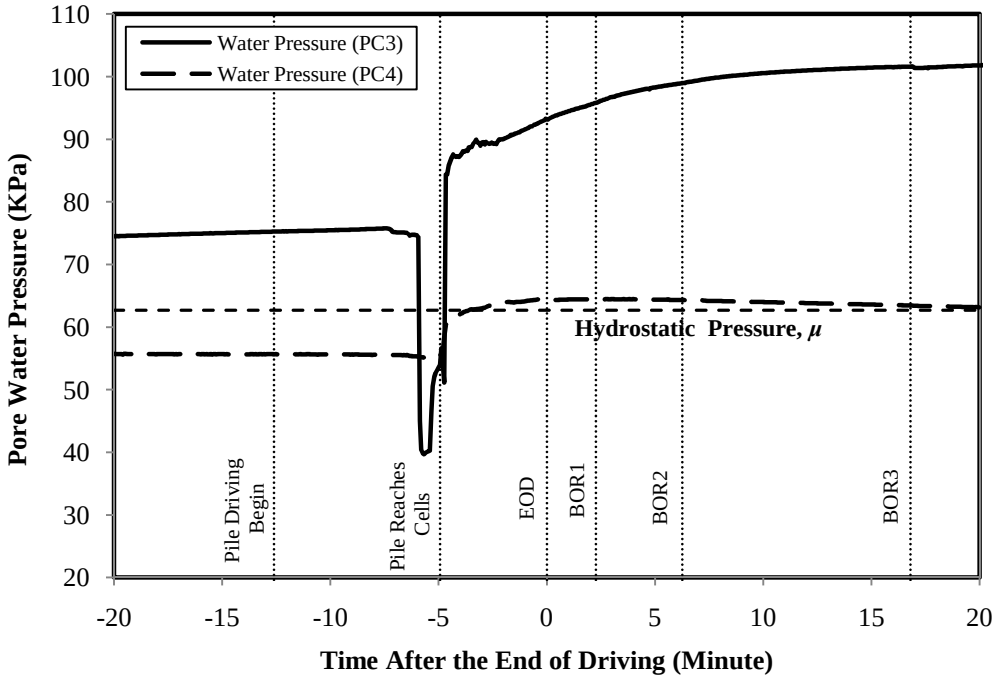


(a) For time in minute

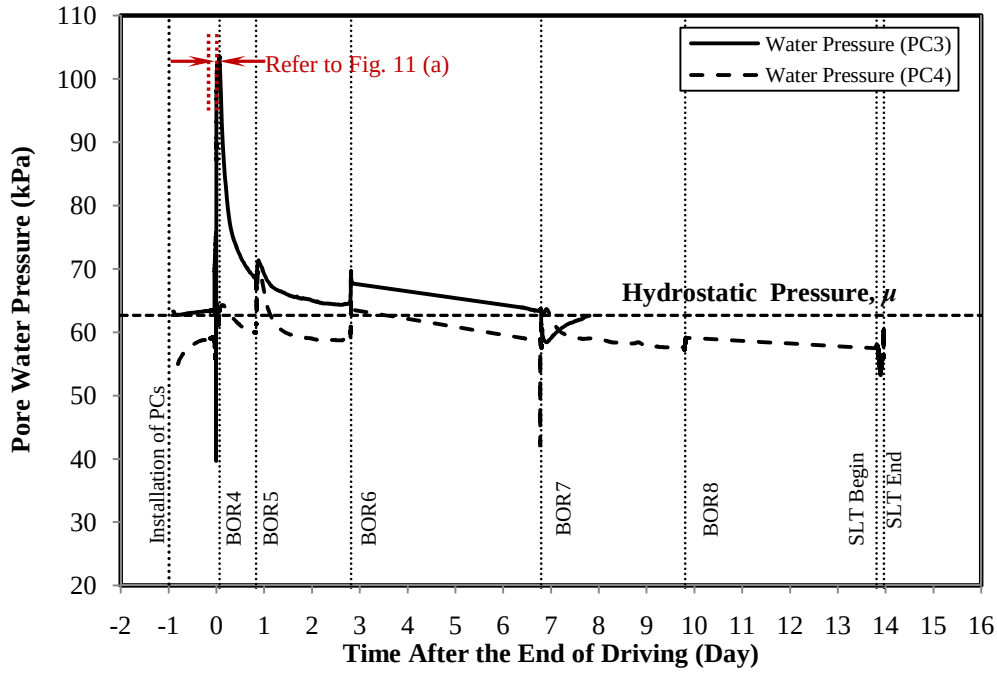


(b) For time in day

Figure 3.13: Pore water pressure recorded by push-in pressure cells (PC3 and PC4) at ISU6 as function of time considered after EOD in (a) minutes; and (b) days

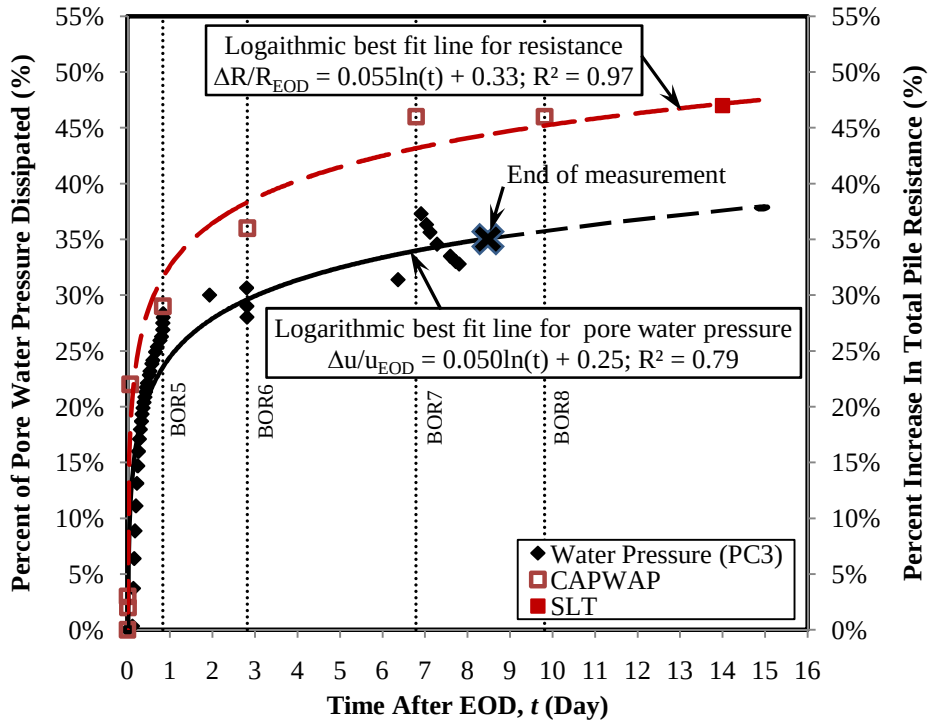


Figure 3.14: Comparison between pore water pressure dissipation and pile setup for ISU6

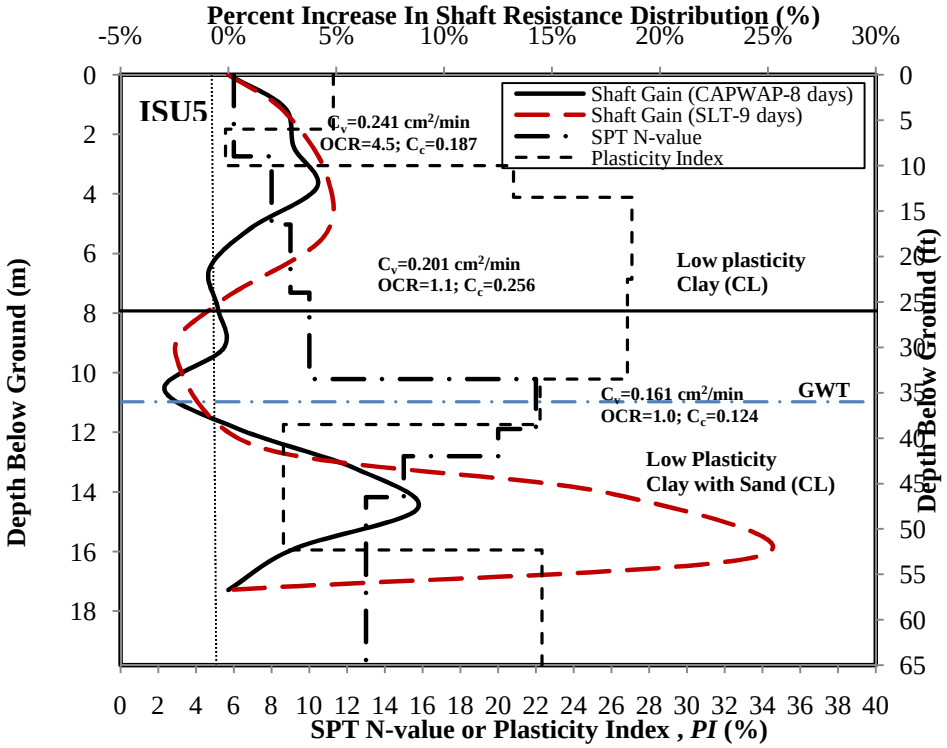


Figure 3.15: Relationship between percent increase in shaft resistance and soil properties for ISU5

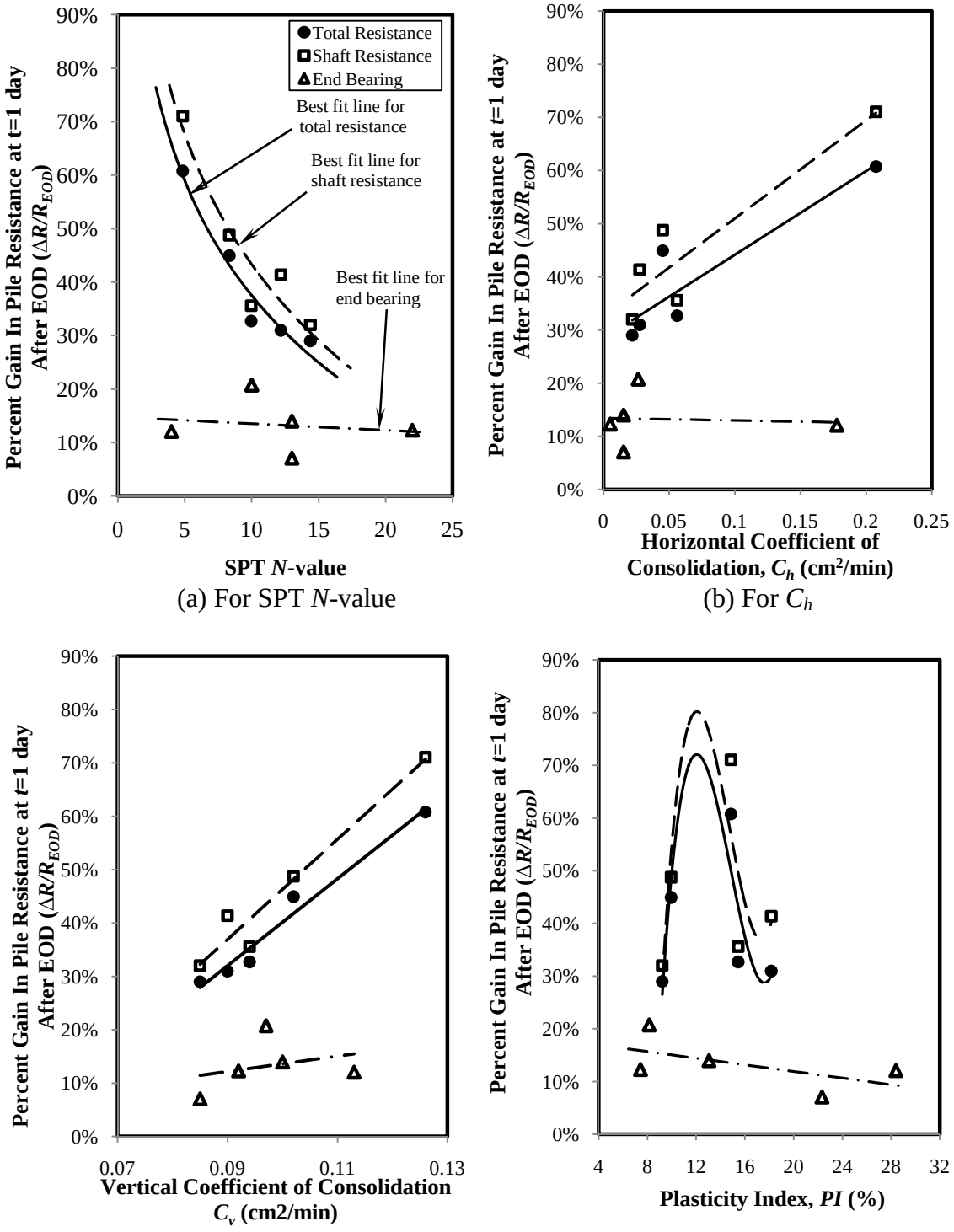


(a) For SPT *N*-value (b) For $C_h$

(c) For $C_v$ (d) For *PI*

Figure 3.16: Relationships between (a) SPT *N*-value; (b) $C_h$; (c) $C_v$; and (d) *PI* and percent gain in pile resistances estimated at a time of 1 day after the EOD for all sites

# CHAPTER 4: PILE SETUP IN COHESIVE SOIL WITH EMPHASIS ON LRFD: ANALYTICAL QUANTIFICATIONS AND DESIGN RECOMMENDATIONS

Ng, K. W.[1]; Suleiman, M. T.[2]; and Sritharan, S.[3]

A paper to be submitted to the Journal of Geotechnical and Geoenvironmental Eng., ASCE

## 4.1. Abstract

Using field test data presented in a companion paper for steel H-piles driven in cohesive soils, this paper establishes a methodology to quantify the pile setup. Existing methods found in the literature for the same purpose usually require inconvenient restrikes at the construction site and rarely use soil properties despite their significant influence on pile setup. Following a critical evaluation of the existing methods, a new approach for estimating pile setup was developed using dynamic measurements and analyses in combination with measured soil properties; mainly focusing on the average Standard Penetration Test (SPT) *N*-value and the horizontal coefficient of consolidation. Using pile setup information available in the literature, it has been shown that the proposed approach provides very good estimate for setup of different types and sizes of driven piles. Suitable design recommendations for incorporating pile setup within the Load and Resistance Factor Design (LRFD) framework are also presented.

**CE Database Keywords:** Pile Setup; SPT; Coefficient of Consolidation; PDA; WEAP; CAPWAP; Restrikes; Static load test; LRFD

---

[1]Ph.D. Candidate, Dept. of Civil, Construction and Environmental Engineering, Iowa State Univ., Ames, IA 50011. E-mail: kwng@iastate.edu
[2]Assistant Professor, Dept. of Civil and Environmental Engineering, Lehigh University, Bethlehem, PA 18015. E-mail: mts210@lehigh.edu
[3]Wilson Engineering Professor and Associate Chair, Dept. of Civil, Construction and Environmental Engineering, Iowa State Univ., Ames, IA 50011. E-mail: sri@iastate.edu

## 4.2. Introduction

Dynamic and static studies for steel H-piles and the corresponding measured soil properties described in the companion paper (Ng et al. 2011b) showed that pile setup in cohesive soils is a function of soil properties; mainly the SPT N-value and the coefficient of consolidation. The existing pile setup methods available in the literatures require inconvenient testing and/or have not incorporated soil properties into the pile setup equations. Therefore, these equations have not been incorporated into the AASHTO (2010) Specifications. Although, an accurate integration of pile setup will lead to a cost-effective foundation designs, AASHTO (2010) acknowledges that it is not feasible in practices to perform static load or dynamic restrike tests over an adequate period of time to quantify the pile setup. Recognized the benefits of pile setup and motivated by the correlation between pile setup and soil properties presented in the companion paper, a new analytical pile setup quantification method was developed based on five recently completed Iowa State University (ISU) field tests. Not only the proposed method incorporates the surrounding soil properties in the setup quantifications, but it also avoids the performance of inconvenient restrikes during construction to demonstrate its economic advantages. This proposed method was validated using both local and external case studies.

In this paper, the existing pile setup estimation methods and their associated limitations were discussed. In addition, to developing the proposed pile setup method using the results of the five tests conducted by the research team and summarized in Ng et al. (2011a), twelve data sets of PIle LOad Test database of the Iowa Department of Transportation (PILOT) and five well-documented tests completed by other researchers and reported in literatures on steel H-piles embedded in cohesive soils were used to validate the proposed method. During the development, the practicality and use of the proposed method within the Load and Resistance Factor Design (LRFD) framework during pile design was given specific consideration. In addition, the compatibility of the proposed method for different pile types and sizes was evaluated. This paper also discusses the confidence levels of the proposed pile setup method, the design recommendations within the LRFD framework, and includes a detailed design example in the Appendix to illustrate the application of the

proposed pile setup method in a practical foundation design.

### 4.3. Existing Pile Setup Estimation Methods

Five pile setup estimation methods, chronologically summarized Table 4.1 are available in the literature. Pei and Wang (1986) purely empirical setup equation has no incorporation of any soil properties and was specifically developed for Shanghai's soils. Furthermore, this method requires the determination of a maximum pile resistance ($R_{max}$) defined at 100% consolidation of the surrounding soil, which is usually difficult to be estimated in practice. Alternatively, Zhu (1988) equation included cohesive soil sensitivity ($S_t$) and was developed to estimate a pile resistance at $14^{th}$ day ($R_{14}$), which is also not practical due to the inflexibility of the method to predict a pile resistance at any time other than $14^{th}$ day.

Skov and Denver (1988) proposed a setup equation, which requires a restrike performed at 1 day after EOD ($t_o$) to estimate a reference pile resistance ($R_o$). Although they recommended the setup factor ($A$) of 0.6 based on Yoldia clay and 250 mm square concrete piles, the variability of soil and pile types yields a range of $A$ values from 0.1 to 1.0 (Bullock et al., 2005 and Yang et al., 2006). To verify these observations, the ISU field test results, including both from restrikes and static load tests, are plotted in Figure 4.1 and compared with the Skov and Denver (1988) setup equation. Figure 4.1 shows that the Skov and Denver (1988) method with the recommended $A$ value of 0.60 does not match the field test results. A good agreement can only be achieved if the $A$ value is reduced to 0.074, which is smaller than the range reported by Bullock et al. (2005) and Yang et al. (2006). In addition, the non-uniqueness of the $A$ values, which are usually determined from restrikes, have no correlations developed in terms of any soil properties limiting the general application of this equation. Although Svinkin and Skov (2000) method has taken into an account the actual time after EOD by allowing the reference pile resistance to be estimated at the EOD condition, the alternative soil dependent setup factor ($B$) value has also not been quantified in terms of soil properties for general practical applications.

Karlsrud et al. (2005) has incorporated the plasticity index (*PI*) and overconsolidation ratio (*OCR*) in their setup method based on a database of the Norwegian Geotechnical Institute (NGI), which consisted of 36 well documented pile tests on steel pipe piles with outer diameters greater than 200 mm. Fellenius (2008) concluded that the reference resistance at 100 days ($R_{100}$) by assuming complete pore water dissipation at this time is not true and not feasible in practice. To validate this method on steel H-piles, ISU field test results were used to extrapolate the $R_{100}$ for each test pile by best fitting a logarithmic trend through the estimated pile resistances determined using CAse Pile Wave Analysis Program (CAPWAP) from restrikes and the measured pile resistance obtained from static load test and later reading the $R_{100}$ from the trend at the 100 days. The estimated pile resistances and the measured pile resistance for each test pile were normalized by its respective $R_{100}$ to determine the pile resistance ratio ($R_t/R_{100}$) as plotted in Figure 4.2. Using the estimated $R_{100}$ value, the average *PI* value, and the average *OCR* value for each site, the pile resistances ($R_t$) at different times within 100 days were estimated using the pile setup equation of Karlsrud et al. (2005) and plotted in Figure 4.2. The poor comparison between the ISU field test results and the Karlsrud et al. (2005) method suggests that this pile setup method cannot be generally applied to different soil and pile conditions.

## 4.4. Pile Setup

### 4.4.1. Pile setup observations

As discussed in the companion paper (Ng et al. 2011b), steel H-pile is the most common foundation type used to support bridges in the United States based on a recent survey of State Departments of Transportation (AbdelSalam et al., 2010). The field test results on five HP 250 × 63 steel piles embedded in cohesive soils as explicitly described in the companion paper show a linear relationship between a normalized pile resistance ($R_t/R_{EOD}$) and a logarithmic normalized time ($\mathrm{Log}_{10}(t/t_{EOD})$) as plotted in Figure 4.3. To eliminate the pile resistance gain resulting from the additional pile penetrations during restrikes, the normalized pile resistance was corrected by multiplying with the normalized pile embedded pile length ($L_{EOD}/L_t$). In order to satisfy the logarithmic relationship and to

consider the immediate gain in pile resistance measured after the EOD, the time at the EOD ($t_{EOD}$) was assumed to be 1 minute (6.94E-3 day). Both CAse Pile Wave Analysis Program (CAPWAP) and Wave Equation Analysis Program (WEAP) with SPT *N*-value based method (SA as referred by Pile Dynamic, Inc. 2005) were selected for the following pile setup evaluations. Figure 4.3 presents the CAPWAP results by five linear best fits representing the five test piles. A similar evaluation was also performed for the WEAP-SA method shown in Figure 4.4. Each best fit line was generated using a linear regression analysis based on the restrike results indicated by open markers. All linear relationships shown in Figure 4.3 and Figure 4.4 except ISU3 of WEAP analysis fit reasonably with the normalized pile resistances, confirmed by good coefficients of determination ($R^2$). For a comparative purpose, static load test results, indicated by solid markers, are also included in the figures. The slope (*C*) of the best fit line describes the rate of a pile resistance gain; i.e., a larger slope indicates a higher percentage of pile setup or provides a larger normalized pile resistance ($R_t/R_{EOD}$) at a given time. Figure 4.3 and Figure 4.4 show that ISU2 (the short-dashed line) embedded in a relative soft cohesive soil (i.e., average SPT *N*-value of 5) has the largest slope of 0.167 for CAPWAP and 0.178 for WEAP. On the other hand, ISU5 (the long-dashed and dotted line) embedded in a relative stiff cohesive soil (i.e., average SPT *N*-value of 12) has the smallest slope of 0.088 for CAPWAP, and ISU4 (the long-dashed line) embedded in a relative stiff cohesive soil (i.e., average SPT *N*-value of 10) has the smallest slope of 0.141 for WEAP.

### 4.4.2. Development of pile setup rate

Given that all test steel H-piles have the same size and the additional pile penetration was corrected for using the normalized embedded pile length ($L_{EOD}/L_t$), the non-uniqueness of the slopes or pile setup rates (*C*) shown in Figure 4.3 and Figure 4.4 confirms that its variation depends on the surrounding soil properties. The general form of the proposed pile setup equation is

$$\frac{R_t}{R_{EOD}} = \left[C\log_{10}\left(\frac{t}{t_{EOD}}\right) + 1\right]\left(\frac{L_t}{L_{EOD}}\right) \tag{4.1}$$

In order to characterize the pile setup rate ($C$) with soil properties, the normalized embedded pile length ($L_t/L_{EOD}$), which ranged between 1 and 1.06 based on all field tests, was assumed unity. Differentiating Eq. (4.1) with respect to time and applying the product rule, Eq. (4.1) yields Eq. (4.2).

$$\frac{1}{R_{EOD}}\frac{dR_t}{dt} = \frac{dC}{dt}\left[\log_{10}\left(\frac{t}{t_{EOD}}\right)\right] + \frac{C}{t\ln(10)} \tag{4.2}$$

Given that the rate of pile setup for a test site is a constant with time ($t$) (i.e., the slope $C$ shown in Figure 4.3 and Figure 4.4), the first term on the right side of $\frac{dC}{dt}$ equals to zero and is eliminated. Since Figure 4.5 shows a poor relationship between the pile setup rate ($C$) and the initial pile resistance ($R_{EOD}$), estimated using either CAPWAP or WEAP, the $C$ is also assumed to be independent of $R_{EOD}$. The rearrangement of Eq. (4.2) shows that the pile setup rate ($C$) is directly proportional to the rate of pile resistance gain ($dR_t/dt$) given by

$$C \propto \frac{dR_t}{dt} \tag{4.3}$$

Assuming the dissipation of excess pore water pressure occurs mainly in the horizontal direction along the embedded pile length, Soderberg (1962) suggested that the increase in pile resistance with time ($dR_t/dt$) could be related to a non-dimensional time factor $T_h$ given by

$$T_h = \frac{C_h t}{r_p^2} \tag{4.4}$$

where $r_p$ = pile radius or equivalent pile radius based on its cross sectional area; and $C_h$ = horizontal coefficient of consolidation. This relationship is consistent with the observation made in the companion paper where the increase in shaft resistance ($\Delta R$) is proportional to $C_h$. In addition, the field test results indicate an inverse relationship between the rate of pile resistance gain ($dR_t/dt$) and an average SPT $N$-value ($N_a$). Results presented in the

companion paper also show that pile setup mostly occurs along the pile shaft. Therefore, only the cohesive soil layers along the pile shaft are considered in the calculation of the $N_a$. The average SPT *N*-value is calculated by weighting the measured *N*-value ($N_i$) at each cohesive soil layer *i* along the pile shaft by its thickness ($l_i$) for total of *n* cohesive layers situated along the embedded pile length, or it is simply expressed as

$$N_a = \frac{\sum_{i=1}^{n} N_i l_i}{\sum_{i=1}^{n} l_i} \tag{4.5}$$

As discussed before, the best fit lines demonstrate that the pile setup rate (*C*) for a specific site is independent of the time (*t*) and $R_{EOD}$. Therefore, Eq. (4.3) can be presented by replacing ($dR_t/dt$) with the horizontal coefficient of consolidation and the average SPT *N*-value as shown below.

$$C \propto \frac{C_h}{N_a r_p^2} \tag{4.6}$$

The $C_h$ values were estimated from pore water pressure dissipation tests during CPT and calculated using the strain path method reported by Houlsby and Teh (1988). In case $C_h$ was not measured, it can be estimated from its respective SPT *N*-value based on the correlation study discussed in the companion paper using Eq. (4.7)

$$C_h(cm^2/min) = \frac{3.179}{N^{2.08}} \tag{4.7}$$

The $C_h$ value in Eq. (4.6) was taken to be an average value calculated using an equation similar to Eq. (4.5). The soil parameters ($C_h$ and $N_a$) are listed in Figure 4.6. An equivalent pile radius ($r_p$) of 5.05 cm was calculated from the 80 $cm^2$ cross-sectional area of HP 250 × 63. Plotting the *C* values determined from Figure 4.3 for CAPWAP and from Figure 4.4 for WEAP-SA with the $\frac{C_h}{N_a r_p^2}$ values in Figure 4.6, the relationship for Eq. (4.6) can be best expressed as

$$C = f_c\left(\frac{C_h}{N_a r_p^2}\right) + f_r \tag{4.8}$$

where $f_c$ = consolidation factor; and $f_r$ = remolding recovery factor, which are tabulated in Figure 4.6 for both the CAPWAP and WEAP-SA. Since pile setup is influenced by the superposition of soil consolidation and recovery of the surrounding remolded soils, the effect of soil consolidation is best described by the first term on the right $\left(\frac{f_c\, C_h}{N_a r_p^2}\right)$ and the effect of recovery of the remolded soils is best accounted for by the remolding recovery factor ($f_r$). The two distinct best fit lines shown in Figure 4.6 indicate that a larger *C* value will be estimated based on the factors ($f_c$ and $f_r$) calibrated for the WEAP-SA analyses. The difference in the two best fit lines was attributed to the larger initial pile resistances estimated at EOD ($R_{EOD}$) using CAPWAP, which resulted in the smaller *C* values determined from Figure 4.3. Furthermore, a better match was observed for CAPWAP, represented with a higher coefficient of determination ($R^2$) of 0.95. In other words, Eq. (4.8) based on CAPWAP has a better accuracy than that based on WEAP-SA in predicting the *C* value.

### 4.4.3. Proposed method

The pile setup rate (*C*) has been successfully quantified using Eq. (4.8). Substituting Eq. (4.8) into setup Eq. (4.1), the proposed pile setup equation is expressed as

$$\frac{R_t}{R_{EOD}} = \left[\left(\frac{f_c C_h}{N_a r_p^2} + f_r\right)\log_{10}\left(\frac{t}{t_{EOD}}\right) + 1\right]\left(\frac{L_t}{L_{EOD}}\right) \tag{4.9}$$

It is important to note that this proposed pile setup equation is developed from ISU field tests based on one size steel H-piles embedded in cohesive soils. Although it needs to be validated for other piles sizes and types (discussed later), when compared with the existing pile setup methods discussed early, the proposed pile setup method in Eq. (4.9) provides the following advantages and simplifications for designers:-

1. Considering a reference pile resistance at EOD which can be conveniently estimated using either WEAP-SA or CAPWAP;

2. Accounting for the actual time elapsed immediately after a pile installation and assumes the time at the EOD ($t_{EOD}$) as small as 1 minute;
3. Incorporating measureable soil parameters from SPTs and CPTs for a general pile setup rate estimation;
4. Not requiring any inconvenient restrikes during constructions; and
5. Accounting for the soil parameters at different layers along a pile shaft.

## 4.5. Validation

The proposed pile setup equation was developed using one-size steel H-piles (HP 250 × 63) installed in cohesive soils. Therefore, to generalize the use of the proposed method, it is necessary to validate the equation for different sizes of steel H-piles and for different pile types and sizes. This section summarizes this validation process using data records available in PILOT and in the literature. Since the proposed equation was established to quantify pile setup experiences in cohesive soil, its application for a mixed soil profile is evaluated using a recently completed steel H-pile ISU8.

### 4.5.1. Steel H-pile

It is important to validate the proposed pile setup method using both Iowa data records from the PILOT (Roling et al., 2010) as well as using data available in the literature that represent different steel H-piles embedded in cohesive soils. The PILOT contains twelve data records in cohesive soils that have sufficient pile, soil and hammer information for pile setup evaluations using the WEAP-SA. However; it contains no Pile Driving Analyzer (PDA) records required for CAPWAP analysis. Table 4.2 summarizes the essential information of the twelve records for the proposed pile setup estimations. Although other pile sizes were used, HP 250 × 63 was the most commonly used steel piles, and they were embedded in primarily cohesive soils. Since CPTs with dissipation tests were not performed at these sites, the average $C_h$ values were estimated from Eq. (4.7) using SPT $N$-values. SLTs were performed between 1 and 8 days after the EOD, and the measured pile resistances were determined based on the Davisson's criterion. The pile resistances at the EOD

condition ($R_{EOD}$) were estimated using the WEAP-SA method.

In addition, five well documented steel H-piles tested by other researchers and available in the literature were used for examining the validity of Eq. (4.9) and these tests are summarized in Table 4.3. These researchers used three different pile sizes, namely HP250, HP 310 and HP 360. The average $C_h$ values were estimated from SPT $N$-values using Eq. (4.7). The measured pile resistances determined either from SLTs or restrikes using CAPWAP were listed with respect to the time when the tests were performed. The estimated pile resistances at the EOD condition ($R_{EOD}$) using both CAPWAP and WEAP-SA methods provided in the literature were also summarized. In three cases, marked with a superscript "a", the $R_{EOD}$ values were estimated using WEAP-SA based on the reported information.

Using the information provided in Table 4.2 and Table 4.3 as well as the results of the five field tests conducted by the research team, Figure 4.7 and Figure 4.8 compare the measured pile resistances ($R_m$) with pile resistances ($R_t$) estimated at the EOD condition and those estimated using the proposed pile setup equation (Eq. (4.9)) at the time ($t$) of the SLTs or restrikes for CAPWAP and WEAP-SA, respectively. A linear best fit (the dashed line) calculated using a linear regression analysis was plotted and compared with an equal line (the solid line). Both figures show that the proposed pile setup method successfully predicted the pile resistances (i.e., shifting the best fit lines towards the equal lines). It should be emphasized that although the proposed pile setup method was developed for one steel H-pile size (HP 250 × 63), the results presented in Figure 4.7 and Figure 4.8 show good predictions for other H-pile sizes.

To avoid the bias created from the local conditions, pile resistance ratios ($R_m/R_t$), the ratio between the measured pile resistances ($R_m$) and the estimated pile resistances ($R_t$) using Eq. (4.9) with pile setup consideration, based only on data available in the literature summarized in Table 4.3 presented in normal distribution curves for both CAPWAP and WEAP-SA as shown in Figure 4.9. A similar statistical evaluation was performed based on pile resistance ratios ($R_m/R_{EOD}$) for the EOD condition and included in Figure 4.9. When the normal distribution curves for the EOD condition and distributions accounting for pile setup

were compared using the proposed methods, Figure 4.9 shows the shifting of mean values ($\mu$) towards unity (from 1.53 to 1.04 for CAPWAP and from 1.78 to 1.06 for WEAP-SA) and the reduction of standard of deviations ($\sigma$) (from 0.32 to 0.17 for CAPWAP and from 0.39 to 0.20 for WEAP-SA). The results clearly show that the proposed pile setup Eq. (4.9) has adequately and consistently predicted the increase in pile resistances in different cohesive soil conditions for steel H-piles with different sizes. Similar observations presented in Figure 4.10 based on all data records were shown. This statistical assessment validates the proposed pile setup method for steel H-piles.

### 4.5.2. Other pile types

Similar assessment was performed to evaluate the application of the proposed method on other pile types installed in cohesive soils. Six well documented cases were used for this purpose as summarized in Table 4.4, which include the following information: (1) SPT *N*-values; (2) initial pile resistances at EOD ($R_{EOD}$); (3) CAPWAP measured pile resistances at the beginning of restrikes (BORs) and/or measured pile resistances from SLTs ($R_m$); and (4) times of restrikes and/or SLTs ($t$). Pile types comprised of closed-ended pipe piles (CEP) and opened-ended pipe piles (OEP), square precast prestressed concrete piles (PCP) and steel monotube piles (MP). The pile sizes or diameters ranged from 244 mm to 750 mm. Furthermore, the number of piles, embedded pile lengths, hammer type, and brief soil profile descriptions were also included in Table 4.4. To differentiate between the small displacement and large displacement piles, a pile area ratio (*AR*) (i.e., a ratio between pile embedded surface area and pile tip area) was calculated for each pile type and compared with a quantitative boundary of 350 suggested by Paikowsky et al. 1994. Since the largest estimated *AR* is 278 for 273 mm OEP was smaller than 350, all piles were classified as large displacement piles.

The comparison between pile resistances obtained during restrikes and SLTs ($R_m$) and initial pile resistances at EOD ($R_{EOD}$) reported in the literatures are plotted in Figure 4.11 shows that the $R_m$ values are larger than the $R_{EOD}$ values (most data points above the solid equal line) confirming the occurrence of pile setup. Using the reported $R_{EOD}$ value, estimated

average SPT *N*-value ($N_a$) calculated using Eq. (4.5), horizontal coefficient of consolidation ($C_h$) estimated using Eq. (4.7), and pile radius ($r_p$), a pile resistance was estimated using the proposed pile setup method presented in Eq. (4.9) at the time of restrike or SLT. With the consideration of pile setup using the proposed method, Figure 4.12 shows that the data points represented with a linear best fit dashed line shifts towards the solid equal line of measured and estimated resistances.

For comparative purposes, means ($\mu$) and standard deviations ($\sigma$) of pile resistance ratios for both EOD condition ($R_m/R_{EOD}$) and the proposed setup method ($R_m/R_t$) were calculated based on two pile categories: (1) pile sizes equal to and greater than 600 mm (referred to as large diameter piles); and (2) pile sizes smaller than 600 mm (referred to small diameter piles). Based on the $\mu$ and $\sigma$ values summarized in Figure 4.11, large diameter piles exhibited a greater pile setup than smaller piles, supported by larger $\mu$ and $\sigma$ values of 1.663 and 0.591, respectively. The consideration of pile setup using the proposed method not only reduces the $\mu$ values from 1.663 to 1.184 and from 1.454 to 1.063 for large and small diameter piles, respectively, but it also reduces the $\sigma$ values. When comparing the $\mu$ and $\sigma$ values given in Figure 4.12, the smaller $\mu$ and $\sigma$ values of 1.063 and 0.274, respectively, reveal that the proposed setup method provides a better pile setup prediction for smaller diameter piles. When compared with the values computed based on steel H-piles given in Figure 4.10 ($\mu$ = 1.024 and $\sigma$ = 0.153), the results confirm that the proposed setup method provides a better setup prediction for low displacement piles (steel H-piles) than large displacement piles. This assessment provides a potential for future refinement of the pile setup method for large displacement piles, providing that detailed soil information and pile response measurements as similarly performed on steel H-piles.

### 4.5.3. Mixed soil profile

The application of the proposed Eq. (4.9) to quantifying the increase in pile resistance of a steel H-pile embedded in a mixed soil profile was evaluated using the field test results of a recently completed test pile ISU8. It is a HP 250 × 63 steel pile embedded in a layer of approximately 6.4 m (21 ft) low plasticity clay (CL) underlying with approximately 5.18 m

(17 ft) well-graded sand (SW) and a 5.21 m (17 ft) sand, silt, and clay mixture. The ground water table (GWT) was located approximately 7.6 m (25 ft) below the ground surface. The detailed soil profile was given in Table 4.5. Also, the corresponding average SPT N-values and the horizontal coefficients of consolidation ($C_h$) were listed. The necessary information at different stages of pile testing was listed in Table 4.6. The listed measured pile resistances were referred to resistances determined at EOD and beginning of restrikes (BOR) using CAPWAP, and using a static load test (SLT) performed 15 days after EOD. Using the soil information given in Table 4.5, the weighted average SPT N-value ($N_a$) and $C_h$ value were determined to be 8.6 and 0.075 $cm^2$/minute (0.012 $in^2$/minute), respectively. Based on the measured pile resistance at EOD ($R_{EOD}$) of 621 kN (140kips), pile resistances corresponded to the time of restrikes and SLT were estimated using Eq. (4.9). Assumed the excess pore water pressure induced during pile driving dissipates immediately at the cohesionless soil layers (i.e., well-graded sand, silty sand, clayey sand, or sandy silt), no pile setup was considered at these layers. As a result, the originally-estimated pile resistances, which were determined for a fully embedded cohesive soil profile, were corrected with respect to the proportion of cohesive soil thickness to the embedded pile length. However, due to the presence of cohesionless soil layers overlaying and/or underlying the cohesive soil layers, the excess pore water pressure induced during pile driving at the cohesive soil layers can dissipate through the cohesionless layers. It is believed that the excess pore water pressure in a cohesive layer with a double drainage path (i.e., overlaying and underlying with cohesionless soil layers) dissipates faster than that with a single drainage path. Assuming the excess pressure dissipated immediately at a total thickness of a cohesive layer with a double drainage path and at half thickness of a cohesive layer with a single drainage path, the proportion of effective cohesive soil layers, that were believed to exhibit increase in pile resistance, was reduced by 50% (i.e., ratio of effective cohesive layer to the embedded pile length reduced from about 0.64 to 0.32). Based on abovementioned assumption, the estimated pile resistances were further adjusted as given in Table 4.6.

The measured and estimated pile resistances were normalized by the initial pile resistance at EOD ($R_{EOD}$) of 621 kN (140kips) and were plotted as a function of the time ($t$)

in Figure 4.13. It was expected that the originally-estimated pile resistances using Eq. (4.9) were higher than the measured values. In addition, the corrected pile resistances with proportioning to the cohesive soil thickness did not capture the actual pile responses. On the other hand, the pile resistances estimated using Eq. (4.9) and adjusted accordingly to the 50% effective cohesive soil layers correlated very well with the measured values. This study concluded the followings:

1. The amount of pile setup exhibited in a mixed soil profile was smaller than that expected in a complete cohesive soil profile,
2. The observed pile setup in the mixed soil profile followed the logarithmic trend as observed at those test piles embedded in cohesive soil profile and as predicted using Eq. (4.9), and
3. The amount of pile setup in a mixed soil profile not only depends on the proportion of the cohesive soil layers to the embedded pile length, but also depends on the stratigraphic layers of cohesive and cohesionless soils that influence the dissipation of the induced excess pore water pressure.

It is important to note that the aforementioned study was performed based on only a field test of ISU8, additional similar field tests on piles embedded in the mixed soil profile will be beneficial in the future to justify the conclusions, to further refine the methodology and assumptions made, and to accurately quantify the pile setup.

## 4.6. Confidence Level

In order to confidently implement the proposed pile setup method in practices, pile designers prefer to know the reliability of the method in advance, so the difference between actual and estimated pile setup values falls within an expectable tolerance. The confidence of the method in terms of the pile resistance ratio ($R_m/R_t$) can be expressed at different confidence levels given by

$$\left(\frac{R_m}{R_t}\right)_{\substack{\text{upper}\\\text{bound}}} = \mu + z \times \frac{\sigma}{\sqrt{n}};\ \left(\frac{R_m}{R_t}\right)_{\substack{\text{lower}\\\text{bound}}} = \mu - z \times \frac{\sigma}{\sqrt{n}} \tag{4.10}$$

where $\mu$ = mean value of the pile resistance ratio; $z$ = standard normal parameter based on a chosen percent of confidence interval (*CI*); $\sigma$ = standard of deviation of the pile resistance ratio; and $n$ = sample size. Using the statistical parameters ($\mu$, $\sigma$ and $n$) calculated early and given in Figure 4.10 for steel H-piles, the upper and lower limits of the population mean values of the pile resistance ratios for 80%, 85%, 90%, 95%, and 98% *CIs* were calculated using Eq. (4.10) and plotted in Figure 4.14 for the proposed setup method based on both CAPWAP and WEAP-SA. Figure 4.14 shows that the upper limits increase and the lower limits decrease with increasing *CI* values from 80% to 98%. In an attempt to determine an average pile setup factor that can be confidently applied directly on the production piles for a North Carolina Department of Transportation highway construction project, Kim and Kreider (2007) suggested the use of 90% and 98% *CIs* for representing a pile group foundation considering redundancy and an individual pile with no redundancy, respectively. Applying this recommendation for the case of an individual pile by considering a *CI* of 98%, the pile resistance ratio ($R_m/R_t$) for CAPWAP ranges between 0.94 and 1.11. In other words, the proposed pile setup Eq. (4.9) using CAPWAP with a 98% *CI* will neither over predict the $R_t$ so that the $R_m/R_t$ value falls below 0.94 nor under predict the $R_t$ that allows the $R_m/R_t$ value to exceed 1.11. A similar explanation applies to WEAP-SA at a *CI* of 98% with the $R_m/R_t$ ratio ranges between 0.92 and 1.07. Based on the largest upper bound $R_m/R_t$ value of 1.11 and the smallest lower bound $R_m/R_t$ value of 0.92 for a 98% *CI*, the proposed pile setup Eq. (4.9) will generally estimate $R_t$ values, so that the difference between the $R_m$ and $R_t$ values falls within 11%. Similarly, in the case of an individual pile foundation by considering a *CI* of 90%, the proposed pile setup Eq. (4.9) will generally estimate $R_t$ values, so that the difference between the $R_m$ and $R_t$ values falls within 8%.

Similar studies of confidence level were conducted for other pile types. For the case of an individual pile by considering a *CI* of 98%, Figure 4.15 shows that the $R_m/R_t$ for small diameter piles (i.e., diameter $\leq$ 600 mm) ranges between 0.97 and 1.16, while $R_m/R_t$ for large

diameter piles (i.e., diameter > 600 mm) ranges between 1.03 and 1.34. Based on the largest upper bound $R_m/R_t$ values, the proposed pile setup Eq. (4.9) will generally estimate $R_t$ values, so that the differences between the $R_m$ and $R_t$ values fall within 16% and 34% for small and large diameter piles, respectively. For the case of an individual pile foundation by considering a *CI* of 90%, the differences between the $R_m$ and $R_t$ values fall within 13% and 29% for small and large diameter piles, respectively.

## 4.7. Application

The application of the proposed pile setup method in pile foundation design can be accomplished by following design recommendations suggested in these three areas: (1) soil investigations; (2) pile setup estimations; and (3) Load Resistance Factor Design (LRFD) framework. This paper and the companion paper recommend soil investigations using SPTs and CPTs with pore water pressure dissipation tests. These soil investigations shall be performed near the foundation, and the soil parameters (SPT *N*-values and $C_h$) of different cohesive soil layers shall be measured in order to compute their average values using Eq. (4.5). However, if the pore water pressure dissipation tests are not successfully performed during CPTs, the $C_h$ values can be estimated from the measured SPT *N*-values using Eq. (4.7).

The inconvenient restrikes will not be required as part of the pile setup estimation using Eq. (4.9). However, the concern is the selection of an appropriate setup time ($t$) after EOD for design. The field test results conducted within the State of Iowa revealed that pile resistances increased immediately and rapidly within a day after the EOD and continuously increased at a slower rate after the second day. Moreover, the PILOT data records listed in Table 4.2 indicate that the SLTs were performed, in average, after 5 days of the EOD. The AASHTO (2010) Specifications recommend the performance of a static load test 5 days after a pile installation. Therefore, it is reasonable to suggest the time ($t$) of at least 5 days after the EOD. However, a different time can be assumed based upon local conditions and experiences.

## 4.8. Integration of Pile Setup Into LRFD

The AASHTO (2010) LRFD Bridge Design Specifications recommended a single resistance factor ($\varphi$) for each dynamic analysis method, because the measured nominal pile resistance obtained from the dynamic pile restrike test is assumed to be a single random variable (i.e., the uncertainties associated with pile resistance and pile setup estimations are assumed to be the same). On the other hand, the proposed method (Eq. (4.9)) consists two resistance components: (1) the initial pile resistance at EOD ($R_{EOD}$) estimated using the dynamic analysis method; and (2) pile setup resistance which is the difference of $R_t$ and $R_{EOD}$ ($R_{setup}=R_t - R_{EOD}$). Each resistance component has its own source of uncertainties, such as those resulting from the in-situ measurement of soil properties, which shall be separately accounted for in order to compile with the LRFD philosophy. Therefore, it is not only conceptually inappropriate to establish a single resistance for both the resistance components, but also the resulting factored resistance ($\varphi R$) could be overestimated. In order to incorporate the setup effects in the LRFD framework and to concurrently address the impact of different uncertainties associated with the estimations of $R_{EOD}$ and $R_{setup}$, the fundamental LRFD framework ($\sum_i^n \gamma_i Q_i \leq \varphi R$) shall be expanded enabling the computation of a separate resistance factor for each resistance component given by Eq. (4.11)

$$\sum_i^n \gamma_i Q_i \leq \varphi R = \varphi_{EOD} R_{EOD} + \varphi_{setup} R_{setup} \tag{4.11}$$

where $\gamma_i$ = load factor; $Q_i$ = applied load; $\varphi_{EOD}$ = resistance factor for $R_{EOD}$; and $\varphi_{setup}$ = resistance factor for $R_{setup}$. Accordingly, Yang and Liang (2006) used the First Order Reliability Method (FORM) to determine the resistance factors specifically for Skov and Denver (1988) setup equation. Yang and Liang recommended a $\varphi_{setup}$ value of 0.30 at a target reliability index ($\beta$) of 2.33 (corresponding to 1% probability of failure) as recommended by Paikowsky et al. (2004) for representing redundant pile groups. Because the FORM requires a special written program with an iterative procedure to simultaneously adjust the load and resistance components for the resistance factor calculation, it creates a challenge for pile designers to implement pile setup during design. Thus, a simpler,

welcoming, and closed-form method, which follows the expanded LRFD framework (Eq. (4.11)), to compute the resistance factor will be beneficial in the future for integrating the proposed pile setup method into the LRFD.

## 4.9. Conclusions

Although pile setup depends of the properties of surrounding soil, the existing pile setup estimation methods available in the literature rarely use any soil properties and usually require inconvenient pile restrikes in estimating pile setup. These limitations and the successful correlation between pile setup and soil parameters described in the companion paper (Ng et al. 2011b) motivate the development of a new pile setup method. From the analyses of the pile and soil test data, the following conclusions were drawn:

1. The proposed pile setup equation incorporates the commonly used SPT *N*-value and the horizontal coefficient of consolidation ($C_h$) to representing the surrounding soils and employ an equivalent pile radius to representing the pile geometry. The proposed method also utilizes the initial pile resistance estimated at the EOD using either CAPWAP or WEAP-SA, which eliminates the need for performing any inconvenient restrikes. The proposed method accounts for the actual time immediately after a pile installation and uses a reference time at the EOD ($t_{EOD}$) to be as small as 1 minute to quantify the pile setup occurring after the EOD.
2. The proposed setup method was validated using additional twelve steel H-pile data records from Iowa and five other well-documented tests found in the literature with different H-pile sizes. It has been shown that the proposed method adequately and confidently estimates the setup for steel H-piles, so that the difference between measured and predicted pile resistances falls within 8% and 11% for 90% and 98% confidence intervals, respectively.
3. The proposed method was also validated using six cases available in the literature for large displacement piles with different types and sizes providing satisfactory pile setup estimations with better prediction for small diameter piles (pile

diameter smaller than 600 mm). For small diameter piles, the differences between the measured and estimated pile resistances fall within 13% and 16% for 90% and 98% confidence intervals, respectively. For large diameter piles, the differences between the measured and estimated pile resistances fall within 29% and 34% for 90% and 98% confidence intervals, respectively.

4. The analytical study performed based on the test pile ISU8 embedded in a mixed soil profile concluded that the amount of pile setup was smaller than that expected in a complete cohesive soil profile. The observed pile setup followed the logarithmic trend. The amount of pile setup not only depends on the proportion of the cohesive soil layers to the embedded pile length, but also depends on the stratigraphic layers of cohesive and cohesionless soils.
5. Pile design recommendations including pile setup application are categorized into soil investigations, pile setup estimations, and LRFD framework. Because the proposed pile setup method consists two resistance components (i.e., initial and setup resistances), with which different uncertainties were associated, the concept of computing a separate resistance factor for each component is recommended in order to compile with the LRFD philosophy.

## 4.10. Acknowledgment

The authors would like to thank the Iowa Highway Research Board for sponsoring the research presented in this paper. We would like to thank the members of the Technical Advisory Committee: Ahmad Abu-Hawash, Bob Stanley, Curtis Monk, Dean Bierwagen, Gary Novey, John Rasmussen, Ken Dunker, Kyle Frame, Lyle Brehm, Michael Nop, and Steve Megivern of this research project for their guidance. Special thanks are due to Sherif S. AbdelSalam, Matthew Roling, and Douglas Wood for their assistance with the field tests.

## 4.11. Appendix: An Example of a Practical Pile Design Procedure

Design a steel-H pile foundation at an integral abutment to support a total 73.15 m long by 12.2 m wide two spanned, pretensioned and prestressed concrete beam bridge over I-

35 at Clarke County, Iowa. The dead load including the safety barrier rail was given as 3323 kN. The dead load for 0.96 kN/m$^2$ future wearing surface was given as 156 kN. The three lanes of HL-93 live load with impact and a 0.85 lane reduction was given as 1339 kN. These loads were distributed to the foundation based on simple span assumptions. The most common ASTM A572 Grade 50 HP 250 × 63 steel pile with a cross sectional area of 80 cm$^2$ was selected for the foundation. Based on the AASHTO (2010) strength I load combination, the factored loads were calculated as

Factored dead load = 1.25 × 3323 kN + 1.5 × 156 kN = 4388 kN
Factored live load = 1.75 × 1339 kN = 2343 kN
Total factored load = 4388 kN + 2443 kN = 6831 kN

*Soil Investigations*

Standard Penetration Test was performed near the foundation location and the results were listed as below. Although the embedded pile length is initially not known during the design process, this site with 100% clay soil layers was classified to be a cohesive soil profile. Thus, the proposed pile setup Eq. (4.9) can be used in the pile designs. Since Piezocone Penetration Test (CPT) was not performed, the horizontal coefficient of consolidation ($C_h$) values were estimated using Eq. (4.7)

| Depth (m) | Soil types | SPT *N*-value | Estimated $C_h$ (cm$^2$/min) |
|---|---|---|---|
| 0 to 2.43 | Low plasticity clay | 6 | 0.0765 |
| 2.43 to 4.86 | Low plasticity clay | 8 | 0.0421 |
| 4.86 to 6.99 | Low plasticity clay | 9 | 0.0329 |
| 6.99 to 9.42 | Low plasticity clay | 10 | 0.0264 |
| 9.42 to 11.85 | Low plasticity clay with sand | 22 | 0.0051 |
| 11.85 to 12.76 | Low plasticity clay with sand | 20 | 0.0063 |
| 12.76 to 13.98 | Low plasticity clay with sand | 15 | 0.0114 |
| 13.98 to 18.25 | Low plasticity clay with sand | 13 | 0.0153 |

*Design Stage*

Prior to pile driving, the foundation was initially designed using any preferred static analysis method that complies with local or state requirements. For instance, Iowa DOT (2008) LRFD Bridge Design Manual has limited the structural pile stress to 41 MPa with the intention to control pile settlement under the Structural Resistance Level-1 (SRL-1). Also,

geotechnical resistance charts given in the design manual were used for pile designs, especially to determine the number of piles and embedded pile lengths. Based on this static analysis method, fourteen (14) piles with each having an embedded length of approximately 16.76 m were initially estimated. Based on the estimated pile length of 16.76 m, the average SPT *N*-value was calculated as 12.2 using Eq. (4.5). Similarly, the average $C_h$ was calculated to be 0.0297 $cm^2$/min.

$$N_a = \frac{2.43\times6+2.43\times8+2.13\times9+2.43\times10+2.43\times22+0.91\times20+1.22\times15+2.78\times13}{16.76} = 12.20$$

*Construction Stage*

Based on driving information on a trial pile using a Delmag D16-32 diesel hammer, a hammer blow count of 85 blow/m was recorded at the EOD. Based on a bearing chart generated using the WEAP-SA shown below, the pile resistance at the EOD ($R_{EOD}$) was estimated to be 635 kN.

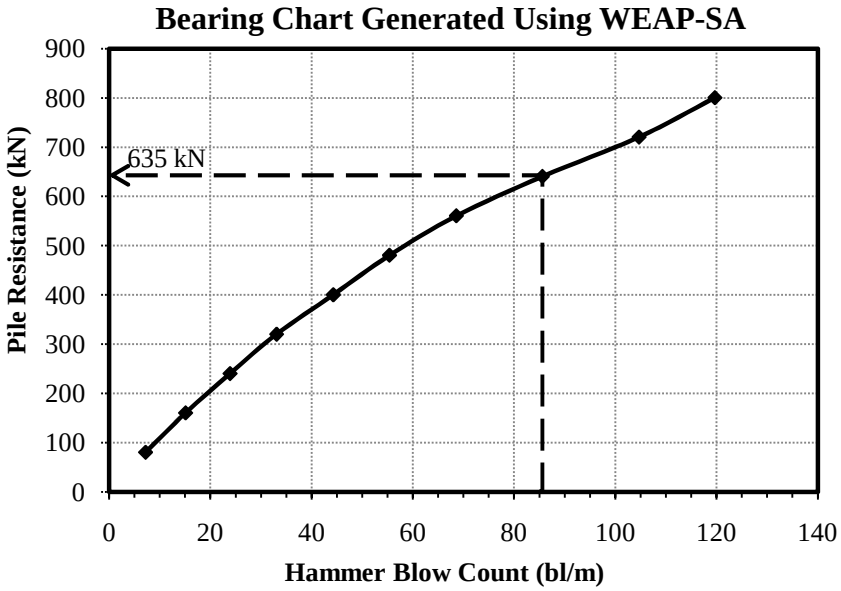


The equivalent pile radius ($r_p$) was determined to be 4.97 cm and a time ($t$) of 5 days for accounting pile setup was assumed. The nominal pile resistance at the time of 5 days after the EOD ($R_t$) was estimated using the proposed pile setup Eq. (4.9), and the difference between $R_t$ and $R_{EOD}$ yielded the pile setup resistance ($R_{setup}$).

$$R_t(\text{WEAP}-\text{SA}) = 635\left[\left(\frac{13.78\times0.0297}{12.2\times4.97^2}+0.1495\right)\log_{10}\left(\frac{5\times24\times60}{1}\right)+1\right]\left(\frac{16.76}{16.76}\right) = 1005 \text{ kN}$$

$R_{setup} = R_t - R_{EOD} = 1005 - 635 = 370$ kN

Next, the factored pile resistance ($\varphi R$) was calculated by applying $\varphi_{EOD}$ of 0.65, which was regionally-calibrated for the State of Iowa in Chapter 6 to $R_{EOD}$ and by assuming $\varphi_{setup}$ of 0.30 to $R_{setup}$ for a redundant pile group condition ($\beta_T$ = 2.33). Compared with the results estimated using the static analysis method, the number of piles required has been reduced from 14 to 13, at which the pile design procedure and the economic advantages of incorporating pile setup using the proposed method in the LRFD have been demonstrated.

$\varphi R = \varphi_{EOD}R_{EOD} + \varphi_{setup}R_{setup} = 0.65 \times 635 + 0.30 \times 370 = 524$ kN

The revised number of piles required = 6831/524 = 13 piles

*Conclusion*

Since the number of piles has been reduced from 14 to 13 with pile setup consideration, the efficiency of the pile foundation to support the bridge structure has been improved, and the economic advantages of incorporating pile setup have been demonstrated.

## 4.12. Notation

| | |
|---|---|
| *A, B* | = Setup factor used in Skov & Denver (1988) or Svinkin and Skov (2000) method |
| *AR* | = Pile area ratio |
| *C*, $C_h$ | = Proposed pile setup rate or horizontal coefficient of consolidation |
| *CI, COV* | = Confidence interval or coefficient of variation |
| $f_c$, $f_r$ | = Empirical consolidation factor or remolding recovery factor |
| *n*, $N_a$ | = Sample size or average SPT N-value |
| *OCR* | = Overconsolidation ratio |
| *PI* | = Plasticity index |
| $Q_D$, $Q_L$ | = Dead load or live load |
| $r_p$ | = Pile radius |

$R_m$, $R_t$ = Measured pile resistance or estimated pile resistance at any time t after the EOD

$R_{EOD}$, $R_{setup}$ = Pile resistance at the EOD or pile setup resistance

$S_t$,$T_h$ = Sensitivity of cohesive soil or Non-dimensional time factor

$z$, $\beta$ = Standard normal parameter or reliability index

$\mu$, $\sigma$ = Mean value or standard of deviation

$\gamma$, $\varphi$ = Load factor or resistance bias factor or resistance factor

## 4.13. References

AbdelSalam, S. S., Sritharan, S., and Suleiman, M. T. (2010). "Current Design and Construction Practices of Bridge Pile Foundations with Emphasis on Implementation of LRFD." *Journal of Bridge Engineering*, ASCE, 15(6), pp. 749-758.

American Association of State Highway and Transportation Officials. (AASHTO). (2010) LRFD Bridge Design Specifications. Customary U.S. Units, 5th Edition, 2010 Interim Revisions, Washington, D.C.

Bowles, J. E. (1977). *Foundation Analysis and Design*. Second Edition, McGraw-Hill Book Company, New York, 85-86.

Bullock, P. J., Schmertmann, J. H., Mc Vay, M. C., and Townsend, F. C. (2005). "Side Shear Setup I: Test Piles Driven in Florida." *J. of Geotech. Geoenviron. Eng.*, ASCE, 131(3), 292-300.

Chen, S.M. and Ahmad, S. A. (1988). "Dynamic Testing Versus Static Loading Test: Five Case Histories." *Proc. of 3rd Int. Conf. on the Application of Stress-Wave Theory to Piles*, B. H. Fellenius, ed., Ottawa, Ontario, Canada, 477-489.

Clarke, J. I., and Meyerhof, G. G. (1972). "The behavior of piles driven in clay. I. An investigation of soil stress and pore water pressure as related to soil properties." *Can. Geotech. J.,*Vol. 9 (4), pp.351-373.

Fellenius, B. H. (2002). "Pile Dynamics in Geotechnical Practice-Six Case Histories." *Geotechnical Special Publication No. 116,* ASCE, Proc. Of Int. Deep Foundations Congress 2002, Feb 14-16, M. W. O'Neill and F. C. Townsend, ed., Orlando, Florida,

619-631.

Fellenius, B. H. (2008). "Effective Stress Analysis and Set-up for Shaft Capacity of Piles in Clay." *From Research To Practice In Geotechnical Engineering*, GSP No. 180, ASCE, 384-406.

Houlsby, G., & Teh, C. (1988). "Analysis of the Peizocone in Clay." *Penetration Testing 1988, 2*, 777-783.

Huang, S. (1988). "Application of Dynamic Measurement on Long H-Pile Driven into Soft Ground in Shanghai." *Proc. of 3rd Int. Conf. on the Application of Stress-Wave Theory to Piles*, B. H. Fellenius, ed., Ottawa, Ontario, Canada, 635-643.

Karlsrud, K., Clausen, C. J. F., and Aas, P. M. (2005). "Bearing Capacity of Driven Piles in Clay, the NGI Approach." *Proc., 1st Int. Symp. on Frontiers in Offshore Geotechnics*, Balkema, Perth, Australia, 775-782.

Karna, U.L. (2001). Characterization of Time Dependent Pile Capacity in Glacial Deposits by Dynamic Load Tests." Degree of Engineer Project, New Jersey Institute of Technology, Newark, New Jersey.

Kim, K. J., and Kreider, C. A. (2007). "Measured Soil Setup of Steel HP Piles from Windsor Bypass Project in North Carolina." *Transportation Research Record*, Transportation Research Board, National Academy Press, Washington, D. C., 3-11.

Kim, D., Bica, A. V. D., Salgado, R., Prezzi, M., and Lee, W. (2009). "Load Testing of a Closed-Ended Pipe Pile Driven in Multilayered Soil." *J. of Geotech. Geoenviron. Eng.*, ASCE, 135(4), 463-473.

Long, J. H., Maniaci, M., and Samara, E. A. (2002). "Measured and Predicted Capacity of H-Piles." *Geotechnical Special Publication No.116,* Advances in Analysis, Modeling & Design, Proc. Of Int. Deep Foundations Congress 2002, ASCE, Feb 14-16, M. W. O'Neill and F. C. Townsend, ed., Orlando, Florida, 542-558.

Lukas, R. G., and Bushell, T. D. (1989). "Contribution of Soil Freeze to Pile Capacity." *Foundation Engineering: Current Principles and Practices*, Vol. 2. Fred H. Kulhawy, ed., ASCE, 991-1001.

Ng, K. W., Suleiman, T. M., Roling, M., AbdelSalam, S. S., and Sritharan, S. (2011a). "Development of LRFD Design Procedures for Bridge Piles in Iowa – Volume II:

Field Testing of Steel Piles in Clay, Sand and Mixed Soils." Final Report Vol. II. IHRB Project No. TR-583. *Institute of Transportation*, Iowa State Univeristy, Ames, Iowa.

Ng, K.W., Roling, M., AbdelSalam, S. S., Suleiman, M.T., and Sritharan, S. (2011b). "Pile Setup in Cohesive Soil with Emphasis on LRFD:An Experimental Investigation." *Journal of Geotechnical and Geoenvironmental Engineering*, ASCE (in progress of submitting).

Paikowsky, S.G., Regan, J.E., and McDonnell, J.J. (1994). "A Simplified Field Method for Capacity Evaluation of Driven Piles." *Rep. No. FHWA-RD-94-042*, Federal Highway Administration, Washington, D. C.

Paikowsky, S.G., Birgisson, B., McVay, M., Nguyen, T., Kuo,C.,Baecher, G., Ayyab, B., Stenersen, K., O'Malley, K., Chernauskas, L., and O'Neill, M. (2004). "Load and Resistance Factor Design (LRFD) for Deep Foundations." *NCHRP Report 507*, Transportation Research Board, Washington, D.C.

Pei, J., and Wang, Y. (1986). "Practical Experiences on Pile Dynamic Measurement in Shanghai." *Proc, Int. Conf. on Deep Foundations*, Beijing, China, 2.36-2.41.

Pile Dynamic, Inc. (2005). *GRLWEAP Wave Equation Analysis of Pile Driving: Procedures and Model Version 2005*. Cleveland, Ohio.

Roling, M., Sritharan, S., and Suleiman, M. T. (2010). Development of LRFD design procedures for bridge piles in Iowa – Electronic Database. Final Report Vol. I, Project No. TR-573, *Institute of Transportation*, Iowa State University, Ames, IA.

Skov, R., and Denver, H. (1988). "Time-Dependence of Bearing Capacity of Piles." *Proc. of 3rd Int. Conf. on the Application of Stress-Wave Theory to Piles*, B. H. Fellenius, ed., Ottawa, Ontario, Canada, 879-888.

Svinkin, M. R., and Skov, R. (2000). "Set-Up Effect of Cohesive Soils in Pile Capacity." *Proc., 6th Int. Conf. on Application of Stress-Waves Theory to Piles*, Niyama, S., and Beim, J., ed., Balkema, A. A., Sao Paulo, Brazil, 107-111.

Soderberg, L. O. (1962). "Consolidation Theory Applied to Foundation Pile Time Effects." *Geotechnique*, 12(3), 217-225.

Thibodeau, E., and Paikowsky, S.G. (2005). "Performance Evaluation of A Large Scale Pile

Load Testing Program in Light of Newly Developed LRFD Parameters." *GeoFrontiers 2005–LRFD and Reliability Based Design of Deep Foundations*, Geo-Institute of ASCE, Austin, Texas.

Thompson, W.R., Held., L., and Saye, S. (2009). "Test Pile Program to Determine Axial Capacity and Pile Setup for the Biloxi Bay Bridge." Deep Foundation Institute Journal, Vol. 3 No.1, 13-22.

Yang, L., and Liang, R. (2006). "Incorporating Set-Up into Reliability-Based Design of Driven Piles in Clay." *Can. Geotech. J.*, 43, 946-955.

Zhu, G. Y. (1988). "Wave Equation Applications for Piles in Soft Ground." *Proc. of 3rd Int. Conf. on the Application of Stress-Wave Theory to Piles*, B. H. Fellenius, ed., Ottawa, Ontario, Canada, 831-836.

Table 4.1: Summary of existing methods of estimating pile setup

| Reference | Setup equation | Limitations |
|---|---|---|
| Pei and Wang (1986) | $\frac{R_t}{R_{EOD}} = 0.236[\log(t) + 1]\left(\frac{R_{max}}{R_{EOD}} - 1\right) + 1$ | – Purely empirical<br>– Site specific<br>– No soil property<br>– Unknown or difficult to determine $R_{max}$ |
| Zhu (1988) | $\frac{R_{14}}{R_{EOD}} = 0.375S_t + 1$ | – Only predict pile resistance at 14th day<br>– No consolidation effect is considered |
| Skov and Denver (1988) | $\frac{R_t}{R_o} = A\log\left(\frac{t}{t_o}\right) + 1$ | – Require restrikes<br>– Wide range and non-uniqueness of $A$ |
| Svinkin and Skov (2000) | $\frac{R_t}{R_{EOD}} = B[\log(t) + 1] + 1$ | – Require restrikes<br>– $B$ value has not been extensively quantified<br>– No clear relationship between $B$ value and soil properties. |
| Karlsrud et al. (2005) | $\frac{R_t}{R_{100}} = A\log\left(\frac{t}{t_{100}}\right) + 1$ ;<br>$A = 0.1 + 0.4\left(1 - \frac{PI}{50}\right)OCR^{-0.8}$ | – Assumed complete dissipation after 100 days is not true<br>– Not practical to use $R_{100}$ |

$R_t$: pile resistance at any time $t$ considered after EOD; $R_{EOD}$: pile resistance at EOD; $R_{max}$: maximum pile resistance assuming after completing soil consolidation; $R_o$: reference pile resistance; $R_{14}$: pile resistance at 14 days after EOD; $R_{100}$: pile resistance at 100 days after EOD; $S_t$: soil sensitivity; $A$: pile setup factor defined by Skov and Denver (1988); $B$: pile setup factor defined by Svinkin and Skov (2000); $PI$: plasticity index; and $OCR$: overconsolidation ratio.

Table 4.2: Summary of the twelve data records from PILOT

| Project ID | County in Iowa | Pile type | Emb. pile length (m) | Hammer type | Soil profile description | Average SPT *N*-value, $N_a$ | Estimated average $C_h$ using Eq. (4.7) ($cm^2$/min) | Time after EOD, *t* (day) | SLT measured Davisson's pile resistance at *t* (kN) | WEAP-SA estimated pile resistance at EOD (kN) |
|---|---|---|---|---|---|---|---|---|---|---|
| 6 | Decatur | HP 250 × 63 | 16.2 | Gravity #732 | Glacial clay | 14.47 | 0.041 | 3 | 525 | 323 |
| 12 | Linn | HP 250 × 63 | 7.25 | Kobe K-13 | Glacial clay | 29.9 | 0.003 | 5 | 907 | 679 |
| 42 | Linn | HP 250 × 63 | 7.16 | Kobe K-13 | Glacial clay | 22.2 | 0.01 | 5 | 365 | 375 |
| 44 | Linn | HP 250 × 63 | 11.1 | Delmag D-22 | Sandy silty clay | 22.34 | 0.005 | 5 | 605 | 410 |
| 51 | Johnson | HP 250 × 63 | 8.99 | Kobe K-13 | Silt/glacial clay | 40 | 0.001 | 3 | 845 | 562 |
| 57 | Hamilton | HP 250 × 63 | 17.4 | Gravity #2107 | Glacial clay | 9.77 | 0.03 | 4 | 747 | 405 |
| 62 | Kossuth | HP 250 × 63 | 13.7 | MKT DE-30B | Glacial clay | 36.05 | 0.018 | 5 | 445 | 335 |
| 63 | Jasper | HP 250 × 63 | 19.2 | Gravity | Silt/glacial clay | 8.32 | 0.043 | 2 | 294 | 265 |
| 64 | Jasper | HP 250 × 63 | 21.7 | Gravity | Silt/glacial clay | 10.52 | 0.031 | 1 | 543 | 320 |
| 67 | Audubon | HP 250 × 63 | 9.76 | Delmag D-12 | Glacial clay | 20 | 0.006 | 4 | 623 | 542 |
| 102 | Poweshiek | HP 250 × 63 | 13.1 | Gravity #203 | Silt/glacial clay | 16.45 | 0.04 | 8 | 578 | 372 |
| 109 | Poweshiek | HP 310 × 79 | 15.6 | Delmag D-12 | Glacial clay | 17.36 | 0.013 | 3 | 783 | 673 |

Table 4.3: Summary of five external sources from literatures on steel H-piles embedded in cohesive soils

| Reference; Location | Pile type | Emb. pile length (m) | Hammer type | Soil profile description | Average SPT *N*-value, $N_a$ | Estimated average $C_h$ using Eq. (4.7) ($cm^2$/min)(4.7) | Time after EOD, *t* (day) | Measured pile resistance at *t* from SLT (Davisson) or restrikes (kN) | CAPWAP estimated pile resistance at EOD (kN) | WEAP-SA estimated pile resistance at EOD (kN) |
|---|---|---|---|---|---|---|---|---|---|---|
| Huang (1988); China | HP 360 × 410 × 176 | 74.2 | Kobe KB60 | Silty clay to clay over silty sand | 6.13 | 0.873 | 1.67<br>31 | 4485[e]<br>7250[d] | 2983 | 3220[a] |
| Lukas & Bushell (1989); Illinois | HP 250 × 63 | 25.6 | Vulcan 80C | Fill overlaying soft to hard clay | 15.48[b] | 0.017 | 10<br>26 | 1139[d]<br>1308[d] | - | 671[a] |
| Long et al. (2002); Illinois | HP 310 × 79 | 9.4 to 11.5 | Delmag D19-32 | Silty clay/loam overlaying sandy till | 6.63 | 0.291 | 7<br>22 | 1202[d]<br>2537[d] | 1068<br>1472[c] | 1174<br>1677[c] |
| Fellenius (2002); Canada | HP 310 × 110 | 70 | Delmag D30-32 | Mixture of sand silt and clay overlaying glacial till | 13.57 | 0.076 | 7<br>13<br>15<br>16<br>18<br>21<br>28<br>32<br>44 | 2300[e]<br>2500[e]<br>2570[e]<br>2821[e]<br>2714[e]<br>2554[e]<br>3000[e]<br>3107[e]<br>3071[e] | 1917 | 1339[a] |
| Kim & Kreider (2007); North Carolina | Structures 3 & 4: HP 310 × 79 & HP 360 × 109<br>Structure 5: HP 310 × 79 | 24.4 to 30.2 | Delmag D19-42 | Sand overlaying silty clay and clayey silt | 10.06 | 0.048 | 1<br>2<br>3<br>4<br>6<br>1 | 1380[f]<br>1538[f]<br>1607[f]<br>1519[f]<br>1471[f]<br>1144[f] | -<br>-<br>-<br>-<br>-<br>649 | 984<br>1157<br>1508<br>916<br>970<br>763 |

[a] – pile resistance estimated by research team based on reported hammer blow rate; [b] – estimated from reported unconfined compressive strength based on Bowles (1977) recommended correlations for cohesive soils; [c] – estimated pile resistance at the EOD condition was taken 7 days after the pile installation; [d] – measured pile resistance using SLT based on Davisson's criteria; [e] – pile resistance estimated using CAPWAP during restrike; and [f] – an average pile resistance estimated using WEAP during restrikes.

Table 4.4: Summary of six external sources from literatures on other pile types embedded in cohesive soils

| Reference; Location | Pile types | No. of pile | Average emb. pile length (m) | Hammer type | Soil profile description | Average SPT *N*-value, $N_a$ | BOR and SLT | Time after EOD, *t* (day) | Ave. *AR* |
|---|---|---|---|---|---|---|---|---|---|
| Cheng & Ahmad (2002); Canada | 244 mm × 13.8 mm closed end steel pipe pile | 1 | 14.3 | Berming Hammer B-400 | Silt to clayey silt and sandy silt | 34 (Site 3) | BOR<br>SLT | 1<br>1 | 115 |
| Karna (2001); Newark-New Jersey | 600 mm × 12.5 mm closed end steel pipe pile | 12 | 36.9 to 48.9 | ICE 206S | Glacial deposit with clayey silt and clay | 23 (South) and 36 (North) | BOR1<br>SLT | 5 to 39<br>6, 28 | 136 |
| Fellenius (2002); Alberta-Canada | 273 mm opened end steel pipe pile | 1 | 24.0 | - | Silt and clay overlaying clay till | 30 | BOR | 0.625 | 278 |
| | 273 mm closed end steel pipe pile | 1 | 24.0 | | | | BOR | 0.625 | 176 |
| Thibodeau and Paikowsky (2005); Connecticut | 324 mm closed end steel pipe pile | 1 | 36.7 | HMC Model 86 and HPSI Model 2000 | Organic silt overlaying glacio-deltaic deposit | 15 (Area A) and 20 (Area B) | BOR<br>SLT | 1, 10<br>56 | 227 |
| | 356 mm square precast prestressed concrete pile | 1 | 30.0 | | | | BOR<br>SLT | 1<br>42 | 169 |
| | 406 mm square precast prestressed concrete pile | 3 | 30.6, 34.9 and 35.2 | | | | BOR<br>SLT | 1, 8, 11, 23<br>41, 44, 45 | 165 |
| | 457 mm steel monotube pile | 2 | 28.9 and 36.7 | | | | BOR<br>SLT | 1, 9, 12<br>54, 55 | 124 |
| | 457 mm closed end steel pipe pile | 3 | 36.3, 37.0 and 43.1 | | | | BOR<br>SLT | 1, 7, 14, 15<br>45, 50, 50 | 170 |
| | 610 mm closed end steel pipe pile | 1 | 47.9 | | | | BOR<br>SLT | 1, 12<br>54 | 157 |
| Kim et al. (2009); Indiana | 356 mm×12.7 mm closed end steel pipe pile | 3 | 17.4 to 18.1 | ICE 42S | Mixture of silty sand, silty clay, and clayey silt | 22 (S1) and 35 (S2) | BOR<br>SLT | 1 to 154<br>50, 90 | 100 |
| Thompson et al. (2009); Mississippi | 600 mm square precast prestressed concrete pile | 7 | 25.9 to 32.0 | Delmag 30-32, DKH-10U, Conmaco5200, and Conmaco300E | Mixture of low and high plasticity clay with some layers of clayey sand | 6 | BOR<br>SLT | 10 to 46<br>22 | 190 |
| | 750 mm square precast prestressed concrete pile | 3 | 27.7, 29.3 and 29.3 | | | | BOR<br>SLT | 6 to 23<br>24 | 151 |

Table 4.5: Soil information along the test pile ISU8

| Soil Layer | Soil Description (USCS) | Soil Thickness (m) | Average SPT N-value | Average $C_h$ ($cm^2$/min) |
|---|---|---|---|---|
| 1 | Clay to silty clay (CL) | 6.40 | 5 | 0.1118[(a)] |
| 2 | Sand (SW) | 5.18 | 2 | - |
| 3 | Clayey silt to silty clay (CL) | 0.92 | 10 | 0.02644[(a)] |
| 4 | Sand to silty sand | 0.31 | 10 | - |
| 5 | Clayey silt to silty clay (CL) | 0.61 | 10 | 0.02644[(a)] |
| 6 | Silty sand to sandy silt | 0.30 | 10 | - |
| 7 | Clayey silt to silty clay (CL) | 0.30 | 10 | 0.02644[(a)] |
| 8 | Silty sand to sandy silt | 0.30 | 10 | - |
| 9 | Sandy silt to clayey silt (CL) | 1.22 | 10 | 0.02644[(a)] |
| 10 | Clayey silt to silty clay (CL) | 1.22 | 24 | 0.00438[(b)] |

[(a)] – estimated using Eq. (4.8); and [(b)] – determined from cone penetration test.

Table 4.6: Summary of field test results and estimated pile resistance for ISU8

| Stage of Testing | Emb. Pile Length (m) | Time After EOD, t (day) | Measured Pile Resistance From Restrikes Using CAPWAP or SLT, $R_t$ (kN) | Estimated Pile Resistance Using Eq. (4.9), $R_t$ (kN) | Proportion of Cohesive Soil Thickness to Emb. Pile length | Estimated Pile Resistance With Amount of Setup Proportional to Cohesive Soil Thickness, $R_t$ (kN) | Estimated Pile Resistance With Amount of Setup Proportional to 50% of the Cohesive Soil Thickness, $R_t$ (kN) |
|---|---|---|---|---|---|---|---|
| EOD | 16.77 | 0.000694 | 621 | 621 | 0.6364 | 621 | 621 |
| BOR1 | 16.93 | 0.0070 | 637 | 691 | 0.6399 | 666 | 644 |
| BOR2 | 17.11 | 0.0112 | 651 | 712 | 0.6437 | 679 | 650 |
| BOR3 | 17.23 | 0.039 | 680 | 751 | 0.6460 | 705 | 663 |
| BOR4 | 17.30 | 0.97 | 689 | 846 | 0.6476 | 767 | 694 |
| BOR5 | 17.37 | 3.97 | 706 | 889 | 0.6490 | 795 | 708 |
| BOR6 | 17.44 | 4.95 | 710 | 899 | 0.6504 | 802 | 711 |
| SLT | 17.44 | 15 | 721 | 931 | 0.6504 | 823 | 722 |

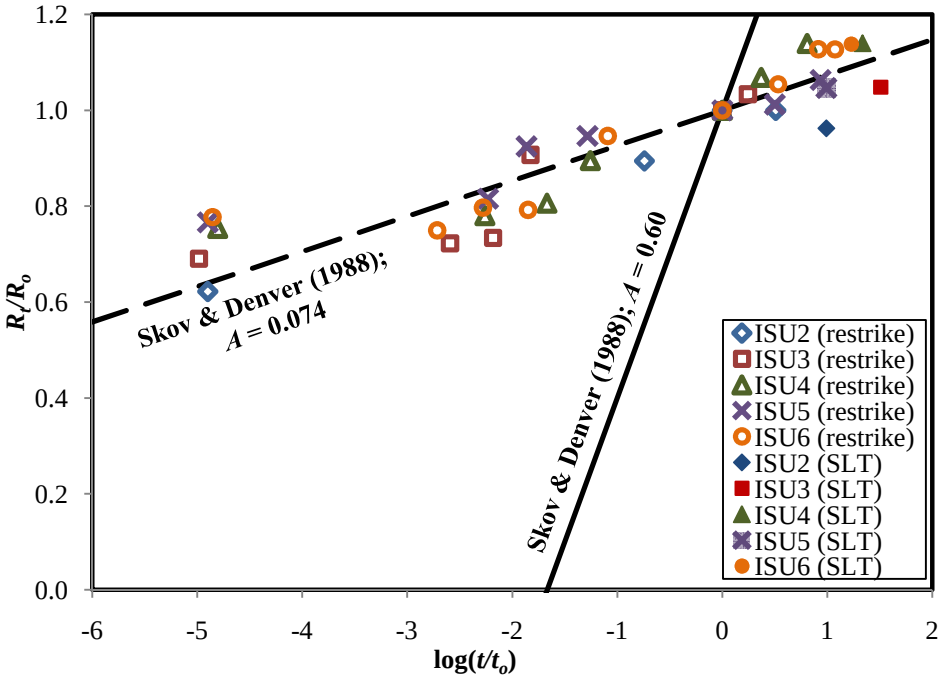


Figure 4.1: Comparison between ISU field test results and Skov and Denver (1988) pile setup method

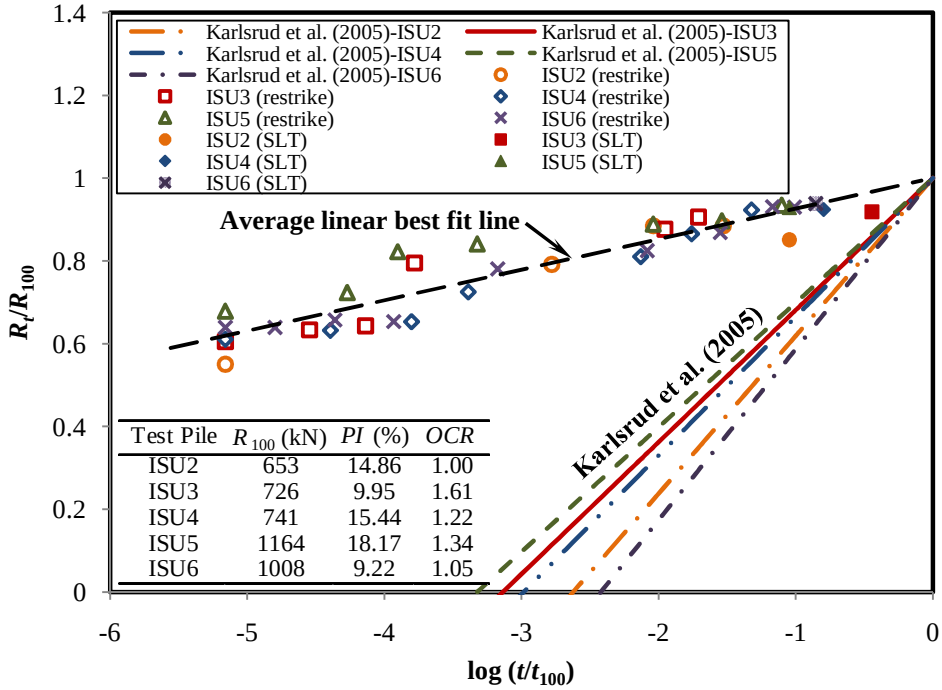


Figure 4.2: Comparison between ISU field test results and Karlsrud et al. (2005) pile setup method

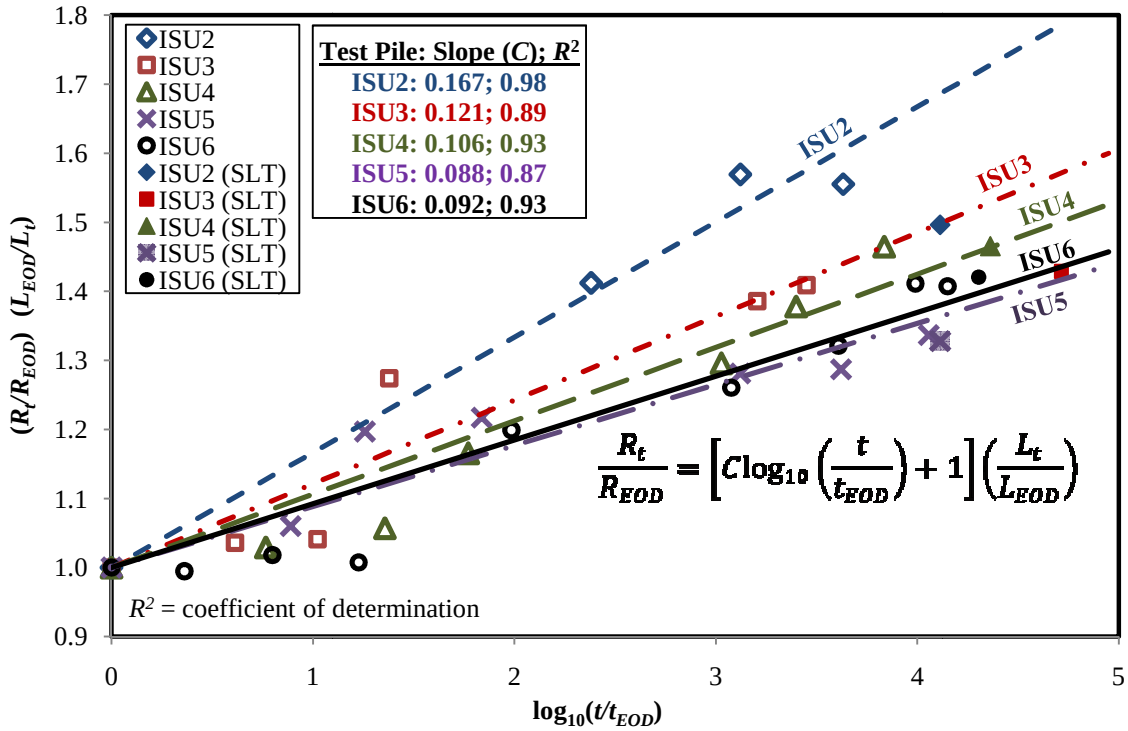


Figure 4.3: Linear best fits of normalized pile resistances as a function of logarithmic normalized time based on CAPWAP analysis

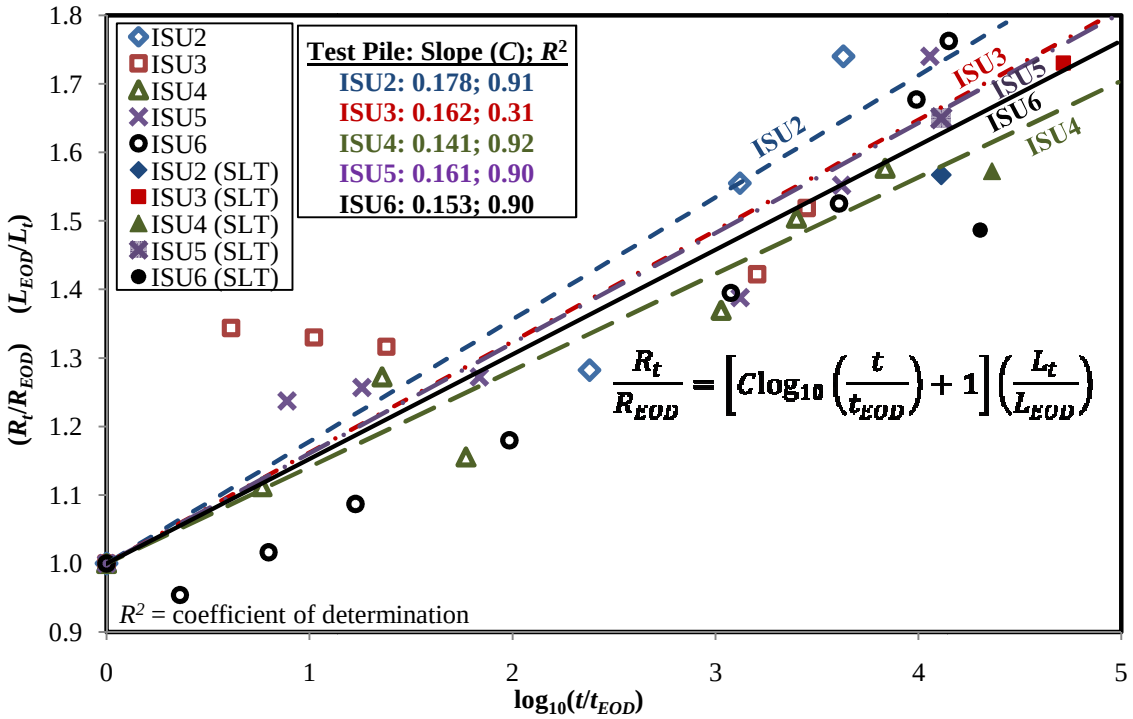


Figure 4.4: Linear best fits of normalized pile resistance as a function of logarithmic normalized time based on WEAP-SA analysis

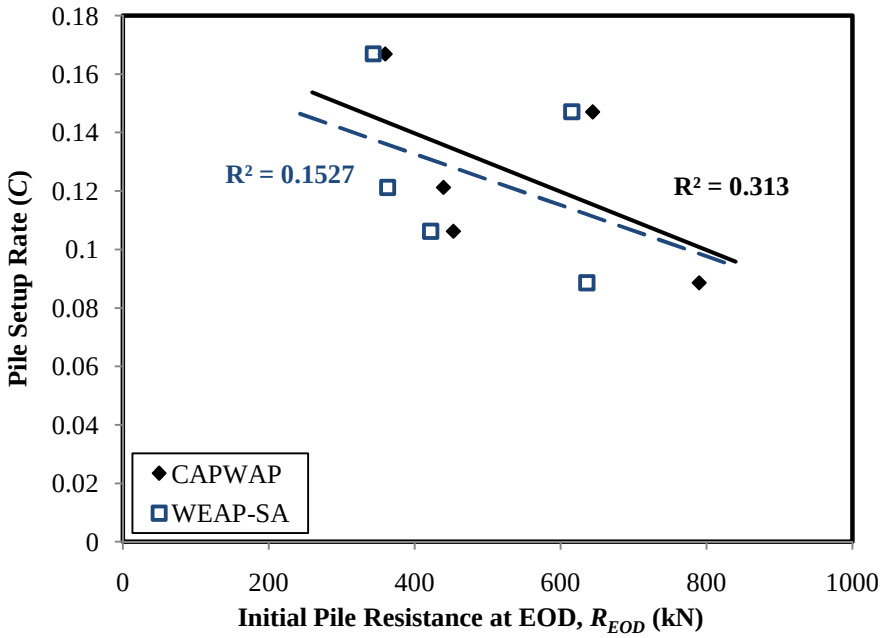


Figure 4.5: Comparison of pile setup rate ($C$) to initial pile resistance

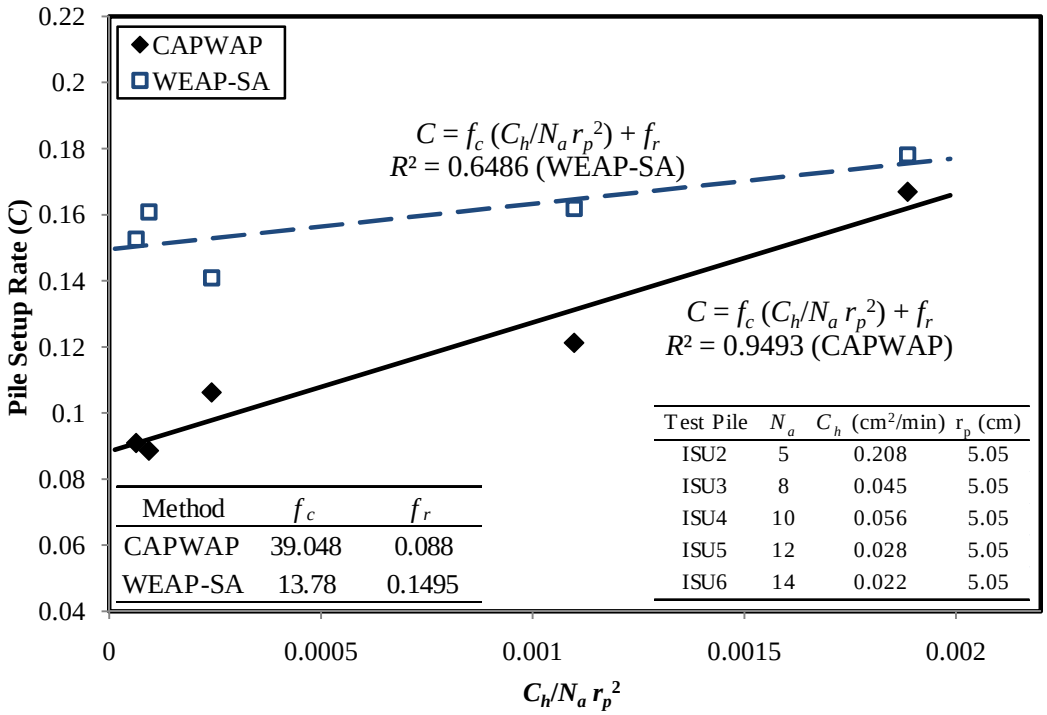


Figure 4.6: Correlations between pile setup rate ($C$) for different ISU field tests and soil parameters as well as equivalent pile radius

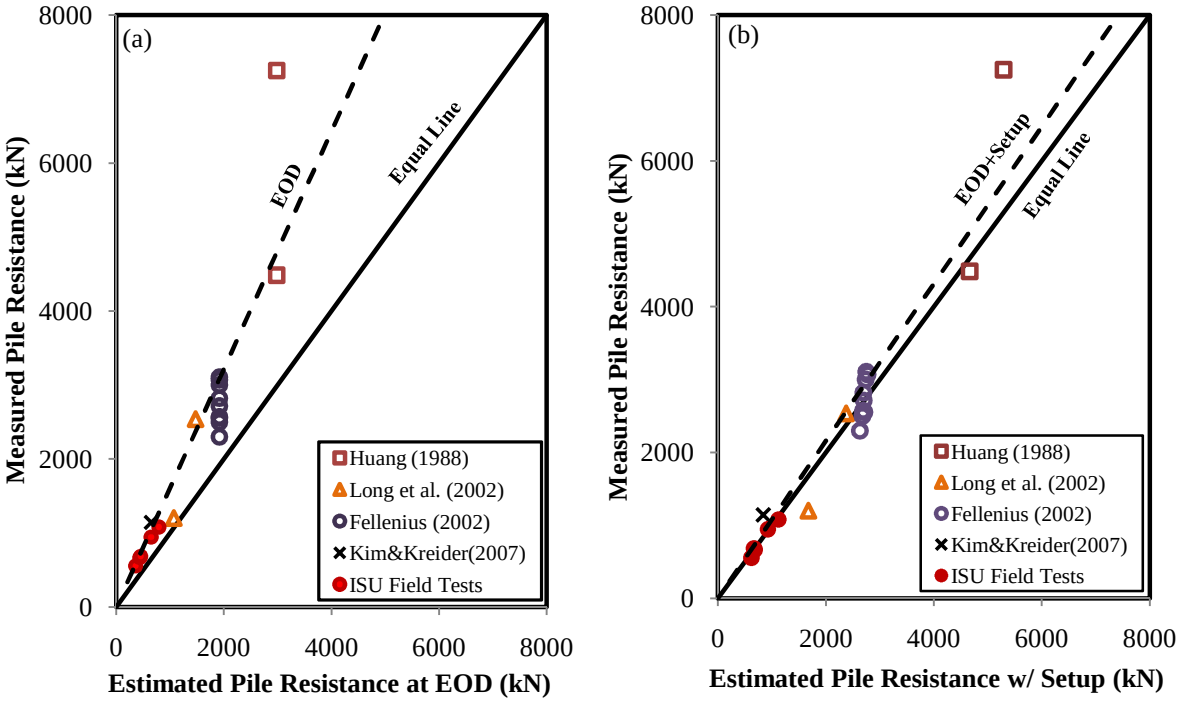


Figure 4.7: Comparison between measured and estimated pile resistances using CAPWAP considered (a) at EOD condition and (b) pile setup using Eq. (4.9)

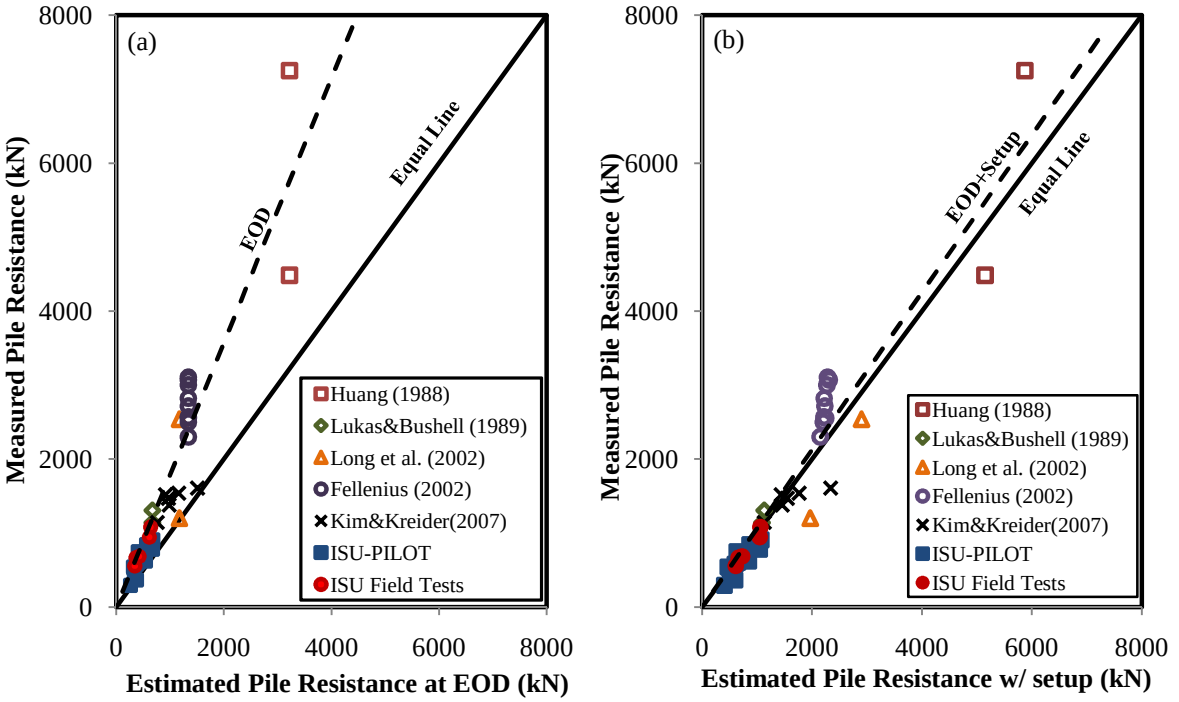


Figure 4.8: Comparison between measured and estimated pile resistances using WEAP considered (a) at EOD condition and (b) pile setup using Eq. (4.9)

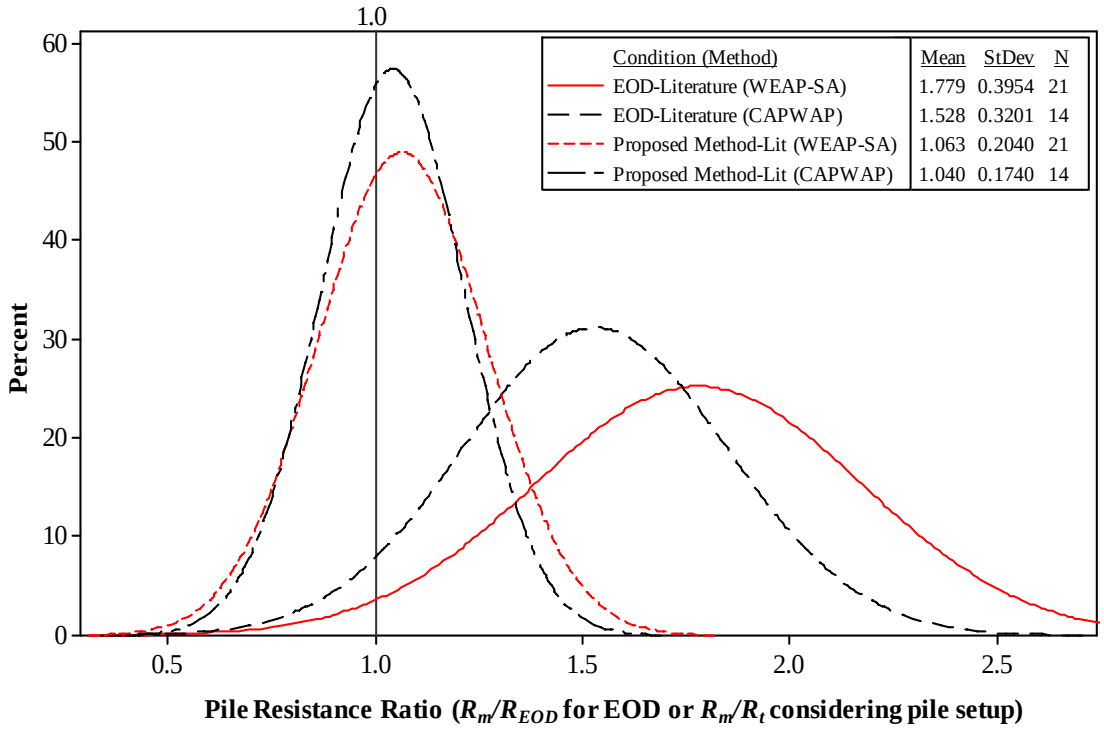


Figure 4.9: Statistical assessment of the proposed pile setup method based only on data points from literatures

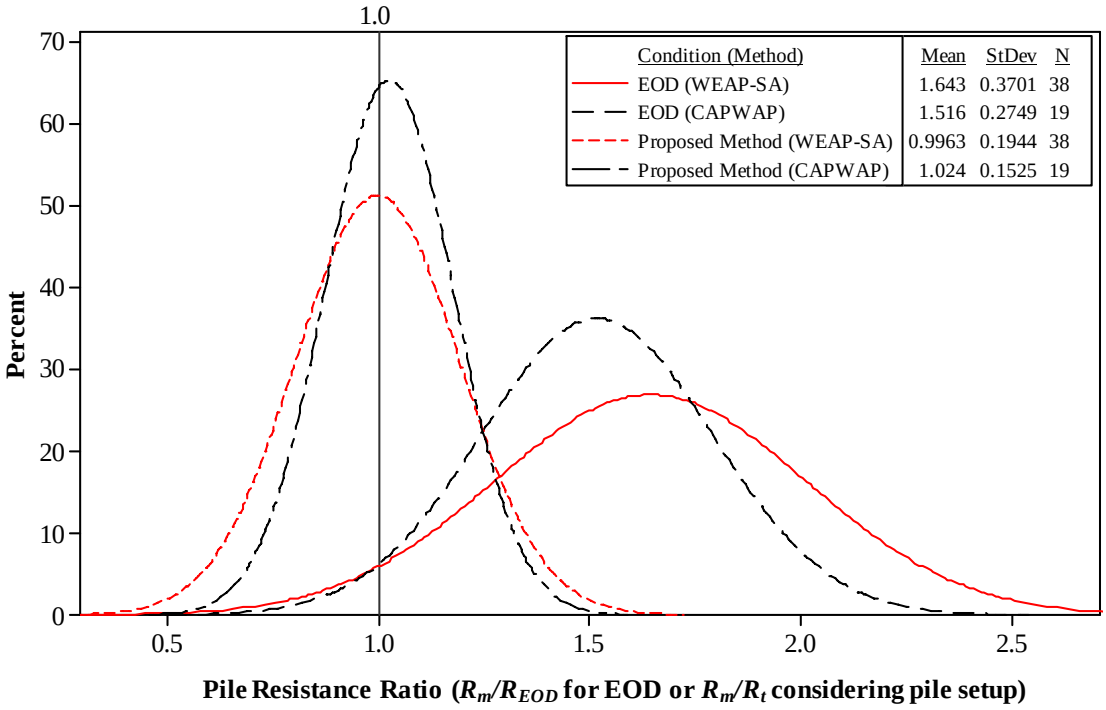


Figure 4.10: Statistical assessment of the proposed pile setup method based on all data points

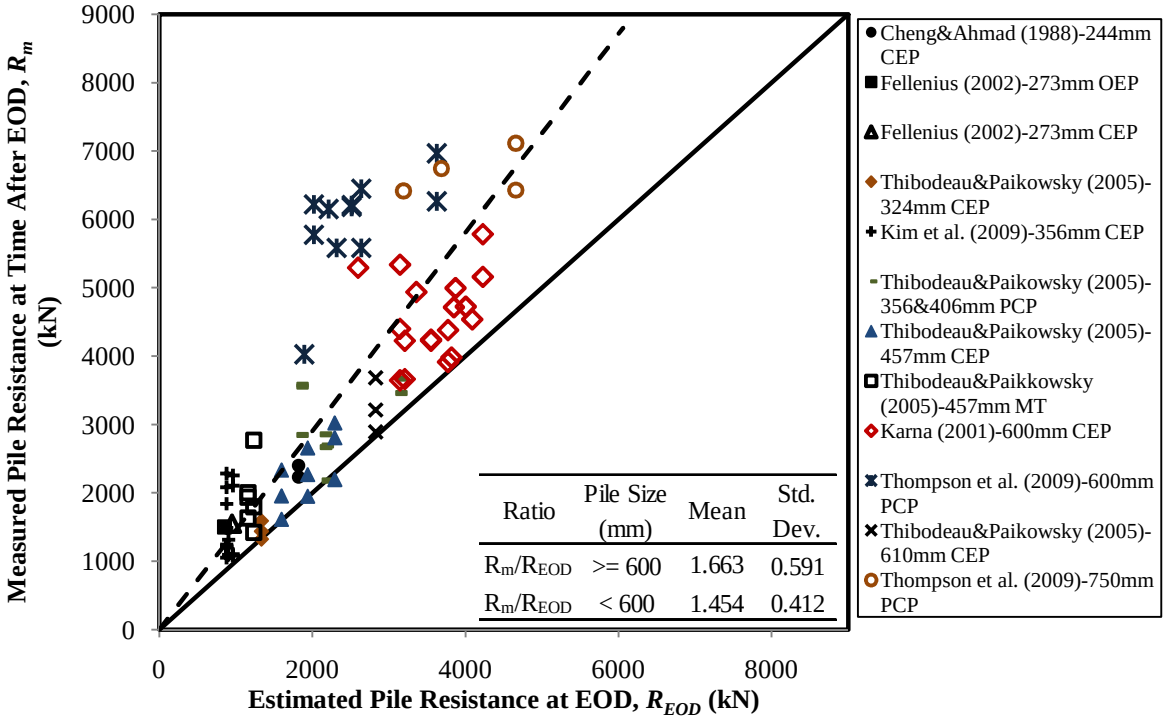


Figure 4.11: Comparison between measured pile resistances at any time (t) and reported pile resistances at EOD

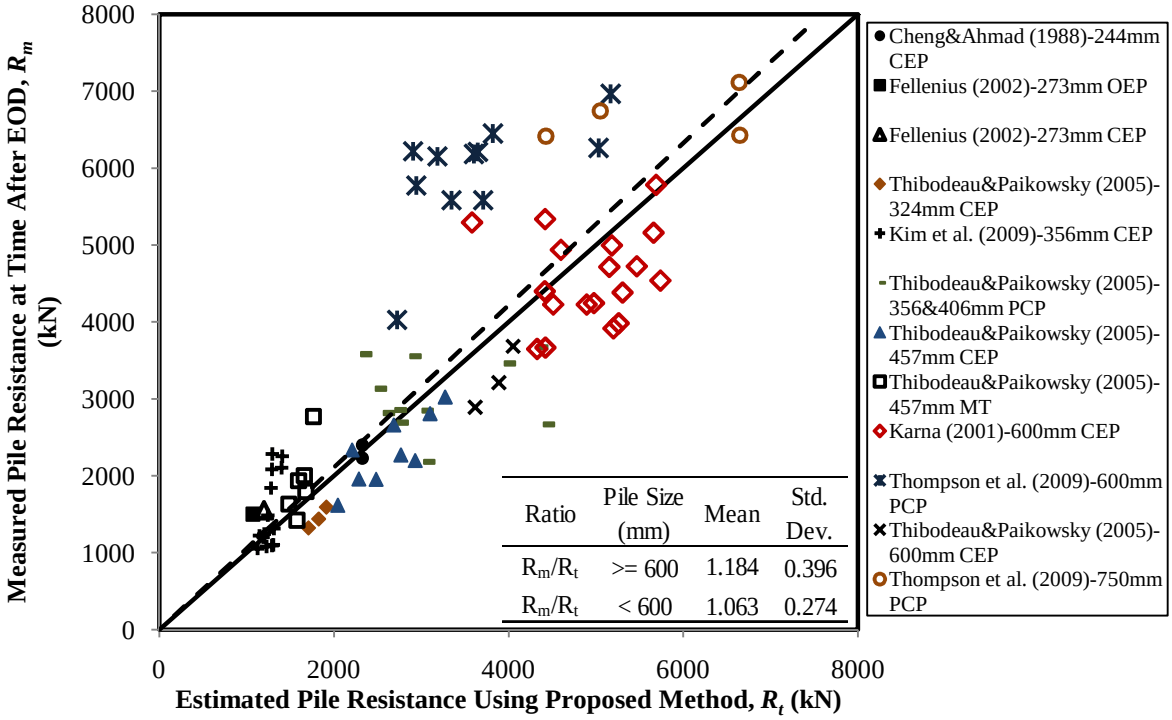


Figure 4.12: Comparison between measured pile resistances at any time (*t*) and estimated pile resistances using the proposed pile setup method

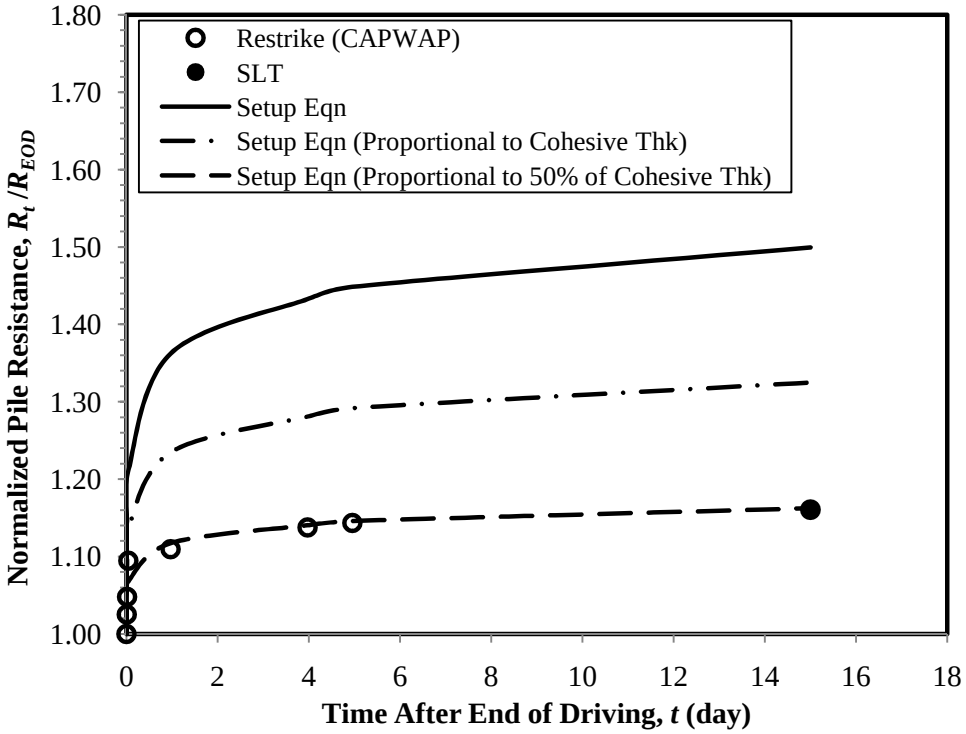


Figure 4.13: Normalized pile resistance as a function of time after EOD for the test pile ISU8 embedded in a mixed soil profile

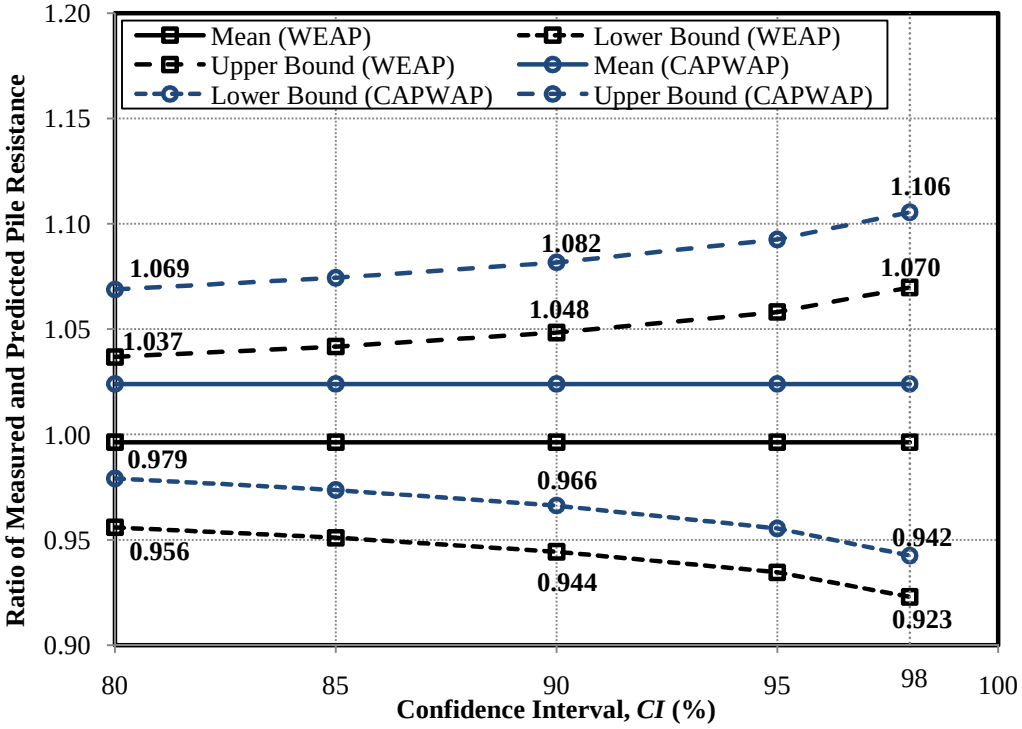


Figure 4.14: The confidence intervals of the proposed pile setup method for steel H-piles

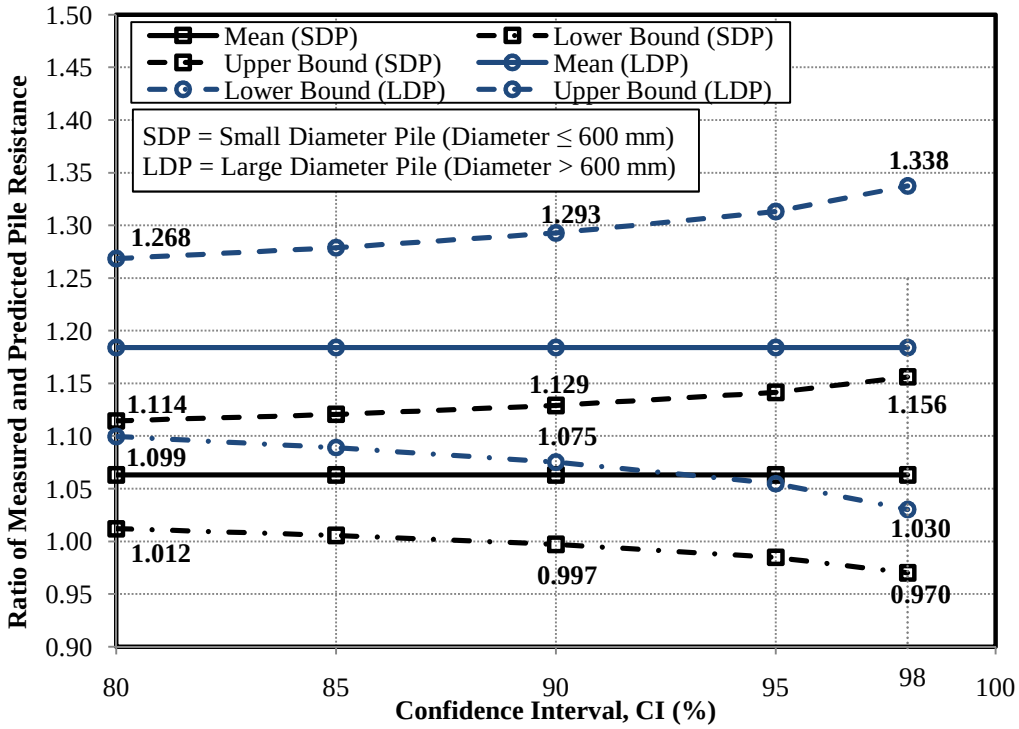


Figure 4.15: The confidence intervals of the proposed pile setup method for other small and large diameter piles

# CHAPTER 5: A PROCEDURE FOR INCORPORATING PILE SETUP IN LOAD AND RESISTANCE FACTOR DESIGN OF STEEL H-PILES IN COHESIVE SOILS

Kam W. Ng, Sri Sritharan, and Muhannad T. Suleiman

The paper was accepted for a poster presentation at the Transportation Research Board 90th Annual Conference and will be submitted to Canadian Geotechnical Journal

## 5.1. Abstract

In a recent study, time-dependent increase in axial load resistance of steel H-piles embedded in cohesive soils due to setup has been systematically quantified using measured soil properties. However, this quantification has its own uncertainties resulting from in-situ measurements of soil properties and the semi-empirical approach adapted for the effects of setup. Given that the impact of these uncertainties should be addressed concurrently with those associated with the estimation of the initial pile resistance at the end of driving condition, a procedure for incorporating the pile setup in Load and Resistance Factor Design (LRFD) was established using the reliability theory to include economic advantages of pile setup during pile designs. The procedure, which uses the First Order Second Moment (FOSM) method, not only allows incorporation of any form of setup estimate to the estimated pile resistance at EOD, but also facilitates inclusion of two resistances affected by each other to reach a target reliability within the FOSM framework. Constant resistance factors for both EOD and setup can be easily calculated based on any regional database that reflects the local soil conditions, pile types, and setup quantification methods, so a practical implementation of this procedure can be appreciated.

## 5.2. Introduction

Pile setup is referred to the increase in resistance of driven piles embedded in cohesive soils over time, which is the result of healing of remolded cohesive soils

surrounding the pile and the consolidation of cohesive soils from pore water pressure dissipation induced by pile driving (Soderberg (1962) and Randolph et al. (1979)). To account for the pile setup in design, the American Association of State Highway and Transportation Officials (AASHTO) (2010) suggests the use of dynamic tests involving time consuming pile restrikes and/or completing static load tests over a sufficient length of time although it is not feasible in practice to perform these tests. Furthermore, the measured nominal pile resistance obtained from the pile tests is assumed to be a single random variable (i.e., the uncertainties associated with pile resistance and pile setup estimations are assumed to be the same), and thus a single resistance factor is suggested in accordance with the Load and Resistance Factor Design (LRFD) framework.

Alternatively, pile setup can be accounted for using empirical methods (e.g., Skov and Denver (1988); Svinkin and Skov (2000)) or analysis-based semi-empirical methods as described in Chapter 4, and the setup estimation using each approach has its own uncertainty. For example, based on extensive field evaluation, Chapter 4 concludes that setup can be satisfactorily estimated using the initial pile resistance obtained from a bearing graph (ultimate pile resistance versus hammer blow count) generated using Wave Equation Analysis Program with SPT *N*-value based method (WEAP-SA) (Pile Dynamic, Inc (2005)) and soil parameters as detailed in Eq. (5.1) without performing any restrikes or load tests.

$$R_{setup} = R_{EOD}\left[\left(\frac{f_c C_h}{N_a r_p^2} + f_r\right)\log_{10}\left(\frac{t}{t_{EOD}}\right)\right] \tag{5.1a}$$

$$R_t = R_{EOD} + R_{setup} \tag{5.1b}$$

where,

$R_{setup}$ = the pile setup resistance, kN or kips,

$R_{EOD}$ = the initial pile resistance at EOD estimated using WEAP-SA, kN or kips,

$R_t$ = the total nominal pile resistance at time ($t$), kN or kips;

$f_c$ = consolidation factor (13.78 for using WEAP-SA in estimating $R_{EOD}$),minute,

$C_h$ = horizontal coefficient of consolidation determined from CPT pore water pressure dissipation tests and strain path method, $cm^2$/min. or $in.^2$/minute,

$N_a$ = average SPT *N*-value by weighting to cohesive soil thicknesses,

$r_p$ = equivalent pile radius based on cross-sectional area, $cm^2$ or $in.^2$,

$f_r$ = remolding recovery factor (use 0.149 for the WEAP-SA method),

$t$ = time elapsed after EOD, minute, and

$t_{EOD}$ = time at the end of driving (assumes a value of 1 minute).

Detailed derivation and validation of Eq. (5.1a) can be found in Chapter 4 as well as for CAse Pile Wave Analysis Program (CAPWAP). However, Eq. (5.1a) for WEAP-SA was selected throughout the paper based on a database of steel H-piles to illustrate the proposed procedure of incorporating pile setup in accordance with LRFD. Nevertheless, the proposed procedure can be generally and practically implemented based on any regional database that reflects the local soil conditions, pile types, and setup quantification methods.

According to Eq. (5.1b), the total nominal pile resistance ($R_t$) comprises both initial pile resistances at EOD ($R_{EOD}$) estimated using WEAP and pile setup resistance ($R_{setup}$) from either Eq. (5.1a) or any other existing empirical setup methods. Unlike the aforementioned setup evaluation involving the pile tests, each of the pile resistance components has its own source of uncertainties, such as those resulting from the in-situ measurement of soil properties and the semi-empirical approach adapted for Eq. (5.1a). To incorporate such a pile setup estimate in LRFD satisfactorily, it should be realized that the impact of the uncertainties associated with the $R_{EOD}$ and the $R_{setup}$ components are different and they should be accounted simultaneously to reach the same target reliability index. While ensuring that the reliability theory based LRFD framework is adequately followed in this process, it enables incorporation of two resistance factors: one for the setup and the other for the pile resistance at the EOD condition. The concept of separately addressing the different uncertainties associated with $R_{EOD}$ and $R_{setup}$ has been recognized by Komurka et al. (2005), but this procedure was suggested using separate safety factors for both resistances. Furthermore, Yang and Liang (2006) used an intensive computational First Order Reliability

Method (FORM) to calculate resistance factors specifically for the Skov and Denver (1988) empirical method. The FORM requires an iterative procedure by simultaneously adjusting the load and resistance components until a minimum reliability index is determined. In order to provide a general and closed-form solution for practical resistance factor calculations, this paper presents the derivation of the resistance factor for pile setup based on a simpler First Order Second Moment (FOSM) method.

## 5.3. Uncertainties of pile Resistance

### 5.3.1. Evaluation Based on Resistance Ratio

For an illustration purpose, evaluation of uncertainties associated with setup was examined for steel H-piles embedded in cohesive soils using a database containing restrike and/or static load test data. Steel H-pile was chosen because it is the most common foundation type used to support bridges in the United States (AbdelSalam et al. (2010)). The database as shown in Table 5.1 comprises five recently completed full-scale pile tests within the State of Iowa (data sets 1 to 5; see Chapter 3 and Ng et al. (2011) for more details), ten data sets from PIle LOad Test database of the Iowa Department of Transportation (PILOT) (data sets 6 to 15; see more details in Roling et al. (2010)), and four well-documented tests (data sets 16 to 19) found in published literature (Huang (1988), Lukas and Bushell (1989), Long et al. (2002), and Fellenius (2002)). One of the important information listed for pile setup evaluations is the elapsed time ($t$), which is the time at pile restrike or static load test (SLT) following the end of pile driving. To compare various sources of uncertainties in terms of coefficient of variation ($COV_R$), five different resistance ratio ($RR$) combinations were calculated as shown in Table 5.1. The resistance ratio (RR) is defined as a ratio of the measured pile resistance ($R_m$) and the estimated pile resistance ($R_e$). The $R_m$ values were obtained from either SLTs or restrikes using CAse Pile Wave Analysis Program (CAPWAP). Pile resistances obtained from CAPWAP were assumed to be $R_m$ values based on the following reasons:

1. The signal matching performed by CAPWAP is based on pile force and velocity

records measured using Pile Driving Analyzer (PDA);

2. CAPWAP is the most reliable method that closely matches the static load test, substantiated by the small difference in resistance factors between CAPWAP (0.65 for at least 2% production piles or 0.75 for 100% production piles) and SLT (0.80 for at least 2% production piles) recommended by AASHTO (2010);
3. In order to illustrate the procedure for incorporating pile setup estimated using Eq. (5.1a) without the need of pile restrikes or load tests in LRFD, the actual pile setup development can be reasonably quantified using either the most reliable CAPWAP or SLT as similarly employed by Yang and Liang (2006); and
4. It is practically infeasible to measure pile resistances at EOD using SLT and such information cannot be found presently in literature. Thus, pile setup measured using CAPWAP can be effectively used to compare with that estimated using Eq. (5.1a). Nevertheless, resistance factors proposed in this paper can be improved using the same proposed calibration procedure in the future providing with sufficient pile setup measurements using only the SLT.

Whereas, the estimated pile resistance ($R_e$) is referred to pile resistances obtained using WEAP-SA or the pile setup resistances estimated using Eq. (5.1a).

The first *RR* ($R_{m\text{-}t}/R_{e\text{-}restrike}$), a ratio of measured pile resistance at any time ($t$) and pile resistance estimated using WEAP-SA from restrike events, were calculated to evaluate the uncertainty associated with pile resistances estimated using WEAP-SA. In case 2, an uncertainty was also evaluated for the typically used *RR* ($R_{m\text{-}t}/R_{e\text{-}EOD}$), a ratio of measured pile resistance at any time ($t$) and estimated initial pile resistance at EOD without considering the effects of setup. In case 3, the *RR* ($R_{m\text{-}t}/R_{e\text{-}t}$) for any time ($t$) was computed based on a ratio of the measured pile resistance and the sum of the initial pile resistance estimated using WEAP and the setup resistance using Eq. (5.1a). In case 4, the *RR* for the EOD ($R_{m\text{-}EOD}/R_{e\text{-}EOD}$), a ratio of the measured and estimated initial pile resistances at EOD, was computed to evaluate the uncertainty associated with initial pile resistance. In case 5, the *RR* for pile setup ($R_{m\text{-}setup}/R_{e\text{-}setup}$), a ratio of the measured pile setup resistance and the setup resistance

estimated using Eq. (5.1a), was calculated to evaluate the uncertainty associated with the pile setup resistance. The measured pile setup resistance ($R_{m\text{-}setup}$) was the difference between the measured pile resistance at any time ($t$) obtained using either SLT or CAPWAP and the initial measured pile resistance at EOD obtained using CAPWAP. These *RR* values in cases 4 and 5 were essential for the computation of separate resistance factors.

Table 5.1: Five cases of the pile resistance ratio (RR)

| Data Set | References [Location] | Time Elapsed after EOD, $t$ (day) | Case 1 *RR* for restrike, ($R_{m\text{-}t}/R_{e\text{-}restrike}$) | Case 2 Typical *RR*, ($R_{m\text{-}t}/R_{e\text{-}EOD}$) | Case 3 *RR* at time $t$, ($R_{m\text{-}t}/R_{e\text{-}t}$) | Case 4 *RR* for EOD, ($R_{m\text{-}EOD}/R_{e\text{-}EOD}$) | Case 5 *RR* for Setup, ($R_{m\text{-}setup}/R_{e\text{-}setup}$) |
|---|---|---|---|---|---|---|---|
| 1 | ISU2 [Mills] | 9 | 0.90[a] | 1.62[a] | 0.91[a] | 1.05[b] | 0.74[a] |
| 2 | ISU3 [Polk] | 36 | 1.14[a] | 1.84[a] | 1.00[a] | 1.21[b] | 0.76[a] |
| 3 | ISU4 [Jasper] | 16 | 1.00[a] | 1.62[a] | 0.94[a] | 1.07[b] | 0.76[a] |
| 4 | ISU5 [Clarke] | 9 | 0.95[a] | 1.70[a] | 1.02[a] | 1.24[b] | 0.68[a] |
| 5 | ISU6 [Buchanan] | 14 | 0.84[a] | 1.54[a] | 0.90[a] | 1.05[b] | 0.69[a] |
| 6 | PILOT [Decatur] | 3 | | 1.63[a] | 1.05[a] | | 1.14[a] |
| 7 | PILOT [Linn] | 5 | | 1.34[a] | 0.85[a] | | 0.58[a] |
| 8 | PILOT [Linn] | 5 | | 0.97[a] | 0.62[a] | | -0.05[c] |
| 9 | PILOT [Linn] | 5 | | 1.48[a] | 0.94[a] | | 0.82[a] |
| 10 | PILOT [Johnson] | 3 | | 1.50[a] | 0.97[a] | | 0.93[a] |
| 11 | PILOT [Hamilton] | 4 | – | 1.84[a] | 1.18[a] | – | 1.48[a] |
| 12 | PILOT [Kossuth] | 5 | | 1.33[a] | 0.84[a] | | 0.56[a] |
| 13 | PILOT [Jasper] | 1 | | 1.70[a] | 1.15[a] | | 1.45[a] |
| 14 | PILOT [Poweshiek] | 8 | | 1.56[a] | 0.96[a] | | 0.91[a] |
| 15 | PILOT [Poweshiek] | 3 | | 1.16[a] | 0.75[a] | | 0.52[a] |
| 16 | Huang (1988) [China] | 2 | – | 1.39[b] | 0.87[b] | 0.93[b] | 0.78[b] |
| | | 31 | | 2.25[a] | 1.23[a] | | 1.61[a] |
| 17 | Lukas & Bushell (1989) [Illinois] | 10 | – | 1.70[a] | 1.05[a] | – | 1.12[a] |
| | | 26 | | 1.95[a] | 1.16[a] | | 1.38[a] |
| 18 | Long et al. (2002) [Illinois] | 7 | 0.77[a] | 1.02[a] | 0.61[a] | 0.91[b] | 0.04[c] |
| | | 22 | 1.11[a] | 2.16[a] | 0.87[a] | | 0.85[a] |
| 19 | Fellenius (2002) [Canada] | 7 | – | 1.72[b] | 1.07[b] | 1.43[b] | 1.19[b] |
| | | 13 | | 1.87[b] | 1.13[b] | | 0.67[b] |
| | | 15 | | 1.92[b] | 1.16[b] | | 0.74[b] |
| | | 16 | | 2.11[b] | 1.27[b] | | 1.02[b] |
| | | 18 | | 2.03[b] | 1.22[b] | | 0.89[b] |
| | | 21 | | 1.91[b] | 1.14[b] | | 0.70[b] |
| | | 28 | | 2.24[b] | 1.32[b] | | 1.16[b] |
| | | 32 | | 2.32[b] | 1.36[b] | | 1.26[b] |
| | | 44 | | 2.29[b] | 1.33[b] | | 1.19[b] |

[a] measured pile resistance using SLT; [b] measured pile resistance using CAPWAP; [c] pile setup was insignificant thus neglected.

### 5.3.2. Results of Conventional FOSM Analysis

Table 5.2 presents the resistance biases ($\lambda_R$) and coefficients of variation ($COV_R$) calculated for all five *RR* (Cases 1 to 5) using the database given in Table 5.1. Table 5.2 shows that pile resistances obtained from restrikes (Case 1) has the least uncertainty as indicated by the lowest $COV_R$ value of 0.14. The large difference in $COV_R$ values between EOD (0.157 in Case 4) and setup (0.317 in Case 5) confirms the disparity in the associated uncertainties and promotes the development of resistance factors separately for the EOD condition and for the effects of setup.

In compliance with the LRFD limit state (i.e., $\varphi R \geq \gamma Q$) and assuming the load ($Q$) and resistance ($R$) are mutually independent and lognormally distributed, the resistance factors ($\varphi$) for Cases 1 to 4 were calibrated in accordance to the FOSM method as suggested by Barker et al. (1991) (see Eq. (5.2)). With the focus on the axial pile resistance, the AASHTO (*3*) strength I load combination is considered here. The numerical values for the different probabilistic characteristics of dead ($Q_D$) and live ($Q_L$) loads ($\gamma$, $\lambda$, and $COV$) as documented by Nowak (1999) and similarly used by Paikowsky et al. (2004) are recapitulated in parentheses given in the definition of each parameter

$$\varphi = \frac{\lambda_R \left(\frac{\gamma_D Q_D}{Q_L} + \gamma_L\right) \sqrt{\left[\frac{\left(1+COV_D^2+COV_L^2\right)}{\left(1+COV_R^2\right)}\right]}}{\left(\frac{\lambda_D Q_D}{Q_L} + \lambda_L\right) e^{\left\{\beta_T \sqrt{\ln\left[\left(1+COV_R^2\right)\left(1+COV_D^2+COV_L^2\right)\right]}\right\}}} \tag{5.2}$$

where,

$\lambda_R$ = the resistance bias factor of the resistance ratio,

$COV_R$ = the coefficient of variation of the resistance ratio,

$\gamma_D$, $\gamma_L$ = the dead load factor (1.25) and live load factor (1.75),

$\lambda_D$, $\lambda_L$ = the dead load bias (1.05) and live load bias (1.15),

$COV_D$, $COV_L$ = the coefficients of variation of dead load (0.1) and live load (0.2), and

$Q_D/Q_L$ = dead to live load ratio (2.0).

Table 5.2: Comparison of Resistance Factors Obtained using the Conventional LRFD framework based on WEAP-SA

| Case | Resistance Ratio (RR) | Sample Size | $\lambda_R$ | $COV_R$ | Nominal Pile Resistance ($R$) | $\beta_T$ = 2.33 | | $\beta_T$ = 3.00 | |
|---|---|---|---|---|---|---|---|---|---|
| | | | | | | $\varphi$ | $\varphi/\lambda$ | $\varphi$ | $\varphi/\lambda$ |
| 1 | $R_{m\text{-}t}/R_{e\text{-}restrike}$ | 7 | 0.959 | 0.140 | $R_{e\text{-}restrike}$ | 0.69 | 0.72 | 0.58 | 0.61 |
| 2 | $R_{m\text{-}t}/R_{e\text{-}EOD}$ | 30 | 1.723 | 0.211 | $R_{e\text{-}EOD}$ | 1.11 | 0.65 | 0.91 | 0.53 |
| 3 | $R_{m\text{-}t}/R_{e\text{-}t}$ | 30 (28) | 1.029 (1.059) | 0.190 (0.156) | $R_{e\text{-}t}$ (Eq. 5.1) | 0.69 | 0.67 | 0.57 | 0.55 |
| 4 | $R_{m\text{-}EOD}/R_{e\text{-}EOD}$ | 8 | 1.111 | 0.157 | $R_{e\text{-}EOD}$ | 0.78 | 0.71 | 0.65 | 0.59 |
| 5 | $R_{m\text{-}setup}/R_{e\text{-}setup}$ | 28 | 0.950 | 0.317 | *Not applicable for Eq. (5.2)* | | | | |

The target reliability indices ($\beta_T$) of 2.33 (corresponding to 1% probability of failure) and 3.00 (corresponding to 0.1% probability of failure) as recommended by Paikowsky et al. (2004) for representing redundant and non-redundant pile groups, respectively, were used in the calculations.

Based on the calculated resistance biases and coefficients of variation, the respective resistance factors ($\varphi$) and efficiency factors ($\varphi/\lambda$) were calculated using Eq. (5.2) as listed in Table 5.2. Due to the occurrence of pile setup in each data point that was measured using a SLT conducted several days (ranging between 1 and 44 days) after EOD, a large $\lambda_R$ value of 1.723 and a moderate $COV_R$ of 0.211 were determined for Case 2 ($R_{m\text{-}t}/R_{e\text{-}EOD}$), and unrealistic high resistance factors of 1.11 and 0.91 were yielded for the $\beta_T$ values of 2.33 and 3.00, respectively. It should be recognized that a constant "pseudo pile setup factor" resulted from a relative large $\lambda_R$ value during the resistance factor calibration using Eq. (5.2), regardless of cohesive soil properties and time elapsed, was indirectly included in the resistance factors. Although the total pile resistances were effectively estimated using Eq. (5.1a), as shown in Case 3 with the $\lambda_R$ value (1.029) closes to unity and a moderate $COV_R$ of 0.190, the difference between the $COV_R$ value of 0.190 for Case 3 and 0.317 for setup (Case 5) confirms that the conventional LRFD calibrating procedure cannot account for the difference uncertainties associated with the initial pile resistance ($R_{EOD}$) and the setup resistance ($R_{setup}$) within the conventional LRFD frame work. Even if the same sample size of 28 for setup is evaluated for Case 3, the $COV_R$ value reduces to 0.156, which is again different from that for setup. Therefore, use of a single resistance factor of 0.69 when $\beta_T$ of

2.33 or 0.57 when $\beta_T$ of 3.00 to both $R_{EOD}$ and $R_{setup}$ having different probabilistic characteristics violates the LRFD philosophy.

## 5.4. Statistical Evaluations

To consider the pile setup resistance estimated using Eq. (5.1a) in pile designs that conform with the reliability theory in accordance with LRFD framework, the principle of strength limit state function ($g$) corresponding to a safety of margin is expanded as in Eq. (5.3), which is valid only if the initial pile resistance at EOD ($R_{EOD}$), pile setup resistance ($R_{setup}$) and both dead ($Q_D$) and live ($Q_L$) loads have lognormal distribution.

$$g = \ln(R_{EOD}) + \ln(R_{setup}) - \ln(Q_D) - \ln(Q_L) \tag{5.3}$$

To verify the pile resistances given in Table 5.1 follow the lognormal distributions, a hypothesis test based on Anderson-Darling (1952) normality method was used to assess the Goodness of Fitting of the assumed lognormal distributions. The reason for selecting the Anderson-Darling method is because it is one of the best normality tests for a database with relative small sample size (Romeu, 2010). Figure 5.1 shows that the Anderson-Darling ($AD$) values of 0.255 and 0.374 are smaller than the critical $P$-values of 0.620 and 0.392 within the 95% confident interval ($CI$) for EOD and setup conditions, respectively. Hence, the hypothesis test confirms the assumed lognormal distributions for both resistances. Since both resistances and loads (as assumed by Nowak (1999)) follow lognormal distributions, natural logarithm of resistances and loads follow normal distributions and the safety margin ($g$) follows a normal distribution such that the relationship between probability of failure ($P_f$) and reliability index ($\beta$) is validly given by Eq. (5.4)

$$P_f = 1 - \Phi(\beta) \tag{5.4}$$

where,

$\beta$ = ratio of E($g$) and $\sigma_g$,

$\Phi$ () = cumulative distribution function,

E($g$) = expected value or mean of the limit state function $g$, and

$\sigma_g$ = standard deviation of the limit state function $g$.

In order to conform the independent relationship among the random variables assumed in the FOSM method, the correlation between the *RR* for EOD (let $R_{m\text{-}EOD}/R_{e\text{-}EOD}$ to be $E$) and for setup (let $R_{m\text{-}setup}/R_{e\text{-}setup}$ to be $S$) was assessed through the calculation of a correlation coefficient ($\rho$) using Eq. (5.5)

$$\rho = \frac{cov(E,S)}{\sigma_E \sigma_S} \tag{5.5}$$

where,

$cov$ ($E$,$S$) = covariance between the resistance ratio for EOD and setup, and

$\sigma_E$, $\sigma_S$ = standard deviation of the resistance ratio for EOD or setup.

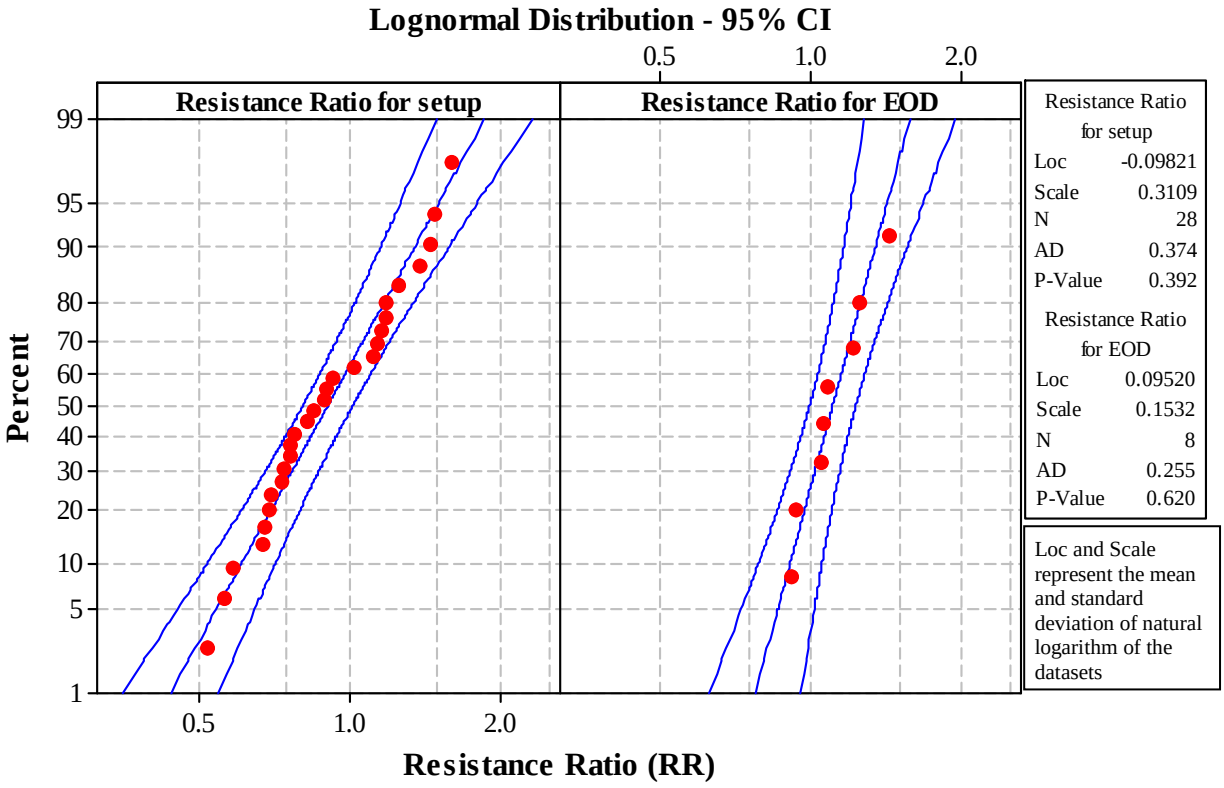


Figure 5.1: Normality test using Anderson-Darling method for setup and EOD

A total of 17 points given in Table 5.1 having both resistance ratio *E* and *S* were selected for the correlation analysis, and the correlation coefficient ($\rho$) was calculated to be 0.071. Compared with the $\rho$ value of -0.243 computed for the Skov and Denver (*3*) empirical pile setup method which led to the independent relationship claimed by Yang and Liang (2006), the calculated $\rho$ value of 0.071 is smaller. Thus, pile resistances for EOD (*E*) and for setup (*S*) are concluded to be mutually independent. The lognormal distribution and independent relationship of the loads and resistances satisfy the assumptions of the FOSM method.

## 5.5. Improved FOSM method for setup

Satisfying the lognormal distributions and independent relationships of loads and resistances and considering only dead ($Q_D$) and live ($Q_L$) loads as per the AASHTO (2010) strength I load combination, the reliability index ($\beta$) is expanded to

$$\beta = \frac{\mathrm{E}(g)}{\sigma_g} = \frac{\mathrm{E}(\ln(R_{EOD})) + \mathrm{E}\left(\ln\left(R_{setup}\right)\right) - \mathrm{E}(\ln(Q_D)) - \mathrm{E}(\ln(Q_L))}{\sqrt{\sigma^2_{\ln(R_{EOD})} + \sigma^2_{\ln(R_{setup})} + \sigma^2_{\ln(Q_D)} + \sigma^2_{\ln(Q_L)}}} \tag{5.6}$$

where,

$R_{EOD}$ = initial pile resistance at EOD,

$R_{setup}$ = pile setup resistance, and

$\mathrm{E}(\ln(R_{EOD}))$, $\sigma_{\ln(R_{EOD})}$ = expected value (mean) and standard deviation of the natural logarithm of the initial pile resistance at EOD, which are similarly defined for other random variables.

To express Eq. (5.6) in terms of simple means ($\bar{R}$ and $\bar{Q}$) and coefficients of variation (*COV*) for loads and resistances of the normal distributions, the mean and standard deviation of lognormal distribution for any load or resistance can be transformed using the following general expressions

$$\mathrm{E}(\ln(R)) = \ln(\bar{R}) - 0.5\ln(1 + COV_R^2) \tag{5.7}$$

$$\sigma^2_{\ln(R)} = \ln(1 + COV_R^2) \tag{5.8}$$

Using these expressions for the four random variables ($R_{EOD}$, $R_{setup}$, $Q_D$ and $Q_L$) and substituting them into Eq. (5.6), the reliability index can be expressed as follows:

$$\beta = \frac{\ln\left(\frac{\bar{R}_{EOD}+\bar{R}_{setup}}{\bar{Q}_D+\bar{Q}_L}\right) + \ln\left(\sqrt{\frac{1+COV_{Q_D}^2+COV_{Q_L}^2+2COV_{Q_D}^2COV_{Q_L}^2}{1+COV_{R_{EOD}}^2+COV_{R_{setup}}^2+2COV_{R_{EOD}}^2COV_{R_{setup}}^2}}\right)}{\sqrt{\ln\left[\left(1+COV_{R_{EOD}}^2+COV_{R_{setup}}^2+2COV_{R_{EOD}}^2COV_{R_{setup}}^2\right)\left(1+COV_{Q_D}^2+COV_{Q_L}^2+2COV_{Q_D}^2COV_{Q_L}^2\right)\right]}} \tag{5.9}$$

Replacing the simple mean values with their respective bias factors ($\lambda$), a ratio between average measured and predicted values ($\frac{\bar{R}_m}{R}$ or $\frac{\bar{Q}_m}{Q}$), and neglecting the terms with the multiplication of two coefficients of variation square ($COV^2COV^2$) as they would yield insignificantly small values, the expression for $\beta$ is simplified as

$$\beta = \frac{\ln\left(\frac{\lambda_{R_{EOD}}R_{EOD}+\lambda_{R_{setup}}R_{setup}}{\lambda_D Q_D+\lambda_L Q_L}\right) + \ln\left[\sqrt{\frac{\left(1+COV_{Q_D}^2+COV_{Q_L}^2\right)}{\left(1+COV_{R_{EOD}}^2+COV_{R_{setup}}^2\right)}}\right]}{\sqrt{\ln\left[\left(1+COV_{R_{EOD}}^2+COV_{R_{setup}}^2\right)\left(1+COV_{Q_D}^2+COV_{Q_L}^2\right)\right]}} \tag{5.10}$$

Equating the LRFD strength limit state equation ($\gamma Q = \varphi R$) and replacing the $\varphi R$ with $\varphi_{EOD}R_{EOD}+\varphi_{setup}R_{setup}$, the $R_{setup}$ can be rearranged as

$$R_{setup} = \frac{\gamma_D Q_D + \gamma_L Q_L - \varphi_{EOD}R_{EOD}}{\varphi_{setup}} \tag{5.11}$$

Substituting Eq. (5.11) into Eq. (5.10) and isolating the $\varphi_{setup}$ parameter to the left side by rearranging Eq. (5.10), the preliminary form of the resistance factor for pile setup can be expressed in the following form.

$$\varphi_{setup} = \frac{\lambda_{setup}[\gamma_D Q_D + \gamma_L Q_L - \varphi_{EOD} R_{EOD}]}{\frac{(\lambda_D Q_D + \lambda_L Q_L) e^{\beta \sqrt{\ln\left[\left(1+cov_{R_{EOD}}^2+cov_{R_{setup}}^2\right)\left(1+cov_{Q_D}^2+cov_{Q_L}^2\right)\right]}}}{\sqrt{\frac{\left(1+cov_{Q_D}^2+cov_{Q_L}^2\right)}{\left(1+cov_{R_{EOD}}^2+cov_{R_{setup}}^2\right)}}} - \lambda_{EOD} R_{EOD}} \tag{5.12}$$

Normalizing the above expression by the total load ($Q_D$ + $Q_L$) and further expressing Eq. (5.12) in terms of the ratio of dead load to live load ($Q_D/Q_L$) and the ratio of initial pile resistance at EOD to total load using $\alpha \left(i.e.,\ \alpha = \frac{R_{EOD}}{Q_D+Q_L}\right)$, the final equation of the resistance factor for pile setup at a target reliability index ($\beta_T$) yields to

$$\varphi_{setup} = \frac{\lambda_{setup}\left[\frac{\gamma_D\left(\frac{Q_D}{Q_L}\right)+\gamma_L}{1+\left(\frac{Q_D}{Q_L}\right)} - \varphi_{EOD}\alpha\right]}{\frac{\left(\frac{\lambda_D\left(\frac{Q_D}{Q_L}\right)+\lambda_L}{1+\left(\frac{Q_D}{Q_L}\right)}\right) e^{\beta_T \sqrt{\ln\left[\left(1+cov_{R_{EOD}}^2+cov_{R_{setup}}^2\right)\left(1+cov_{Q_D}^2+cov_{Q_L}^2\right)\right]}}}{\sqrt{\frac{\left(1+cov_{Q_D}^2+cov_{Q_L}^2\right)}{\left(1+cov_{R_{EOD}}^2+cov_{R_{setup}}^2\right)}}} - \lambda_{EOD}\alpha} \tag{5.13}$$

## 5.6. Resistance Factors For Setup

The aforementioned derivation resulted in Eq. (5.13) reveals that the $\varphi_{setup}$ value is dependent on various parameters. Considering only the AASHTO (2010) strength I load combination, the probabilistic characteristics ($\gamma$, $\lambda$ and $COV$) of the random variables $Q_D$ and $Q_L$ are defined in Eq. (5.2) as documented by Nowak (1999). The probabilistic characteristics ($\lambda$ and $COV$) of the random variables $R_{EOD}$ and $R_{setup}$ were selected from Cases 4 and 5 of Table 5.2, respectively. Therefore, the following analyses focus on the influence of the remaining random variables ($\beta_T$, $\alpha$, $\varphi_{EOD}$ and $Q_D/Q_L$) on the $\varphi_{setup}$ value.

Since the uncertainty for the pile resistance at EOD is lower than that for setup ($COV_{EOD}$ of 0.157 versus $COV_{setup}$ of 0.317) and both resistance mean biases are closer to unity ($\lambda_{EOD}$ = 1.111 and $\lambda_{setup}$ = 0.950), the calculated $\varphi_{EOD}$ values will likely higher than the

$\varphi_{setup}$ values. At a fixed dead to live load ratio of 2.0, Figure 5.2 shows that the $\varphi_{setup}$ values decrease with increasing $\alpha$ values. It is reasonable for Eq. (5.13) to yield a smaller $\varphi_{setup}$ value when the estimated $R_{EOD}$ is overly higher than the loads because the computed total factored pile resistances are not overly larger than the factored loads, resulting in an over conservative design. Therefore, an efficient driven pile system shall consider a shorter pile length or a smaller α value. The $\varphi_{setup}$ values decrease with increasing $\beta_T$ values for $\alpha$ values in the range between 0.2 to 1.2. The $\varphi_{setup}$ values become insensitive to $\beta_T$ values when $\alpha$ value = 1.4, indicating by a nearly horizontal dashed line with triangular markers. However, the $\varphi_{setup}$ values decrease when $\beta_T$ is smaller than 2.50 and $\alpha$ is greater than 1.4.

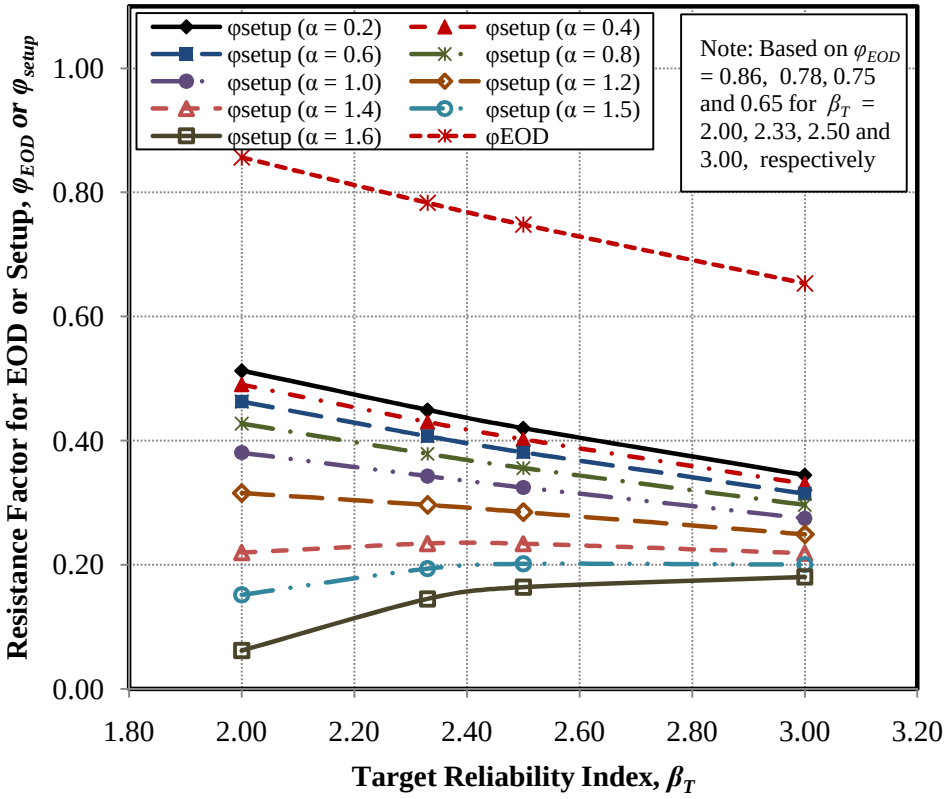


Figure 5.2: Relationship between resistance factor and target reliability index

Based on a fixed $Q_D/Q_L$ of 2.0 and $\varphi_{EOD}$ values of 0.78 and 0.61 (see Table 5.2) for the $\beta_T$ values of 2.33 and 3.00, respectively, Figure 5.3 shows that the increase in $\alpha$ values from 0.2 to 1.6 reduce the $\varphi_{setup}$ values by a factor of 3 and 2 for $\beta_T$ values of 2.33 and 3.00,

respectively. It can be seen that the $\varphi_{setup}$ values for $\beta_T$ value of 2.33 are always greater than those for $\beta_T$ value of 3.00; however, an opposite trend is seen for $\alpha$ values greater than 1.47. The continuous increase in $\alpha$ values reduce the $\varphi_{setup}$ values to approaching zero. This means that the pile setup effect becomes irrelevant at an extremely high $R_{EOD}$ value with respect to total load, specifically at $\alpha$ values greater than 1.8 and 2.16 for the $\beta_T$ values of 2.33 and 3.00, respectively. Similar observations are observed for the efficiency factors ($\varphi/\lambda$). Due to the impact of higher uncertainty associated with pile setup, the maximum $\varphi/\lambda$ values of 0.49 and 0.37 for both $\beta_T$ values of 2.33 and 3.00, respectively, are smaller than those for the EOD condition (0.71 and 0.59, respectively) given in Table 5.2.

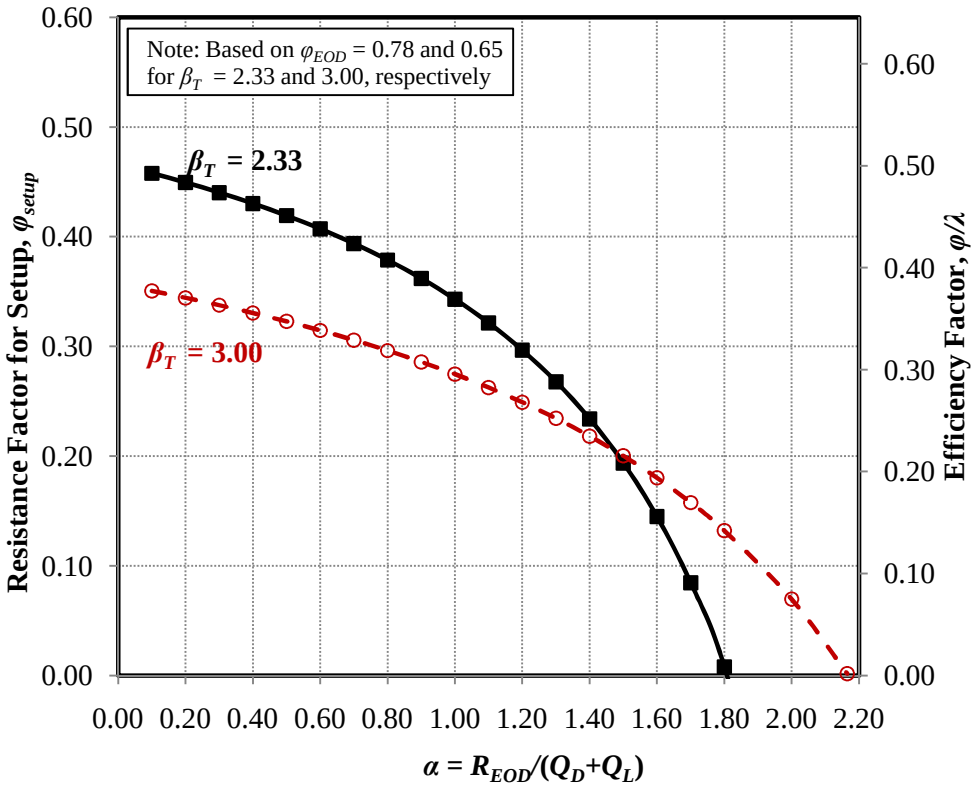


Figure 5.3: Relationship between resistance factor for setup and the ratio of initial pile resistance at EOD to total load ($\alpha$)

Because a constant $\varphi_{EOD}$ value as similarly shown in Table 5.2 and a fixed α value will be chosen during pile designs, a constant $\varphi_{setup}$ value will be recommended. However, in order to illustrate the possibility of different $\varphi_{EOD}$ values for reflecting different regional soil

conditions and design practices, Figure 5.4 shows the variation of $\varphi_{setup}$ values based on a constant $Q_D/Q_L$ ratio of 2. Figure 5.4 shows that larger $\varphi_{setup}$ values will be recommended if larger $\varphi_{EOD}$ values are calibrated for $\alpha$ values ranging between 0.2 and 1.2. The $\varphi_{setup}$ values become less sensitive to $\varphi_{EOD}$ values at $\alpha$ value of 1.4. However, if a local design method yields conservative pile designs (i.e., α values larger than 1.5) and results in a $\varphi_{EOD}$ value greater than 0.75, pile setup resistance becomes dispensable for satisfying the total factored load.

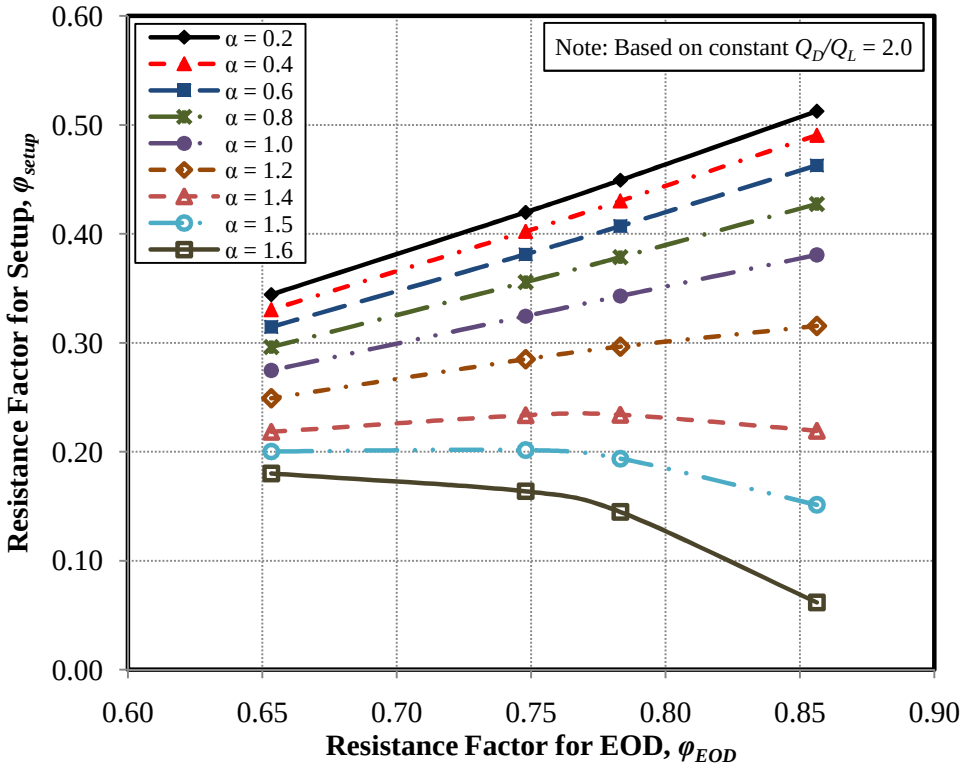


Figure 5.4: Relationship between resistance factors for setup and for EOD

The aforementioned observations shown in Figure 5.2, 5.3 and 5.4 are based on a fixed $Q_D/Q_L$ of 2, and it is of interest to investigate the influence of this ratio, which is a function of the span length of a bridge, on the $\varphi_{setup}$ values. Based on the AASHTO (2003) Specifications, the following dead to live load ratios 0.52, 1.06, 1.58, 2.12, 2.64, 3.00, and 3.53 are suggested for span lengths of 9, 18, 27, 36, 45, 50, and 60 m. For an illustration purpose, $\alpha$ values of 1.0 and 1.5 were selected as shown in Figure 5.5(a) and (b),

respectively. Figure 5.5 illustrates that the $\varphi_{setup}$ values reduce gradually with increasing $Q_D/Q_L$ ratios from 0.52 to about 2.12, and the $\varphi_{setup}$ values reduce at a slower rate thereafter. Figure 5.5(a) indicates that the increase in $Q_D/Q_L$ ratio by a factor of 6.8 from 0.52 to 3.53 only reduces the $\varphi_{setup}$ values by a small factor of about 1.2. Hence, it can be generally concluded that the $\varphi_{setup}$ values are not sensitive to the $Q_D/Q_L$ ratios. However, the sensitivity increases at a larger $\alpha$ value of 1.5 as shown in Figure 5.5(b), indicated by the faster decrease in the $\varphi_{setup}$ values. In order to optimize the pile setup contribution by selecting an $\alpha$ value of 1.0 during pile designs, $\varphi_{setup}$ values of 0.32 and 0.26 can be conservatively recommended for $\beta_T$ values of 2.33 and 3.00, respectively.

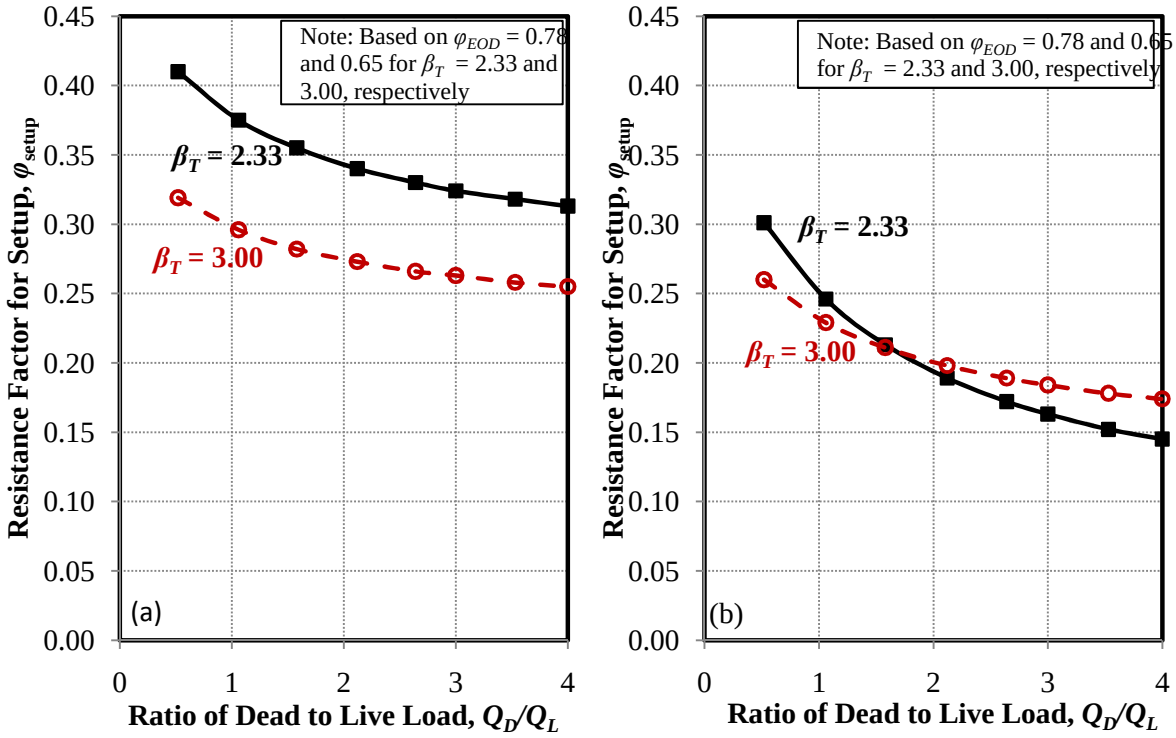


Figure 5.5: Relationship between resistance factor for setup and dead to live load ratio for (a) $\alpha$ value = 1.0; and (b) $\alpha$ value = 1.5

## 5.7. Dependability

Although separate resistance factors have been developed to account for the difference in uncertainties, it is important to demonstrate the dependability of the proposed

procedure in pile designs. Two construction bridge sites at the locations of recently completed field tests in Iowa listed in Table 5.1 (data sets 1 and 4) were selected for a comparative study. The soil profile at each of these sites is cohesive, and a total dead load of 3000 kN (674 kips) and total live load of 1500 kN (337 kips) were assumed for all bridge abutments. HP 250×63 (HP 10×42) production piles were driven with embedded lengths of 29 m (95 ft) and 21 m (69 ft) closed to test sites ISU2 and ISU5, respectively.

Four factored pile resistances based on: (1) EOD condition ($\varphi_{EOD}R_{EOD}$); (2) a single resistance factor as described in Case 3 of Table 5.2 ($\varphi(R_{EOD}+R_{setup})$); (3) the proposed procedure ($\varphi_{EOD}R_{EOD}+\varphi_{setup}R_{setup}$); and (4) SLTs ($\varphi_{SLT}R_{SLT}$) were determined by establishing the minimum number of piles required to support the assumed applied loads. For comparison purposes, each computed number of piles was not rounded to the next higher integer number. A fixed time of 7 days elapsed after pile installation was assumed in the pile setup calculations in Eq. (5.1a). The respective resistance factors are given in Figure 5.6. The $\varphi_{setup}$ values were calculated using Eq. (5.13) based on the recommended probabilistic characteristics of the loads recapitulated in Eq. (5.2) and of the pile resistances given in Table 5.2. The $\varphi_{SLT}$ of 0.80 for measured pile resistances using SLTs was adapted from the AASHTO (2010) recommendations. These resistance factors were selected based on a target reliability index ($\beta_T$) of 2.33.

Figure 5.6 clearly shows that the incorporation of pile setup reduces the number of piles needed, comparing the EOD condition with others. On average the proposed procedure reduces the number of piles required by about 8.6% when compared to the EOD condition ($\varphi_{EOD}R_{EOD}$). The procedure using a single resistance factor for both initial pile resistance and pile setup ($\varphi(R_{EOD}+R_{setup})$) requires the least number of piles, which is less than those determined based on the measured pile resistances ($\varphi_{SLT}R_{SLT}$). This approach will lead to a lower reliability index than that targeted because it is implied in Figure 5.6 that the resistant factor is not the same for both $R_{EOD}$ and $R_{setup.}$ On the other hand, the proposed procedure ($\varphi_{EOD}R_{EOD}+\varphi_{setup}R_{setup}$) compares compatibly with those from measured pile resistances as the number of piles determined based on both combinations are almost similar. This implies that

the proposed procedure provides a better dependability in accordance with LRFD framework. In other words, by taking into account for the different uncertainties associated with pile setup, the proposed LRFD procedure will less likely overestimate the total factored pile resistance and under design the pile foundation system as observed for the case with using a single resistance factor.

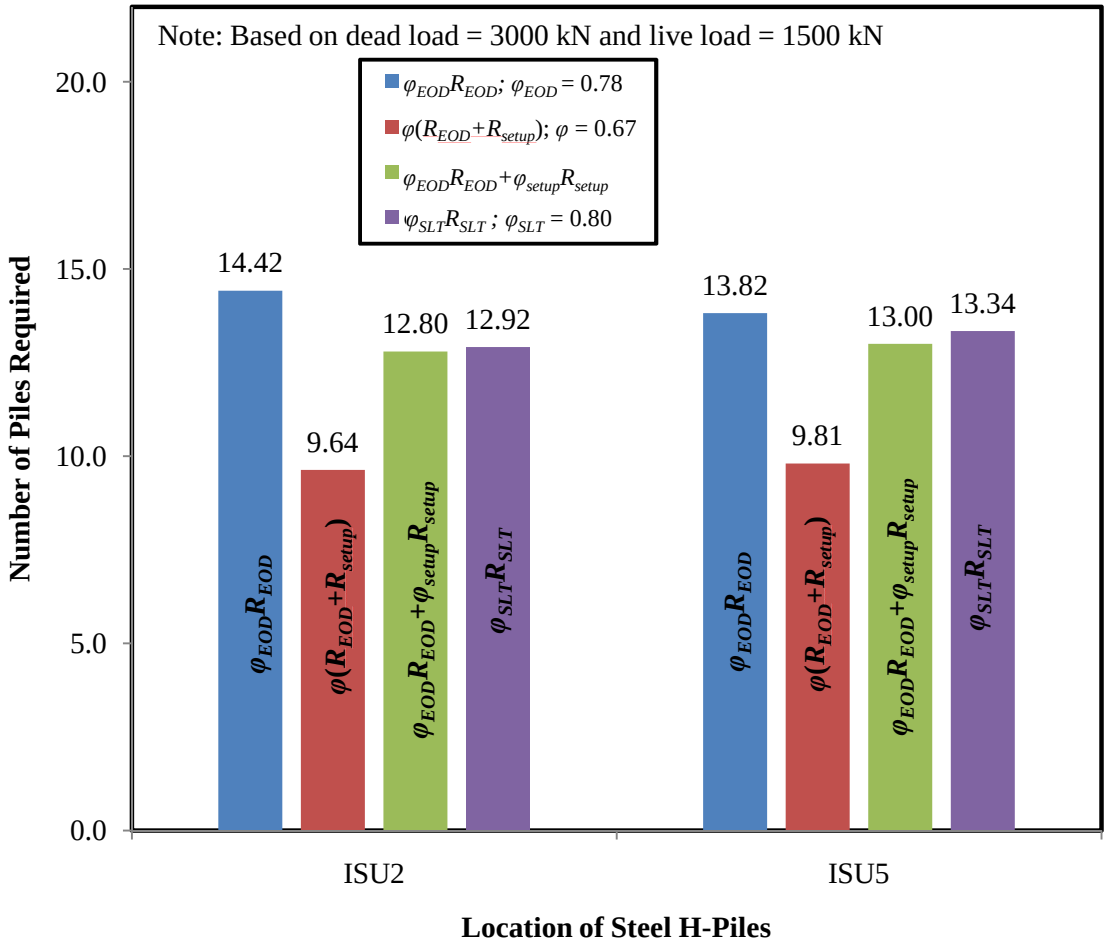


Figure 5.6: Dependability of various procedures to account for setup

## 5.8. Conclusions

AASHTO (2010) acknowledges that it is not feasible in practices to perform static load or dynamic restrike tests over an adequate period of time to quantify the pile setup. To overcome this limitations, pile setup can accounted for using the existing empirical pile setup

estimation methods (e.g. Skov and Denver (1988); Svinkin and Skov (5)) or a semi-empirical method developed Chapter 4. However, the existing calibration procedure cannot separately account the different sources of uncertainties associated with the initial pile resistance ($R_{EOD}$) and the pile setup resistance ($R_{setup}$). Hence, a new and general calibration procedure given by Eq. (5.13) was developed in accordance with LRFD framework to separately calculate the resistance factors for both resistance components, so the economic advantages of pile setup can be recognized during pile designs. In particular, the incorporation of pile setup in LRFD reduces the number of piles required to support the applied loads or prevents additional pile penetrations into an extremely dense soil layer that could cause pile damages. On the other hand, the use of a single resistance factor to both initial pile resistance and pile setup will overestimate the total factored pile resistance and results in an under designed pile foundation. It is concluded that the proposed procedure provides a more dependable pile foundation design while maintaining a target reliability level.

Although the paper illustrates a range of resistance factors for setup ($\varphi_{setup}$) that depends on possible variations of resistance factor for EOD ($\varphi_{setup}$), target reliability index ($\beta_T$), initial pile resistance to total load ratio ($\alpha$), and ratio of dead load to live load ($Q_D/Q_L$), a fixed $\varphi_{setup}$ value can be easily calculated using Eq. (5.13) based on any regional database that reflects the local soil conditions, pile types, and setup quantification methods. For example, $\varphi_{setup}$ values of 0.32 and 0.26 can be conservatively recommended for $\beta_T$ values of 2.33 and 3.00, respectively, based on the database presented in Table 5.1 for steel H-piles embedded in clay and a selected $\alpha$ value of 1.0 in order to optimize the pile setup contribution during pile designs.

## 5.9. Acknowledgments

The authors would like to thank the Iowa Highway Research Board for sponsoring the research presented in this paper. We would like to thank the members of the Technical Advisory Committee: Ahmad Abu-Hawash, Bob Stanley, Curtis Monk, Dean Bierwagen, Gary Novey, John Rasmussen, Ken Dunker, Kyle Frame, Lyle Brehm, Michael Nop, and

Steve Megivern of this research project for their guidance. Special thanks are due to Sherif S. AbdelSalam, Matthew Roling and Douglas Wood for their assistance with the field tests and to Donald Davidson and Erica Velasco for their assistance with the laboratory soil tests.

## 5.10. References

AbdelSalam, S. S., Sritharan, S., and Suleiman, M. T. (2010). "Current Design and Construction Practices of Bridge Pile Foundations with Emphasis on Implementation of LRFD." Journal of Bridge Engineering, ASCE, 15(6), pp. 749-758.

American Association of State Highway and Transportation Officials. (AASHTO). (2003). LRFD Bridge Design Specifications 2nd Edition. 1998 with 2003 Interim., Washington, D.C.

American Association of State Highway and Transportation Officials (AASHTO) (2010). LRFD Bridge Design Specifications Customary U. S. Units 4th Edition. 2008 Interim, Washington, D.C.

Anderson, T. W., and Darling, D. A. (1952). "Asymptotic Theory of Certain "Goodness-of-Fit" Criteria Based on Stochastic Processes." Annals of Mathematical Statistics, 23, pp. 193-212.

Barker, R., Duncan, J., Rojiani, K., Ooi, P., Tan, C., and Kim, S. (1991). NCHRP Report 343: Manuals for the Design of Bridge Foundations. Transportation Research Board, Washington, D.C.

Fellenius, B. H. (2002). "Pile Dynamics in Geotechnical Practice-Six Case Histories." Geotechnical Special Publication No. 116: Proceedings of International Deep Foundations Congress 2002, ASCE, Feb 14–16, Edited by M. W. O'Neill and F. C. Townsend, Orlando, Florida, pp. 619-631.

Huang, S. (1988). "Application of Dynamic Measurement on Long H-Pile Driven into Soft Ground in Shanghai." Proceedings of 3rd International Conference on the Application of Stress-Wave Theory to Piles, Edited by B. H. Fellenius, Ottawa, Ontario, Canada, pp. 635–643.

Komurka, V. E., Winter, C. J., and Maxwell, S. (2005). "Applying Separate Safety Factors to

End-Of-Drive and Set-up Components of Driven Piles Capacity." Geotechnical Applications for Transportation Infrastructure: Proceedings of the 13th Great Lakes Geotechnical and Geoenvironmental Conference, Milwaukee, Wisconsin. Edited by H. H. Titi. Geotechnical Practice Publication 3, ASCE, pp. 65-80.

Long, J. H., Maniaci, M., and Samara, E. A. (2002). "Measured and Predicted Capacity of H-Piles." Geotechnical Special Publication No.116: Advances in Analysis, Modeling & Design, Proceedings of International Deep Foundations Congress 2002, ASCE, Feb 14–16, Edited by M. W. O'Neill and F. C. Townsend, Orlando, Florida, pp.542-558.

Lukas, R. G., and Bushell, T. D. (1989). "Contribution of Soil Freeze to Pile Capacity." Foundation Engineering: Current Principles and Practices, Vol. 2. Edited by Fred H. Kulhawy, ASCE, pp.991-1001.

Ng, K. W., Suleiman, T. M., Roling, M., AbdelSalam, S. S., and Sritharan, S. (2011). Development of LRFD Design Procedures for Bridge Piles in Iowa – Volume II: Field Testing of Steel Piles in Clay, Sand and Mixed Soils. IHRB Project No. TR-583. Institute of Transportation, Iowa State Univeristy, Ames, IA.

Nowak, A. (1999). Calibration of LRFD Bridge Design Code. NCHRP Report 368, Transportation Research Board, Washington, D. C.,.

Paikowsky, S.G. with Contributions from Birgisson, B., McVay, M., Nguyen, T., Kuo, C., Baecher, G., Ayyab, B., Stenersen, K., O'Malley, K., Chernauskas, L., and O'Neill, M. (2004). Load and Resistance Factor Design (LRFD) for Deep Foundations. NCHRP Report 507, Transportation Research Board, Washington, D.C.

Pile Dynamic, Inc. (2005). GRLWEAP Wave Equation Analysis of Pile Driving: Procedures and Model Version 2005, Cleveland, OH.

Roling, M. J., Sritharan S., and Suleiman M. T. (2010). "Electronic Database for PIle LOad Tests in Iowa (PILOT-IA): Paradigm for Data Archiving Needed for Regional LRFD Calibration." Transportation Research Board 89th Annual Meeting, January 10–14, Washington, D.C., pp. 10-1023.

Romeu, J. L. (2010). Anderson-Darling: A Goodness of Fit Test for Small Samples Assumptions. START 2003-5, Vol. 10, Number 5, Reliability Analysis Center,

Rome, NY, (http:www.theriac.org/riacapps/startsheets/?category=Reliability).

Skov, R., and Denver, H. (1988). "Time-Dependence of Bearing Capacity of Piles." Proceedings of the 3rd International Conference on the Application of Stress-Wave Theory to Piles, Edited by B. H. Fellenius, Ottawa, Ontario, Canada, pp. 879-888.

Soderberg, L. O. (1962). "Consolidation Theory Applied to Foundation Pile Time Effects." *Geotechnique*, 12(3), pp. 217-225.

Svinkin, M. R., and Skov, R. (2000). Set-Up Effect of Cohesive Soils in Pile Capacity. Proceedings of the 6th International Conference on Application of Stress-Waves Theory to Piles, Edited by Niyama, S., and Beim, J., Sao Paulo, Brazil, pp. 107-111.

Yang, L., and Liang, R. (2006). "Incorporating Set-Up into Reliability-Based Design of Driven Piles in Clay." Canadian Geotechnical Journal, 43, pp.946-955.

# CHAPTER 6: INTEGRATION OF CONSTRUCTION CONTROL AND PILE SETUP INTO DESIGN

Ng, K. W.[1]; Sritharan, S.[2]; and Suleiman, M. T.[3]

A paper to be submitted to a journal

## 6.1. Abstract

The main objective of this paper is to establish regional Load and Resistance Factor Design (LRFD) recommendations for bridge pile designs, based on a historical PIle LOad Test (PILOT) database and 10 recently completed field tests. Resistance factors were developed for the Wave Equation Analysis Program (WEAP) and CAse Pile Wave Analysis Program (CAPWAP) using the First Order Second Moment (FOSM) method. Compared with the latest American Association of State Highway and Transportation Officials (AASHTO) (2010) recommendations, the regionally-calibrated resistance factors were improved for WEAP and CAPWAP. Using these calibrated results, the design and construction efficiencies of piles were enhanced by minimizing the discrepancy between design and field pile resistances. This was achieved by integrating WEAP and CAPWAP as construction control methods as part of the design process. Furthermore, the effect of pile setup in a clay profile, which was explicitly discussed in Chapters 3 and 4, was incorporated into the LRFD recommendations to elevate the efficiency of bridge foundations attaining the economic advantages of pile setup.

**CE Database Keywords:** WEAP; PDA; CAPWAP; Dynamic Analysis Methods; Resistance Factors; Efficiency Factor; Construction Control; Pile Setup; FOSM; LRFD.

---

[1]Ph.D. Candidate, Dept. of Civil, Construction and Environmental Engineering, Iowa State Univ., Ames, IA 50011. E-mail: kwng@iastate.edu

[2]Wilson Engineering Professor and Associate Chair, Dept. of Civil, Construction and Environmental Engineering, Iowa State Univ., Ames, IA 50011. E-mail: sri@iastate.edu

[3]Assistant Professor, Dept. of Civil and Environmental Engineering, Lehigh University, Bethlehem, PA, 18015. E-mail: mts210@lehigh.edu

## 6.2. Introduction

Allowable Stress Design (ASD) philosophy has long been used for the design of pile foundations for decades. Uncertainties associated with load (Q) and resistance (R) are addressed in this approach through a factor of safety (SF), and the selection of factor of safety is highly dependent on the pile designers' judgments and experiences. Thus, a consistent and reliable performance of bridge foundations cannot be ensured. To overcome this limitation, the Load and Resistance Factor Design (LRFD) philosophy has been progressively developed since the early 1990s with the primary objective of ensuring a uniform reliability of bridge foundations in the United States. The LRFD framework is expressed in Eq. (6.1) as noted by the American Association of State Highway and Transportation Officials (AASHTO) (2001) LRFD Bridge Design Specifications.

$$\sum \gamma_i Q_i \leq \varphi R \tag{6.1}$$

where,

$Q_i$ = applied load,

$R$ = nominal pile resistance,

$\gamma_i$ = load factor corresponding to load $Q_i$, and

$\varphi$ = resistance factor.

The uncertainties associated with the resistance (R) principally originate from site characterization, soil variability, design method, and construction practice. These uncertainties are significantly different from those that affect the applied load (Q) (Paikowsky et al., 2004). Thus, the suitable resistance factor ($\varphi$) and load factor ($\gamma$) are separately multiplied to the resistance and applied load, respectively. As a result, the uncertainties of resistance and applied load can be individually accounted for in achieving a consistent and reliable performance of bridge foundations.

Recognizing the advantages of LRFD philosophy, the Federal Highway Administration (FHWA) mandated all new bridges initiated after October 1, 2007 should follow the LRFD design approach. Unfortunately, the current AASHTO (2007) LRFD

Bridge Design Specifications have been developed for general soil conditions and pile types. These AASHTO Specifications cannot reflect the local soil conditions, design methods, and construction practices, which may result in conservative foundation designs. Even though AASHTO allows the use of regionally-calibrated resistance factors in LRFD pile designs, regional usable pile data, such as pile driving data with PDA records, is insufficient for developing the resistance factors. In recognizing these problems, extensive soil investigations and 10 field pile tests described in Chapter 3 and Ng et al. (2011) were conducted to populate the existing historical PIle LOad Tests (PILOT) database, which has been electronically compiled by Roling et al. (2010). Given that a recent survey of more than 30 State Departments of Transportation (DOTs) conducted by AbdelSalam et al. (2010) revealed that steel H-pile is the most common foundation type used for bridges in the United States, the research studies focus on the most commonly used steel H-pile foundations. Using the PILOT database and the recently completed pile test results, the regionally-calibrated LRFD resistance factors are computed specifically for the construction control methods, Wave Equation Analysis Program (WEAP) and CAse Pile Wave Analysis Program (CAPWAP), using the First Order Second Moment (FOSM) method suggested by Barker et al. (1991).

Since piles are typically designed using static analysis methods and their performances are verified using the construction control methods during construction, it has been a challenge to attain the design pile resistance during construction. As a result of the discrepancy, pile driving specifications are normally adjusted accordingly, such as increasing pile length. This adjustment may increase construction costs, delay construction schedule, and cause contractual challenges. To enhance the design and construction efficiencies of piles, a methodology was developed by the writers to minimize the discrepancy between the design and field pile resistances by integrating the WEAP and CAPWAP as part of the design process.

Although the incorporation of pile setup into pile designs improves the efficiency of bridge foundations, it has not been accounted for in the latest AASHTO (2010) LRFD Specifications. Using the pile setup quantification method developed in Chapters 3 and 4

and the calibration procedure proposed in Chapter 5, the effect of pile setup was incorporated into the LRFD recommendations to elevate the efficiency of bridge foundations attaining the economic advantages of pile setup.

## 6.3. Background

The different pile design and construction practices results in a discrepancy between design and field pile resistances. For instance, in current Iowa practices, piles are designed using the Iowa DOT in-house method (Iowa Blue Book), and the designed pile performances are verified in the field using dynamic analysis methods. The disagreement in the pile resistances incurs additional construction costs, delays the construction schedule, and may provoke contractual challenges. To overcome this problem, the regionally-calibrated results were used to minimize the difference in pile resistances through a probabilistic approach. Construction control factors ($\xi$) for the static analysis method (i.e., Iowa Blue Book) with respect to different dynamic analysis methods at different soil profiles were determined. The corrected resistance factors were limited to ensure the corrected pile resistance remained smaller than the measured resistances obtained from the static load test. This proposed construction control procedure assimilates the construction control capability of dynamic analysis methods in pile designs and overcomes the limitations concerning the design method.

## 6.4. Development of Resistance Factors

The development of regionally-calibrated resistance factors requires sufficient pile load test data records with good quality hammer, pile, and soil information. Both historical Iowa DOT database and 10 recently completed field test results were used in calculating the resistance factors for WEAP, while only the recent field test results containing PDA data were used for CAPWAP. With the focus on the axial pile resistance, the AASHTO Strength I load combination (i.e., dead and live loads only) was considered, and the FOSM method suggested by Barker et al. (1991) was used to determine the resistance factors. Furthermore, resistance factors for pile setup were determined using the calibration procedure proposed in

Chapter 5. The resistance factors were compared with those presented in the NCHRP Report 507 and the latest AASHTO (2010) Specifications.

### 6.4.1. PIle LOad Test (PILOT) database

The Iowa DOT conducted a total of 264 static pile load tests between 1966 to 1989 to improve their pile foundation design practices. These historical test records were compiled, and an electronic PIle LOad Test (PILOT) database was developed by Roling et al. (2010) to allow for efficient analyses performed on the amassed dataset. Of these tests in PILOT, 164 were performed on steel H-piles, but only 32 of them had the hammer, pile, and soil information required for pile resistance estimation using WEAP. Table 6.1, which shows that steel HP 250×63 (HP 10×42) was the most commonly used pile size in Iowa, lists the measured pile resistances obtained from static load tests (SLTs) based on the Davisson's criterion (Davisson, 1972) and the estimated pile resistances using WEAP. For the WEAP analysis, five different soil profile input procedures (i.e., ST, SA, Iowa Blue Book, Iowa DOT and DRIVEN) described in Chapter 2 were used. It is essential to note that all pile resistances estimated using WEAP were based on hammer blow counts (i.e., number of hammer impacts on each pile to achieve 300 mm pile penetration) recorded at the end of driving (EOD) condition, while the static load tests were conducted between 1 and 32 days after the EOD.

To avoid mixing the uncertainties resulting from different soil behaviors, the PILOT database was sorted into sand, clay, and mixed soil profiles, and the resistance factors were individually calculated for each soil type. This grouping was consistent with the AASHTO (2007) LRFD Specifications. Although AASHTO (2007) did not explain the criterion for defining the soil profiles, a methodology for defining a site using a 70%-rule has been accepted by AbdelSalam et al. (2011) in the development of LRFD resistance factors for static analysis methods. A site is identified as sand or clay profile, if the most predominant soil type classified in accordance with the Unified Soil Classification System (USCS) exists more than 70% along the pile shaft embedded length. In contrast, a site with less than 70% sand or clay is identified to have a mixed soil profile. Among the 32 data records listed in

Table 6.1, 11 in sand, 12 in clay, and 9 in mixed soils were used for LRFD resistance factors calibration for WEAP at the EOD condition.

Unfortunately, the PILOT database contains no pile strain and acceleration measurements, recorded using a Pile Driving Analyzer (PDA) described in Chapter 2. These measurements are required in CAPWAP analysis as boundary conditions for pile resistance estimations.

### 6.4.2. Field tests data

To collect the pile strain and acceleration records for CAPWAP analysis and pile setup data as well as to populate the existing PILOT database, 10 full-scaled pile tests were conducted to cover all five geological regions in the State of Iowa. These pile tests involved detailed site characterization using both in-situ subsurface investigations and laboratory soil tests. Prior to pile driving, the test piles were instrumented with strain gauges along the embedded pile length for axial strain measurements during SLTs. Steel HP250 piles were selected for all test piles denoted from ISU1 to ISU10, as listed in Table 6.2. Applying the 70%-rule, test piles ISU9 and ISU10 were embedded in sand profiles, test piles ISU2, ISU3, ISU4, ISU5, and ISU6 were embedded in clay profiles, and test piles ISU1, ISU7, and ISU8 were embedded in mixed soil profiles. During pile driving, EOD and restrikes, the PDA measurements and pile driving resistances in terms of hammer blow counts were recorded. After completing the last restrike, a vertical SLT was performed on each test pile following the “Quick Test” procedure of ASTM D 1143. Details of the field tests were described in Chapter 3 and Ng et al. (2011).

Table 6.2 lists the time of SLTs after the EOD and the Davisson’s measured pile resistances. Also, the estimated pile resistances at the EOD condition for both WEAP and CAPWAP were summarized, whereas the pile resistances estimated from the last restrike tests for both WEAP and CAPWAP are summarized in Table 6.3. These pile resistances were used for LRFD resistance factors calibration for WEAP and CAPWAP at both the EOD and the beginning of restrike (BOR) conditions.

### 6.4.3. Calibration method

First-Order Second-Moment (FOSM), suggested by Barker et al. (1991), is the simplest statistical method used in the resistance factors calibration (see Eq. (6.4)). Compared with the rigorous and invariant First Order Reliability Method (FORM), Paikowsky et al. (2004) concluded that the difference in the outcomes of using the two methods is approximately 10% with the FOSM method leading to smaller resistance factors. Furthermore, an advanced Monte-Carlo method employed by Allen (2005) produced factors similar to the FOSM. Thus, it is justifiable to use the less sophisticated FOSM method to determine the resistance factors for dynamic analysis methods.

Kim (2002) stated that the application of the FOSM method requires both the load (Q) and resistance (R) to be lognormally distributed and mutually independent. With the focus on the axial pile resistance, the AASHTO (2007) Strength I load combination (i.e., dead and live loads only) was considered here. Nowak (1999) observed the lognormal distribution better characterizes the loads and suggested the numerical values for the different probabilistic characteristics of dead ($Q_D$) and live ($Q_L$) loads ($\gamma$, $\lambda$, and COV), as recapitulated in parentheses given in Eq. (6.4). To verify that the pile resistance follows a lognormal distribution, a hypothesis test, based on Anderson-Darling (AD) (1952) normality method, was used to assess the Goodness of Fitting of the assumed lognormal distributions. The reason for selecting the Anderson-Darling method is because it is one of the best normality tests for a database with a relative small sample size (Romeu, 2010). Since the AD values calculated using Eq. (6.2) are smaller than the respective critical values (CV) determined using Eq. (6.3), Figure 6.1, 6.2, 6.3, and 6.4 show that all resistances follow the lognormal characteristics, except the resistance estimated using CAPWAP for all soil conditions shown in Figure 6.4 (AD = 1.173 > CV = 0.685).

$$\mathrm{AD} = \sum_{i=1}^{N} \frac{1-2i}{N} \{\ln(F_o[Z_i]) + \ln(1 - F_o[Z_{N+1-i}])\} - N \qquad (6.2)$$

$$CV = \frac{0.752}{1 + \frac{0.75}{N} + \frac{2.25}{N^2}} \tag{6.3}$$

where,

$F_o[Z_i]$ = the cumulative density function of Z at i data = Pr ($Z \leq z_i$),

Pr ( ) = probability function,

Z = standardized normal distribution of expected resistance bias $\lambda_R$ or $\ln(\lambda_R)$,

$z_i$ = standardized normal distribution of estimated resistance bias $\lambda_R$ or $\ln(\lambda_R)$ = $\frac{R_i - \mu_R}{\sigma_R}$ or $\frac{\ln(R_i) - \mu_{\ln(R)}}{\sigma_{\ln(R)}}$,

$\lambda_R$ = resistance bias, a ratio of estimated and measured pile resistances, and

N = sample size.

The normality test revealed the necessity of categorizing the sites into three soil profiles, because the case with all soil conditions increased the uncertainties and deviated from the typical characteristic of a lognormal distribution. The hypothesis test generally confirms the assumed lognormal distribution for the resistances. In addition, Nowak (1999) concluded that load and resistance are mutually independent. Therefore, the resistance factors were determined using the FOSM closed-form equation given by

$$\varphi = \frac{\lambda_R \left(\frac{\gamma_D Q_D}{Q_L} + \gamma_L\right) \sqrt{\left[\frac{(1+COV_D^2+COV_L^2)}{(1+COV_R^2)}\right]}}{\left(\frac{\lambda_D Q_D}{Q_L} + \lambda_L\right) e^{\left\{\beta_T \sqrt{\ln[(1+COV_R^2)(1+COV_D^2+COV_L^2)]}\right\}}} \tag{6.4}$$

where,

$\lambda_R$ = the resistance bias factor of the resistance ratio,

$COV_R$ = the coefficient of variation of the resistance ratio,

$\gamma_D$, $\gamma_L$ = the dead load factor (1.25) and live load factor (1.75),

$\lambda_D$, $\lambda_L$ = the dead load bias (1.05) and live load bias (1.15),

$COV_D$, $COV_L$ = the coefficients of variation of dead load (0.1) and live load (0.2),

$\beta_T$ = target reliability index, and

$Q_D/Q_L$ = dead to live load ratio.

The LRFD resistance factors calibration requires a proper selection of a set of target reliability levels represented by target reliability indices ($\beta_T$), which describe the probability of failures ($P_f$). According to Barker et al. (1991), the target reliability index for driven piles can be reduced to a value between 2.0 and 2.5, especially for a group system effect. The initial target reliability indices used by Paikowsky et al. (2004) was between 2 and 2.5 for a pile group, and as high as 3.0 for a single pile. After following the reviews, Paikowsky et al. (2004) recommended target reliability indices of 2.33 (corresponding to 1% probability of failure) and 3.00 (corresponding to 0.1% probability of failure) for representing redundant and non-redundant pile groups, respectively. To maintain consistency, the recommended $\beta_T$ values were selected for this study.

Based on the AASHTO (2003) Specifications, the following dead to live load ratios ($Q_D/Q_L$) of 0.52, 1.06, 1.58, 2.12, 2.64, 3.00, and 3.53 were suggested for span lengths of 9, 18, 27, 36, 45, 50, and 60 m (30, 59, 89, 148, 164, and 197 ft), respectively. Paikowsky et al. (2004) used a $Q_D/Q_L$ ratio ranging from 2.0 to 2.5, while Allen (2005) used a conservative ratio of 3.0. Due to the frequent use of short span bridges in the State of Iowa, the Iowa DOT used a $Q_D/Q_L$ ratio of 1.5. However, Paikowsky et al. (2004) concluded that resistance factors are insensitive to the choice of a $Q_D/Q_L$ ratio. To strike a balance between two extremes (0.52 for 9 m and 3.53 for 60 m bridge spans), an average $Q_D/Q_L$ ratio of 2.0 was selected for this study.

The foregoing FOSM method is appropriately used for calculating a resistance factor for a pile resistance (R) defined as a single random variable (i.e., the pile resistance is determined from a single procedure or method). However, the incorporation of pile setup in the LRFD requires a new calibration procedure that can separately and simultaneously account for the different uncertainties associated with the initial pile resistance at EOD ($R_{EOD}$), and for the pile setup resistance ($R_{setup}$) to reach a same target reliability level. The different uncertainties arise from the different procedures engaged in estimating the two resistance components ($R_{EOD}$ is estimated using the dynamic analysis method, and $R_{setup}$ is estimated using the proposed setup equation described in Chapter 4). This new calibration

procedure has been described in Chapter 5, and the LRFD framework considering that the pile setup has been revised to Eq. (6.5) by multiplying different resistance factors $\varphi_{EOD}$ and $\varphi_{setup}$ to $R_{EOD}$ and $R_{setup}$, respectively.

$$\sum \gamma_i Q_i \leq \varphi_{EOD} R_{EOD} + \varphi_{setup} R_{setup} \tag{6.5}$$

The $\varphi_{EOD}$ value was determined using the FOSM Eq. (6.4), and the $\varphi_{setup}$ value was determined using the proposed Eq. (6.6) derived in Chapter 5. To ensure consistency, the same probabilistic characteristics ($\gamma$, $\lambda$, COV) of the loads recommended by Nowak (1999) as recapitulated in Eq. (6.4), the $Q_D/Q_L$ ratio of 2.0, and both $\beta_T$ values of 2.33 and 3.00 were selected. The calculated probabilistic characteristics ($\lambda$, COV) and the $\varphi_{EOD}$ value were used in Eq. (6.6). A conservative $\alpha$ value, a ratio of initial pile resistance at EOD, and a total applied load of 1.60 were chosen for this study.

$$\varphi_{setup} = \frac{\lambda_{setup}\left[\frac{\gamma_D\left(\frac{Q_D}{Q_L}\right)+\gamma_L}{1+\left(\frac{Q_D}{Q_L}\right)} - \varphi_{EOD}\alpha\right]}{\left(\frac{\lambda_D\left(\frac{Q_D}{Q_L}\right)+\lambda_L}{1+\left(\frac{Q_D}{Q_L}\right)}\right) e^{\beta_T\sqrt{\ln\left[\left(1+COV_{R_{EOD}}^2+COV_{R_{setup}}^2\right)\left(1+COV_{Q_D}^2+COV_{Q_L}^2\right)\right]}}} - \lambda_{EOD}\alpha \tag{6.6}$$
$$\sqrt{\frac{\left(1+COV_{Q_D}^2+COV_{Q_L}^2\right)}{\left(1+COV_{R_{EOD}}^2+COV_{R_{setup}}^2\right)}}$$

### 6.4.4. Resistance factors

Figure 6.1 shows five lognormally distributed cumulative density function (CDF) plots of various resistance ratios (RRs), based on the five soil input procedures (ST, SA, Iowa Blue Book, Iowa DOT and DRIVEN) used in WEAP for the sand profile. Figure 6.2 and Figure 6.3 show similar plots of RRs for WEAP in clay and mixed soil profiles, respectively, and Figure 6.4 shows the plots of RRs for CAPWAP. The resistance ratio (RR) is generally defined as a ratio of the measured pile resistance obtained from SLT and the estimated pile resistance as tabulated in Table 6.1, Table 6.2, Table 6.3, or Table 6.4. The detailed descriptions of various RRs for the three soil profiles are provided as follows:

a. For sand and mixed soil profiles

1. RR for EOD is a ratio of SLT measured pile resistance at any time (t) and the estimated pile resistance determined at the EOD condition, using either WEAP or CAPWAP (see Table 6.1 and Table 6.2).

b. For clay profile

1. RR for EOD is a ratio of SLT measured pile resistance adjusted from time (t) to the EOD condition (see Table 6.4) using the proposed SPT-based setup Eq. (6.7) to the estimated pile resistance determined at the EOD condition using either WEAP or CAPWAP (see Table 6.1 and Table 6.2). Equation (6.7) was similarly developed using the same procedure and validated using the same data points as outlined in Chapter 4 for SPT and CPT-based setup equation. The detailed description of this SPT-based setup method was included in Ng et al. (2011).

$$R_{EOD} = \frac{R_t}{\left[\frac{a \log_{10}\left(\frac{t}{t_{EOD}}\right)}{(N_a)^b} + 1\right]\left(\frac{L}{L_{EOD}}\right)} \tag{6.7}$$

where,

$R_{EOD}$ = pile resistance at the end of driving condition,
$R_t$ = pile resistance at time t,
a = empirical scale factor (see Table 6.5),
b = empirical concave factor (see Table 6.5),
$N_a$ = weighted average SPT N-value,
$L_{EOD}$ = embedded pile length at the end of driving condition, and
L = embedded pile length at time t.

2. RR for BOR is a ratio of SLT measured pile resistance at any time (t) and estimated pile resistance determined from the beginning of last restrike test, using either WEAP or CAPWAP (see Table 6.3).

3. RR for setup is a ratio of measured pile setup resistance and estimated pile setup resistance as listed in Table 6.4. The measured pile setup resistance is the difference between SLT measured pile resistance at any time (t) and the pile resistance at the EOD condition estimated, using either WEAP or CAPWAP. The estimated pile setup resistance was determined using the proposed SPT-based setup equation.

Because the CDF plots shown in Figure 6.1, 6.2, 6.3, and 6.4 were lognormally distributed, the mean and standard deviation were represented with "Loc" and "Scale", respectively. To implement Eqs. (6.4) and (6.6), the normally distributed resistance bias ($\lambda_R$) was back-calculated using Eq. (6.8), and the normally distributed coefficient of variation ($COV_R$) was back-calculated using Eq. (6.9).

$$\lambda_R = e^{[Loc+0.5\ln(1+COV_R^2)]} \tag{6.8}$$

$$COV_R = \sqrt{\left(e^{Scale^2}-1\right)} \tag{6.9}$$

Using these probabilistic characteristics of resistances ($\lambda_R$ and $COV_R$), the regional resistance factors were calculated and are given in Table 6.6 and Table 6.7 for WEAP and CAPWAP, respectively. Table 6.6 shows that the resistance factors for the same soil profile and resistance condition (EOD, BOR, or setup) are similar, which concludes the insensitivity of different soil input procedures and the validity of the 70%-rule used in classifying the soil profile. However, the soil input procedure with the highest resistance factor does not necessarily provide the most efficient and economic pile design, since different procedures provide different nominal pile resistance estimations. For instance, in the clay profile and at the EOD condition, the DRIVEN procedure has the highest φ value of 0.66 when compared with 0.65 for the Iowa Blue Book method. Using the estimated nominal pile resistances of ISU6 (601 kN for DRIVEN and 624 kN for the Iowa Blue Book) as listed in Table 6.2, the factored pile resistance ($\varphi R_{EOD}$) for DRIVEN becomes 397 kN, which is smaller than 405 kN

for the Iowa Blue Book. To evaluate the efficiency of different procedures relative to the measured pile performance, efficiency factors ($\varphi/\lambda$) are calculated. A higher $\varphi/\lambda$ value correlates to a better economic pile design. Procedures with the highest $\varphi/\lambda$ values are boldly highlighted in Table 6.6. The results show no unique procedure has the best efficiency among various soil and resistance conditions. For ease of practical applications and due to the minimal difference in the $\varphi/\lambda$ values, a single procedure is recommended in Section 6.6 for WEAP analysis. Nevertheless, the regionally-calibrated $\varphi$ and $\varphi/\lambda$ values are higher than those recommended in the NCHRP Report 507 (Paikowsky et al., 2004), based on a general national database that may not reflect the local soil conditions and construction practices. Similarly, the $\varphi$ values have been improved based on the regional database, comparing with the latest AASHTO (2010) recommendations.

Table 6.7 shows the regionally-calibrated results for CAPWAP. When compared with the results for WEAP given in Table 6.6, CAPWAP provides better pile resistance estimations relative to the measured pile resistances, indicated by $\lambda_R$ values closer to unity and smaller $COV_R$ values. Thus, higher $\varphi$ and $\varphi/\lambda$ values are calculated for CAPWAP. Similar to WEAP, the regionally-calibrated results are higher than those of the NCHRP Report 507 (Paikowsky et al., 2004) and the latest AASHTO (2010) recommendations. Overall, the calibrated results have been improved based on the regional database.

Furthermore, the effect of pile setup in clay profile was incorporated in the LRFD by computing the $\varphi_{setup}$ values for the proposed SPT-based setup equation, based on the Iowa Blue Book and Iowa DOT procedures for WEAP in Table 6.6 and CAPWAP in Table 6.7. Due to a higher uncertainty involved in estimating the pile setup resistance (higher $COV_R$) and the selection of a conservative $\alpha$ value of 1.60, smaller $\varphi_{setup}$ values (0.21 for WEAP-Iowa Blue Book, 0.26 for WEAP-Iowa DOT, and 0.37 for CAPWAP based on $\beta_T$=2.33) were determined using Eq. (5.13). However, it is believed that the $\varphi_{setup}$ values can be increased in the future by using more quality pile setup data, continuous improvement of the SPT-based setup equation to increase accuracy of the pile setup estimations, and elevate confidence level by selecting a smaller $\alpha$ value (smaller $R_{EOD}$ relative to total loads).

## 6.5. Construction Control Considerations

### 6.5.1. Introduction

Construction control involves procedures or methods for nondestructive verification of designed pile resistances during pile driving. The Iowa DOT currently uses the Iowa Blue Book (originally written by Dirks and Kam, 1989) method to design piles and uses either WEAP or CAPWAP as a construction control method to verify the designed pile resistance during construction. If the desired pile resistance is not attained during construction, pile driving specifications will be adjusted accordingly, such as increasing pile length. The adjustment may increase construction costs, delay construction schedule, and cause contractual challenges. The construction control method is also used to detect any pile damage and to check pile integrity. To improve the accuracy of pile resistance and cost estimations during the design stage and to ensure an adequate pile performance, the construction control method using either WEAP or CAPWAP is integrated as part of the design procedure. To ensure consistent and practical pile designs, the Iowa Blue Book soil input procedure used in WEAP was selected for the following construction control evaluations and analyses. Databases from both PILOT and the recently completed field tests were selected for WEAP, while only the field tests were used for the CAPWAP evaluation. The total data points for WEAP in the clay, mixed, and sand profiles were 17, 12, and 13, respectively, and the total data points for CAPWAP in the clay, mixed, and sand profiles were 5, 2, and 2, respectively. The construction control evaluations were performed for three resistance conditions—EOD, setup, and BOR. Referring to Table 6.8 for the construction control method using WEAP, construction control evaluations for EOD were performed for all three soil profiles, while evaluation for setup was only applied to clay. On the other hand, construction control evaluations for all three resistance conditions were performed for clay, and an evaluation for only BOR was applied to sand and mixed soil profiles.

### 6.5.2. Methodology

Construction control was accounted for by multiplying a construction control factor ($\xi$) for the respective resistance condition to the original resistance factor ($\varphi$) of the Blue

Book method computed by AbdelSalam et al. (2010) as listed in Table 6.8. Adopting the suggestion given by Paikowsky et al. (2004) for other affecting factors, the LRFD framework for the construction control consideration can be expressed as:

$$\sum \gamma_i Q_i \leq \Pi \xi_i \varphi R \tag{6.10}$$

The product of construction control factors ($\Pi\xi_i$) can be expressed specifically for various resistance conditions as follows:

1. EOD condition: $\Pi\xi_i = \xi_{EOD}$,
2. EOD condition including setup in clay: $\Pi\xi_i = \xi_{EOD} \times \xi_{setup}$, or
3. BOR condition: $\Pi\xi_i = \xi_{BOR,}$

where,

$\gamma_i$ = load factor,

$Q_i$ = applied load,

$\Pi\xi_i$ = product of all applicable construction control factors,

$\varphi$ = originally developed resistance factor for Iowa Blue Book,

R = nominal pile resistance estimated using Iowa Blue Book,

$\xi_{EOD}$ = construction control factor at the end of driving condition,

$\xi_{setup}$ = construction control factor for considering pile setup, and

$\xi_{BOR}$ = construction control factor for beginning of restrike condition.

The construction control factors were determined using a probabilistic approach. This probabilistic approach relies on a cumulative distribution curve of a ratio of the factored pile resistance predicted using either WEAP or CAPWAP to that estimated using the Iowa Blue Book method as shown in Figure 6.5 and Figure 6.6, respectively. The cumulative percent on the y-axis indicates the chance at which the factored pile resistance predicted using the selected construction control method is less than that estimated using the Iowa Blue Book. The blue straight line represents the theoretical, cumulative, normal distribution of the factored resistance ratios (i.e., the red data points), and the variation in the red data points along the theoretical straight line indicates the data are not a perfect normal distribution. The

two blue curved lines represent the 95% confidence interval of the theoretical normal distribution. Figure 6.5 and Figure 6.6 show all data points fall within the 95% confidence interval. Thus, the theoretical normal distribution line can be confidently used to determine the factored resistance ratio at the corresponding desired cumulative percent. To minimize the average discrepancy in the factored pile resistances estimated using any construction control method and the Iowa Blue Book, a 50% cumulative value is used as similarly suggested by Long et al. (2009) in improving the agreement between estimated and actual field driven pile lengths for the Illinois DOT. The factored resistance ratio on the x-axis corresponding to the recommended 50% cumulative value is referred to as the construction control factor ($\xi$). The construction control factors are tabulated in Table 6.8 for various soil and resistance conditions.

After applying the desired construction control factors to the originally calculated factored resistance ($\varphi R$) estimated using the Iowa Blue Book, it is believed that the modified factored resistance ($\Pi\xi_i\varphi R$) remains smaller than the factored resistance determined from a static load test ($\varphi_{SLT}R_{SLT}$). This is believed to be due to the resistance factors for the construction control methods being calibrated from the measured pile resistance ($R_{SLT}$), which is the same value used in calibrating the resistance factor for the Iowa Blue Book. Although this reason seemingly convinces the adequacy of the aforementioned construction control methodology, the target reliability index ($\beta_T$) reduces with the potential increase in the modified resistance factors ($\Pi\xi_i\varphi$), as illustrated using the rearranged FOSM relationship given by Eq. (6.11).

$$\beta_T = \frac{\ln\left[\lambda_R\left(\frac{\gamma_D Q_D}{Q_L}+\gamma_L\right)\sqrt{\frac{(1+COV_D^2+COV_L^2)}{(1+COV_R^2)}}\right]-\ln\left[\frac{\lambda_D Q_D}{Q_L}+\lambda_L\right]-\ln\left[\Pi\xi_i\varphi\right]}{\sqrt{\ln[(1+COV_R^2)(1+COV_D^2+COV_L^2)]}} \tag{6.11}$$

The reduction in the $\beta_T$ value increases the probability of failure, and therefore, it is necessary to set a maximum limit on the construction control factor ($\Pi\xi_i$) or on the modified resistance factor ($\Pi\xi_i\varphi$). The maximum construction factor was established, so the resulting

modified resistance factor ($\Pi\xi_i\varphi$) does not exceed the resistance factor of 0.80 (see Table 6.8), as recommended by AASHTO (2010) for an SLT ($\varphi_{SLT}$).

For an illustrative purpose, Figure 6.7 shows the primary relationship between the factored pile resistances estimated using WEAP and the Iowa Blue Book (on the left y-axis) for a mixed soil profile together with the construction control correction factor ($\xi_{EOD}$) on the x-axis. A construction control factor ($\xi_{EOD}$) of 1.07 and a modified resistance factor ($\xi_{EOD}\varphi$) of 0.64 as similarly found in Figure 6.5 were confirmed by equating the primary factored resistance ratio (left y-axis) to one. Figure 6.7 also shows the secondary relationship (on the right y-axis) between the factored pile resistances measured using SLT and estimated using the Iowa Blue Book considering the construction control correction factor ($\xi_{EOD}$) on the x-axis. The maximum limits for $\xi_{EOD}$ and modified resistance factor ($\xi_{EOD}\varphi$) are determined 1.90 and 1.14, respectively, by equating the secondary factored resistance ratio (right y-axis) to one. Since the initially calculated $\xi_{EOD}$ value of 1.07 is smaller than the maximum limit of 1.90 or the recommended $\xi_{EOD}\varphi$ of 0.64 is smaller than the calculated maximum limit of 1.14 as well as 0.80, based on AASHTO (2010), the $\xi_{EOD}$ value of 1.07 is suggested in Table 6.8. Figure 6.8 shows the normal distribution curves of the factored resistances ratio for WEAP and the Iowa Blue Book (i.e., $\varphi_{weap}R_{weap}/\varphi_{BB}R_{BB}$) before and after considering the construction control. The effect of construction control consideration shifts the mean towards unity and reduces the standard of deviation from 0.27 to 0.25, which indicates that the average pile resistances estimated using WEAP and the Iowa Blue Book has been matched, minimizing the overall discrepency between design and field verified pile resistances.

### 6.5.3. Construction control results

Table 6.8 summarized the results obtained from the foregoing construction control evaluations. If WEAP is specified as the construction control method during pile driving, the calculated construction controls for clay and sand are 0.87 and 0.94, respectively. In other words, the average factored pile resistances estimated using WEAP are smaller than those using the Iowa Blue Book. The Iowa Blue Book's value may have to be reduced to match

with WEAP's. However, considering the economic advantages and the original efficiency of the Iowa Blue Book method, a construction control factor of 1.00 was suggested (i.e., the construction control consideration was neglected for clay and sand soil profiles). On the other hand, in the case with a mixed soil profile, the construction control consideration using WEAP has increased the original φ value of the Iowa Blue Book from 0.60 to 0.64 or improved the φ value by 7%.

Similarly, Table 6.8 shows the construction control method using CAPWAP has increased the original φ values of the Iowa Blue Book for all three soil profiles. The reasons are attributed to the accuracy of the CAPWAP method and the performance of restrike tests, which enhance the verification of pile resistances. In particular, construction control using CAPWAP increases the original φ value of the Iowa Blue Book for the clay profile from 0.60 to 0.68 (or improved by 8%), considering both the EOD and setup resistance conditions. In addition, the construction control method using CAPWAP, based on the restrike condition, improves the φ values for clay, mixed soil, and sand profiles by 27%, 18%, and 6%, respectively. It is important to highlight the construction control of 1.27 instead of 1.38 for clay was suggested to limit the modified φ value to 0.80.

## 6.6. Recommendations

The recommended resistance factors of the Iowa Blue Book with WEAP and CAPWAP as construction control methods, for a reliability index of 2.33 (redundant pile group) were summarized in Table 6.9. To maintain a consistency between pile designs and constructions, the Iowa Blue Book soil input procedure was selected among the other procedures (i.e., ST, SA, DRIVEN and Iowa DOT procedures) for WEAP. The modified resistance factors for the Iowa Blue Book listed in Table 6.8 were transferred to Table 6.9 under the "Design" stage. Under the "Construction" stage, the resistance factors of WEAP listed in Table 6.6 as well as resistance factors of CAPWAP listed in Table 6.7 were recommended in Table 6.9. Compared with the AASHTO (2010) recommendations, these regionally-calibrated resistance factors have been improved, based on the local Iowa database.

Furthermore, these LRFD recommendations account for the effect of pile setup in clay. Different resistance factors ($\varphi_{EOD}$ and $\varphi_{setup}$) have been separately developed for the initial pile resistance at EOD ($R_{EOD}$) estimated using either WEAP or CAPWAP, and the pile setup resistance ($R_{setup}$) estimated using the proposed SPT-based setup equation. The application of these resistance factors follows the revised LRFD framework given by Eq. (6.5).

## 6.7. Summary and Conclusions

The paper presents the successful establishment of regional Load and Resistance Factor Design (LRFD) recommendations for bridge pile designs in the State of Iowa, based on a historical database and 10 recently completed field tests. When compared with the recommendations presented in the NCHRP Report 507 by Paikowsky et al. (2004) and the latest AASHTO (2010) LRFD Bridge Design Specifications, the regionally-calibrated resistance factors calculated using the FOSM method for both WEAP and CAPWAP approaches were improved in all soil profiles. For the WEAP approach considering the EOD condition, the regionally-calibrated resistance factors were 0.55, 0.65, and 0.83 for the sand, clay, and mixed soil profile, respectively, which were higher than the AASHTO's recommended value of 0.50. For the CAPWAP approach considering the BOR condition, the regionally-calibrated resistance factors were 0.77, 0.80, and 0.93 for the sand, clay, and mixed soil profile, respectively, which were all higher than the ASSHTO's recommended value of 0.75.

A construction control procedure was established to enhance pile resistance estimations during design. Construction control factors were calculated using a proposed probabilistic approach. These factors were multiplied to the resistance factors of the Iowa Blue Book to minimize the discrepancy between design and field pile resistances and to integrate WEAP and CAPWAP as construction control methods as part of the design process. The construction control consideration increases the originally-calibrated resistance factors for Iowa Blue Book method by as high as 27%.

Furthermore, the procedure of incorporating pile setup into the LRFD framework as described in Chapter 5 was employed to determine different resistance factors ($\varphi_{EOD}$ and $\varphi_{setup}$) for the initial pile resistance at EOD ($R_{EOD}$) estimated using either WEAP or CAPWAP, and the pile setup resistance ($R_{setup}$) estimated using the proposed SPT-based setup equation. The consideration of pile setup in LRFD further elevates the efficiency of bridge foundations attaining the economic advantages of a pile setup. Due to the tremendous benefits of the proposed LRFD recommendations, the results presented in this paper will be adopted by the Iowa DOT as part of the bridge foundation design guidelines.

## 6.8. Acknowledgments

The authors would like to thank the Iowa Highway Research Board for sponsoring the research presented in this paper. We would like to thank the members of the Technical Advisory Committee: Ahmad Abu-Hawash, Bob Stanley, Curtis Monk, Dean Bierwagen, Gary Novey, John Rasmussen, Ken Dunker, Kyle Frame, Lyle Brehm, Michael Nop, and Steve Megivern of this research project for their guidance. Special thanks are due to Sherif S. AbdelSalam, Matthew Roling, and Douglas Wood for their assistance with the field tests and to Donald Davidson and Erica Velasco for their assistance with the laboratory soil tests.

## 6.9. References

American Association of State Highway and Transportation Officials. (AASHTO). (2001). LRFD Bridge Design Specifications. Washington, D.C.

American Association of State Highway and Transportation Officials. (AASHTO). (2003) LRFD Bridge Design Specifications. Customary U.S. Units, 2nd Edition, Washington, D.C.

American Association of State Highway and Transportation Officials. (AASHTO). (2007) LRFD Bridge Design Specifications. Customary U.S. Units, 4th Edition, 2008 Interim, Washington, D.C.

American Association of State Highway and Transportation Officials. (AASHTO). (2010) LRFD Bridge Design Specifications. Customary U.S. Units, 5th Edition, 2010 Interim

Revisions, Washington, D.C.

AbdelSalam, S., Sritharan, S., Suleiman, M. T., Ng, K. W., & Roling, M. J. (2010). Development of LRFD Procedures for Bridge Pile Foundations In Iowa - Volume III: Recommended Resistance Factors with Consideration to Construction Control and Setup. Institute of Transportation, Iowa State Univeristy, Ames, IA.

AbdelSalam, S., Sritharan, Sri, and Suleiman, T. M. (2011). "LRFD Resistance Factors for Design of Driven H-Piles in Layered Soils." Journal of Bridge Engineering, ASCE. (under review).

Allen, T. M. (2005). Development of the WSDOT Pile Driving Formula and Its LRFD Calibration. FHWA Report, Washington State DOT, WA.

Anderson, T. W., and Darling, D. A. (1952). "Asymptotic Theory of Certain "Goodness-of-Fit" Criteria Based on Stochastic Processes." Annals of Mathematical Statistics, 23, pp. 193-212.

Barker, R., Duncan, J., Rojiani, K., Ooi, P., Tan, C., and Kim, S. (1991). NCHRP Report 343: Manuals for the Design of Bridge Foundations. Transportation Research Board,Washington, D.C.

Davisson, M. (1972). "High Capacity Piles." Soil Mechanics Lecture Series on Innovations in Foundation Construction, ASCE, Chicago, IL, pp. 81-112.

Dirks, K. and Kam, P. (1989). Foundation Soils Information Chart. Iowa Department of Transportation, Office of Road Design, Ames, IA.

Kim, Kyung Jun. (2002). Development of Resistance Factors for Axial Capacity of Driven Piles in North Carolina. PhD Dissertation submitted to the Graduate Faculty of North Carolina State University. 272 pp.

Long, James H., Hendrix, Joshua, and Baratta, Alma. (2009). Evaluation/Modification of IDOT Foundation Piling Design and Construction Policy. Research Report FHWA-ICT-09-037, Illinois Center for Transportation, University of Illinois at Urbana-Champaign, IL, March.

Ng, K. W., Suleiman, M. T., Sritharan, S., Roling, M., and AbdelSalam, S. S. (2011). Development of LRFD Design Procedures for Bridge Piles in Iowa: SoilInvestigation and Full-Scaled Pile Tests. Final Report Vol. II. IHRB Project No.TR-573. Institute

of Transportation, Iowa State Univeristy, Ames, IA.

Nowak, A. (1999). NCHRP Report 368: Calibration of LRFD Bridge Design Code. Transportation Research Board, Washington, D.C.

Paikowsky, S.G. with Contributions from Birgisson from Birgisson, B., McVay, M., Nguyen, T., Kuo, C., Baecher, G., Ayyab, B., Stenersen, K., O'Malley, K., Chernauskas, L., and O'Neill, M. (2004). Load and Resistance Factor Design (LRFD) for Deep Foundations, NCHRP Report 507, Transportation Research Board, Washington, D.C.

Romeu, J. L. (2010). Anderson-Darling: A Goodness of Fit Test for Small Samples Assumptions. START 2003-5, Vol. 10, Number 5, Reliability Analysis Center, Rome, NY, (http:www.theriac.org/riacapps/startsheets/?category=Reliability).

Roling, M., Sritharan, S., and Suleiman, M. T. (2010). Development of LRFD design procedures for bridge piles in Iowa – Electronic Database. Final Report Vol. I, Project No. TR-573, Institute of Transportation, Iowa State University, Ames, IA.

Table 6.1: Summary of data records for three soil profiles from PILOT

| Soil profile | ID | Iowa County | Pile type | Hammer type | Time of SLT (day) | SLT measured Davisson's pile resistance (kN) | Hammer blow count (bl/300mm) | Estimated pile resistance at EOD using WEAP (kN) | | | | |
|---|---|---|---|---|---|---|---|---|---|---|---|---|
| | | | | | | | | ST | SA | Iowa Blue Book | Iowa DOT | DRIVEN |
| Sand | 10 | Ida | HP 250×63 | Gravity | 2 | 516 | 5 | 272 | 305 | 284 | 237 | 327 |
| | 34 | Dubuque | HP 250×63 | Delmag D-12 | 7 | 996 | 37 | 703 | 711 | 688 | 642 | 705 |
| | 48 | Black Hawk | HP 250×63 | Gravity | 5 | 641 | 10 | 621 | 621 | 578 | 539 | 619 |
| | 17 | Fremont | HP 250×63 | Gravity | 5 | 587 | 13 | 913 | 848 | 973 | 812 | 1092 |
| | 20 | Muscatine | HP 250×63 | Kobe K-13 | 5 | 534 | 40 | 811 | 821 | 770 | 713 | 828 |
| | 24 | Harrison | HP 250×63 | Gravity | 9 | 818 | 23 | 1073 | 1057 | 1108 | 1147 | 1439 |
| | 70 | Mills | HP 250×63 | Delmag D-12 | 5 | 569 | 30 | 613 | 621 | 622 | 568 | 665 |
| | 74 | Benton | HP 250×63 | Kobe k-13 | 32 | 667 | 34 | 634 | 602 | 617 | 633 | 786 |
| | 99 | Wright | HP 250×63 | Gravity | 7 | 463 | 7 | 429 | 395 | 411 | 443 | 513 |
| | 158 | Dubuque | HP 360×132 | Kobe K-42 | 4 | 2589 | 60 | 3154 | 3225 | 2961 | 2716 | 3241 |
| | 151 | Pottawattamie | HP 250×63 | Delmag D-22 | 4 | 890 | 11 | 590 | 595 | 604 | 501 | 597 |
| Clay | 6 | Decatur | HP 250×63 | Gravity | 3 | 525 | 8 | 628 | 323 | 314 | 366 | 307 |
| | 12 | Linn | HP 250×63 | Kobe K-13 | 5 | 907 | 46 | 564 | 679 | 689 | 755 | 684 |
| | 42 | Linn | HP 250×63 | Kobe K-13 | 5 | 365 | 19 | 409 | 375 | 378 | 411 | 359 |
| | 44 | Linn | HP 250×63 | Delmag D-22 | 5 | 605 | 24 | 641 | 410 | 418 | 496 | 400 |
| | 51 | Johnson | HP 250×63 | Kobe K-13 | 3 | 845 | 36 | 716 | 562 | 570 | 624 | 560 |
| | 57 | Hamilton | HP 250×63 | Gravity | 4 | 747 | 11 | 503 | 405 | 416 | 493 | 411 |
| | 62 | Kossuth | HP 250×63 | MKT DE-30B | 5 | 445 | 21 | 716 | 335 | 336 | 367 | 325 |
| | 63 | Jasper | HP 250×63 | Gravity | 2 | 294 | 13 | 499 | 265 | 263 | 400 | 267 |
| | 64 | Jasper | HP 250×63 | Gravity | 1 | 543 | 15 | 556 | 320 | 315 | 394 | 321 |
| | 67 | Audubon | HP 250×63 | Delmag D-12 | 4 | 623 | 24 | 567 | 542 | 536 | 618 | 544 |
| | 102 | Poweshiek | HP 250×63 | Gravity | 8 | 578 | 13 | 550 | 372 | 375 | 433 | 347 |
| | 109 | Poweshiek | HP 310×79 | Delmag D-12 | 3 | 783 | 48 | 1440 | 673 | 653 | 817 | 674 |

Table 6.1: (continue)

| Soil profile | ID | Iowa County | Pile type | Hammer type | Time of SLT (day) | SLT measured Davisson's pile resistance (kN) | Hammer blow count (bl/300mm) | Estimated pile resistance at EOD using WEAP (kN) | | | | |
|---|---|---|---|---|---|---|---|---|---|---|---|---|
| | | | | | | | | ST | SA | Iowa Blue Book | Iowa DOT | DRIVEN |
| Mixed | 7 | Cherokee | HP 250×63 | Gravity | 6 | 783 | 11 | 389 | 393 | 371 | 471 | 383 |
| | 8 | Linn | HP 250×63 | Kobe K-13 | 8 | 756 | 34 | 630 | 575 | 589 | 640 | 542 |
| | 25 | Harrison | HP 250×63 | Delmag D-12 | 4 | 996 | 36 | 676 | 642 | 653 | 645 | 732 |
| | 43 | Linn | HP 250×63 | Delmag D-22 | 5 | 632 | 22 | 619 | 627 | 625 | 742 | 619 |
| | 46 | Iowa | HP 250×63 | Gravity | 4 | 730 | 11 | 647 | 657 | 635 | 584 | 430 |
| | 66 | Black Hawk | HP 250×63 | Mit M14S | 5 | 801 | 32 | 478 | 514 | 478 | 535 | 724 |
| | 73 | Johnson | HP 250×63 | Kobe K-13 | 6 | 1032 | 30 | 733 | 735 | 678 | 572 | 727 |
| | 90 | Black Hawk | HP 310×79 | Gravity | 4 | 845 | 26 | 940 | 873 | 925 | 868 | 946 |
| | 106 | Pottawattamie | HP 250×63 | Gravity | 6 | 658 | 7 | 316 | 280 | 271 | 334 | 252 |

Table 6.2: Summary of pile records from field tests at EOD

| Test pile ID | Soil profile | Iowa County | Pile type | Time of SLT, *t* (day) | SLT measured Davisson's pile resistance at time *t* (kN) | Estimated pile resistance at EOD using WEAP (kN) | | | | | CAPWAP at EOD (kN) |
|---|---|---|---|---|---|---|---|---|---|---|---|
| | | | | | | ST | SA | Iowa Blue Book | Iowa DOT | DRIVEN | |
| ISU1 | Mixed | Mahaska | HP 250×85 | 100 | 881 | 476 | 453 | 473 | 520 | 582 | 631 |
| ISU2 | Clay | Mills | HP 250×63 | 9 | 556 | 344 | 343 | 343 | 423 | 347 | 359 |
| ISU3 | Clay | Polk | HP 250×63 | 36 | 667 | 363 | 363 | 366 | 411 | 363 | 440 |
| ISU4 | Clay | Jasper | HP 250×63 | 16 | 685 | 437 | 422 | 422 | 509 | 422 | 453 |
| ISU5 | Clay | Clarke | HP 250×63 | 9 | 1081 | 639 | 636 | 635 | 737 | 632 | 790 |
| ISU6 | Clay | Buchanan | HP 250×63 | 14 | 946 | 599 | 615 | 624 | 728 | 601 | 644 |
| ISU7 | Mixed | Buchanan | HP 250×63 | 13 | 236 | 36 | 41 | 41 | 44 | 57 | 51 |
| ISU8 | Mixed | Poweshiek | HP 250×63 | 15 | 721 | 609 | 613 | 607 | 675 | 557 | 621 |
| ISU9 | Sand | Des Moines | HP 250×63 | 25 | 703 | 790 | 712 | 737 | 691 | 821 | 751 |
| ISU10 | Sand | Cedar | HP 250×63 | 6 | 565 | 685 | 708 | 685 | 638 | 719 | 538 |

Table 6.3: Summary of pile records from field tests from last restrike

| Test pile ID | Soil profile | Hammer type | Time at last restrike, *t* (day) | Estimated pile resistance from last restrike using WEAP (kN) | | | | | CAPWAP from last restrike (kN) |
|---|---|---|---|---|---|---|---|---|---|
| | | | | ST | SA | Iowa Blue Book | Iowa DOT | DRIVEN | |
| ISU1 | Mixed | Delmag D19-42 | Not available | | | | | | |
| ISU2 | Clay | Delmag D19-42 | 2.97 | 615 | 617 | 614 | 752 | 620 | 578 |
| ISU3 | Clay | Delmag D19-32 | 1.95 | 715 | 586 | 585 | 714 | 586 | 658 |
| ISU4 | Clay | Delmag D19-42 | 4.75 | 712 | 687 | 688 | 813 | 687 | 685 |
| ISU5 | Clay | Delmag D16-32 | 7.92 | 1160 | 1140 | 1138 | 1311 | 1123 | 1088 |
| ISU6 | Clay | Delmag D19-42 | 9.81 | 1089 | 1121 | 1122 | 1293 | 1101 | 937 |
| ISU7 | Mixed | Delmag D19-42 | 9.76 | 311 | 290 | 292 | 325 | 294 | 331 |
| ISU8 | Mixed | Delmag D19-42 | 4.95 | 815 | 815 | 811 | 899 | 756 | 710 |
| ISU9 | Sand | APE D19-42 | 9.77 | 715 | 649 | 667 | 619 | 739 | 688 |
| ISU10 | Sand | APE D19-42 | 4.64 | 599 | 614 | 593 | 547 | 629 | 526 |

Table 6.4: Summary of adjusted measured pile resistances at EOD and setup resistances for clay profile only

| Source of data | Test pile ID | Adjusted measured pile resistance using SLT at EOD (kN) | | | Measured pile setup resistance (kN) | | | Estimated pile setup resistance (kN) | | |
|---|---|---|---|---|---|---|---|---|---|---|
| | | WEAP-Iowa Blue Book | WEAP-Iowa DOT | CAPWAP | WEAP-Iowa Blue Book | WEAP-Iowa DOT | CAPWAP | WEAP-Iowa Blue Book | WEAP-Iowa DOT | CAPWAP |
| Field test | ISU2 | 316 | 308 | 320 | 316 | 308 | 197 | 242 | 316 | 245 |
| | ISU3 | 359 | 354 | 402 | 359 | 354 | 227 | 274 | 317 | 247 |
| | ISU4 | 396 | 393 | 452 | 396 | 393 | 232 | 285 | 351 | 212 |
| | ISU5 | 649 | 645 | 754 | 649 | 645 | 291 | 392 | 461 | 308 |
| | ISU6 | 561 | 560 | 668 | 561 | 560 | 302 | 394 | 462 | 238 |
| PILOT | 6 | 343 | 342 | - | 343 | 342 | - | 168 | 197 | - |
| | 12 | 602 | 607 | - | 602 | 607 | - | 351 | 429 | - |
| | 42 | 238 | 239 | - | 238 | 239 | - | 201 | 234 | - |
| | 44 | 395 | 397 | - | 395 | 397 | - | 222 | 259 | - |
| | 51 | 579 | 587 | - | 579 | 587 | - | 262 | 334 | - |
| | 57 | 472 | 468 | - | 472 | 468 | - | 243 | 278 | - |
| | 62 | 298 | 301 | - | 298 | 301 | - | 167 | 175 | - |
| | 63 | 190 | 187 | - | 190 | 187 | - | 144 | 227 | - |
| | 64 | 366 | 363 | - | 366 | 363 | - | 153 | 195 | - |
| | 67 | 408 | 410 | - | 408 | 410 | - | 282 | 343 | - |
| | 102 | 365 | 365 | - | 365 | 365 | - | 219 | 260 | - |
| | 109 | 516 | 516 | - | 516 | 516 | - | 339 | 439 | - |

Table 6.5: Summary of the empirical scale and concave factors

| Method | a | b |
|---|---|---|
| CAPWAP | 0.432 | 0.606 |
| WEAP-ST | 0.243 | 0.168 |
| WEAP-SA | 0.217 | 0.141 |
| WEAP-DRIVEN | 0.214 | 0.136 |
| WEAP-Iowa Blue Book | 0.215 | 0.144 |
| WEAP-Iowa DOT | 0.246 | 0.192 |

Table 6.6: Regionally-calibrated results for WEAP

| Source | Soil profile | Condition | Estimated pile resistance | Soil input procedure | $\lambda_R$ | COV $_R$ | $\beta = 2.33$ | | $\beta = 3.00$ | |
|---|---|---|---|---|---|---|---|---|---|---|
| | | | | | | | $\varphi$ | $\varphi/\lambda$ | $\varphi$ | $\varphi/\lambda$ |
| Iowa | Sand | EOD | $R_{EOD}$ | ST | 1.04 | 0.35 | 0.51 | 0.49 | 0.39 | 0.37 |
| | | | | ***SA*** | ***1.04*** | ***0.31*** | ***0.55*** | ***0.53*** | ***0.43*** | ***0.41*** |
| | | | | Iowa Blue Book | 1.05 | 0.33 | 0.54 | 0.51 | 0.41 | 0.39 |
| | | | | Iowa DOT | 1.14 | 0.39 | 0.52 | 0.46 | 0.39 | 0.34 |
| | | | | DRIVEN | 0.95 | 0.36 | 0.46 | 0.48 | 0.35 | 0.37 |
| | Clay | EOD | $R_{EOD}$ | ST | 0.91 | 0.15 | 0.65 | 0.71 | 0.54 | 0.59 |
| | | | | SA | 0.92 | 0.16 | 0.65 | 0.71 | 0.54 | 0.59 |
| | | | | ***Iowa Blue Book*** | ***0.93*** | ***0.16*** | ***0.65*** | ***0.71*** | ***0.55*** | ***0.59*** |
| | | | | Iowa DOT | 0.79 | 0.17 | 0.54 | 0.69 | 0.45 | 0.57 |
| | | | | DRIVEN | 0.93 | 0.16 | 0.66 | 0.70 | 0.55 | 0.59 |
| | | BOR | $R_{restrike}$ | ***ST*** | ***0.92*** | ***0.04*** | ***0.73*** | ***0.79*** | ***0.63*** | ***0.68*** |
| | | | | SA | 0.97 | 0.12 | 0.72 | 0.74 | 0.61 | 0.63 |
| | | | | Iowa Blue Book | 0.97 | 0.18 | 0.72 | 0.74 | 0.61 | 0.63 |
| | | | | Iowa DOT | 0.82 | 0.10 | 0.62 | 0.76 | 0.52 | 0.64 |
| | | | | DRIVEN | 0.97 | 0.11 | 0.73 | 0.75 | 0.62 | 0.64 |
| | | Setup | $R_{setup}$ | Iowa Blue Book | 0.86 | 0.33 | 0.21[a] | 0.25 | 0.19[a] | 0.22 |
| | | | | ***Iowa DOT*** | ***0.62*** | ***0.24*** | ***0.26***[a] | ***0.43*** | ***0.22***[a] | ***0.35*** |
| | Mixed | EOD | $R_{EOD}$ | ST | 1.45 | 0.28 | 0.82 | 0.57 | 0.65 | 0.45 |
| | | | | SA | 1.49 | 0.30 | 0.81 | 0.55 | 0.63 | 0.43 |
| | | | | Iowa Blue Book | 1.52 | 0.31 | 0.80 | 0.53 | 0.62 | 0.41 |
| | | | | ***Iowa DOT*** | ***1.41*** | ***0.26*** | ***0.83*** | ***0.59*** | ***0.66*** | ***0.47*** |
| | | | | DRIVEN | 1.49 | 0.33 | 0.76 | 0.51 | 0.59 | 0.40 |
| NCHRP 507 | All soil | EOD | $R_{EOD}$ | - | 1.66 | 0.72 | 0.39 | 0.24 | 0.25 | 0.15 |
| AASHTO (2010) | All soil | EOD or BOR | $R_{EOD}$ or $R_{restrike}$ | - | - | - | 0.50 | - | 0.40 | - |

[a] based on a conservative $\alpha$ value of 1.60 in the resistance factor calculations using Eq. (5.13).

Table 6.7: Regionally-calibrated results for CAPWAP

| Source | Soil profile | Condition | Estimated pile resistance | $\lambda_R$ | $COV_R$ | β = 2.33 | | β = 3.00 | |
|---|---|---|---|---|---|---|---|---|---|
| | | | | | | φ | φ/λ | φ | φ/λ |
| Iowa | All soil | BOR | $R_{restrike}$ | 1.02[d] | 0.16[d] | 0.71 | 0.70 | 0.59 | 0.58 |
| | Sand | General | R | 0.99 | 0.08 | 0.77 | 0.78 | 0.65 | 0.67 |
| | Clay | EOD | $R_{EOD}$ | 0.96 | 0.06 | 0.75 | 0.78 | 0.64 | 0.67 |
| | | Setup | $R_{setup}$ | 1.00 | 0.18 | 0.37[e] | 0.37 | 0.38[e] | 0.37 |
| | | BOR | $R_{restrike}$ | 0.99 | 0.02 | 0.80 | 0.80 | 0.69 | 0.69 |
| | Mixed | General | R | 1.28 | 0.13 | 0.93 | 0.96 | 0.79 | 0.81 |
| NCHRP Report 507 | All soil | General | R | 1.37 | 0.45 | 0.59 | 0.43 | 0.43 | 0.31 |
| | | EOD | $R_{EOD}$ | 1.63 | 0.49 | 0.64 | 0.39 | 0.46 | 0.28 |
| | | EOD (AR<350 & Bl. Ct. <16 bl/10cm) | $R_{EOD}$ | 2.59 | 0.92 | 0.41 | 0.16 | 0.23 | 0.09 |
| | | BOR | $R_{restrike}$ | 1.16 | 0.34 | 0.65 | 0.56 | 0.51 | 0.44 |
| AASHTO (2010) | All soil | BOR[a] | $R_{restrike}$ | - | - | 0.80 | - | 0.64 | - |
| | | BOR[b] | $R_{restrike}$ | - | - | 0.75 | - | 0.60 | - |
| | | BOR[c] | $R_{restrike}$ | - | - | 0.65 | - | 0.52 | - |

[a] at least one static load test and two dynamic tests per site condition, but no less than 2% of the production piles; [b] dynamic tests on 100% production piles; [c] dynamic tests on at least two piles per site condition, but no less than 2% of the production piles; [d] cannot satisfy the lognormal distribution; and [e] based on a conservative α value of 1.60 in the resistance factor calculation using Eq. (5.13).

Table 6.8: Construction control and resistance factors for the Iowa Blue Book method

| Construction control method | Soil profile | Construction control factor (ξ) | | | | | | Resistance factor (φ) of the Iowa Blue Book for β = 2.33 | | % gain in φ |
|---|---|---|---|---|---|---|---|---|---|---|
| | | EOD | Setup | BOR | Total | Limit | Suggest | Original | Modified | |
| WEAP (Iowa Blue Book procedure) | Clay | 0.75 | 1.16 | - | 0.87 | 1.32 | 1.00[a] | 0.63 | 0.63 | 0% |
| | Mixed | 1.07 | - | - | 1.07 | 1.90 | 1.07 | 0.60 | 0.64 | 7% |
| | Sand | 0.94 | - | - | 0.94 | 1.34 | 1.00[a] | 0.55 | 0.55 | 0% |
| CAPWAP | Clay | 0.87 | 1.25 | - | 1.08 | 1.37 | 1.08 | 0.63 | 0.68 | 8% |
| | | - | - | 1.38 | 1.38 | 1.27 | 1.27[b] | 0.63 | 0.80 | 27% |
| | Mixed | - | - | 1.18 | 1.18 | 1.63 | 1.18 | 0.60 | 0.71 | 18% |
| | Sand | - | - | 1.06 | 1.06 | 1.25 | 1.06 | 0.55 | 0.58 | 6% |

[a] the minimum value of 1.00 was suggested (i.e., construction control consideration is not considered); and [b] this value was suggested so that the modified φ for the Iowa Blue Book does not exceed 0.80.

Table 6.9: Recommended resistance factors for the Iowa Blue Book, WEAP and CAPWAP

| Theoretical analysis[b] | Stage | Construction control (field verification) | | | Resistance factor (φ)[a] | | | | |
|---|---|---|---|---|---|---|---|---|---|
| | | | | | Clay | | | Mixed | Sand |
| | | WEAP | CAPWAP | Restrike | General | EOD | Setup | EOD | EOD |
| Iowa Blue Book | Design[c] | - | - | - | 0.63 | - | - | 0.60 | 0.55 |
| | | Yes[e] | - | - | 0.63 | - | - | 0.64 | 0.55 |
| | | | Yes | - | 0.68[g] | - | - | - | - |
| | | | | Yes | 0.80 | - | - | 0.71 | 0.58 |
| | Construction[d] | Yes[e] | - | - | - | 0.65 | 0.21 | 0.80 | 0.54 |
| | | | - | Yes | 0.72 | - | - | - | |
| | | | Yes[f] | - | - | 0.75 | 0.37 | - | - |
| | | | | Yes | 0.80 | - | - | 0.71 | 0.71 |

[a] provide a minimum of five piles per redundant pile group; [b] use the Iowa Blue Book to estimate the theoretical nominal pile resistance; [c] use the applicable resistance factor to estimate factored resistance during design; [d] use the applicable resistance factor to determine the driving criteria required to achieve the required nominal driving resistance; [e] use the Iowa Blue Book soil input procedure in WEAP analysis; [f] use signal matching to estimate total resistance; and [g] setup effect has been included when WEAP is used to establish driving criteria and CAPWAP is used as a construction control.

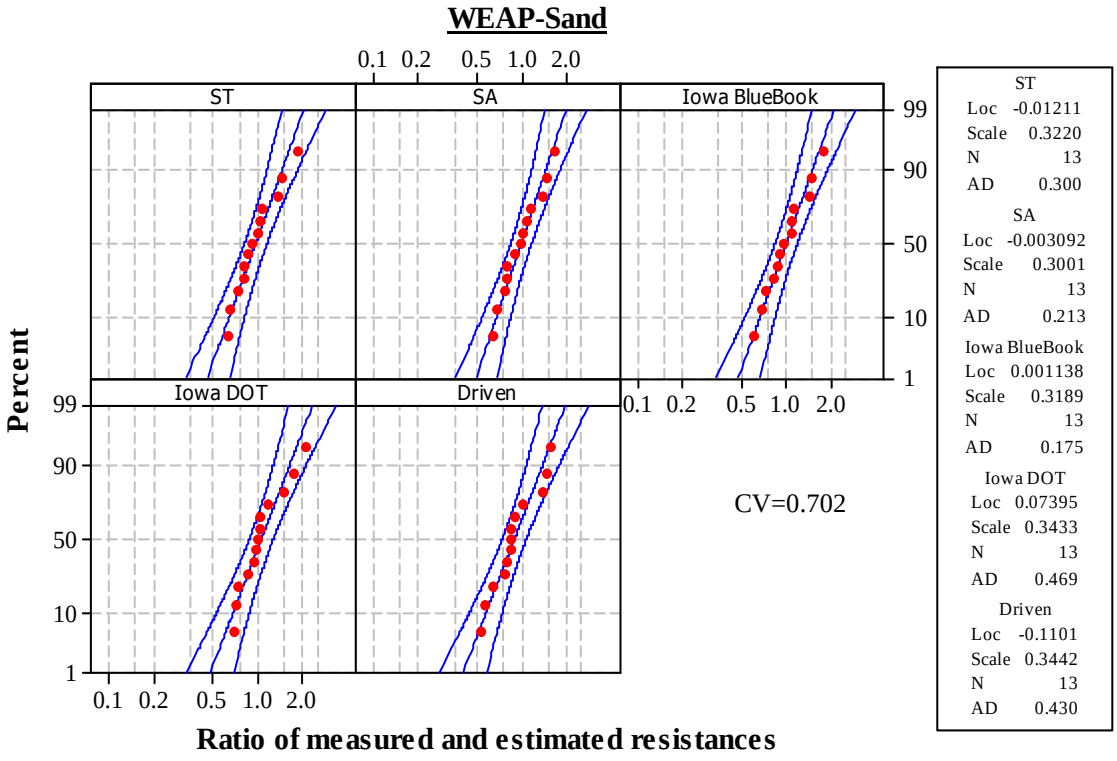


Figure 6.1: Cumulative density functions for WEAP at sand profile

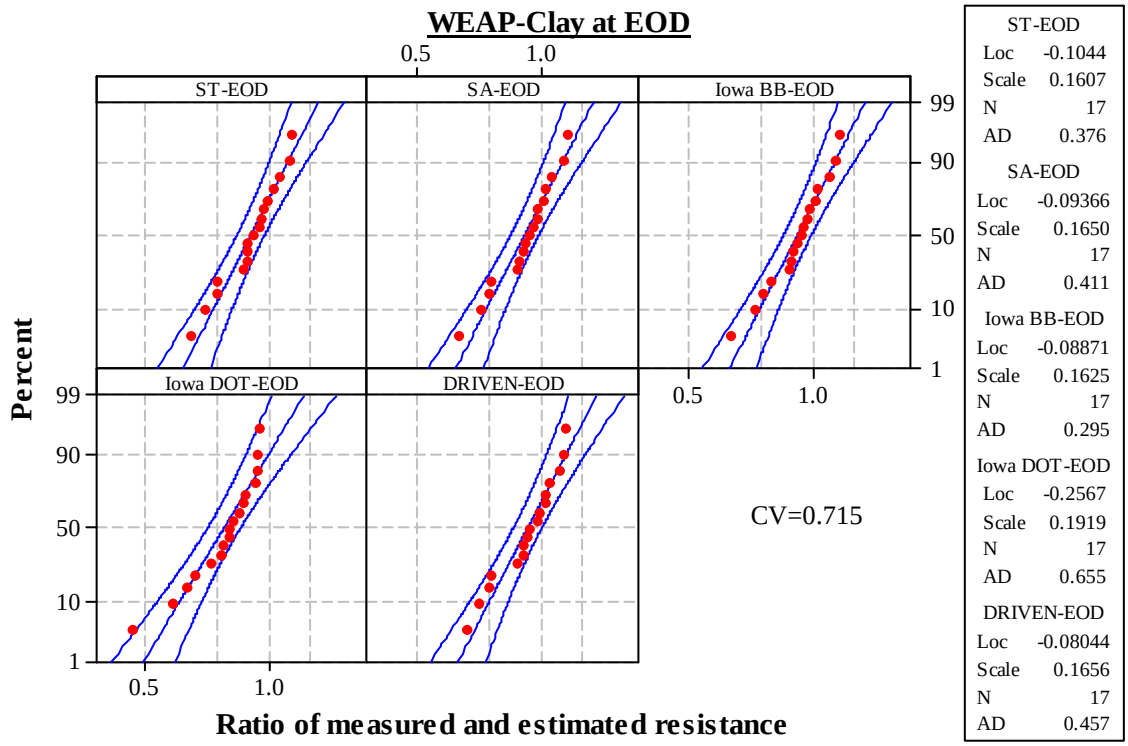


(a) Based on resistances considered at EOD condition

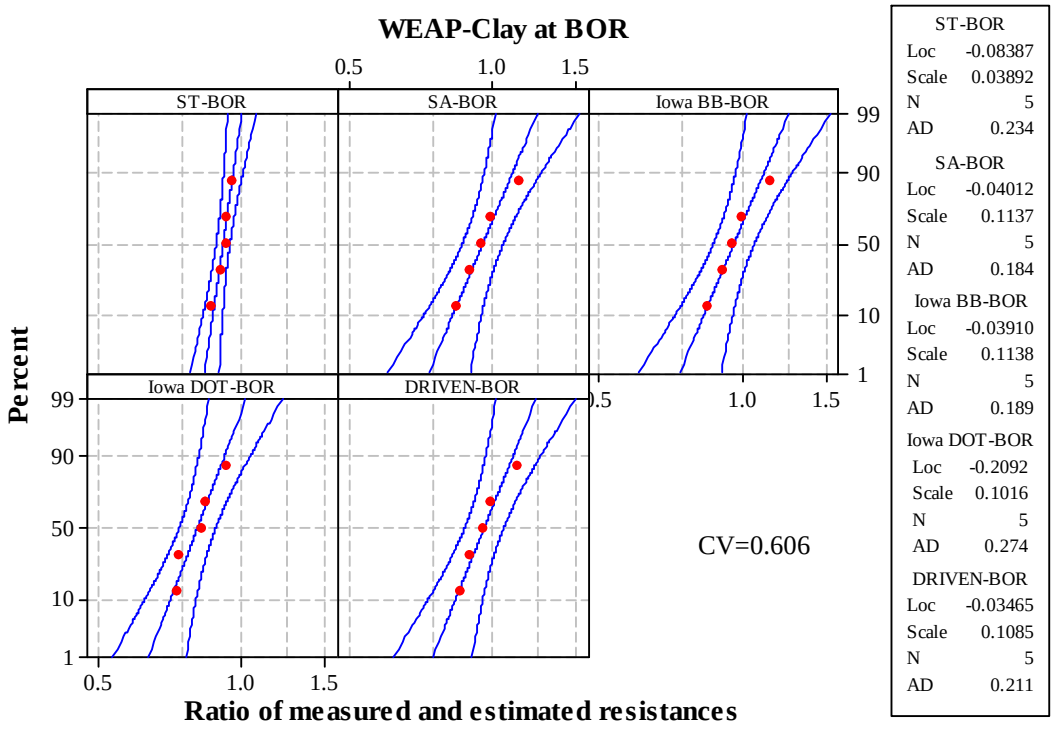


(b) Based on resistances considered at BOR condition

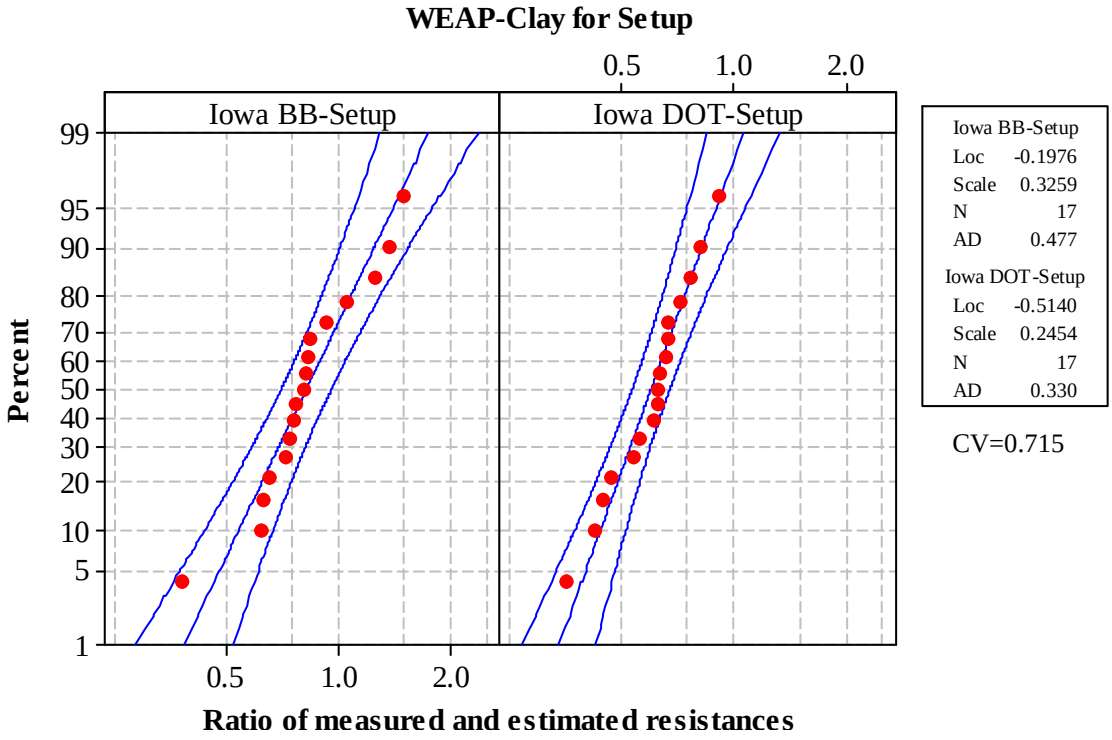


(c) Based on pile setup resistances

Figure 6.2: Cumulative density functions for WEAP at clay profile

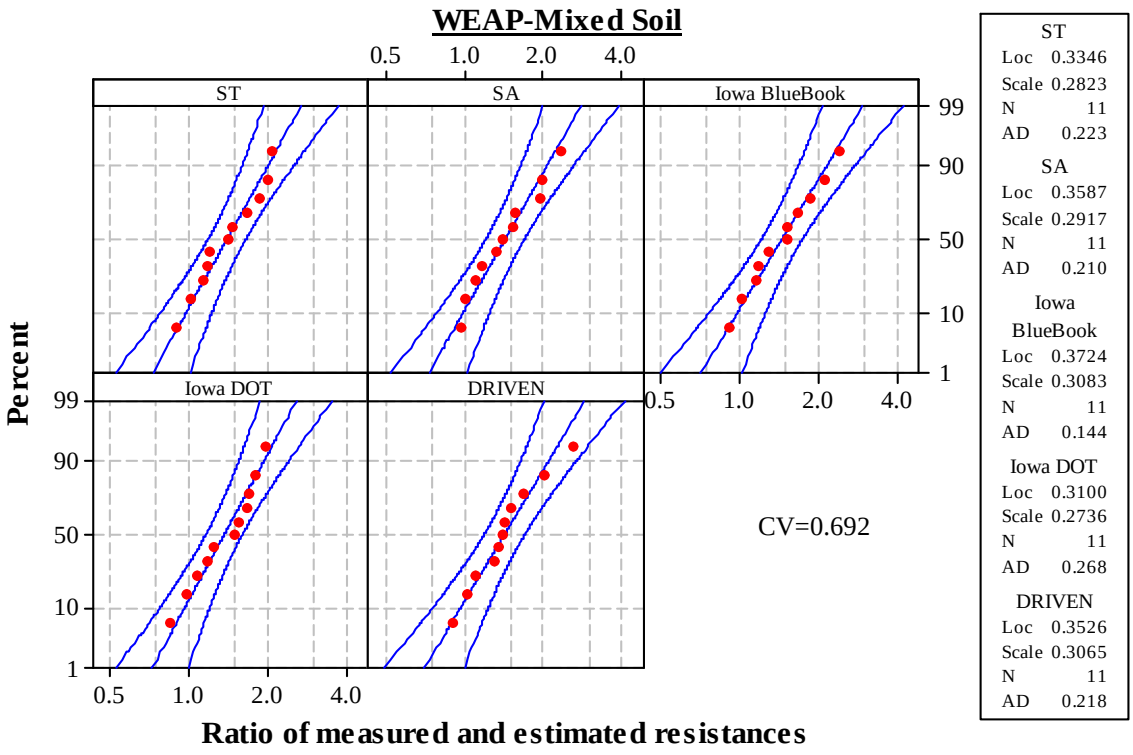


Figure 6.3: Cumulative density functions for WEAP at mixed soil profile

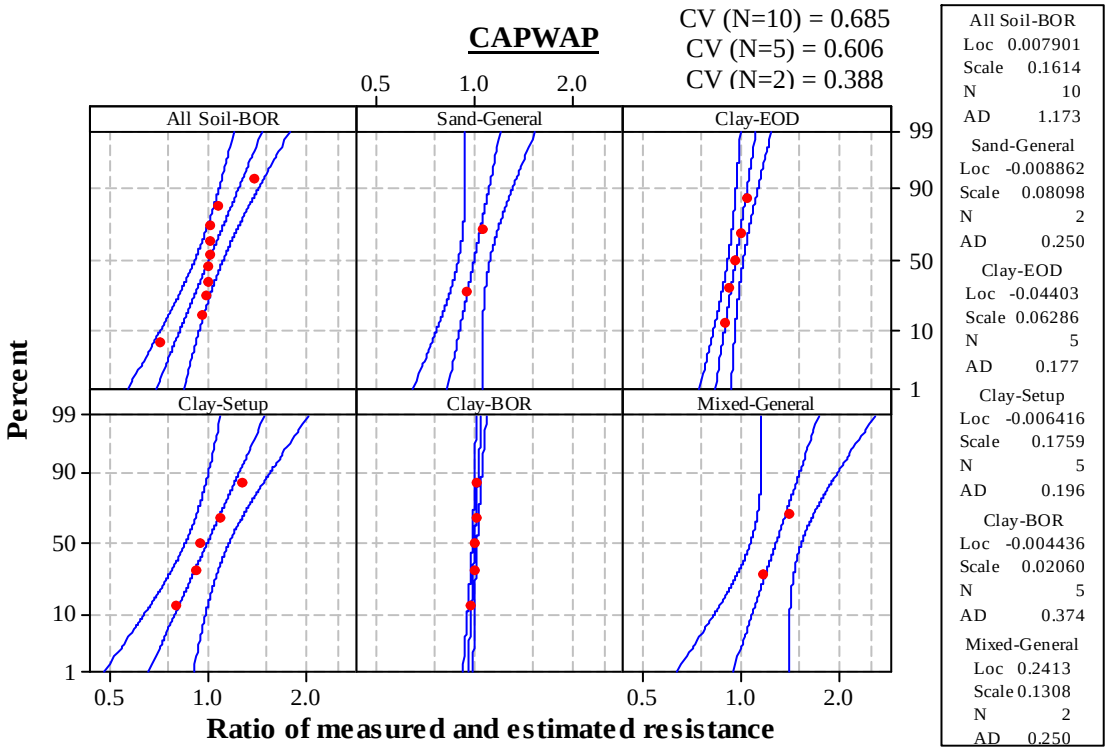


Figure 6.4: Cumulative density functions for CAPWAP

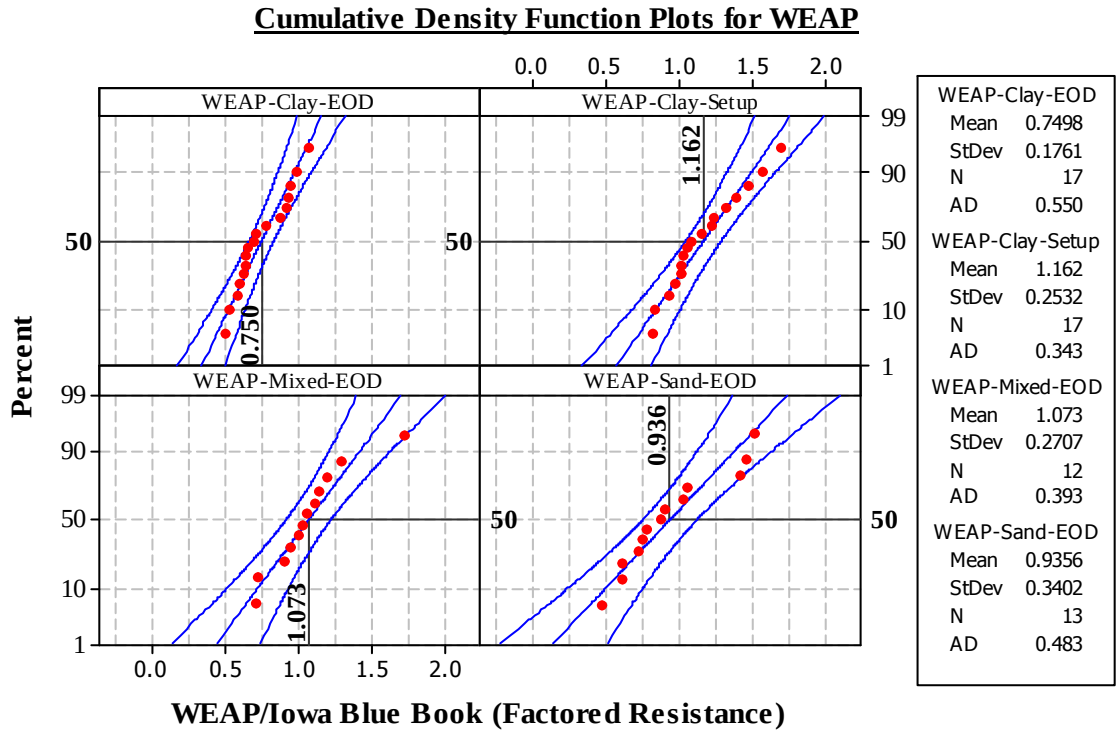


Figure 6.5: Cumulative probability distribution curve of factored resistance ratios for WEAP

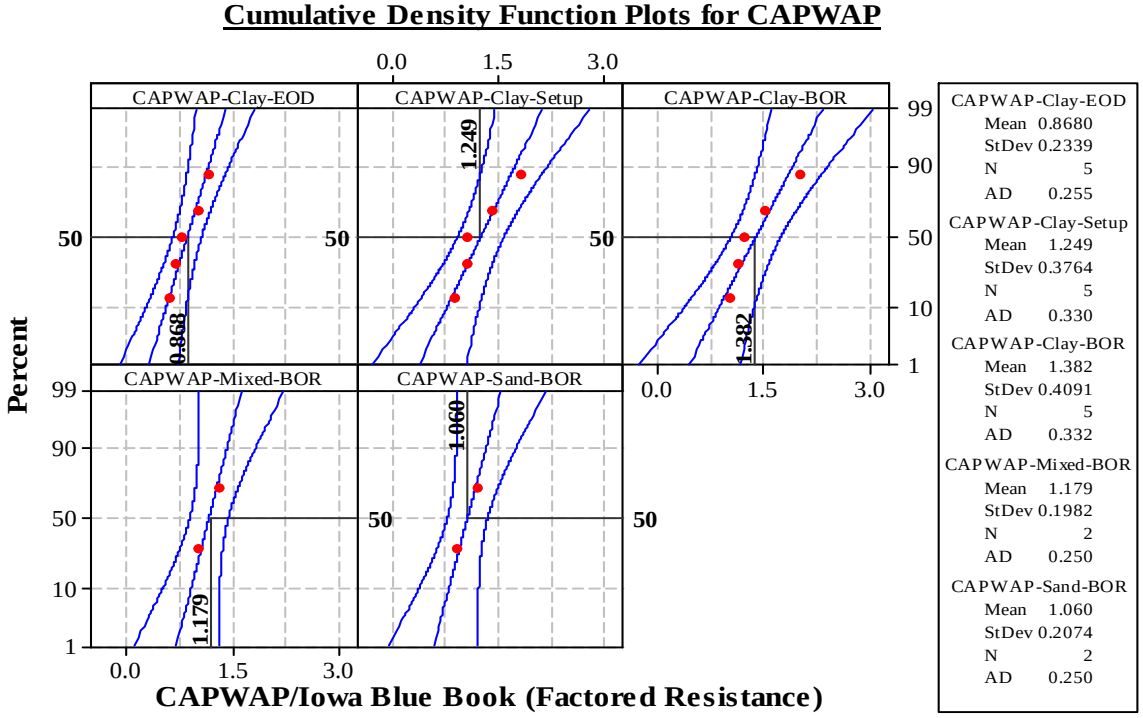


Figure 6.6: Cumulative probability distribution curve of factored resistance ratios for CAPWAP

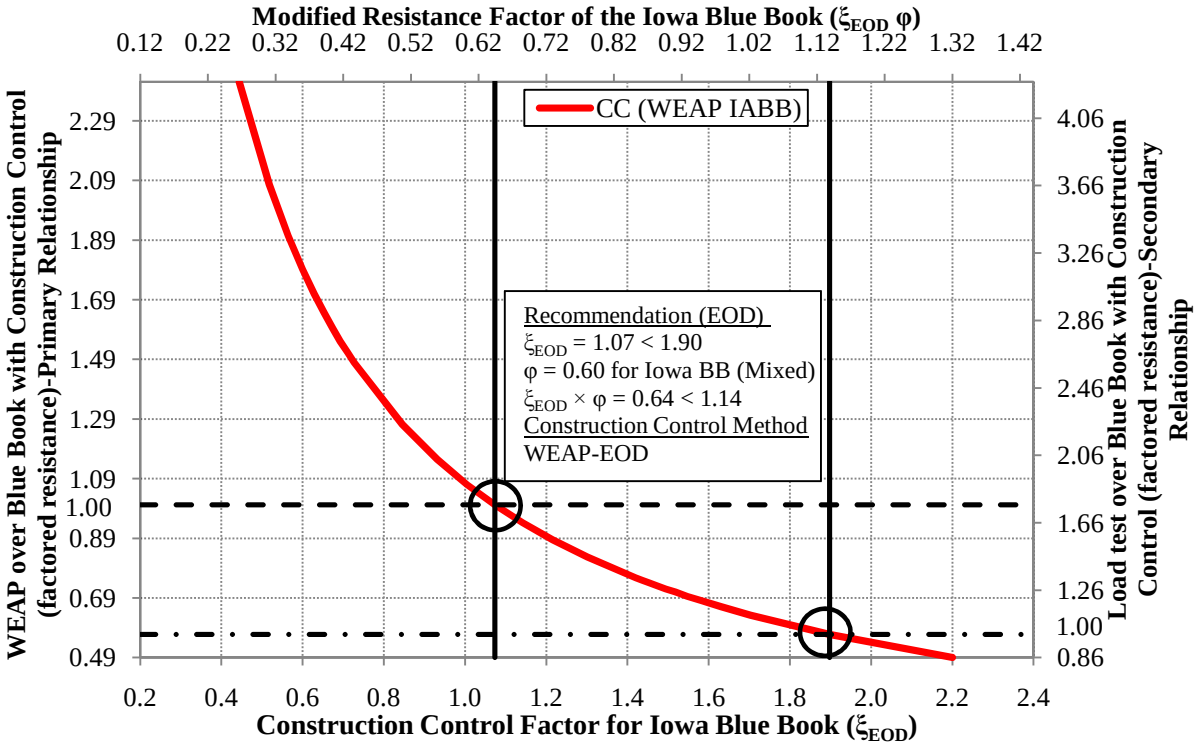


Figure 6.7: Maximum limit of construction control factor for the Iowa Blue Book, based on WEAP (Iowa Blue Book input procedure) for a mixed soil profile

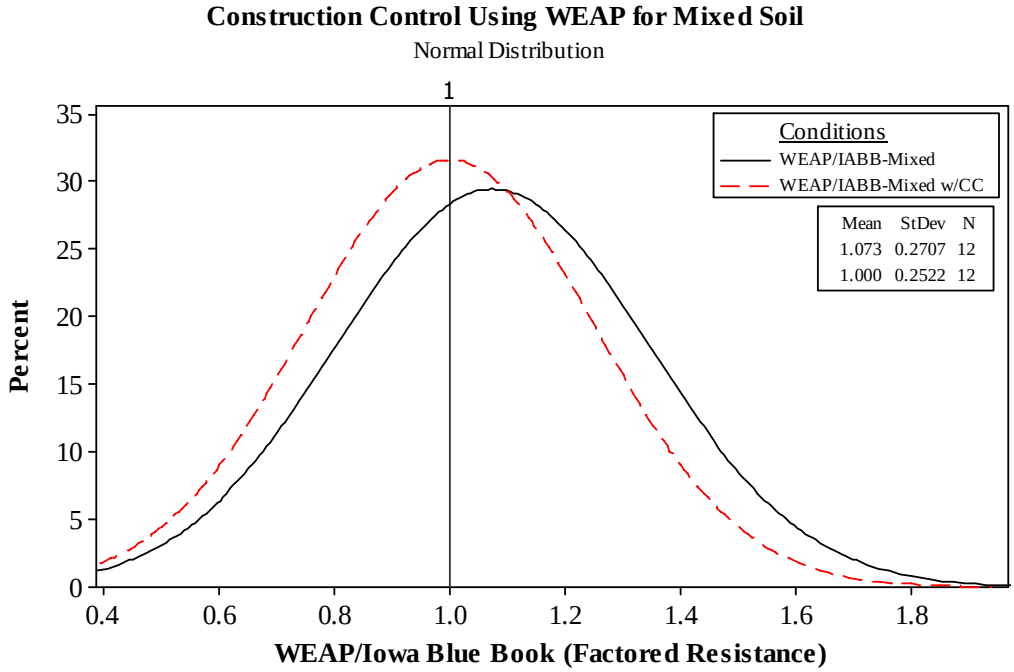


Figure 6.8: Before and after applying construction control using WEAP-Iowa Blue Book procedure for a mixed soil profile

# CHAPTER 7: AN IMPROVED CAPWAP MATCHING PROCEDURE FOR THE QUANTIFICATION OF DYNAMIC SOIL PARAMETERS

Ng, K. W.[1]; Sritharan, S.[2]; and Suleiman, M. T.[3]

A paper to be submitted to the *Computers and Geotechnics Journal*

## 7.1. Abstract

Although dynamic analysis methods have been widely used in estimating axial pile resistance, the accuracy of these methods is highly dependent upon the appropriate selection of dynamic soil parameters, such as damping factor and quake value. Due to the high degree of scatter found during correlation studies and the limitation with the current default CAPWAP matching procedure from which constant parameters are assumed over an entire soil profile, these parameters have not been successfully quantified from any standard geotechnical in-situ or laboratory soil test results. To improve the prediction of these parameters, a systematic CAPWAP matching procedure is proposed, based on variable soil parameters along the pile length. The proposed CAPWAP matching procedure improved the match quality between measured and estimated pile responses to as high as 20%. Correlation studies showed a good relationship between the SPT N-value and shaft dynamic soil parameters at the EOD condition for both cohesive and cohesionless soils. Empirical equations were established with relative high coefficient of determination. Also, the analyses presented herein revealed the influences of pile setup and pile installation on the estimation of the parameters. The application of these parameters was validated based on an independent CAPWAP analysis performed on a recently tested steel H-pile embedded in a mixed soil profile with a 19% match quality improvement.

---

[1]Ph.D. Candidate, Dept. of Civil, Construction and Environmental Engineering, Iowa State Univ., Ames, IA 50011. E-mail: kwng@iastate.edu

[2]Wilson Engineering Professor and Associate Chair, Dept. of Civil, Construction and Environmental Engineering, Iowa State Univ., Ames, IA 50011. E-mail: sri@iastate.edu

[3]Assistant Professor, Dept. of Civil and Environmental Engineering, Lehigh University, Bethlehem, PA, 18015. E-mail: mts210@lehigh.edu

## 7.2. Introduction

Although dynamic analysis methods, such as the Wave Equation Analysis Program (WEAP) and the CAse Pile Wave Analysis Program (CAPWAP), have been widely used in estimating axial pile resistances, the accuracy of these methods is highly dependent upon the proper selection of suitable dynamic soil properties (Liang and Sheng, 1993). These properties include the stiffness (k) and viscous damping coefficient (c) used in the dynamic resistance ($R_d$) of the soil mass surrounding the shaft and toe of a pile (sees Figure 7.1). Smith (1962) developed Eq. (7.1) to calculate the static resistance ($R_s$) at any point x corresponding to the soil spring deformation x on the solid line OABC shown in Figure 7.2.

$$\begin{aligned} R_s = kx = \frac{R_{su}}{q}x \ ; 0 \le x \le q \\ R_s = R_{su} \ ; x > q \end{aligned} \tag{7.1}$$

Soil stiffness (k) was taken as the ratio of an ultimate static soil resistance ($R_{su}$) and quake value (q) within the elastic deformation. Constant values for shaft quake ($q_s$) and toe quake ($q_T$)) have been typically employed in the dynamic analysis methods to define the stiffness of the soil along a pile shaft and at a pile toe, respectively. In addition, Smith (1962) described the dynamic soil resistance ($R_d$) in terms of a damping coefficient (c) and an instantaneous velocity (v) experienced by the viscous damper given by Eq. (7.2). Smith (1962) estimated the damping coefficient as a product of the static resistance calculated using Eq. (7.1) and a damping factor (J). Similar to the quake values, constant shaft damping factor ($J_s$) and toe damping factor ($J_T$) have been used in the dynamic analysis methods to describe the damping characteristics of the soil along the shaft and toe of a pile, respectively. The total soil resistance (R), represented by the dashed line OA′BC shown in Figure 7.2, is defined as the summation of both the static and dynamic soil resistances.

$$R_d = cv = (R_s J)v \tag{7.2}$$

Although improvement to the use of constant Smith quake values and damping factors have been investigated for more than three decades, no significant advancements to

establish relationships between these parameters and soil properties have been accomplished, due to large degree of scatter typically seen for the collected soil parameters as illustrated by McVay and Kuo (1999) and shown in Figure 7.3. These parameters are currently determined through CAPWAP analyses by matching the PDA measured signals representing force and velocity measured near pile top with the computed signals, based on a one-dimensional soil-pile model in Figure 7.1. The large variation among the collected soil parameters shown in Figure 7.3 is attributed to the current approach in performing the CAPWAP analysis with an emphasis in achieving a best signal matching, from which the constant shaft damping factor and the quake value are determined, regardless of the different soil properties alongside of a pile. Furthermore, the fact that this best fit solution achieved from the CAPWAP analysis is not being unique, and that it is influenced by the magnitude of the shaft and toe resistances that may be adjusted arbitrarily in striving to achieve the best signal match. Due to the indeterminate nature of the CAPWAP analysis, the dynamic soil parameters cannot be uniquely quantified. Svinkin and Woods (1998) noted one of the limitations of dynamic analysis methods is the difficulty in quantifying these soil parameters in terms of any standard geotechnical in-situ or laboratory test results. As a result, based on a database collected by Pile Dynamic, Inc. (2000), a possible range of damping factors (0.078 to 1.44 s/m for shaft and toe) and quake values (1.02 to 17.96 mm for shaft and 1.02 to 5.36 mm for toe) are recommended in CAPWAP,.

In lieu of the current setback with dynamic soil parameters quantification, empirical relationships were developed herein to uniquely estimate them using Standard Penetration Test (SPT) N-value. These empirical relationships were established through a systematic approach in performing the signal matching adopted during the CAPWAP analysis, as explicitly described in Section 7.3. The proposed procedure not only provides a realistic distribution of dynamic soil parameters in accordance with the soil stratigraphy, but it also improves the quality of the signal matching.

Svinkin and Woods (1998) suggested the use of variable soil parameters as a function of time to simulate the increase in pile resistance due to pile setup. Recognizing the

difficulty in pile setup investigation based solely on limited data available in the literature (see Section 3.3), the relationship between dynamic soil parameters and time has not been established. To enhance the capability of dynamic analysis methods in accounting for pile setup and to avoid the performance of practically infeasible pile restrikes, two recently completed field results of test piles ISU5 and ISU6, as described in Chapter 3, were selected to examine the effect of pile setup on the dynamic soil parameters.

## 7.3. Background

Although dynamic soil damping factor and quake values have been investigated by many researchers, (e.g. Smith (1962), Coyle et al. (1973), Hannigan et al. (1998), McVay and Kuo (1999), Malkawi and Ayasrah (2000), Liang (2000), and Roling (2010)), a general approach for accurately quantifying these parameters cannot be established from all the recommendations. Based on the experience gained through working extensively with this problem and a limited number of comparisons with static load tests, Smith (1962) suggested constant values, as listed in Table 7.1 for practical applications. After approximately a decade later, Coyle et al. (1973) estimated a set of dynamic parameters for three different soil types (i.e., clay, sand, and silt) from full-scale pile tests, in which the most accurate correlation of the dynamic parameters were achieved. They acknowledged that an extensive data set was not available at that time for the damping characteristics of soils, and the use of more accurate values was recommended if they are available in the future.

Based on pile driving experience, Hannigan et al. (1998) observed that the damping factors vary with the waiting times after the end of driving (EOD), and that higher values may be appropriated for analyses modeling the restrike conditions. They believed damping factors are not a constant for a given soil type and a higher value may be expected for soft soils than hard rock. Due to the lack of dynamic measurements and quantitative analyses, their hypotheses on damping factors have not been validated, and constant values were suggested as listed in Table 7.1. In addition, shaft quakes were recommended at 2.54 mm for the most cases, whereas toe quake values were recommended as the value obtained from the pile diameter (D) divided by 120 for very dense and hard soils and 60 for soft soils.

Although these recommendations have been implemented in current dynamic analysis methods in Wave Equation Analysis Program (WEAP), results obtained from McVay and Kuo (1999) and the recently completed field tests conducted in Iowa using CAPWAP (see Figure 7.3 and Figure 7.4) revealed: (1) the dynamic soil parameters are not constant value as suggested by Hannigan et al. (1998); (2) they have no unique correlation with the SPT N-value as assumed in the current default CAPWAP matching procedure; and (3) the dynamic soil parameters did not vary distinctly as the soil type varies from cohesive soil to cohesionless soil to limestone.

Malkawi and Ayasrah (2000) performed a series of dynamic load tests on a steel, smooth closed ended, pipe pile. With 900 mm length, 61 mm diameter, and 5 mm thickness, this slender pile was comparable to the common pipe piles used in practice. The test pile was driven into a fine to medium, poorly graded sand (SP) compacted to three different relative densities of 35, 50, and 70%. Based on the matching of time-displacement signals, they concluded that damping factors (J) were found to be inversely proportional to pile installation depth, sand relative density, and static sand resistance. These conclusions obtained this test pile are yet to be validated from real pile tests.

Liang (2000) conducted a statistical analysis on the dynamic soil parameters using a database of 611 driven piles collected by Paikowsky et al. (1994). The dynamic soil parameters were estimated via the default CAPWAP signal matching procedure, summarized in Table 7.2, with consideration to soil type (sand and clay) and time of dynamic pile testing (EOD and BOR). These statistical analysis results revealed that the quake values varied minimally with the soil type and time of dynamic testing. The damping factors were found to be influenced more by the time of dynamic testing than by the soil type. Furthermore, the relative high standard of deviation indicated a large scatter in estimating each dynamic soil parameter that could lower the accuracy of pile resistance computations using CAPWAP. Although a larger database was used in these statistical analyses, a unique correlation for dynamic soil parameters quantification cannot be established in terms of soil type and/or time of dynamic testing.

Liang (2000) calculated an average shaft quake of 1.27 mm and toe quake of 3.18 mm, based on SPT tests collected and reported by Goble, Rausche and Likins (GRL) through the default CAPWAP signal matching procedure. Using these quake values, Liang determined the damping factors through a number of consequent iterations using WEAP until the estimated SPT blow count matched the actual recorded SPT N-value at each soil layer for all 23 Ohio Department of Transportation piling project sites. Performing the default CAPWAP signal matching procedure on 34 driven test piles (31 pipe piles and 3 H-piles) at the 23 test sites, Liang independently determined the damping factors and compared them with those estimated using WEAP on SPT. The estimated damping factors obtained from WEAP in this manner for all sites were adjusted by a reduction factor, so its average value was close to the CAPWAP average value as illustrated in Table 7.3 for both 60 and 70% SPT hammer efficiencies. Finally, the correlations between the adjusted damping factors (shaft and toe) and the corresponding SPT N-values generated Eqs. (7.3) and (7.4) for clay and sand, respectively. The validation of these proposed equations has not been provided. Thus, they have not been widely implemented for practical applications.

$$\mathrm{J(s/m)} = \frac{2.089\ \mathrm{N}}{62.5 + \mathrm{N}}\ \text{for Clay} \tag{7.3}$$

$$\mathrm{J(s/m)} = \frac{1.107\ \mathrm{N}}{62.5 + \mathrm{N}}\ \text{for Sand} \tag{7.4}$$

Recognizing the limitation with the current CAPWAP analysis, Roling (2010) proposed a displacement-based signal matching procedure using a commercial finite element analysis program SAP2000 (Computers & Structures, Inc. 2008). Similar to the one-dimensional soil-pile model used in CAPWAP as shown in Figure 7.1, the pile top displacement was generated using SAP2000 and compared with that measured using the PDA. As a result of this proposed matching procedure, the shaft damping factor was determined to be directly proportional to pile installation depth, whereas the shaft quake value decreased with the depth on account of the increasing geostatic pressure. Furthermore, Roling concluded that the magnitude of the damping factor was dependent upon the stage of

pile embedment (i.e., the same soil layer will have a smaller damping factor during pile installation than at the EOD condition, when the pile is fully embedded). Furthermore, Roling discovered that soils near the pile toe in a nearly virgin stage of disturbance will experience much severe degradation (i.e., relatively larger increment in the shaft quake value or larger reduction in stiffness) as opposed to soils above, which have been disturbed by a repetitive cycle of hammer blows.

## 7.4. Methodology

The aforementioned limitations with the current default CAPWAP signal matching procedure suggest the need for a new procedure that can produce a distinctive solution without scarifying the quality of a good signal match achieved using the current procedure. A distinctive solution is referred as the representative shaft and toe static resistances that are weighted accordingly with the surrounding soil types and properties. Concurrently, unique dynamic soil damping factor and quake value at each soil segment along the entire embedded pile length and at pile toe, are characterized during CAPWAP analysis to determine the shaft and toe dynamic pile resistances. To eliminate the current indeterminate CAPWAP procedure of simultaneously adjustment of both static and dynamic resistance components, the static soil resistance distribution was estimated using the Schmertmann's (1978) correlated Cone Penetration Test (CPT) unit skin friction ($f_s$) and unit tip resistance ($q_c$) data. This approach isolates the dynamic resistance component needed to achieve a good signal match and eliminates the burden of striving to adjust a significant number of unknowns during the CAPWAP analysis.

Since the goal of this paper is to quantify these dynamic soil parameters, the static soil resistances at each soil segment alongside of a pile and at pile toe are estimated using the Schmertmann's (1978) method, and are proportionally adjusted so that the total resistance better matched the total pile resistance computed using the current default CAPWAP procedure. This approach not only generates a realistic distribution of the static resistance, but it also ensures comparable pile resistance estimation. The next step is to identify the dynamic soil characteristic of each soil segment described with the one-dimensional pile-soil

model shown in Figure 7.1. Based on the concept of wave propagation, when a uniform pile is impacted by a driving hammer, an impulsive stress wave propagates from the pile top down towards the toe. During wave propagation, the stress wave is partially reflected by the presence of soil resistance along the pile shaft and at pile toe. The downward wave propagation overlaps with the upward wave reflection. The actual response can be recorded near the pile top using a Pile Driving Analyzer (PDA). The influence of a series of soil segments from which the stress wave is reflected can be identified from the actual measured response at a time interval determined by Eq. (7.5)

$$t = \frac{2L}{C} \tag{7.5}$$

where,

L = distance from the PDA instrumentation near pile head to the soil segment of interest, m,

C = pile wave speed = $\sqrt{\frac{E}{\rho}}$, m/s,

E = modulus of elasticity of the pile material, $N/m^2$, and

$\rho$ = mass density of the pile material, $N\text{-}s^2/m^4$.

Therefore, the dynamic characteristic of the specified soil segment of interest can be determined by matching the actual measured response with the CAPWAP computed response up to the time interval (t) that corresponds to the location of the specified soil segment. This approach begins from the first soil segment closest to the ground surface and repeats on consecutive soil segments, together with the dynamic parameters for preceding soil segments during the matching process. Pile response in terms of upward traveling force wave or WaveUp ($W_u$) defined by Eq. (7.6) is selected during the matching process to ensure a consistent comparison between results obtained using this new procedure and the commonly used default CAPWAP procedure

$$W_u = \frac{F(t) + Zv(t)}{2} \tag{7.6}$$

where,

$F(t)$ = measured or estimated pile force near pile head at time t, N,

$Z = \frac{EA}{C}$ = pile impedance, N-s/m,

$v(t)$ = measured or estimated pile velocity near the pile head at time t, m/s, and

$A$ = pile cross sectional area, $m^2$.

As a result of the multiple matching processes up to the final soil segment at a time interval of 2L/C, where L is the entire wave traveling distance, a distribution of damping soil parameters was preliminarily determined. This distribution is further refined and adjusted proportionally until a best match is achieved for the complete time period that includes the rebounding and unloading conditions as illustrated in Figure 7.6. In CAPWAP analysis, the accuracy of a matching is evaluated in terms of a match quality (MQ), which is the normalized, weight sum of the absolute values of the differences between computed and measured responses of the specified time interval. The matching of hammer blow count (i.e., pile set) within the 2L/C during the preliminary estimation of the dynamic soil parameters is not considered and its error is not added to the MQ value; however, this error is included during the final matching for the entire time period.

The aforementioned procedure is applicable for both EOD and BOR conditions. For example, at the EOD condition, the static soil resistances estimated using Schmertmann's (1978) method are adjusted to match with the total CAPWAP estimated pile resistance for the EOD, and the estimated dynamic soil parameters represent the dynamic characteristic of the surrounding soil at the EOD condition.

## 7.5. Quantification of Shaft Dynamic Soil Parameters

As part of this research project, ten steel H-piles were driven and load tested in the field. The pile top responses (strains and accelerations) during driving were recorded using the PDA. With adequate in-situ (Standard Penetration Test (SPT) and Cone Penetration Test (CPT)) and laboratory soil characterizations, five test piles embedded in cohesive soil profile,

which were identified as ISU2, ISU3, ISU4, ISU5, and ISU6, were selected primarily for quantifying the cohesive dynamic soil parameters. To quantify dynamic soil parameters for cohesionless soils, only test pile ISU9 was chosen, but test pile ISU10 was not included due to incomplete CPT results. For accurate correlation studies, piles ISU1, ISU7, and ISU8 embedded in mixed soil profiles were not considered. However, test pile ISU8, which has both SPT and CPT data, was selected for the validation of the estimated parameters. The field tests of these test piles were explicitly described in Chapter 3 and Ng et al. (2011).

Table 7.4 summarizes the average unit tip resistance ($q_c$) and unit skin friction ($f_s$) measured using CPT and the average SPT N-value at the depth of each soil model along the test pile. Referring to Figure 7.1, each soil model represented by a linear elastic-plastic spring and a linear viscous damper was used in CAPWAP to characterize the surrounding soil at the designated soil layer. The soil resistance ($R_s$) at each soil layer estimated using Schmertmann's (1978) method was adjusted proportionally as listed in Table 7.4, so that the total estimated soil resistance matched the total pile resistance estimated based on the default CAPWAP matching procedure. Following the proposed CAPWAP matching procedure described in Section 7.4, the shaft damping factor ($J_s$) and the shaft quake value ($q_s$) were quantified for each soil model. These dynamic soil parameters represent the soil characteristics at the EOD condition, in which the PDA recorded pile responses were engaged during the CAPWAP matching process.

To investigate the effect of pile setup on cohesive dynamic soil parameters, two PDA pile responses recorded from the beginning of the last restrike, BOR6 of test pile ISU5 and BOR8 of test pile ISU6, were selected. The BOR6 of ISU5 performed at 8 days after EOD had a close duration with the BOR8 of ISU6, performed at 10 days after EOD. Aligned with the similar procedure described for the EOD condition, the dynamic soil parameters at the time of last restrikes were determined. Table 7.5 summarizes the location of the soil models, the measured soil properties, and the computed dynamic soil parameters.

### 7.5.1. EOD condition for cohesive soils using SPT

Results summarized in Table 7.4 for test pile ISU5 were selected to illustrate in detail the relationship between the measured soil properties and the computed dynamic soil parameters at EOD along the embedded pile length. Figure 7.7 (a) and (b) show the comparison of the SPT N-values to the computed shaft damping factors ($J_s$) and the shaft quake values ($q_s$), respectively. Figure 7.7 (a) shows a direct relationship between $J_s$ and the SPT N-value, demonstrated by the increase in $J_s$ up to 0.59 s/m at the depth of 10.39 m, where the low plasticity clay (CL) reached its maximum SPT N-value of 22 and by the decrease in the $J_s$ value to 0.31 s/m as the SPT N-value decreased from 22 to 13 before reaching the pile toe at 16.76 m. In contrast, Figure 7.7 (b) shows an inverse relationship between $q_s$ and the SPT N-value, whereby the low plasticity clay at 10.39 m with the maximum SPT N-value of 22 had the smallest $q_s$ value of 1.02 mm. Below the 10.39 m, the $q_s$ value increased to 2.03 mm as the SPT N-value reduced from 22 to 13. Furthermore, these figures show the influence of soil types on the dynamic soil parameters. For instance, unlike the CL layers indicated in Table 7.4, the first 0.82 m fill layer (silt (ML) and sandy clay (SC)), mechanically compacted during road construction, had a relative high $J_s$ value of 2.57 s/m and a relative small $q_s$ value of 0.51 mm. Although the soil layer (CL and SC) near the ground water table (GWT) at 10.8 m shared the same SPT N-value of 22 with the clay soil layer above it, its dynamic soil parameters ($J_s$ = 1.65 s/m and $q_s$ = 1.78 mm) were higher than those for clay soil ($J_s$ = 0.59 s/m and $q_s$ = 1.02 mm). These figures prove that the dynamic soil parameters are not constant throughout the soil profile, as treated in the default CAPWAP matching procedure.

To further expand on the above observations, the dynamic soil parameters computed from all test piles provided in Table 7.4 were compared with SPT N-values. To present a better correlation with the SPT N-value, an average dynamic soil parameter was computed from those values corresponding to the same SPT N-value as plotted in Figure 7.8 to Figure 7.11. Using these correlated data points, best-fit lines and their corresponding 95% confidence intervals were drawn. Figure 7.8 shows a plot for the $J_s$ value at the EOD as a function of SPT N-value (represented by the circular solid markers). Using this data in this

figure, a power relationship in Eq. (7.7) was established satisfactory to quantify the $J_s$ value as indicated by a relative high coefficient of determination ($R^2$) of 0.83. Furthermore, these data points followed the relationship given in Eq. (7.3) suggested by Liang (2000), which further reinstated the direct relationship between the $J_s$ value and the SPT N-value, as opposed to the constant values suggested by Smith (1962) and Hannigan et al. (1998) given in Table 7.1.

$$J_s(s/m) = 0.016\ N^{1.1838};\ \text{for EOD} \tag{7.7}$$

Besides using the damping factor, the damping coefficient ($c_s$) as described in Section 7.2 can be directly implemented in CAPWAP to define the dynamic characteristic of the soil-pile system. Referring to Eq. (7.2), Smith (1962) defined the damping coefficient as a product of damping factor ($J_s$) and its corresponding static soil resistance ($R_s$). Using the data points plotted in Figure 7.8 for EOD, the correlation between $c_s$ and the SPT N-value was plotted in Figure 7.9 (represented by the circular solid markers). Similarly, damping coefficients as tabulated in Table 7.4 were estimated based on Liang's (2000) proposed Eq. (7.3) for $J_s$ value. Next, average damping coefficients were computed and plotted against their respective SPT N-values in Figure 7.9 (represented by asterisk marks). Comparing the two best fit lines for the EOD, the higher $R^2$ value of 0.82, based on the proposed Eq. (7.7), versus the $R^2$ value of 0.79, based on Liang (2000), suggests that they are comparable.

Similar to the aforementioned correlation study between $J_s$ and SPT N-value, the average shaft quake values ($q_s$) were calculated and plotted against the SPT N-values in Figure 7.10. The exponential decaying best fit line given by Eq. (7.8) with a high $R^2$ value of 0.90 confirms the inverse relationship between $q_s$ and SPT N-value observed earlier in Figure 7.7 and contrasts the constant values suggested by Smith (1962) and Hannigan et al. (1998) given in Table 7.1. Although the linear plastic spring of the soil model (see Figure 7.1) is normally characterized using the quake value, it can also be defined in terms of soil stiffness ($k_s$), which is a ratio of static soil resistance ($R_s$) and the quake value. Transforming the data points plotted in Figure 7.10, Figure 7.11 shows a linear relationship between the $k_s$ value and the SPT N-value given by Eq. (7.9). The relatively higher $R^2$ value of 0.96 exhibits a

better confidence in quantifying the $k_s$ value than the $q_s$ value. Unfortunately, the current CAPWAP does not provide a direct input of $k_s$ value; hence, the proposed Eq. (7.8) is recommended.

$$q_s(\text{mm}) = \frac{9.1664}{e^{0.13N}} \text{ ; for EOD} \tag{7.8}$$

$$k_s(\text{kN/m}) = \frac{R_s}{q_s} = 3.4813\ N - 12.453 \text{ ; for EOD} \tag{7.9}$$

### 7.5.2. EOD condition for cohesive soils using CPT

Similar comparisons were performed using the CPT average unit tip resistance ($q_c$), average unit skin friction ($f_s$), and average friction ratio (FR) as summarized in Table 7.4 for ISU5. The friction ratio (FR) is defined as the ratio between the unit skin friction and the total cone tip resistance ($q_t$), reported as a percentage and used as a simple index to identify soil type. Figure 7.12(a) does not show a clear relationship between the $q_c$ value and the shaft damping ($J_s$) value. The $q_c$ value increased from 857 kPa near ground surface to 3310 kPa near pile toe, while the $J_s$ value increased to its maximum value near the GWT and decreased thereafter. On the other hand, Figure 7.12(b) shows an inverse relationship between the $q_c$ value and the shaft quake ($q_s$) value. Considering that dynamic soil parameters could be influenced by the ground water table, the pore water pressure effect was included by correcting the $q_c$ to a total cone tip resistance ($q_t$) using Eq. (7.7) as suggested by Mayne (2007).

$$q_t = q_c + \mu(1 - a_n) \tag{7.10}$$

where,

$\mu$ = measured pore water pressure, kPa, and

$a_n$ = net area ratio (0.80 was used for Type 2 Piezocone with a section area of 10 $cm^2$).

A similar observation to $q_t$ was noticed in Figure 7.13. Figure 7.14 shows no clear

relationship between the $f_s$ value and the dynamic soil parameters. Similarly, Figure 7.15(a) shows an approximate relationship between the FR value and the $J_s$ value, while Figure 7.15(b) shows a more direct relationship between the FR and the $q_s$ value. All of these observations reveal that the difficulty with quantifying the dynamic soil parameters at the EOD condition using the CPT measured soil properties.

To further expand on the above observations made using ISU5, the shaft damping factors ($J_s$) computed from all test piles in cohesive soils given in Table 7.4 were best represented using FR values as plotted in Figure 7.16. As reported by Mayne (2007), low FR values (less than 1%) were observed in clean quartz sands and siliceous sands, whereas clays and clayey silts of low sensitivity exhibit FR values greater than 4%, and sandy silts and silts fall in between. Figure 7.16 shows that medium to hard cohesive soils with SPT N-value greater than 9 exhibit larger $J_s$ values than soft cohesive soils with SPT N-value smaller than or equal to 9. More importantly, Figure 7.16 shows that the $J_s$ values were dependent on the FR value (i.e., soil type). For medium to hard cohesive soils, the $J_s$ value decreased with increasing FR value (i.e., from sandy silts, silts, clayey silts to clays). However, for soft cohesive soils, the $J_s$ value decreased to a FR value of about 4% (i.e., from sandy silts to silts) and remained almost constant at about 0.08 s/m (0.024 s/ft) for clayey silts and clays. To incorporate the FR value and the SPT N-value for a practical quantification of the $J_s$ value, data points presented in Figure 7.16 were plotted against a ratio of SPT N-value to the FR value (N/FR) as shown in Figure 7.17.

$$J_s(\mathrm{s/m}) = 0.0884\left(\frac{N}{FR}\right) + 0.0133 \text{ ; for EOD} \tag{7.11}$$

A linear relationship given by Eq. (7.11) was established to quantify the $J_s$ value, based on different soil denseness and soil types. On the other hand, Figure 7.18 shows an approximate relationship between the shaft quake value ($q_s$) and the CPT measured unit tip resistance ($q_c$). A similar observation was noticed in Figure 7.19 for the CPT measured unit skin friction ($f_s$). These analytical results reveal that the challenge associated with quantifying the quake value using CPT measured soil properties.

### 7.5.3. Post EOD condition for cohesive soils

Based on the data presented in Table 7.5 for ISU5 and ISU6 determined from matching the PDA records obtained from the last restrikes, average dynamic soil parameters for cohesive soils were determined and plotted against the SPT N-value in Figure 7.8 to Figure 7.11 (represented with open markers). Using these data points, best-fit lines and their corresponding 95% confidence intervals were drawn. The difference between these data points and those determined for the EOD condition suggests that the influence of pile setup on the dynamic soil parameters. Figure 7.8 shows that pile setup increases the damping factors, especially cohesive soils with an SPT N-value greater than 8. The damping factor ($J_s$) at duration for about 8 to 10 days after EOD can be best estimated using Eq. (7.12).

$$J_s(s/m) = 0.0052\ N^{1.7327};\ \text{for 8 to 10 days after EOD} \tag{7.12}$$

A similar observation was observed in terms of the damping coefficient ($c_s$) as shown in Figure 7.9, while the estimation for the $c_s$ value with $R^2$ of 0.66 was not as good as the $J_s$ value with $R^2$ of 0.80. Figure 7.10 reveals that the effect of pile setup increases the quake value ($q_s$), while the amount of increase diminishes in a denser cohesive soil with a relatively higher SPT N-value. This quake value after about 8 to 10 days from EOD can be best estimated using Eq. (7.13), which should be cautiously used, based on a relatively lower $R^2$ of 0.69.

$$q_s(mm) = -6.944\ \ln(N) + 24.177\ ;\ \text{for 8 to 10 days after EOD} \tag{7.13}$$

However, an opposite observation was noticed for soil stiffness ($k_s$) as plotted in Figure 7.11. The effect of pile setup reduces the stiffness, and the amount of reduction enlarges with SPT N-value. The foregoing results conclude that the effect of pile setup increases the dynamic resistance of the soil-pipe system, resulting from a larger damping factor or damping coefficient. Furthermore, the consequence of pile setup provides a larger capability of the soil-pile system to dissipate energy, represented by a larger hysteretic envelop of the linear plastic spring, as a result of a larger quake value or a smaller stiffness (see Figure 7.1).

### 7.5.4. EOD condition for cohesionless soils

Correlation studies between dynamic soil parameters and SPT N-value were also performed for cohesionless soils, referred to as silty sand (SM), well-graded sand (SW), and poorly graded sand (SP) in accordance with Unified Soil Classification System (USCS). As shown in Table 7.4, limited data points were available for the cohesionless soil layers, which presented between 4.02 and 6.34 m depth of ISU6 and below 4.05 m depth of ISU9. Based on these data points, Figure 7.20 shows an inverse relationship between damping factor and SPT N-value, which contradicts the relationship generated using Eq. (7.4) as recommended by Liang (2000). Figure 7.20 shows that the damping factor for cohesionless soils can be best estimated using Eq. (7.14). Furthermore, Figure 7.21 also shows an inverse relationship between the quake value and the SPT N-value, which can be best represented with Eq. (7.15).

$$J_s(s/m) = -0.186\ln(N) + 0.6707 \ ; \text{for EOD} \tag{7.14}$$

$$q_s(mm) = -5.261\ln(N) + 17.943 \ ; \text{for EOD} \tag{7.15}$$

In addition, the 95% confidence intervals of the predicted equations are included. Both figures show the variation of dynamic soil parameters with SPT N-value, as opposed to the constant values recommended by Smith (1962) and Hannigan et al. (1998) given in Table 7.1. Nevertheless, the quantification of these dynamic soil parameters for cohesionless soils can be improved with continuously populated data points in the future.

### 7.5.5. Effect of pile installation

It is important to investigate the effect of pile installation on the aforementioned correlation studies of the dynamic soil parameters for the EOD condition in terms of the SPT N-value measured in a nearly virgin stage of disturbance before the pile installation. Dynamic soil parameters ($J_s$ and $q_s$) were selected from Table 7.4 at three designated locations: (1) within 3 m below ground surface; (2) at mid-depth between 6 and 9 m below ground surface; and (3) within 3 m from pile toe, and were plotted separately in Figure 7.22

(a) and (b) for $J_s$ and $q_s$, respectively. It is expected that the soil near the surface would experience a larger number of repetitive cycles of disturbance from the pile installation than the soils near the mid-depth and pile toe. Figure 7.22 (a) shows the dot-dashed best fit line representing the correlation analysis between $J_s$ and SPT N-value of soil layers within 3 m below the ground surface has the least $R^2$ of 0.35. However, soil layers at mid depth, that experienced relatively lesser amount of disturbance, produced a slightly better correlation with a larger $R^2$ of 0.37. As expected, soil layers within 3 m from the pile toe, that experienced the least amount of disturbance, generated the best correlation study with the highest $R^2$ of 0.66. Besides comparing and contrasting the correlation results on $J_s$ value, similar evaluations were achieved based on the $q_s$ value as shown in Figure 7.22 (b). Similar observations were noticed from which soil layers within 3 m below the surface had the poorest correlation with $R^2$ of only 0.05; the best correlation with $R^2$ of 0.82 occurred at soil layers near pile toe, and correlation for soil layers at mid-depth with $R^2$ of 0.72 fell in between. These observations conclude that the effect of pile installation action on the accuracy of the dynamic soil parameters quantification. Nevertheless, it is impracticable to perform the SPT during different stages of pile installation. Hence, it is assumed that the uncertainty associated with the variation in SPT N-values at different stages of a pile installation was indirectly accounted for during the aforementioned correlation analysis performed based on an average dynamic soil parameter corresponding to the same SPT N-value.

## 7.6. Quantification of Toe Dynamic Soil Parameters

Table 7.6 summarizes the measured soil properties near the pile toe, estimated pile toe resistance, toe damping factor ($J_T$), and toe quake value ($q_T$) determined during the proposed CAPWAP matching process for the EOD condition. A poor relationship was observed between measured soil properties, such as SPT N-value, $q_s$, and $f_s$ values, and the toe dynamic soil parameters. For instance, although the low plasticity clay (CL) at the pile toes of ISU4 and ISU5 had the same SPT N-value and shared similar $q_c$ and $f_s$ values, there was a relative large difference in the $J_T$ and $q_T$ values. This observation became apparent when these dynamic soil parameters for cohesive soils (i.e., for all test piles except ISU9)

were plotted against the SPT N-value in Figure 7.23. Referring to the solid best fit lines of the data points, the poor correlation was substantiated with relative low $R^2$ of 0.40 for the $J_T$ value and $R^2$ of 0.47 for the $q_T$ value. For a comparative purpose, the dynamic soil parameters determined from the default CAPWAP matching procedure for the same test piles were similarly plotted against the same SPT N-value in Figure 7.23. The best fitting of these data points (represented by dashed lines of the open-filled circular markers) generated much lower $R^2$ of 0.16 for the $J_T$ value and $R^2$ of 0.26 for the $q_T$ value. In other words, the proposed CAPWAP matching procedure gives a better estimation of these parameters. Despite the challenge with quantifying toe dynamic soil parameters in terms of any measureable soil properties, the results clearly indicate the toe dynamic soil parameters do not follow the typical constant value included in Table 7.1 as recommended by Smith (1962) and Hannigan et al. (1998).

## 7.7. Validation of Proposed Dynamic Soil Parameters

The foregoing correlation studies not only provided successful quantification of the dynamic soil parameters in terms of SPT N-value, but also the match quality (MQ) of each CAPWAP analysis has not been sacrificed during the proposed CAPWAP matching procedure. In fact, the match qualities, as shown in Table 7.7, have been improved by as high as 20%, based on matching the WaveUp ($W_u$) records (i.e., upward traveling force wave defined by Eq. (7.6)). In addition, the match qualities for matching the force and velocity records have been improved in most cases as shown in Table 7.7. The improvement in matching the measured and computed pile responses validates the proposed approach in quantifying the dynamic soil parameters.

To expand the validation, an independent test pile, ISU8, not used in the aforementioned correlation studies, was selected for the CAPWAP analysis, based on the shaft dynamic soil parameters estimated using the proposed equations described in Sections 7.5.1 and 7.5.3 for cohesive and cohesionless soil layers, respectively. Since the actual pile resistance was not measured using a static load test at EOD, the pile resistance of 621 kN estimated using the default CAPWAP matching procedure was maintained, while the

comparison was assessed in terms of match quality as shown in Table 7.7. The application of the proposed shaft dynamic soil parameters, while keeping the toe dynamic soil parameters closer to the values suggested by Smith (1962) during the CAPWAP analysis, has improved the match quality by 19%. This study further validates the proposed method in quantifying the dynamic soil parameters.

## 7.8. Summary and Conclusions

Although dynamic analysis methods have been used in estimating axial pile resistances, the accuracy of these methods is highly dependent upon the proper input of suitable dynamic soil parameters. Unfortunately, these parameters have not been successfully quantified in terms of any measured soil properties, due to a large degree of scatter in the collected parameters resulting from the current default CAPWAP matching procedure, where constant parameters are assumed along the entire pile shaft. In addition, due to the indeterminate nature of the CAPWAP analysis, the dynamic soil parameters cannot be uniquely quantified. As a result, a possible range of damping factors and quake values are recommended in CAPWAP by Pile Dynamic, Inc. (2000). In fact, many researchers have urged the use of improved or better represented dynamic soil parameters in the analysis. To improve the CAPWAP analysis, a new matching procedure, with variation in shaft dynamic soil parameters based on empirical equations, was developed.

The results show that the dynamic soil parameters are not constant along the pile depth, but they vary with different types and properties of soils. For cohesive soils at the EOD condition, the correlation studies revealed a direct relationship between the shaft damping factor and the SPT N-value and an inverse relationship between the shaft quake value and the SPT N-value. Empirical equations were established to quantify these shaft dynamic soil parameters in terms of SPT N-value. Furthermore, correlation studies using CPT measured soil properties concluded that the shaft damping factor was influenced by different soil types. On the other hand, no relationship was observed between the shaft quake value and the CPT measured soil properties. It is believed that the similar process for SPT to pile driving, both subjected to a continuous impulsive hammer force, explains the better

correlation between dynamic soil parameters and SPT N-value.

Pile setup increases the dynamic soil parameters for cohesive soils, which increase the dynamic resistance and provide a larger energy dissipation capability of the soil-pile system. For cohesionless soils at the EOD condition, an inverse relationship between the shaft dynamic soil parameters and the SPT N-value was observed, and empirical equations in terms of SPT N-value were developed for their quantifications. Furthermore, correlation studies performed for soil models at three different locations concluded the influence of pile installation on the shaft dynamic soil parameters estimation with the highest accuracy for soils near pile toe and lowest accuracy for soils near ground surface. The results of similar correlation studies on toe dynamic soil parameters suggested that the difficulty and challenge in quantifying these parameters in terms of measureable soil properties.

The proposed CAPWAP signal matching procedure, based on variation in shaft dynamic soil parameters, not only provides comparable pile resistance estimation but also improves the match quality, indicating the accuracy of matching the measured pile responses. The application of these parameters was validated based on an independent CAPWAP analysis performed on the test pile ISU8 with a 19% match quality improvement. Although the quantification of these dynamic soil parameters was developed based on a static soil resistance distribution estimated using the Schmertmann's (1978) method, the methodology presented in this paper can be adopted for other static analysis methods.

## 7.9. Acknowledgments

The authors would like to thank the Iowa Highway Research Board for sponsoring the research presented in this paper. We would like to thank the members of the Technical Advisory Committee: Ahmad Abu-Hawash, Bob Stanley, Curtis Monk, Dean Bierwagen, Gary Novey, John Rasmussen, Ken Dunker, Kyle Frame, Lyle Brehm, Michael Nop, and Steve Megivern of this research project for their guidance. Special thanks are due to Sherif S. AbdelSalam, Matthew Roling, and Douglas Wood for their assistance with the field tests and to Donald Davidson and Erica Velasco for their assistance with the laboratory soil tests.

## 7.10. References

Computers and Structures, Inc. (CSI). (2008). CSI Analysis Reference Manual For SAP2000®, ETABS®, and SAFE®. Berkeley, CA.

Coyle, H. M, Bartoskewitz, R. E., and Berger, W. J. (1973). "Bearing Capacity by Wave Equation Analysis – State of Art." Texas Transportation Institute, Texas A & M University, August.

Hannigan, P.J., Goble, G.G., Thendean, G., Likins, G.E. and Rausche, F. (1998). Design and Construction of Driven Pile Foundations – Volumn II, FHWA-HI-97-013. National Highway Institute, Federal Highway Administration, U.S. Department of Transportation, Washington, D.C.

Malkawi, A. I. H. and Ayasrah, I. M. (2000). "Identification of Soil-Pile Model Interaction Parameters from Recorded Time-Displacement Signals." Application of Stress-Wave Theory to Piles: Quality Assurance on Land and Offshore Piling: At Taylor & Francis, Balkema, Rotterdam, September, pp. 233-240.

Mayne, P. W. (2007). Cone Penetration Test: A Synthesis of Highway Practice. NCHRP Synthesis 368, Transportation Research Board, Washington, D.C.

McVay, Michael, and Ching Kuo. (1999). Estimate Damping and Quake by Using Traditional Soil Testing. Department of Civil Engineering, University of Florida, Gainesville, FL.

Ng, K. W., Suleiman, M. T., Sritharan, S., Roling, M., and AbdelSalam, S. S. (2011). Development of LRFD Design Procedures for Bridge Pile Foundations in Iowa – Field Testing of Steel Piles in Clay, Sand and Mixed soils and Data Analysis. Final Report Vol. II. IHRB Project No. TR-573. Institute of Transportation, Iowa State Univeristy, Ames, IA.

Paikowsky, S. G., Regan, J. E., and McDonnell, J. J. (1994). A Simplified Field Method for Capacity Evaluation of Driven Piles. FHWA-RD-94-042. Federal Highway Administration, U.S. Department of Transportation, Washington, D.C.

Pile Dynamic, Inc. (2000). CAPWAP for Windows Manual. Pile Dynamic, Inc., Cleveland, OH.

Liang, Y. (2000). "Correlation Study of Smith Damping Coefficient and SPT Blow Count."

Application of Stress-Wave Theory to Piles: Quality Assurance on Land and Offshore Piling: At Taylor & Francis, Balkema, Rotterdam, September, pp. 461-467.

Liang, Y. and Sheng Y. (1993). "Wave Equation Parameters from Driven-Rod Test." Journal of Geotechnical Engineering, ASCE, Vol.119, No.6, June, pp. 1037-1057.

Roling, M. J. (2010). Establishment of a Suitable Dynamic Pile Driving Formula for the Construction Control of Iowa Driven Pile Foundations and its Calibration for Load and Resitance Factor Design. Master Thesis. Department of Civil, Construction, and Environmental Engineering, Iowa State University, Ames, IA.

Schmertmann, J.H. (1978). Guidelines for Cone Penetration Test, Performance and Design. Report No. FHWA-TS-78-209, U.S. Department of Transportation, Washington, D.C., 145 pp.

Smith, E. A. L. (1962). "Pile-Driving Analysis by the Wave Equation." Journal of the Soil Mechanics and Foundations Division, ASCE, Paper No. 3306, Vol. 127, Part 1, pp. 1145-1193.

Svinkin, M. R. and Woods, R. D. (1998). "Accuracy of Determining Pile Capacity by Dynamic Methods." Proceeding of the 7th International Conference and Exhibition on Piling and Deep Foundations, Deep Foundation Institute, 15th to 17th June, Palais, Ferstel, Vienna, Austria, pp. 1.2.1-1.2.8.

Table 7.1: Summary of suggested dynamic soil parameters found in the literature

| Reference | Damping Factor (s/m) | | Quake Value (mm) | |
|---|---|---|---|---|
| | Shaft ($J_S$) | Toe ($J_T$) | Shaft ($q_S$) | Toe ($q_T$) |
| Smith (1962) | 0.16 | 0.49 | 2.54 | 2.54 |
| Coyle et al. (1973) | 0.66 for clay<br>0.16 for sand<br>0.33 for silt | 0.03 for clay<br>0.49 for sand<br>0.49 for silt | 2.54 | 2.54 |
| Hannigan et al. (1998) | 0.66 for cohesive soil<br>0.16 for non-cohesive soil | 0.49 | 2.54 | D/120 for dense and hard soil<br>D/60 for soft soil |

D = Pile width or diameter in mm.

Table 7.2: Statistical summary for dynamic soil parameters (after Liang, 2000)

| Soil Type | Parameters | Statistical Summary | EOD Condition | BOR Condition |
|---|---|---|---|---|
| Sand | $J_S$ (s/m) | Mean | 0.53 | 0.67 |
| | | Std. Dev. | 0.53 | 0.53 |
| | $J_T$ (s/m) | Mean | 0.43 | 0.80 |
| | | Std. Dev. | 0.43 | 0.90 |
| | $q_S$ (mm) | Mean | 3.0 | 3.0 |
| | | Std. Dev. | 4.6 | 3.8 |
| | $q_T$ (mm) | Mean | 6.4 | 5.8 |
| | | Std. Dev. | 3.6 | 3.3 |
| Clay | $J_S$ (s/m) | Mean | 0.43 | 0.73 |
| | | Std. Dev. | 0.40 | 0.53 |
| | $J_T$ (s/m) | Mean | 0.30 | 0.67 |
| | | Std. Dev. | 0.17 | 0.53 |
| | $q_S$ (mm) | Mean | 2.8 | 3.0 |
| | | Std. Dev. | 1.3 | 1.5 |
| | $q_T$ (mm) | Mean | 6.4 | 5.3 |
| | | Std. Dev. | 4.8 | 2.0 |

Table 7.3: Comparison of average damping factors obtained from CAPWAP on test piles and WEAP on SPT (after Liang, 2000)

| SPT Hammer Efficiency | Shaft Damping Factor, $J_S$ (s/m) | | | Toe Damping Factor, $J_T$ (s/m) | | |
|---|---|---|---|---|---|---|
| | CAPWAP (Test Pile) | WEAP (SPT) | Adjusted WEAP (SPT) | CAPWAP (Test Pile) | WEAP (SPT) | Adjusted WEAP (SPT) |
| 60% | 0.58 | 0.59 | 0.59 | 0.36 | 0.95 | 0.95×0.42 = 0.39 |
| 70% | 0.58 | 0.74 | 0.74×0.79 = 0.59 | 0.36 | 1.17 | 1.17×0.35 = 0.39 |

Table 7.4: Summary of measured soil properties, estimated soil resistances, and dynamic soil parameters estimated based on the proposed matching procedure at EOD along the pile shaft

| Test Pile | Depth Below Ground (m) | Soil Type-USCS | Ave. CPT Unit Tip Resis., $q_c$ (kPa) | Ave. CPT Unit Skin Friction, $f_s$ (kPa) | Ave. Friction Ratio, FR (%) | Ave. SPT N-value | Est. Soil Resis., $R_s$ (kN) | Shaft Damping Factor, $J_s$ (s/m) | Shaft Quake Value, $q_s$ (mm) | Damping Coeff. Based On Liang (2000) Eq. (7.3), $c_s$ (kN-s/m) |
|---|---|---|---|---|---|---|---|---|---|---|
| ISU2 | 1.13 | CL/SC | 2721 | 118 | 4.65 | 3 | 31 | 0.24 | 5.08 | 2.92 |
| | 2.32 | | 1852 | 87 | 4.84 | 3 | 28 | 0.27 | 4.83 | 2.64 |
| | 3.51 | | 783 | 37 | 4.10 | 3 | 17 | 0.28 | 5.33 | 1.67 |
| | 4.66 | CL | 823 | 29 | 3.15 | 8 | 12 | 0.11 | 2.03 | 2.73 |
| | 5.85 | | 1420 | 40 | 2.64 | 14 | 14 | 0.21 | 0.76 | 5.20 |
| | 7.04 | | 941 | 24 | 2.44 | 8 | 16 | 0.10 | 2.29 | 3.74 |
| | 8.20 | | 956 | 25 | 2.55 | 3 | 19 | 0.07 | 6.35 | 1.83 |
| | 9.39 | | 983 | 27 | 2.58 | 3 | 17 | 0.08 | 6.35 | 1.62 |
| | 10.58 | | 1004 | 28 | 2.60 | 3 | 19 | 0.07 | 5.08 | 1.86 |
| | 11.73 | | 1275 | 56 | 4.13 | 4 | 25 | 0.05 | 5.08 | 3.13 |
| | 12.92 | | 1522 | 75 | 4.86 | 4 | 26 | 0.05 | 5.08 | 3.23 |
| | 14.11 | | 2582 | 54 | 2.65 | 4 | 26 | 0.06 | 5.08 | 3.33 |
| | 15.27 | | 2189 | 52 | 2.48 | 4 | 26 | 0.06 | 5.08 | 3.24 |
| | 16.46 | | 1182 | 34 | 2.61 | 8 | 22 | 0.11 | 2.54 | 5.17 |
| ISU3 | 0.61 | CL/SC | 6696 | 128 | 3.64 | 8 | 41 | 0.29 | 2.54 | 5.17 |
| | 1.77 | CL | 1623 | 108 | 7.41 | 8 | 40 | 0.32 | 3.56 | 9.49 |
| | 2.96 | | 1516 | 53 | 4.84 | 8 | 37 | 0.19 | 2.54 | 8.73 |
| | 4.11 | CL/SM | 3746 | 139 | 3.86 | 11 | 35 | 0.09 | 0.76 | 10.82 |
| | 5.27 | CL | 1819 | 37 | 2.09 | 5 | 32 | 0.14 | 5.33 | 4.95 |
| | 6.46 | | 1682 | 36 | 2.10 | 5 | 35 | 0.13 | 5.33 | 5.38 |
| | 7.62 | | 1671 | 43 | 2.48 | 7 | 36 | 0.14 | 4.83 | 7.65 |
| | 8.78 | | 1092 | 24 | 2.07 | 7 | 26 | 0.19 | 4.83 | 5.50 |
| | 9.97 | | 916 | 15 | 1.53 | 12 | 20 | 0.80 | 1.52 | 6.62 |
| | 11.13 | | 1804 | 36 | 1.92 | 12 | 33 | 0.67 | 1.78 | 11.00 |
| | 12.28 | | 1719 | 29 | 1.61 | 9 | 30 | 0.28 | 1.52 | 7.85 |
| | 13.47 | | 1318 | 22 | 1.52 | 10 | 25 | 0.73 | 1.52 | 7.10 |
| | 14.63 | | 2278 | 113 | 4.85 | 10 | 40 | 0.50 | 1.52 | 11.55 |
| ISU4 | 0.58 | CL/SC | 2188 | 105 | 7.01 | 3 | 15 | 0.74 | 6.60 | 1.47 |
| | 1.92 | | 1435 | 58 | 4.06 | 3 | 26 | 0.27 | 6.86 | 2.48 |
| | 3.29 | SW-SC | 1223 | 18 | 2.98 | 4 | 16 | 0.33 | 4.83 | 1.98 |
| | 4.63 | CL/SM | 978 | 6 | 0.62 | 5 | 11 | 0.39 | 4.32 | 1.72 |
| | 5.97 | CL/SW | 1384 | 6 | 0.41 | 6 | 18 | 0.39 | 3.05 | 3.26 |
| | 7.32 | CL | 3679 | 146 | 4.36 | 11 | 37 | 0.35 | 2.54 | 11.64 |
| | 8.69 | | 3100 | 165 | 5.32 | 11 | 46 | 0.28 | 2.54 | 14.37 |
| | 10.03 | | 2541 | 171 | 6.74 | 14 | 41 | 0.32 | 1.02 | 15.78 |
| | 11.37 | | 2640 | 167 | 6.32 | 12 | 45 | 0.29 | 1.27 | 15.27 |
| | 12.71 | | 2154 | 89 | 4.06 | 10 | 37 | 0.39 | 1.27 | 10.80 |
| | 14.08 | | 2213 | 76 | 3.25 | 11 | 40 | 0.42 | 1.27 | 12.38 |
| | 15.42 | | 2137 | 69 | 3.12 | 12 | 37 | 0.50 | 1.02 | 12.59 |
| | 16.76 | | 2157 | 91 | 3.12 | 13 | 35 | 0.57 | 1.02 | 12.56 |

Table 7.4: (continue)

| Test Pile | Depth Below Ground (m) | Soil Type-USCS | Ave. CPT Unit Tip Resis., $q_c$ (kPa) | Ave. CPT Unit Skin Friction, $f_s$ (kPa) | Ave. Friction Ratio, FR (%) | Ave. SPT N-value | Est. Soil Resis., $R_s$ (kN) | Shaft Damping Factor, $J_s$ (s/m) | Shaft Quake Value, $q_s$ (mm) | Damping Coeff. Based On Liang (2000) Eq. (7.3), $c_s$ (kN-s/m) |
|---|---|---|---|---|---|---|---|---|---|---|
| | 0.82 | ML/SC | 2185 | 68 | 3.49 | - | 33 | 2.57 | 0.51 | 3.22 |
| | 2.44 | | 857 | 59 | 7.06 | 6 | 68 | 0.09 | 5.59 | 12.38 |
| | 4.02 | | 1482 | 124 | 8.59 | 8 | 71 | 0.09 | 4.32 | 16.76 |
| | 5.61 | CL | 1318 | 110 | 8.80 | 9 | 71 | 0.08 | 4.06 | 18.78 |
| | 7.19 | | 1779 | 113 | 6.37 | 9 | 71 | 0.10 | 4.06 | 18.75 |
| ISU5 | 8.81 | | 1741 | 112 | 6.55 | 10 | 72 | 0.29 | 3.30 | 20.65 |
| | 10.39 | | 1604 | 97 | 6.13 | 22 | 69 | 0.59 | 1.02 | 37.40 |
| | 11.98 | CL/SC | 2334 | 126 | 5.35 | 22 | 70 | 1.65 | 1.78 | 38.06 |
| | 13.56 | | 3468 | 155 | 4.47 | 15 | 77 | 0.36 | 1.78 | 31.33 |
| | 15.18 | CL | 3310 | 128 | 3.97 | 13 | 76 | 0.32 | 2.03 | 27.28 |
| | 16.76 | | 3310 | 127 | 3.72 | 13 | 74 | 0.31 | 2.03 | 26.56 |
| | 0.52 | | 5581 | 87 | 2.08 | 12 | 27 | 0.19 | 5.84 | 4.84 |
| | 1.68 | CL/SC | 2361 | 118 | 5.07 | 12 | 33 | 0.11 | 5.33 | 11.05 |
| | 2.83 | | 2156 | 81 | 4.05 | 12 | 36 | 0.11 | 6.35 | 11.97 |
| | 4.02 | CL/SM | 1149 | 56 | 5.27 | 12 | 33 | 0.11 | 6.10 | 11.11 |
| | 5.18 | SM | 8279 | 77 | 1.04 | 23 | 99 | 0.03 | 2.54 | 29.37 |
| | 6.34 | | 5559 | 58 | 1.63 | 23 | 73 | 0.04 | 2.54 | 21.86 |
| | 7.53 | | 1510 | 46 | 3.61 | 8 | 34 | 0.11 | 4.32 | 7.96 |
| ISU6 | 8.69 | | 979 | 44 | 4.62 | 8 | 32 | 0.06 | 4.32 | 7.55 |
| | 9.85 | | 2582 | 60 | 3.27 | 10 | 42 | 0.09 | 3.56 | 12.07 |
| | 11.03 | | 1626 | 62 | 3.82 | 16 | 36 | 0.49 | 0.76 | 15.28 |
| | 12.19 | CL | 2147 | 81 | 3.76 | 23 | 34 | 0.48 | 0.51 | 18.87 |
| | 13.35 | | 2250 | 83 | 3.65 | 23 | 33 | 0.53 | 0.51 | 18.65 |
| | 14.54 | | 2241 | 78 | 3.44 | 23 | 35 | 0.49 | 0.51 | 19.92 |
| | 15.70 | | 2302 | 78 | 3.42 | 23 | 34 | 0.52 | 0.51 | 19.07 |
| | 16.86 | | 4349 | 150 | 3.25 | 22 | 35 | 0.50 | 0.51 | 18.87 |
| | 2.01 | CL/SC | 4280 | 91 | 3.86 | 8 | 34 | 0.71 | 6.60 | 8.07 |
| | 4.05 | | 1118 | 66 | 5.74 | 4 | 9 | 1.31 | 4.32 | 1.15 |
| | 6.13 | | 8476 | 64 | 1.83 | 6 | 69 | 0.32 | 9.40 | 6.70 |
| ISU9 | 8.17 | SW | 10252 | 58 | 0.57 | 7 | 84 | 0.32 | 8.38 | 9.34 |
| | 10.21 | | 12517 | 69 | 0.55 | 11 | 102 | 0.31 | 5.08 | 16.91 |
| | 12.28 | SP | 14925 | 64 | 0.43 | 13 | 125 | 0.10 | 1.27 | 23.78 |
| | 14.27 | SW | 27415 | 185 | 0.59 | 24 | 233 | 0.10 | 1.02 | 70.60 |

Table 7.5: Summary of measured soil properties, estimated soil resistances, and dynamic soil parameters estimated based on the proposed matching procedure at BOR along the pile shaft

| Test Pile | Depth Below Ground (m) | Soil Type-USCS | Aver. CPT Unit Tip Resis., $q_c$ (kPa) | Ave. CPT Unit Skin Friction, $f_s$ (kPa) | Ave. Friction Ratio, FR (%) | Ave. SPT N-value | Est. Soil Resis., $R_s$ (kN) | Shaft Damping Factor, $J_s$ (s/m) | Shaft Quake Value, $q_s$ (mm) |
|---|---|---|---|---|---|---|---|---|---|
| ISU5 (BOR6 = 8 days after EOD) | 1.10 | ML/SC | 1744 | 60 | 4.48 | 6 | 53 | 0.76 | 0.76 |
| | 2.44 | CL | 921 | 63 | 7.05 | 8 | 76 | 0.16 | 11.18 |
| | 3.78 | | 1392 | 117 | 8.65 | 8 | 78 | 0.16 | 11.18 |
| | 5.15 | | 1432 | 118 | 8.72 | 8 | 86 | 0.15 | 11.68 |
| | 6.49 | | 1468 | 99 | 6.98 | 9 | 78 | 0.16 | 10.41 |
| | 7.83 | | 1953 | 132 | 6.84 | 10 | 84 | 0.21 | 8.64 |
| | 9.17 | | 1678 | 101 | 6.12 | 10 | 77 | 0.41 | 6.86 |
| | 10.55 | | 1589 | 96 | 6.13 | 22 | 81 | 0.98 | 2.79 |
| | 11.89 | CL/SC | 2375 | 129 | 5.38 | 21 | 82 | 1.07 | 2.79 |
| | 13.23 | CL | 3547 | 162 | 4.58 | 15 | 85 | 0.92 | 3.05 |
| | 14.57 | | 3190 | 132 | 4.13 | 13 | 76 | 0.85 | 3.05 |
| | 15.91 | | 3830 | 127 | 3.72 | 13 | 94 | 0.82 | 3.05 |
| | 17.28 | | 3830 | 127 | 3.72 | 13 | 86 | 0.57 | 3.05 |
| ISU6 (BOR8 = 10 days after EOD) | 1.07 | CL/SC | 3851 | 100 | 3.58 | 12 | 51 | 0.25 | 12.70 |
| | 2.26 | | 2404 | 117 | 5.05 | 12 | 62 | 0.09 | 11.43 |
| | 3.41 | | 1727 | 56 | 3.67 | 12 | 54 | 0.09 | 10.16 |
| | 4.57 | SM | 3238 | 50 | 3.76 | 12 | 63 | 0.09 | 10.16 |
| | 5.76 | | 8811 | 85 | 0.96 | 23 | 110 | 0.02 | 0.51 |
| | 6.92 | CL | 2911 | 49 | 2.68 | 8 | 58 | 0.14 | 9.65 |
| | 8.08 | | 1064 | 43 | 4.56 | 8 | 55 | 0.20 | 9.65 |
| | 9.27 | | 2446 | 54 | 3.25 | 10 | 54 | 0.41 | 8.13 |
| | 10.42 | | 1483 | 57 | 3.96 | 16 | 53 | 0.45 | 7.11 |
| | 11.58 | | 1895 | 74 | 3.85 | 23 | 56 | 1.07 | 5.84 |
| | 12.77 | | 2264 | 84 | 3.68 | 23 | 56 | 1.14 | 5.33 |
| | 13.93 | | 2243 | 80 | 3.54 | 23 | 54 | 1.28 | 5.33 |
| | 15.09 | | 2198 | 77 | 3.49 | 23 | 57 | 1.16 | 2.03 |
| | 16.28 | | 2649 | 77 | 2.93 | 23 | 55 | 0.93 | 2.29 |
| | 17.43 | | 5536 | 233 | 4.24 | 22 | 52 | 0.65 | 2.29 |

Table 7.6: Summary of measured soil properties, estimated soil resistances, and dynamic soil parameters estimated based on the proposed matching procedure at EOD near the pile toe

| Test Pile | Soil Type-USCS | CPT Unit Tip Resistance, $q_c$ (kPa) | CPT Unit Skin Friction, $f_s$ (kPa) | SPT N-value | Estimated Toe Resistance, $R_s$ (kN) | Toe Damping Factor, $J_T$ (s/m) | Toe Quake Value, $q_T$ (mm) |
|---|---|---|---|---|---|---|---|
| ISU2 | CL | 1182 | 34 | 12 | 64 | 1.04 | 25.40 |
| ISU3 | CL | 2278 | 113 | 10 | 15 | 0.64 | 1.27 |
| ISU4 | CL | 2157 | 91 | 13 | 48 | 0.08 | 4.83 |
| ISU5 | CL | 3310 | 127 | 13 | 38 | 1.31 | 1.02 |
| ISU6 | ML | 4349 | 150 | 22 | 29 | 0.08 | 20.83 |
| ISU9 | SW | 27415 | 185 | 24 | 95 | 1.02 | 18.30 |

Table 7.7: Comparison between the default and proposed CAPWAP matching procedures in terms of match quality

| Test Pile | EOD/BOR | Match Quality (MQ) | | | | | | Percent Gain (WaveUp) |
|---|---|---|---|---|---|---|---|---|
| | | Default CAPWAP Procedure | | | Proposed CAPWAP Procedure | | | |
| | | Force | Velocity | WaveUp | Force | Velocity | WaveUp | |
| ISU2 | EOD | 10.38 | 6.89 | 4.48 | 8.92 | 6.55 | 3.60 | 20% |
| ISU3 | EOD | 4.43 | 3.43 | 3.47 | 4.10 | 3.24 | 3.48 | 0% |
| ISU4 | EOD | 5.20 | 2.55 | 2.68 | 3.89 | 2.53 | 2.64 | 1% |
| ISU5 | EOD | 2.06 | 1.07 | 1.16 | 5.74 | 0.98 | 1.04 | 10% |
| | BOR6 | 1.73 | 1.91 | 1.42 | 1.83 | 1.49 | 1.39 | 2% |
| ISU6 | EOD | 3.88 | 2.26 | 2.16 | 3.78 | 2.79 | 2.08 | 4% |
| | BOR8 | 1.35 | 1.12 | 1.22 | 1.63 | 1.00 | 1.19 | 2% |
| ***ISU8*** | ***EOD*** | ***2.74*** | ***2.07*** | ***1.96*** | ***2.61*** | ***2.08*** | ***1.59*** | ***19%*** |
| ISU9 | EOD | 2.39 | 2.06 | 1.96 | 2.46 | 1.97 | 1.80 | 8% |

Table 7.8: Summary of soil profile and dynamic soil parameters estimated using proposed equations for ISU8 at EOD

| Test Pile | Depth Below Ground (m) | Soil Type-USCS | Ave.CPT Unit Tip Resistance, $q_c$ (kPa) | Ave. CPT Unit Skin Friction, $f_s$ (kPa) | Ave. CPT friction ratio, FR (%) | Ave. SPT N-value | Est. Soil Resistance, $R_s$ (kN) | Damping Factor, $J_s$ (s/m) | Quake Value, $q_s$ (mm) |
|---|---|---|---|---|---|---|---|---|---|
| ISU8 | 0.40 | CL | 1195 | 57 | 4.37 | 5 | 6 | 0.11 | 4.79 |
| | 1.58 | | 967 | 63 | 6.66 | 5 | 23 | 0.11 | 4.79 |
| | 2.74 | | 1887 | 97 | 5.28 | 6 | 23 | 0.13 | 4.20 |
| | 3.90 | | 1340 | 77 | 5.92 | 5 | 21 | 0.11 | 4.79 |
| | 5.09 | | 1059 | 41 | 4.02 | 4 | 20 | 0.08 | 5.45 |
| | 6.25 | | 1125 | 44 | 3.88 | 5 | 20 | 0.11 | 4.79 |
| | 7.41 | | 846 | 29 | 3.28 | 2 | 16 | 0.04 | 7.07 |
| | 8.60 | | 3342 | 29 | 1.13 | 2 | 22 | 0.04 | 7.07 |
| | 9.75 | SW | 4977 | 29 | 0.57 | 2 | 31 | 0.54 | 14.30 |
| | 10.91 | | 21257 | 133 | 0.65 | 2 | 163 | 0.54 | 14.30 |
| | 12.10 | CL | 11650 | 89 | 1.64 | 11 | 96 | 0.27 | 2.19 |
| | 13.26 | | 4000 | 74 | 2.28 | 11 | 26 | 0.27 | 2.19 |
| | 14.42 | | 3971 | 78 | 2.38 | 10 | 26 | 0.24 | 2.50 |
| | 15.61 | | 2789 | 68 | 2.59 | 17 | 23 | 0.46 | 1.01 |
| | 16.76 | | 3655 | 154 | 3.93 | 24 | 23 | 0.69 | 0.40 |
| | Toe | | 3655 | 154 | 3.93 | 21 | 82 | 0.42 | 2.03 |

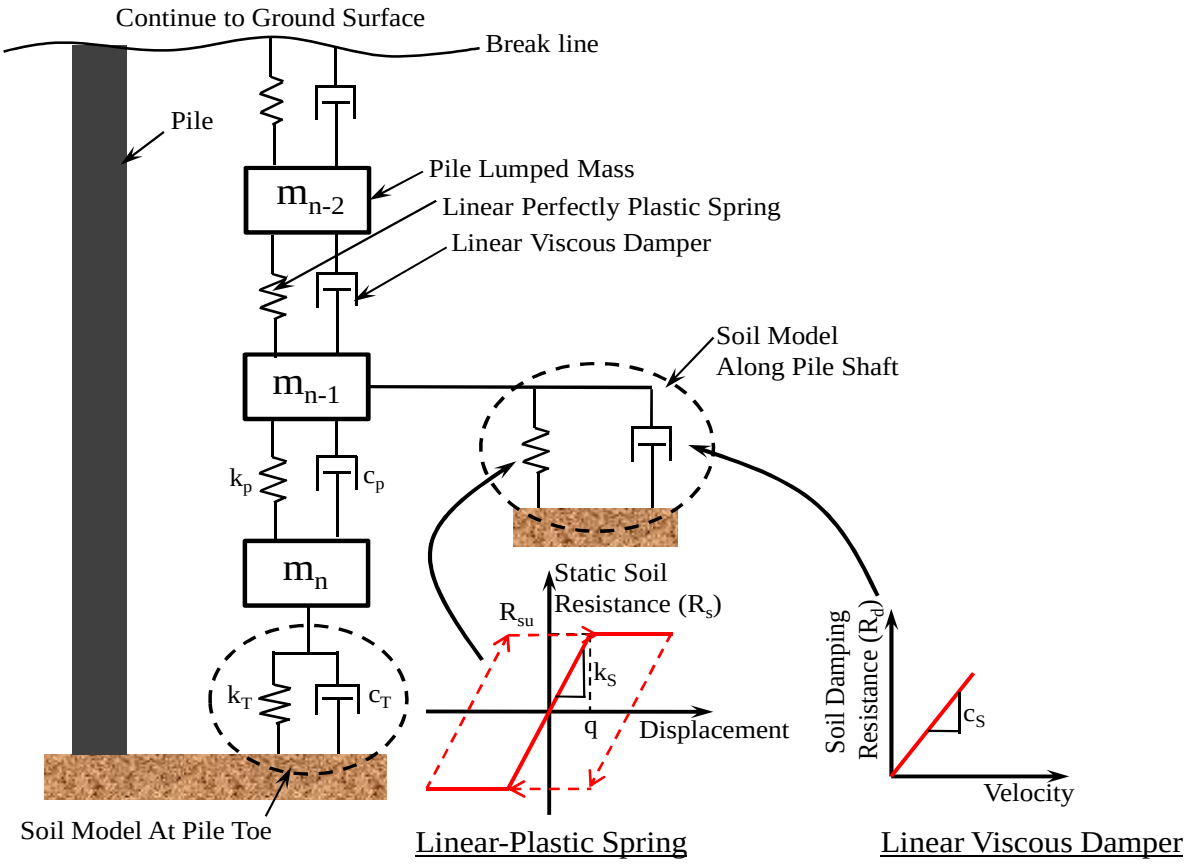


Figure 7.1: One-dimensional soil-pile model

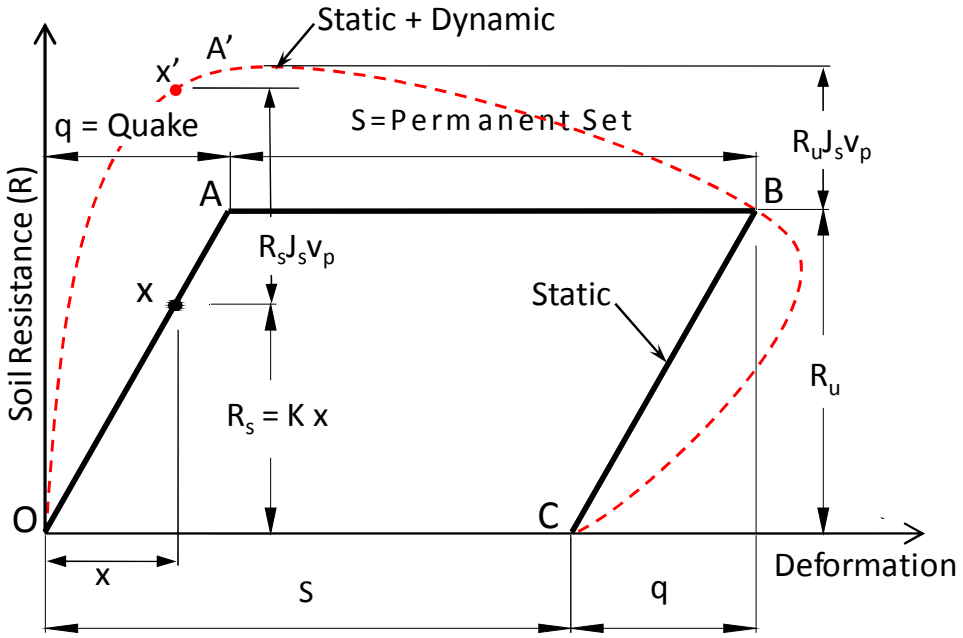


Figure 7.2: Static and dynamic soil resistances at a pile point (after Smith, 1962)

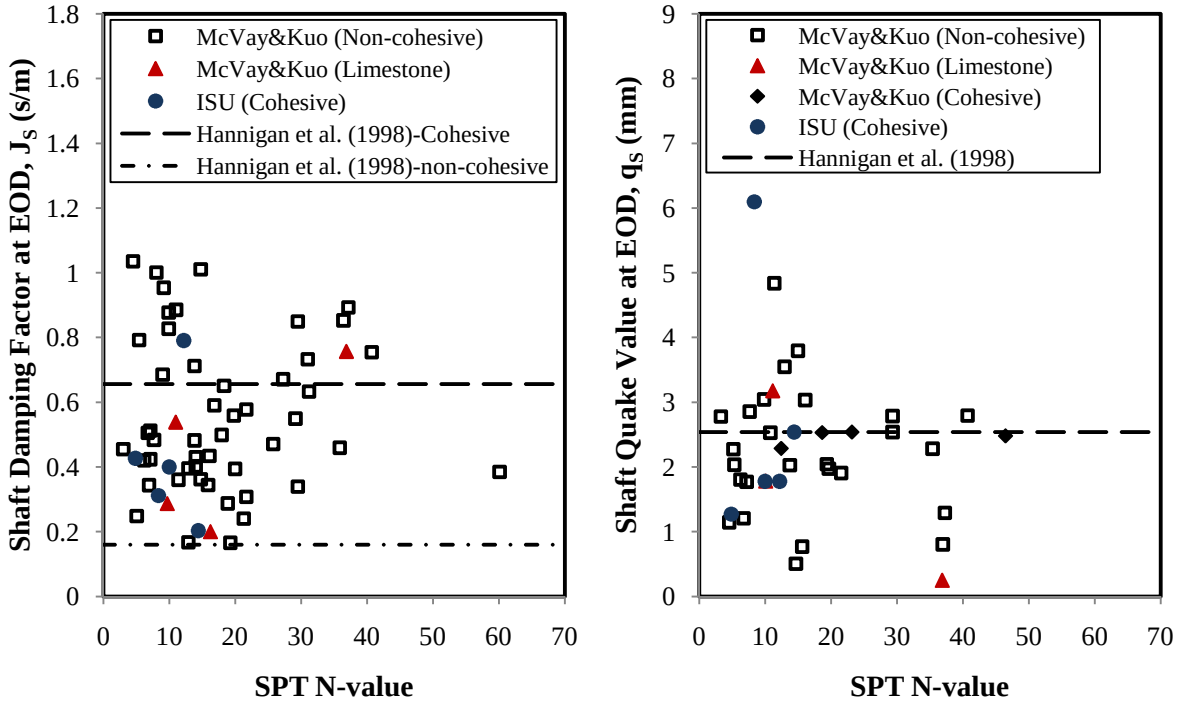


(a) $J_s$ versus SPT N-value (b) $q_s$ versus SPT N-value

Figure 7.3: SPT N-values versus (a) shaft damping factors; and (b) shaft quake values

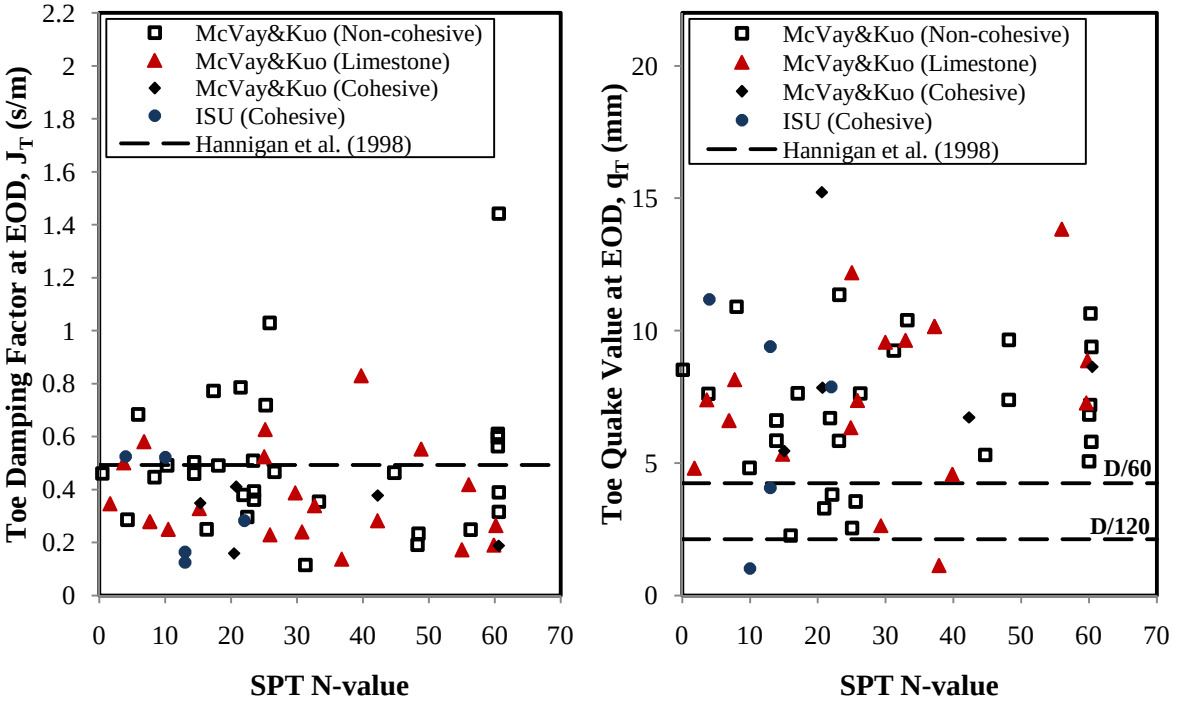


(a) $J_T$ versus SPT N-value (b) $q_T$ versus SPT N-value

Figure 7.4: SPT N-values versus (a) toe damping factors; and (b) toe quake values

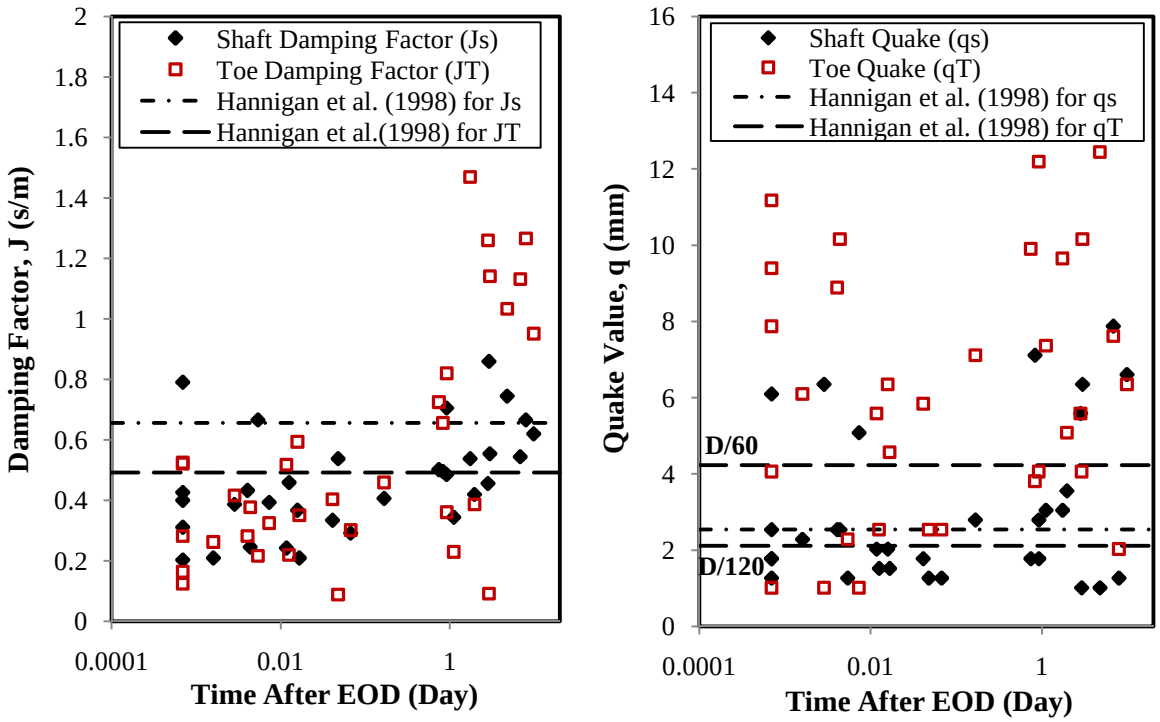


(a) J versus Time (b) q versus Time

Figure 7.5: Time measured after EOD versus (a) damping factors; and (b) quake values obtained from recently completed field tests using CAPWAP for cohesive soils

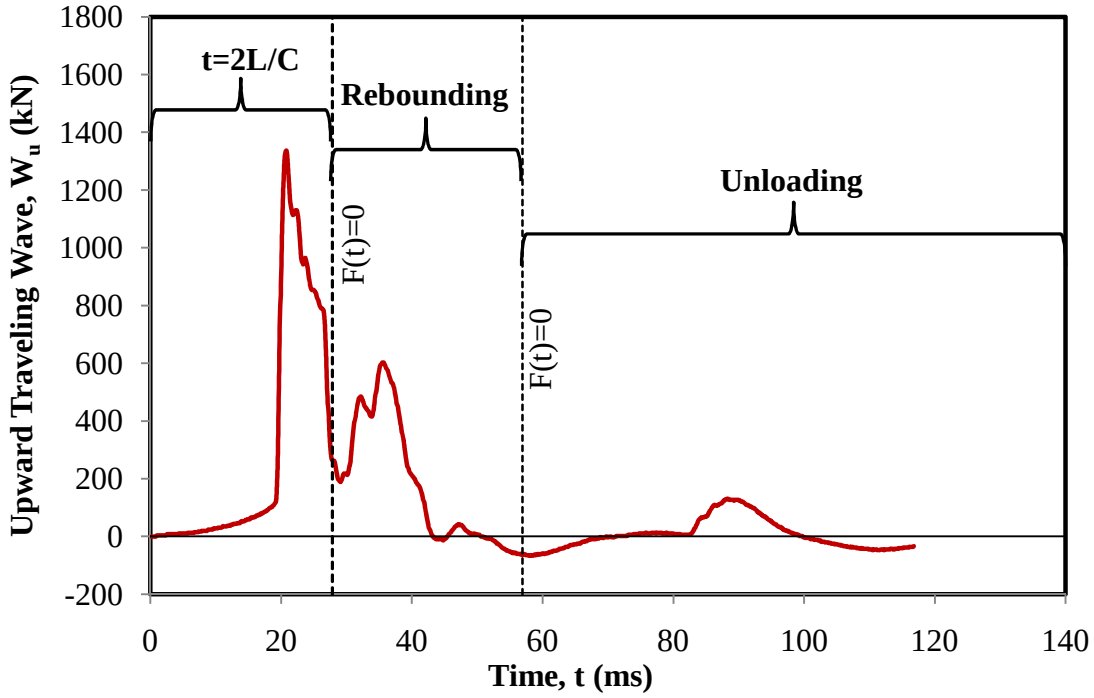


Figure 7.6: Typical upward traveling wave force ($W_u$) collected from the field tests

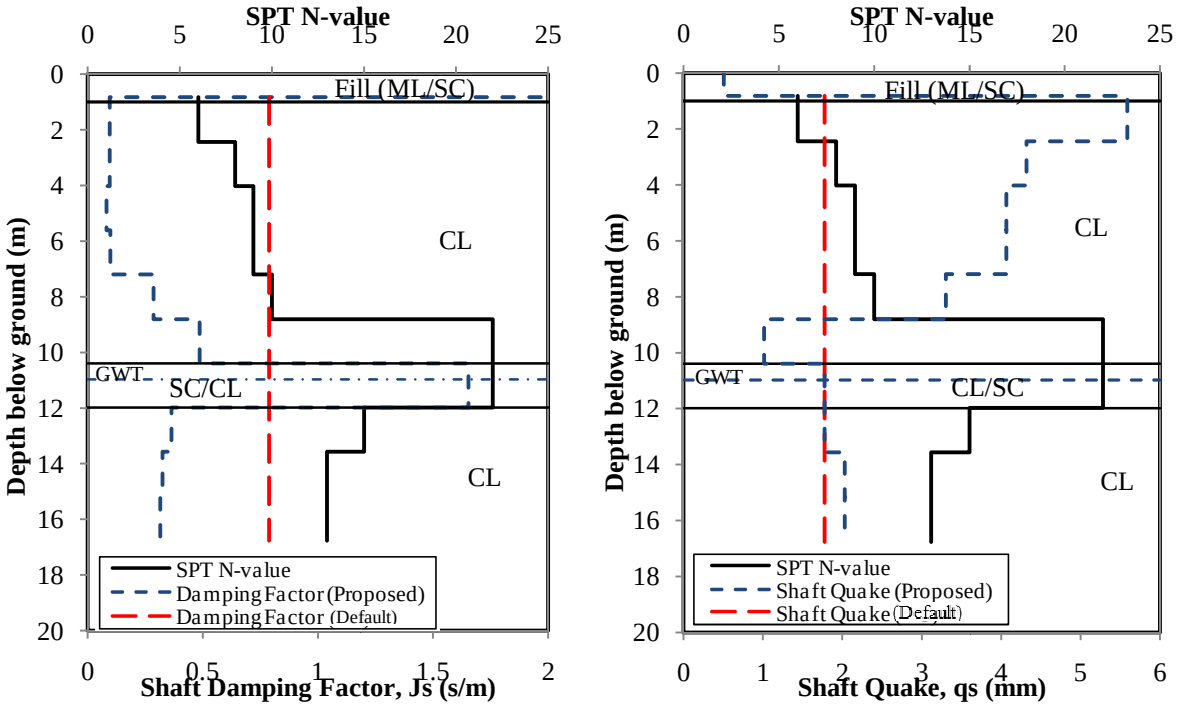


(a) $J_s$ versus SPT N-value (b) $q_s$ versus SPT N-value

Figure 7.7: SPT N-values versus (a) shaft damping factors; and (b) shaft quake values along the embedded pile length of ISU5

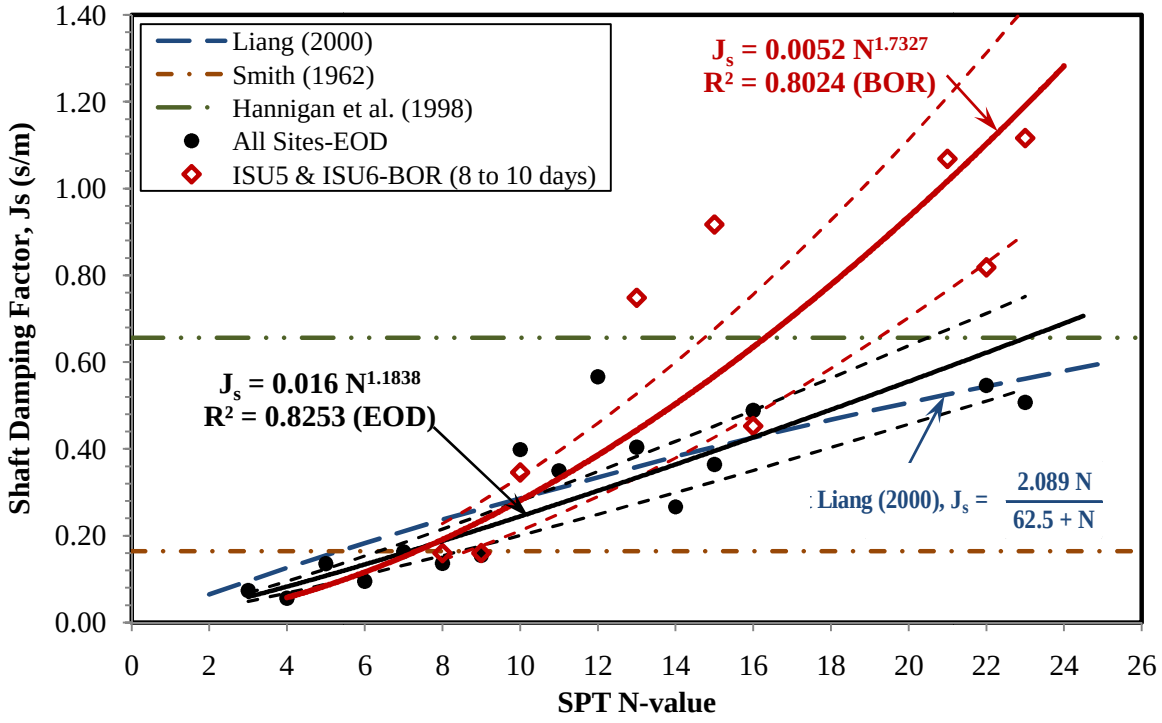


Figure 7.8: Relationship between shaft damping factor for cohesive soils and SPT N-value

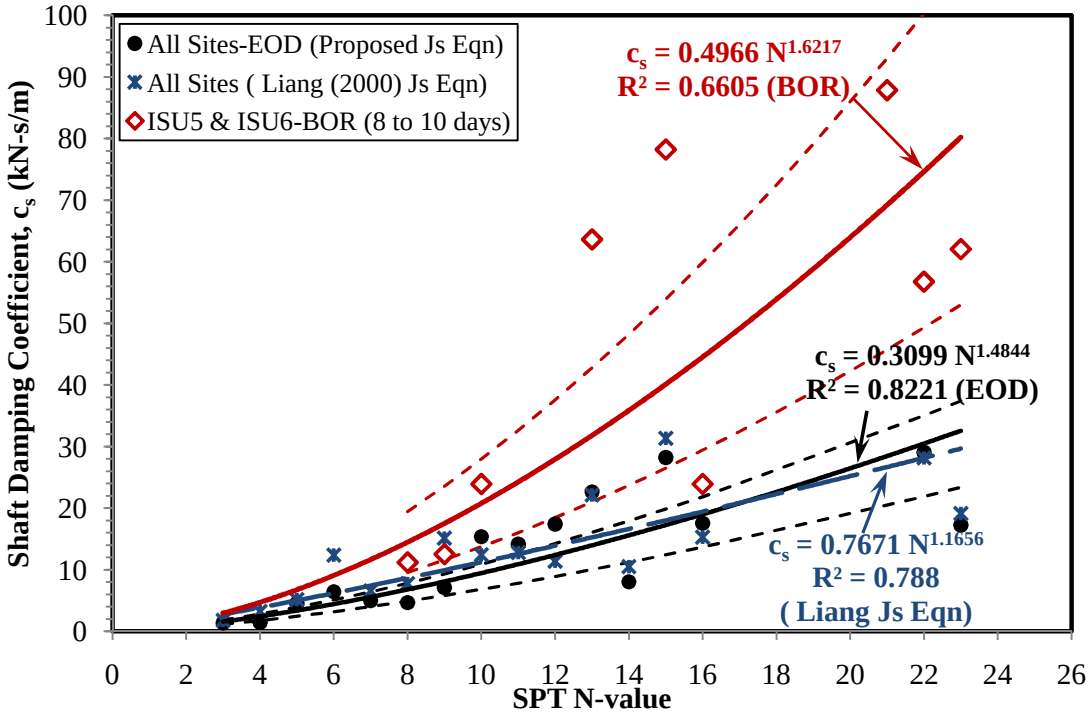


Figure 7.9: Relationship between shaft damping coefficient for cohesive soils and SPT N-value

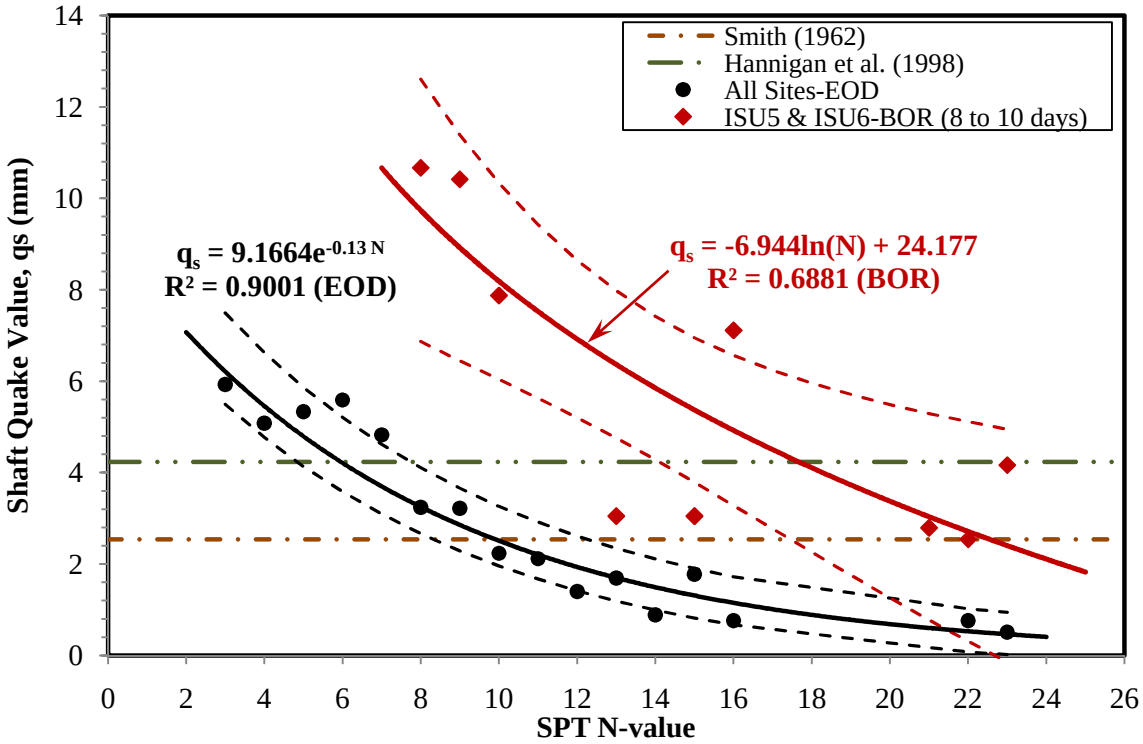


Figure 7.10: Relationship between shaft quake value for cohesive soils and SPT N-value

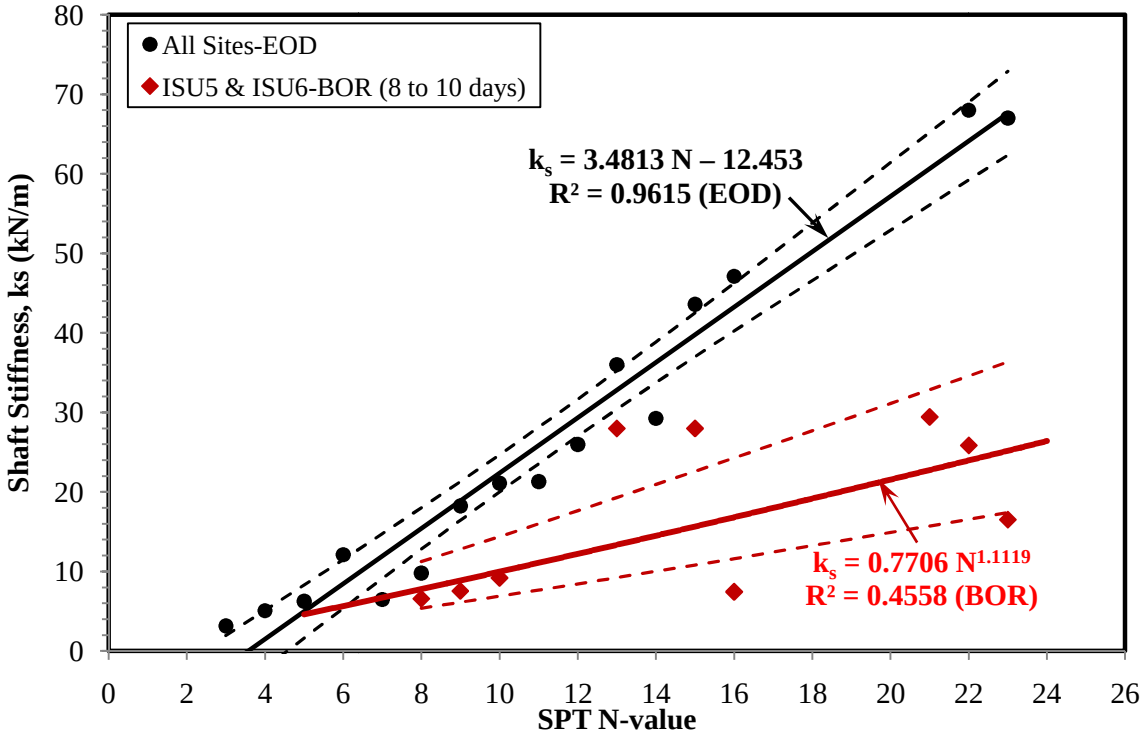


Figure 7.11: Relationship between shaft stiffness for cohesive soils and SPT N-value

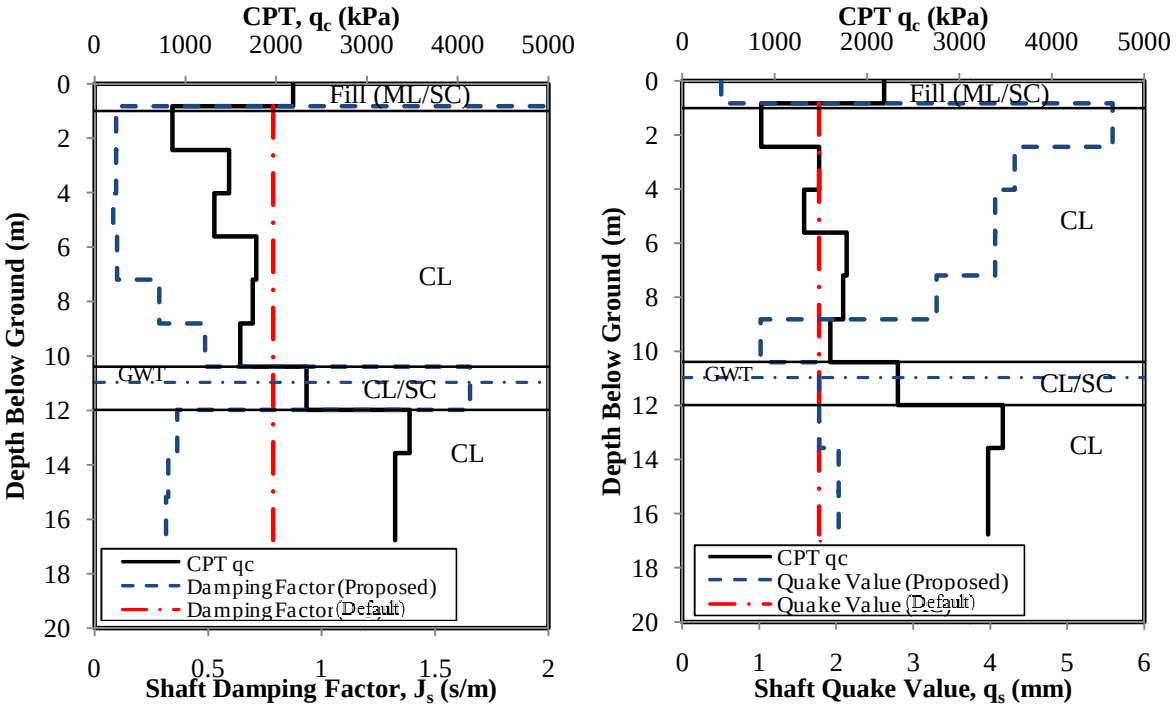


(a) $J_s$ versus $q_c$ (b) $q_s$ versus $q_c$

Figure 7.12: CPT unit tip resistance ($q_c$) versus (a) shaft damping factors; and (b) shaft quake values along the embedded pile length of ISU5

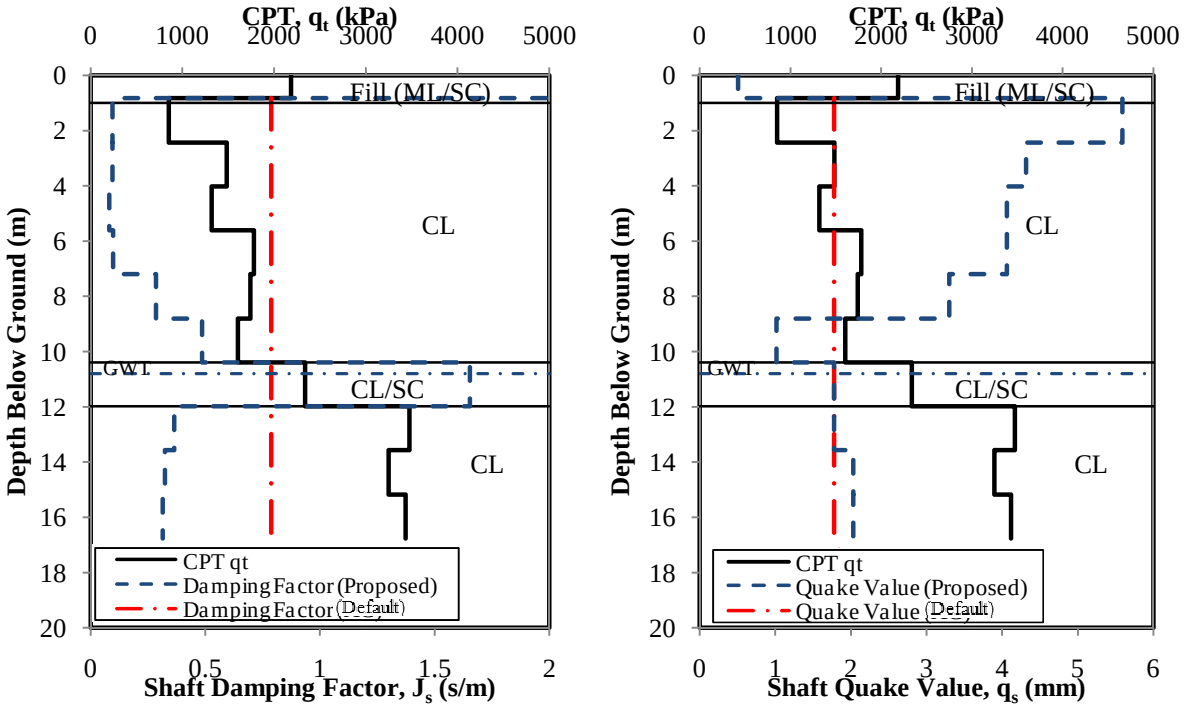


(a) $J_s$ versus $q_t$ (b) $q_s$ versus $q_t$

Figure 7.13: CPT total cone tip resistance ($q_t$) versus (a) shaft damping factors; and (b) shaft quake values along the embedded pile length of ISU5

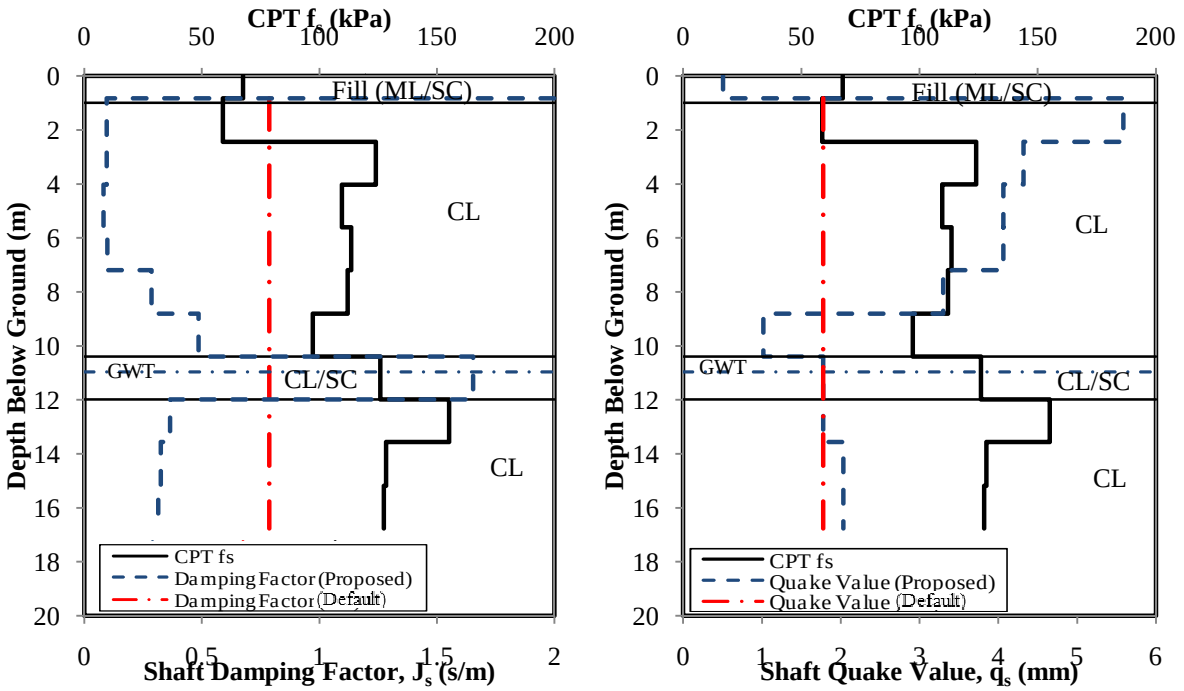


(a) $J_s$ versus $f_s$ (b) $q_s$ versus $f_s$

Figure 7.14: CPT unit skin friction ($f_s$) versus (a) shaft damping factors; and (b) shaft quake values along the embedded pile length of ISU5

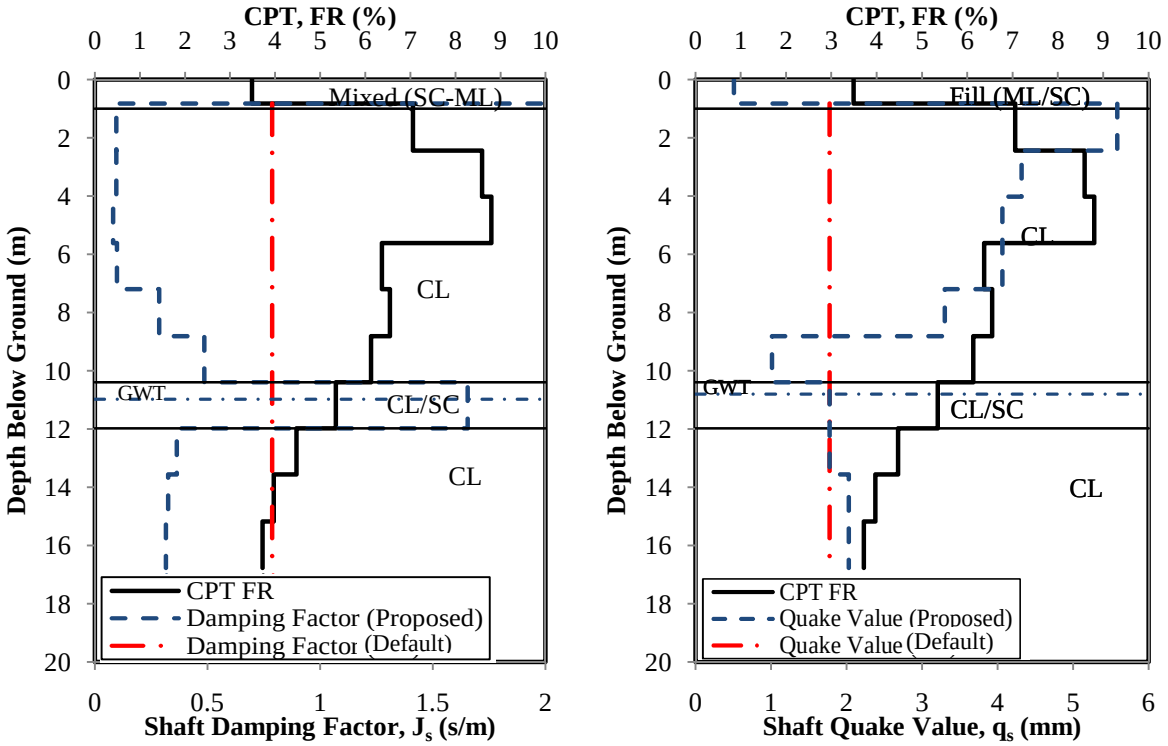


(a) $J_s$ versus FR (b) $q_s$ versus FR

Figure 7.15: CPT friction ratio (FR) versus (a) shaft damping factors; and (b) shaft quake values along the embedded pile length of ISU5

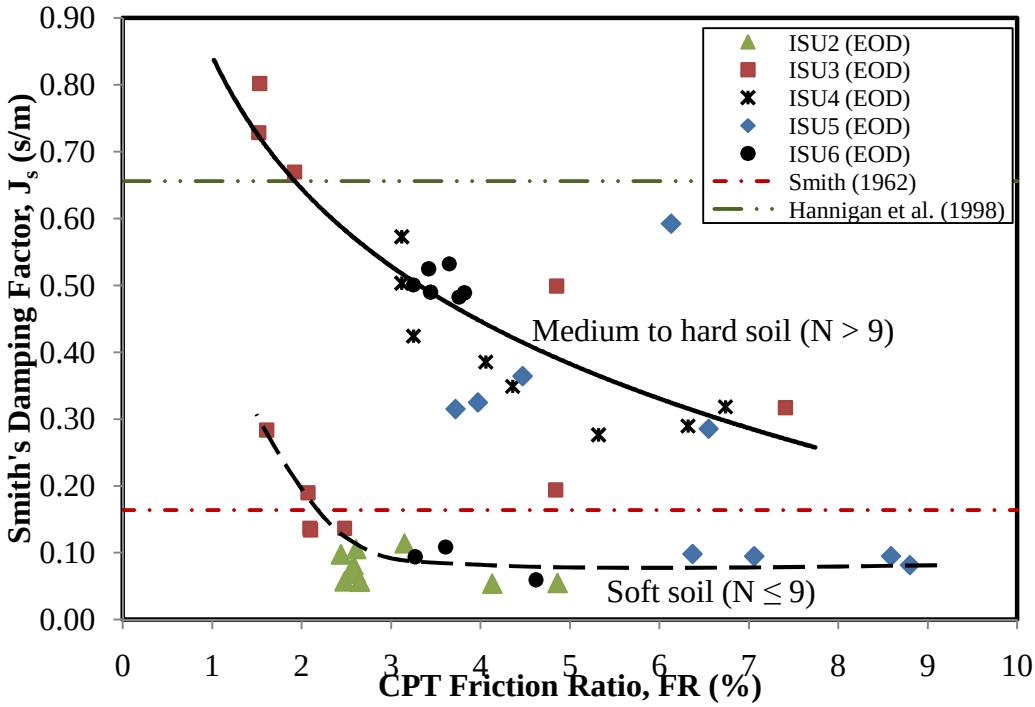


Figure 7.16: Shaft damping factor versus CPT friction ratio

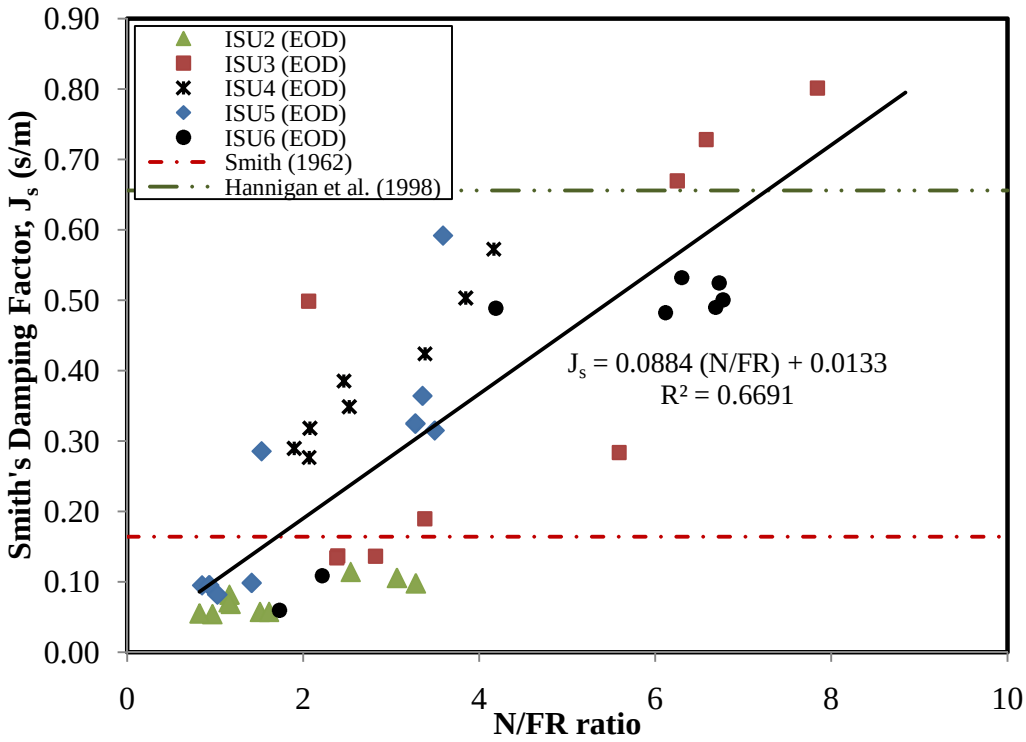


Figure 7.17: Relationship between shaft damping factor and a ratio of SPT N-value to CPT friction ratio

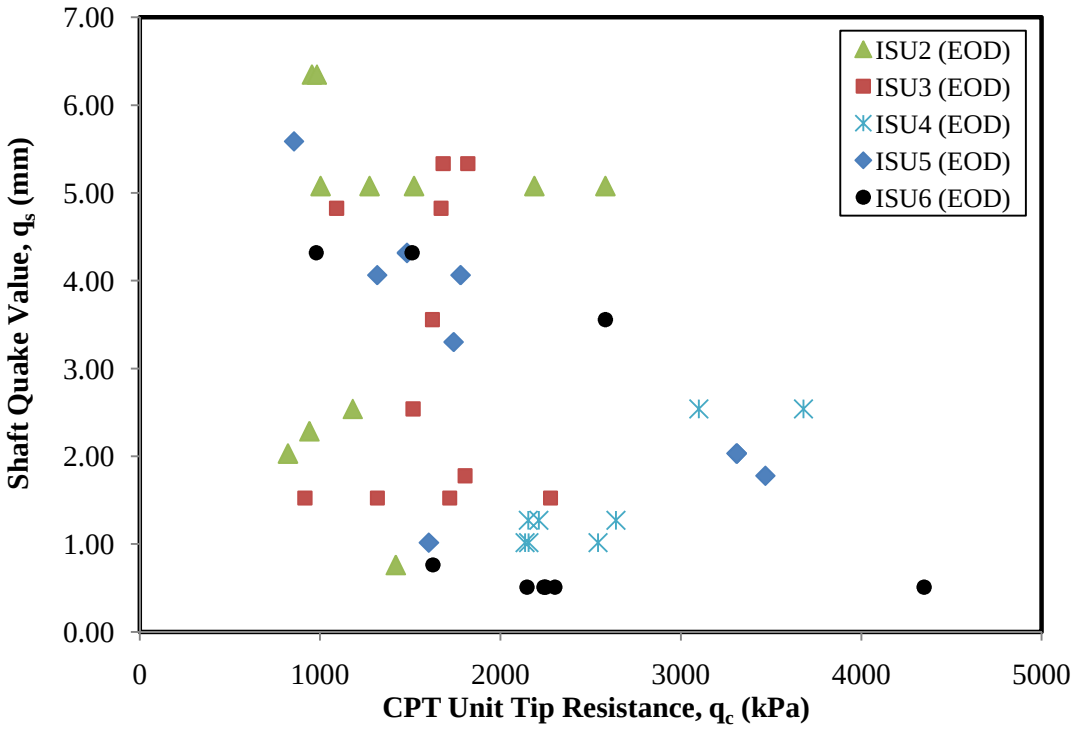


Figure 7.18: Shaft quake value versus CPT unit tip resistance for cohesive soils

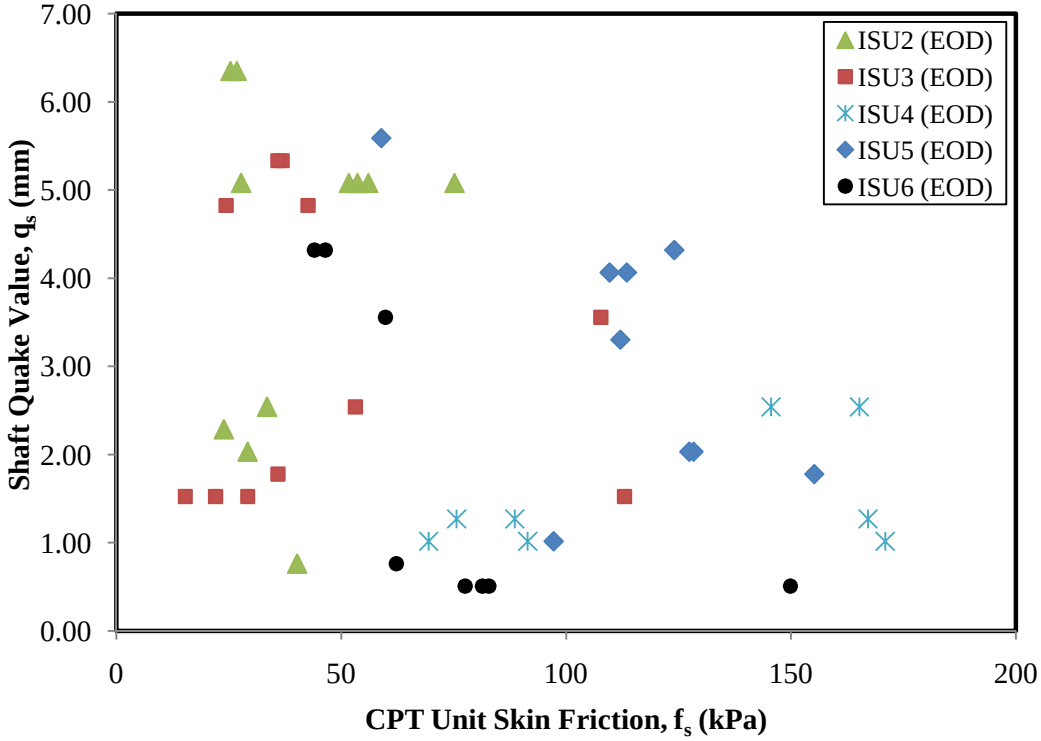


Figure 7.19: Shaft quake value versus CPT unit skin friction for cohesive soils

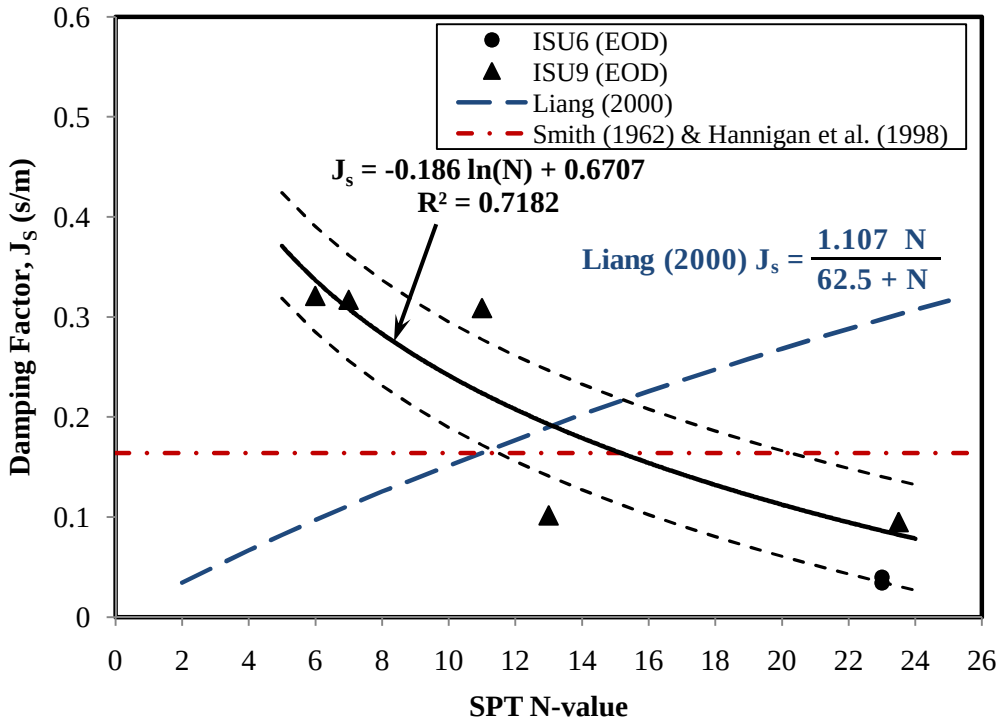


Figure 7.20: Relationship between damping factor and SPT N-value for cohesionless soils

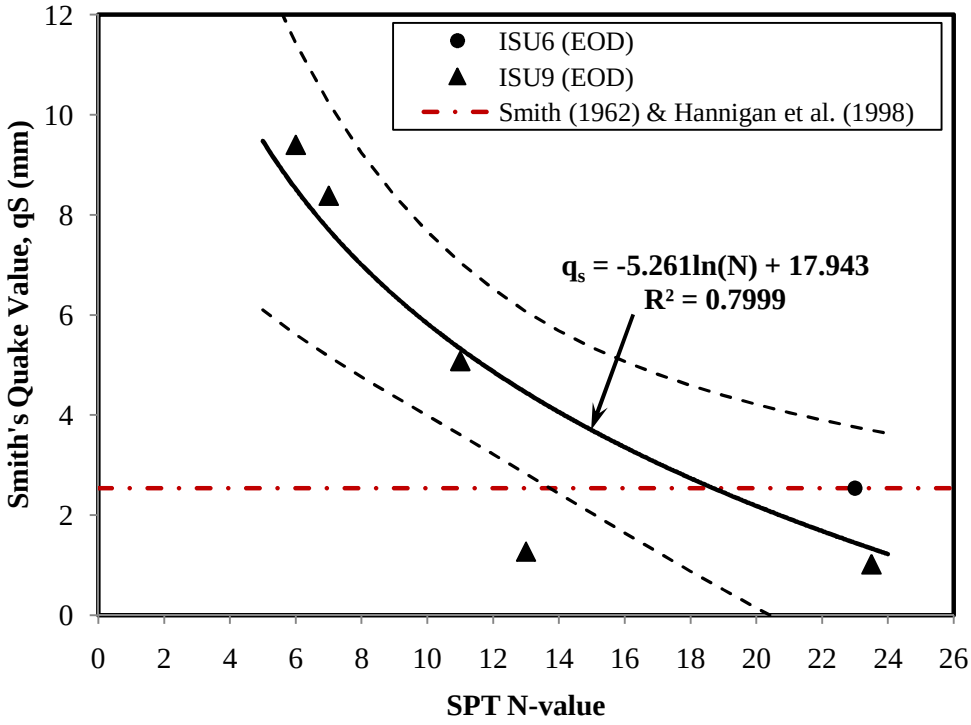


Figure 7.21: Relationship between quake value and SPT N-value for cohesionless soils

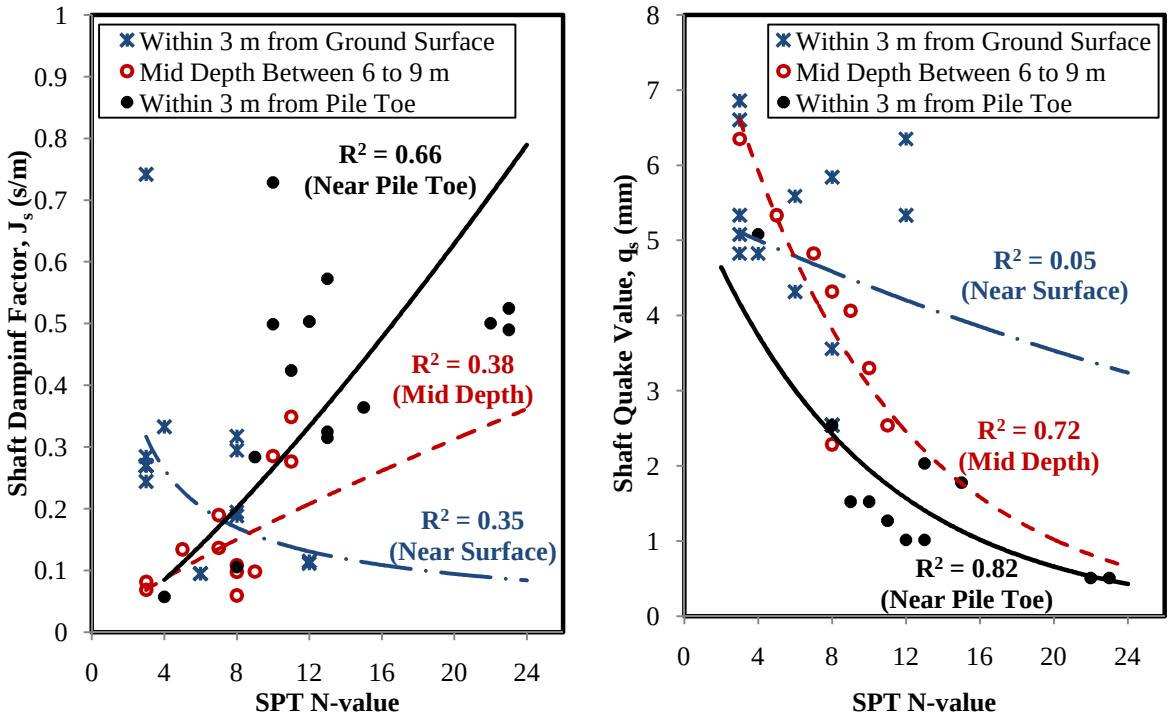


(a) $J_s$ versus SPT N-value (b) $q_s$ versus SPT N-value

Figure 7.22: Effect of pile installation on the correlation studies of (a) damping factor; and (b) quake value at three designated locations along the test pile

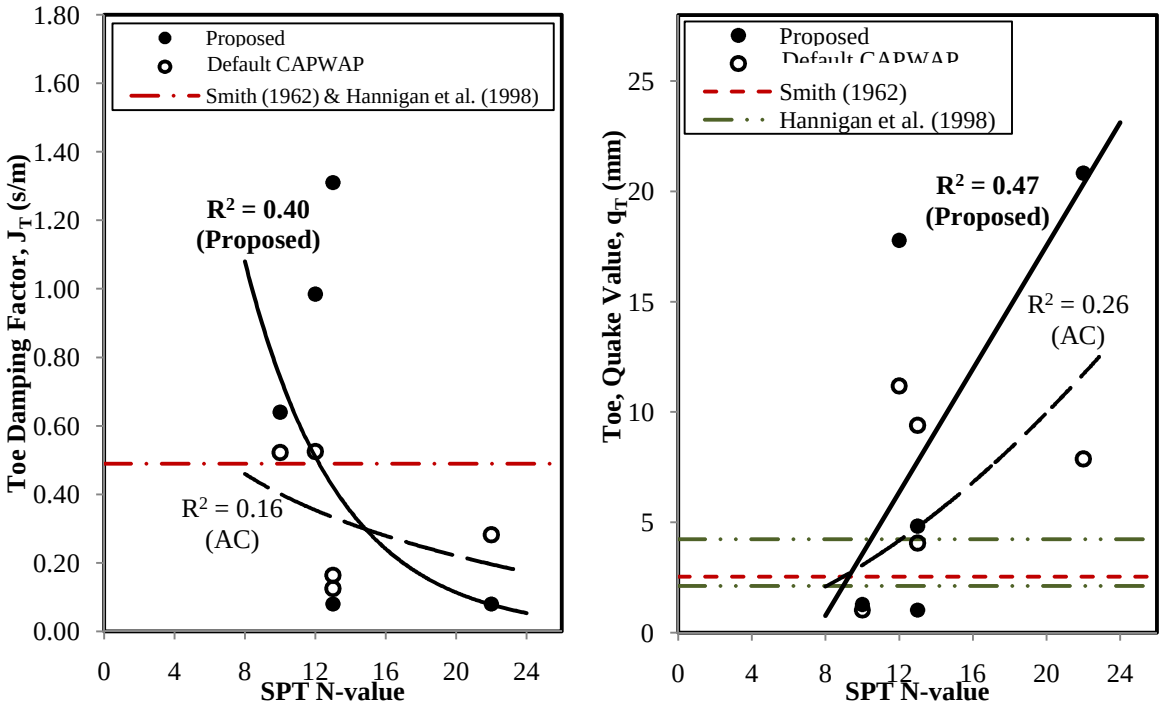


(a) $J_T$ versus SPT N-value (b) $q_T$ versus SPT N-value

Figure 7.23: SPT N-value versus (a) toe damping factor; and (b) toe quake value for cohesive soils

# CHAPTER 8: SUMMARY, CONCLUSIONS AND RECOMMENDATIONS

## 8.1. Summary

Although the Federal Highway Administration (FHWA) has mandated all new bridges initiated after October 1, 2007 should follow the Load and Resistance Factor Design (LRFD) approach, the current American Association of State Highway and Transportation Officials (AASHTO) Specifications do not lead to efficient design of pile foundations. This is because the resistance factors presented for LRFD in the AASHTO Specifications were developed for general soil conditions and pile types that can be used at the national level. Also, the current Iowa Department of Transportation (Iowa DOT) pile design manual does not comply with the LRFD design philosophy, nor does it address the effect of pile setup in cohesive soil profiles, discrepancy between pile resistance estimation and verification, and efficiencies in the dynamic soil parameter quantification.

To overcome the aforementioned challenges, research opportunities were developed and executed by a team of researchers. Presented in this dissertation are work completed by the author which included the following scopes to enhance LRFD approach and construction control of steel H-piles: 1) to characterize soil-pile responses under pile driving impact loads, and (2) to articulate how this information can be implemented to improve design and construction control of piles subjected to vertical loads in accordance with the LRFD philosophy. The main research objective was pile setup investigation in cohesive soils. Other research objectives included (1) to develop regional LRFD recommendations for dynamic analysis methods (WEAP and CAPWAP), (2) to improve pile performance estimations, and (3) to improve dynamic analysis methods. Research was accomplished through extensive literature reviews, comprehensive restrike, and static load tests performed on ten fully instrumented steel H-piles, detailed subsurface monitoring and characterizations, and efficient utilization of historical pile load test data and soil properties compiled in the electronic database PILOT.

Through execution of the above listed objectives, this dissertation was intended to (1) develop reliable, analytical pile setup quantification methods in terms of measurable soil properties without the performance of inconvenient pile restrikes or expensive static load tests currently practiced during construction, (2) establish a calibration procedure for incorporating pile setup in LRFD to elevate the efficiency of pile foundations, (3) improve resistance factors for dynamic analysis methods, (4) enhance the Iowa Blue Book method through construction control evaluations, (5) recommend an improved CAPWAP matching procedure, and (6) quantify dynamic soil parameters in terms of soil types and properties, ultimately impacting the design and construction of bridge pile foundations in Iowa and in the nation.

## 8.2. Conclusions

The major conclusions drawn from the research as described in Chapters 3 through 7 are summarized below.

### 8.2.1. Pile setup investigation and quantification

Pile setup was investigated in Chapter 3 using field test results collected from five fully instrumented HP 250×63 steel piles embedded in cohesive soils. During the field investigation, detailed soil characterization, monitoring of soil total lateral stress and pore water pressure using push-in pressure cells, collection of pile dynamic restrike data as a function of time, and vertical static load tests were completed. Detailed pile setup analyses were performed and a pile setup estimation method was developed in Chapter 4. From the analyses of pile and soil test data, the following conclusions were drawn.

1. Setup was experienced along the pile shaft and at the pile toe in cohesive soils, with the larger setup effect occurring to the shaft resistance between 51 and 71% of the CAPWAP estimated pile resistance at EOD. Despite an average contribution of about 16% towards the total resistance, the end bearing component only increased by 8% to 21% due to setup.
2. Steel H-piles exhibited a logarithmic trend for the gain in total pile resistance with time. The same trend was also true for the shaft resistance. All pile resistances

increased immediately and rapidly within a day after EOD and continuously increased at a slower rate after the second day over the maximum monitored duration of 36 days. A comparison of the gradients of the best fits obtained for various restrike data revealed that the logarithmic increase in total pile resistance generally followed the rate of the pore water pressure dissipation.

3. The experimental investigation confirmed that the amount of setup at a given time depends on soil properties including the coefficient of consolidation, the SPT *N*-value as well as the thicknesses of the cohesive soil layers along the embedded pile length. Piles embedded in a cohesive soil with a larger coefficient of consolidation exhibited higher percent increase in total pile resistances. However, piles embedded in a softer soil characterized by a smaller SPT *N*-value led to a higher percent increase in setup. The collected experimental data showed sufficient information for quantifying the pile setup using properties of surrounding soil, which is not promoted in the past studies.
4. A new pile setup method incorporating the commonly used SPT N-value and horizontal coefficient of consolidation as well as employing an equivalent pile radius was developed. This proposed method utilizes the initial pile resistance estimated at the EOD using either CAPWAP or WEAP, which eliminates the need for performing any inconvenient and costly restrikes or pile load tests. The proposed setup method was successfully validated using additional twelve historical records and five well-documented tests completed by other researchers. The proposed method adequately estimated the pile setup with the difference between measured and predicted pile resistances being 8 and 11% for 90 and 98% confidence intervals, respectively.
6. Based on the analysis performed using six external data sources on large displacement piles, the proposed method provides a better pile setup prediction for piles with diameters smaller than or equal to 600 mm.
7. The analytical study performed based on the test pile ISU8 embedded in a mixed soil profile concluded that the amount of pile setup was smaller than that expected in a complete cohesive soil profile. The observed pile setup followed the

logarithmic trend. The amount of pile setup not only depends on the proportion of the cohesive soil layers to the embedded pile length, but also depends on the stratigraphic layers of cohesive and cohesionless soils.

### 8.2.2. Pile setup in LRFD

The implementation of the proposed pile setup quantification method into the LRFD approach was addressed in Chapter 5. Statistical studies show different uncertainties are associated with the initial pile resistance estimated using dynamic analysis methods and the pile setup resistance quantified using the proposed method. However, the existing calibration procedure cannot separately account for these different sources of uncertainties. Hence, a new and general calibration procedure was developed using the First Order Second Moment (FOSM) method to separately calculate the resistance factors for both resistance components and to ensure both resistance components reach a target reliability level. Compared with the concept of using a single resistance factor to both resistance components, it is concluded that the proposed procedure provides a more dependable pile foundation design. Constant resistance factors for both resistance components can be calculated based upon any regional database that reflects the local soil conditions, pile types, and setup quantification methods. Based on a total 28 data points provided in Chapter 5 on steel H-piles embedded in cohesive soils, the resistance bias ($\lambda_R$) and the coefficient of consolidation ($COV_R$) for pile setup resistance ($R_{setup}$) were determined to be 0.95 and 0.317, respectively. The resistance factors for pile setup were found to be 0.32 and 0.26 for $\beta_T$ values of 2.33 and 3.00, respectively.

### 8.2.3. Regional resistance factors

Chapter 6 presents the establishment of regional Load and Resistance Factor Design (LRFD) recommendations for dynamic analysis methods, based on the historical database and ten recently completed field tests. When compared with the recommendations presented in the NCHRP Report 507 by Paikowsky et al. (2004) and the latest AASHTO (2010) LRFD Bridge Design Specifications, the regionally calibrated resistance factors calculated using the FOSM method for steel H-piles embedded in sand, clay, and mixed soil profiles were

improved. The regionally-calibrated resistance factors are summarized as below:

1. For the WEAP approach considering the EOD condition, the regionally-calibrated resistance factors were 0.55, 0.65, and 0.83 for the sand, clay, and mixed soil profile, respectively, which were higher than the AASHTO's recommended value of 0.50.
2. For the CAPWAP approach considering the BOR condition, the regionally-calibrated resistance factors were 0.77, 0.80, and 0.93 for the sand, clay, and mixed soil profile, respectively, which were all higher than the ASSHTO's recommended value of 0.75.

Using the procedure developed in Chapter 5, the effect of pile setup in a clay profile was incorporated as part of the LRFD recommendations to elevate the efficiency of bridge foundations, so the economic advantages of pile setup can be attained. Due to a higher uncertainty involved in estimating the pile setup resistance (higher $COV_R$) and the selection of a conservative $\alpha$ value of 1.60, smaller $\varphi_{setup}$ values (0.21 for WEAP-Iowa Blue Book, 0.26 for WEAP-Iowa DOT, and 0.37 for CAPWAP based on $\beta_T$=2.33) were determined

### 8.2.4. Construction control

To minimize the discrepancy between design and field pile resistances and to assimilate the construction control capability of dynamic analysis methods during the design stage, a construction control procedure was established in Chapter 6 using a probabilistic approach. This was achieved by integrating WEAP and CAPWAP as construction control methods as part of the design process. Construction control was accounted for by determining a construction control factor corresponding to the 50% cumulative density function of the resistance ratio of the construction control method and the Iowa Blue Book method. These construction control factors were calculated according to the selection of construction control method (WEAP or CAPWAP) during pile driving and the presence of soil type surrounding the pile. A minimum construction control factor of 1.0 was suggested to maintain the economic advantages and the original efficiency of the Iowa Blue Book method. The corrected resistance factor, after considering construction control, was limited

to 0.80, the maximum value recommended by AASHTO (2010). Overall, the construction control consideration has increased the originally-calibrated resistance factors of the Iowa Blue Book method as follow:

1. Construction control using WEAP has increased the original φ value of the Iowa Blue Book from 0.60 to 0.64 or improved the φ value by 7%.
2. Construction control using CAPWAP increases the original φ value of the Iowa Blue Book for the clay profile from 0.60 to 0.68 (or improved by 8%), considering both the EOD and setup resistance conditions.
3. The construction control method using CAPWAP, based on the restrike condition, improves the φ values for clay, mixed soil, and sand profiles by 27%, 18%, and 6%, respectively.

### 8.2.5. Dynamic soil parameters quantification

Due to the limitation with current default CAPWAP matching procedure, in which constant damping factor and quake value are assumed over an entire soil profile and the indeterminate nature of the CAPWAP analysis, Chapter 7 shows the high degree of scatter in the correlation studies between the dynamic soil parameters and the SPT N-value. Although the accuracy of pile resistance estimation using dynamic analysis methods is highly dependent upon the appropriate input of these dynamic soil parameters, these parameters have not been successfully quantified from any standard geotechnical in-situ or laboratory soil test results. Thus, an improved CAPWAP signal matching procedure with variation in shaft dynamic soil parameters was proposed. Its implementation led to the following conclusions:

1. The analytical results show the dynamic soil parameters are not constant over an entire soil profile, but they vary with different soil types and soil properties.
2. For cohesive soils at the EOD condition, the correlation studies revealed a direct relationship between the shaft damping factor and the SPT N-value, and an inverse relationship between the shaft quake value and the SPT N-value. Furthermore, correlation studies using CPT-measured soil properties concluded that the shaft damping factor was influenced by different soil types, while no

relationship was conclusively drawn between the shaft quake value and the CPT-measured soil properties. Since the process of conducting the SPT is similar to pile driving, both are subjected to a continuous impulsive hammer force, the dynamic soil parameters were found to be correlated well with SPT N-value.

3. For cohesionless soils at the EOD condition, an inverse natural algorithmic relationship between the shaft dynamic soil parameters and the SPT N-value was observed.
4. The effect of pile setup increases the dynamic soil parameters for cohesive soils, which increases the dynamic resistance and provides a larger energy dissipation capability of the soil-pile system.
5. The correlation studies concluded that the influence of pile installation on the shaft dynamic soil parameters estimation, showing the highest accuracy for soils near pile toe and lowest accuracy for soils near ground surface.
6. The results of similar correlation studies on toe dynamic soil parameters suggest that the difficulty and challenge with quantifying these parameters in terms of any measureable soil properties. The proposed matching procedure not only provides comparable pile resistance estimation, but also improves match quality.

## 8.3. Recommendations for Future Work

In the future, additional detailed restrikes and static load tests on piles embedded in cohesive soils as similarly employed in this research will further improve the correlation studies between the pile setup and soil properties. The actual measurement of pile resistances at the EOD and over a period of time on a series of piles using a static load testing system will help validate the pile setup estimated using the dynamic analysis methods, and serves as a reference in the resistance factors calibration. Besides pile setup, piles experiencing a decrease in resistance (i.e., pile relaxation) in sandy soils may be investigated. The regional resistance factor calibration may be extended to other pile types, such as drilled shafts and end bearing piles. The uncertainties associated with the estimations of shaft resistance and end bearing may be accounted for by separately providing sufficient data points on the pile resistance distribution. The implementation of the proposed CAPWAP

signal matching procedure in future research and practice would generate more representative dynamic soil parameters to further improve the correlation studies, eventually leading to more accurate pile resistance estimations.

# ACKNOWLEDGMENTS

I was one of the fortunate graduate students, who received a research assistantship from Dr. Sri Sritharan in a short period of time after submitting my PhD application to the graduate school. It is my privilege to have Dr. Sritharan as my major advisor. I would like to thank him for his guidance and support throughout these years. I also greatly enjoy the competitive squash games we have played.

I would like to thank Dr. Muhannad T. Suleiman for his advice and assistance during this research. Special thanks to my colleagues, Dr. Sherif S. AbdelSalam and Matthew J. Roling, for their collaboration on the same research project.

Drs. Fouad Fanous, Jeramy Ashlock, Jennifer Shane, and Igor Beresnev served as members of my Program of Study committee. I am indebted to their advice and cooperation in completing this dissertation.

Outside my committee, Dr. Say Kee Ong served as a mentor starting from my undergraduate education at Iowa State University. His encouragement and advice are greatly appreciated.

The research presented in this dissertation was funded by the Iowa Highway Research Board (IHRB). I express my gratitude to members of the IHRB and the following members of the project Technical Advisory Committee for their guidance and advice: Ahmad Abu-Hawash, Dean Bierwagen, Lyle Brehm, Ken Dunker, Kyle Frame, Steve Megivern, Curtis Monk, Michael Nop, Gary Novey, John Rasmussen, and Bob Stanley. The members of this committee represent the Office of Bridges and Structures, Soils, Design Section, and the Office of Construction of the Iowa DOT, FHWA Iowa Division, and Iowa County Engineers.

Special thanks are due to Douglas Wood, Donald Davidson, and Erica Velasco for their assistance with the field tests and laboratory soil tests. The author would also like to thank various bridge contractors and soil investigation contractors, Team Services Inc., and Geotechnical Services Inc. (GSI), for their contribution to the field tests.